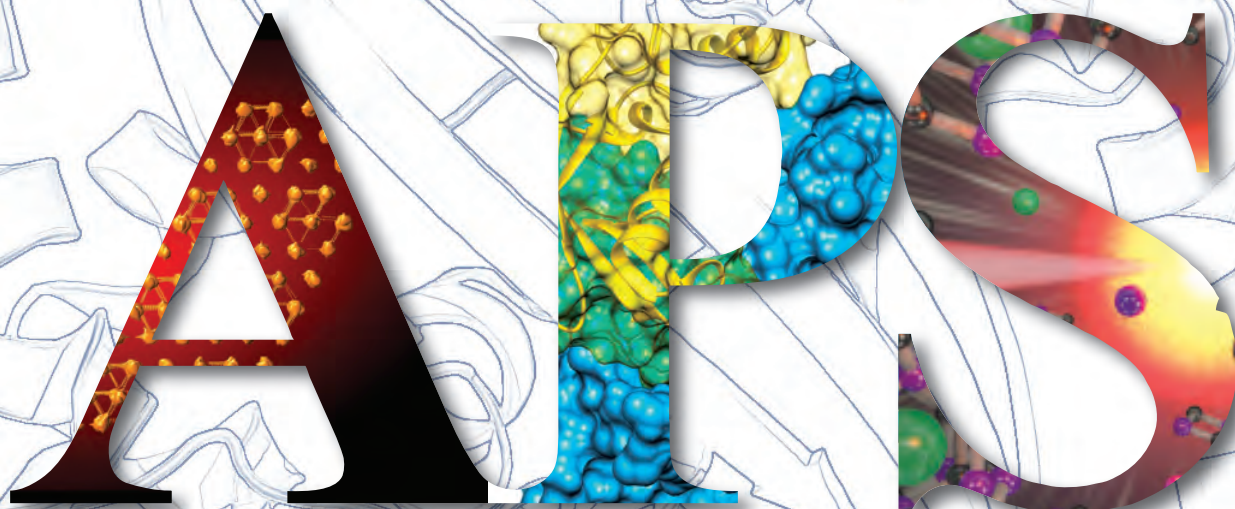


ANL-21/06 Vol.1
ISSN 1931-5007
January 2021

APS Science

2020 VOLUME 1



APS

RESEARCH AND ENGINEERING HIGHLIGHTS
FROM THE
ADVANCED PHOTON SOURCE AT
ARGONNE NATIONAL LABORATORY

Includes APS research into the SARS-CoV-2 virus

Argonne 
NATIONAL LABORATORY

About Argonne National Laboratory

Argonne is a U.S. Department of Energy laboratory managed by UChicago Argonne, LLC under contract DE-AC02-06CH11357. The Laboratory's main facility is outside Chicago, at 9700 South Cass Avenue, Lemont, Illinois 60439. For information about Argonne and its pioneering science and technology programs, see www.anl.gov.

DOCUMENT AVAILABILITY

Online Access: U.S. Department of Energy (DOE) reports produced after 1991 and a growing number of pre-1991 documents are available free at OSTI.GOV (<http://www.osti.gov/>), a service of the US Dept. of Energy's Office of Scientific and Technical Information.

Reports not in digital format may be purchased by the public from the National Technical Information Service (NTIS): U.S. Department of Commerce National Technical Information Service
5301 Shawnee Rd
Alexandria, VA 22312
www.ntis.gov
Phone: (800) 553-NTIS (6847) or (703) 605-6000
Fax: (703) 605-6900
Email: orders@ntis.gov

Reports not in digital format are available to DOE and DOE contractors from the Office of Scientific and Technical Information (OSTI):

U.S. Department of Energy
Office of Scientific and Technical Information
P.O. Box 62
Oak Ridge, TN 37831-0062
www.osti.gov
Phone: (865) 576-8401
Fax: (865) 576-5728
Email: reports@osti.gov

Disclaimer

This report was prepared as an account of work sponsored by an agency of the United States Government. Neither the United States Government nor any agency thereof, nor UChicago Argonne, LLC, nor any of their employees or officers, makes any warranty, express or implied, or assumes any legal liability or responsibility for the accuracy, completeness, or usefulness of any information, apparatus, product, or process disclosed, or represents that its use would not infringe privately owned rights. Reference herein to any specific commercial product, process, or service by trade name, trademark, manufacturer, or otherwise, does not necessarily constitute or imply its endorsement, recommendation, or favoring by the United States Government or any agency thereof. The views and opinions of document authors expressed herein do not necessarily state or reflect those of the United States Government or any agency thereof, Argonne National Laboratory, or UChicago Argonne, LLC.

On the cover: Background: Structure of the SARS-CoV-2 N protein N2b domain, PDB ID 6WZQ..

APS Science

2020 VOLUME 1

RESEARCH AND ENGINEERING HIGHLIGHTS
FROM THE
ADVANCED PHOTON SOURCE AT
ARGONNE NATIONAL LABORATORY

Argonne is a U.S. Department of Energy (DOE) laboratory managed by UChicago Argonne, LLC.
The Advanced Photon Source is a DOE Office of Science user facility
operated for the DOE Office of Science by Argonne National Laboratory under Contract No. DE-AC02-06CH11357.

Table of Contents

The Advanced Photon Source Facility at Argonne National Laboratory iv

Contact Us iv

Plan View of the Argonne 400-Area Facilities; APS Sectors v

APS Beamlines vi

Double-Safe in the Time of the Pandemic viii

Engineering Materials and Applications 1

Caging a New Class of Carbon-Boron Clathrates 2

Printing Ultrathin 2-D Polymer Electronics 4

Obstacles to Sodium-Ion Battery Performance: When Too Much Order is a Bad Thing 8

For Lithium-Ion Cathodes, Partial Order Up 10

A New Lease on Life for Electrocatalysts 12

Single-Site Electrocatalyst Synthesis and Model Validation Increases Green Energy Options 14

Water Adsorption in Metal-Organic Frameworks 16

Slow Flow and Sudden Avalanches Relax Stress in Glasses 18

Putting a Shine on Metal 3-D Printing 20

Making Strong Plastics from Silk 22

A Short, Sharp Shock to Gold Structure 24

Shocking Cerium into a New Phase 26

Electronic and Magnetic Materials 29

Peeling Back the Layers on GdTe₃ 30

High-Resolution RIXS System Reveals Dynamic Spin Correlations in Na₂IrO₃ 32

Ferroelectric Domain Wall Movement in a Complex Oxide Thin Film 34

Nematoelastic Coupling Reveals the Nematic Correlation Lengths of Three Fe-Based Superconductors 38

How Tantalum Clustering Leads to Charge Density Wave Lattice Distortions in 2H-TaSe₂ 40

Growing the Skinniest Magnets 42

Double-Safe in the Time of the Pandemic: Paul Rossi 44

Soft Materials and Liquids 45

Crystals Could Reveal a New Spin on Quantum Physics 46

Putting the Starch in Tissue-Like Materials 48

X-rays Paint a “Grainy” Portrait of Coarsening Soft Materials 50

Finding the Recipe for Protein-Based Drugs 52

Double-Safe in the Time of the Pandemic: Tiffany Freedman 54

Chemical Science 55

Catalytic Magic 56

A Deeper Look into Bio-Inspired Catalysts 58

Reversible Isomerization Reaction Drives a COF-Based Humidity Sensor 60

Chromium-Zinc Catalysts Expand Potential for Synthetic Gas and Non-Petroleum-Based Manufacturing 62

Designing a Catalyst 64

New Pathways to Advance Adsorbent Technologies for Alkene Purification 66

Double-Safe in the Time of the Pandemic: Mike Fries 68

Life Science 69

Key Insights into an Inherited Muscle Disease 70

Developing Tiny Sensors to Test Oxygen Passage in Lung Membranes 72

Effects of Gravity on the Open Circulatory Systems of Invertebrates 74

Uncovering Unique Structural Features in Protein Regions Associated with ALS 76

Double-Safe in the Time of the Pandemic: Cassandra Hayden 78

Structural Biology 79

Discoveries from First SARS Outbreak Jump-Start COVID-19 Treatment Development 80

Viral Life Cycle Inspires New Approaches to Drug Design for SARS-CoV-2 82

Deciphering Coronavirus Protein Behavior 84

Dexamethasone and COVID-19: All Patients Are Not Alike 86

How SARS-CoV-2 RNA Evades Host Immune Responses 88

Compact Llama Antibody Combats Coronavirus 90

3-D Structure of SARS-CoV-2 Explains High Infectivity vs. Other Coronaviruses 92

Repurposing Existing Treatments to Fight Emerging Viral Pathogens 94

New Zika Virus Vaccine May Also Protect Against Dengue Virus	96
A Novel, Potent Pharmaceutical for the Treatment of Prostate Cancer	99
Mamba Snake Toxin Unlocks Potential for Future Drug Discoveries	100
Solving the Structure of a Clinically Interesting Protein Associated with Schizophrenia	102
Probing the Kinetics of Cooperation in Hemoglobin	104
Two Keys, One Protein, Diverse Pathways	106
Bringing Phages and Yeast Together for Peptide Discovery	108
Preventing a Bacterium from Getting a Taste of Its Own Medicine	110
Enzyme-Assisted Molecular Strain Contributes to Successful Reaction	112
Transfer RNA Conformation Aids Efficient Ribosome Recycling	114
Structural Analyses Reveal Key Insights into Clinically Relevant Nanomachines	116
Double-Safe in the Time of the Pandemic: Jeff McGhee	118
Environmental, Geological, and Planetary Science	119
<i>In Situ</i> Imaging of Methane Hydrate Formation and Dissolution	120
A Comparison of Large and Supersized Rhyolitic Eruptions in Taupo, New Zealand	122
A Deeper Look into the Surface Chemistry and Mineralogy of Titan	124
Keeping Heavy Metals Out of the Food Chain	126
Double-Safe in the Time of the Pandemic: Elroy Chang	128
Nanoscience	129
Using Cutting-Edge Nanoscale Imaging to Gain Molecular Insights about Parkinson's Disease	130
Silver Nanostructures Show Promise for Improved Medical Probes	132
APS X-ray Availability and Reliability	134
Typical APS Machine Parameters	134
Novel Accelerator and X-ray Techniques and Instrumentation	135
An X-ray Waveguide Probe into Ultra-thin Nanostructure Films	136
Using X-Rays and Rare Earth Elements to Generate Ultra-High Resolution Images	138
Data	140
Photon Sciences Directorate Organization Chart	141
APS Source Parameters	142
Acknowledgments	144

Access to Beam Time at the Advanced Photon Source

Five types of beam-time proposals are available at the APS: general user, partner or project user, collaborative access team (CAT) member, CAT staff, and APS staff. All beam time at the APS must be requested each cycle through the web-based Beam Time Request System. Each beam-time request (BTR) must be associated with one of the proposals mentioned above.

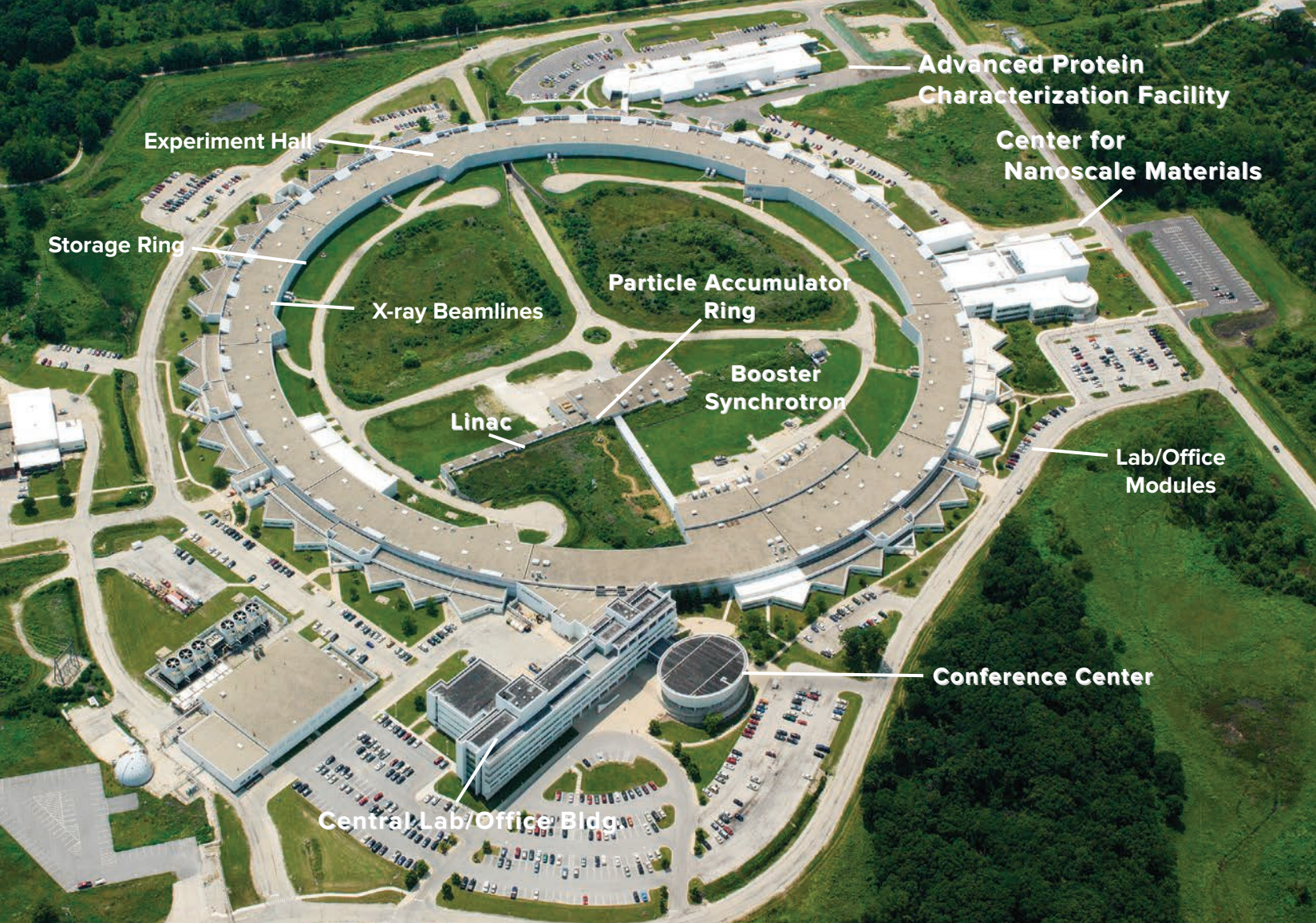
GENERAL-USER PROPOSALS AND BTRS Proposals are peer reviewed and scored by a General User Proposal Review Panel, and time is allocated on the basis of scores and feasibility. A new BTR must be submitted each cycle; each cycle, allocation is competitive. Proposals expire in two years or when the number of shifts recommended in the peer review has been utilized, whichever comes first.

PARTNER- OR PROJECT-USER PROPOSALS AND BTRS Proposals are peer reviewed by a General User Proposal Review Panel and reviewed further by a subcommittee of the APS Scientific Advisory Committee and by APS senior management. Although a new BTR must be submitted each cycle, a specific amount of beam time is guaranteed for up to three years.

CAT-MEMBER PROPOSALS from CAT members are typically much shorter and are reviewed by processes developed by individual CATs. Allocation/scheduling is determined by each CAT's management.

CAT AND APS STAFF-MEMBER PROPOSALS AND BTRS These proposals are also very short and are reviewed through processes developed by either the CAT or the APS. Each CAT/beamline determines how beam time is allocated/scheduled. Collaborative access team and/or APS staff may submit general-user proposals, in which case the rules for general-user proposals and BTRs are followed.

In addition to the above, the APS has developed an industrial measurement access mode (MAM) program to provide a way for industrial users to gain rapid access for one-time measurements to investigate specific problems. A MAM proposal expires after one visit. The APS User Information page (www.aps.anl.gov/Users-Information) provides access to comprehensive information for prospective and current APS users.



The Advanced Photon Source Facility at Argonne National Laboratory

The U.S. Department of Energy's Advanced Photon source (APS) is one of the world's most productive x-ray light source facilities. Each year, the APS provides high-brightness x-ray beams to a diverse community of more than 5,000 researchers in materials science, chemistry, condensed matter physics, the life and environmental sciences, and applied research. Researchers using the APS produce over 2,000 publications each year detailing impactful discoveries, and solve more vital biological protein structures than users of any other x-ray light source research facility. APS x-rays are ideally suited for explorations of materials and biological structures; elemental distribution; chemical, magnetic, electronic states; and a wide range of technologically important engineering systems from batteries to fuel injector sprays, all of which are the foundations of our nation's economic, technological, and physical well-being.

The APS occupies an 80-acre site on the Argonne campus, about 25 miles from downtown Chicago, Illinois. It shares a site with the Center for Nanoscale Materials and the Advanced Protein Characterization Facility.

For directions to Argonne, see <https://www.anl.gov/visiting-argonne>.

CONTACT US

For more information about the APS send an email to apsinfo@aps.anl.gov or write to APS Info, Bldg. 401, Rm. A4113, Argonne National Laboratory, 9700 S. Cass Ave., Lemont, IL 60439.

To order additional copies of this, or previous, issues of *APS Science* send email to apsinfo@aps.anl.gov.

To download PDF versions of *APS Science* back issues go to www.aps.anl.gov/Science/APS-Science

Visit the APS on the Web at www.aps.anl.gov

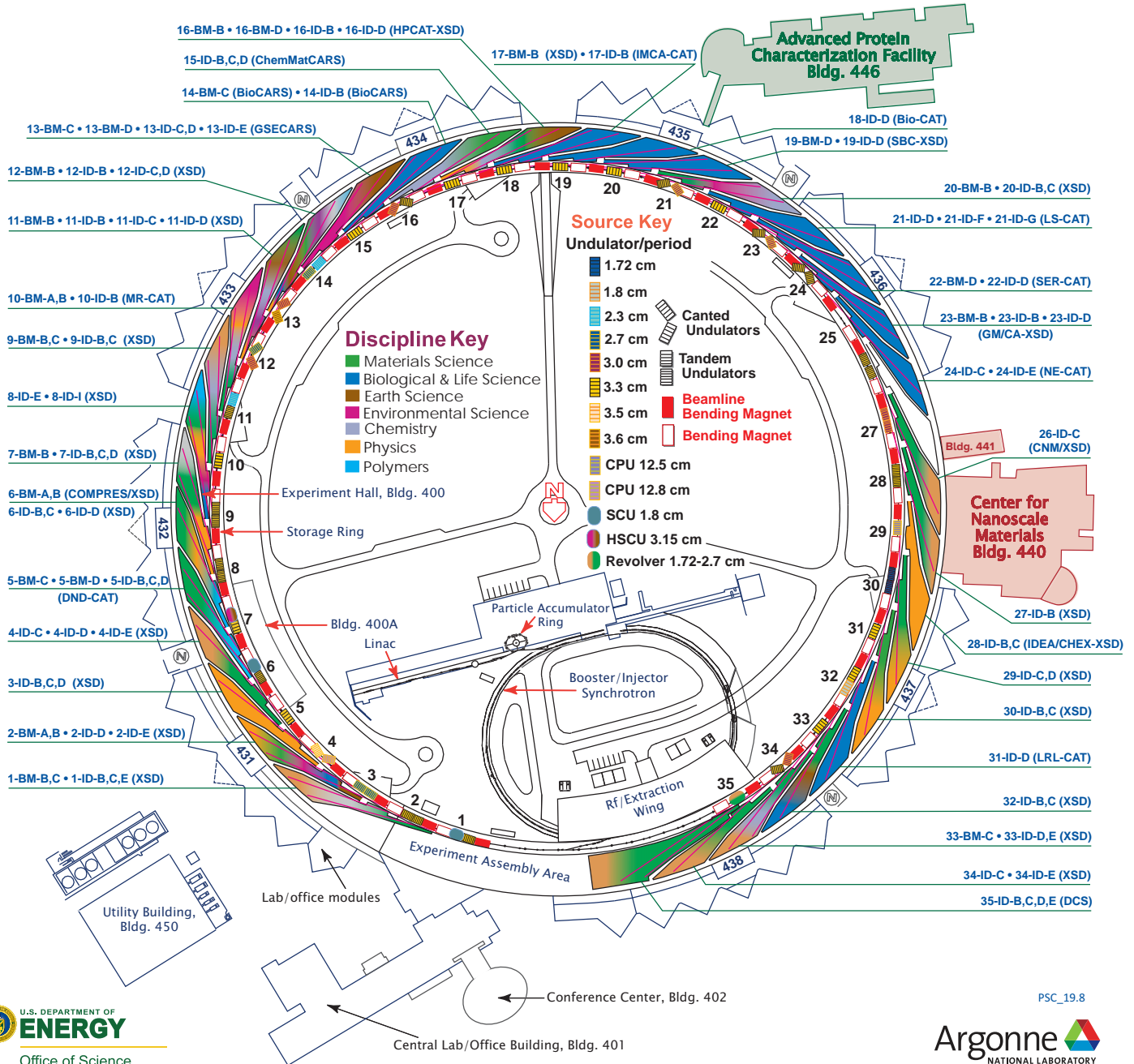
ARGONNE NATIONAL LABORATORY 400-AREA FACILITIES

ADVANCED PHOTON SOURCE

(Beamlines, Disciplines, and Source Configuration)

ADVANCED PROTEIN CHARACTERIZATION FACILITY

CENTER FOR NANOSCALE MATERIALS



PSC_19.8



APS sectors: At the APS, a “sector” comprises the radiation sources (one bending magnet and nominally one insertion device, although the number of insertion devices in the straight sections of the storage ring can vary) and the beamlines, enclosures, and instrumentation that are associated with a particular storage ring sector. The APS has 35 sectors dedicated to user science and experimental apparatus. X-ray Science Division (XSD) sectors comprise those beamlines operated by the APS. Collaborative access team (CAT) sectors comprise beamlines operated by independent groups made up of scientists from universities, industry, and/or research laboratories both federal and private.

APS BEAMLINES

KEY: BEAMLINE DESIGNATION • SECTOR OPERATOR • DISCIPLINES • TECHNIQUES • RADIATION SOURCE ENERGY • USER ACCESS MODE(S) • GENERAL-USER STATUS

1-BM-B,C • **X-RAY SCIENCE DIVISION (XSD)** • MATERIALS SCIENCE, PHYSICS • OPTICS TESTING, DETECTOR TESTING, TOPOGRAPHY, WHITE LAUE SINGLE-CRYSTAL DIFFRACTION • 6-30 keV, 50-120 keV • ON-SITE • ACCEPTING GENERAL USERS

1-ID-B,C,E • XSD • MATERIALS SCIENCE, PHYSICS, CHEMISTRY, LIFE SCIENCE • HIGH-ENERGY X-RAY DIFFRACTION, TOMOGRAPHY, SMALL-ANGLE X-RAY SCATTERING, FLUORESCENCE SPECTROSCOPY, PAIR DISTRIBUTION FUNCTION, PHASE CONTRAST IMAGING • 41-136 keV, 45-116 keV • ON-SITE • ACCEPTING GENERAL USERS

2-BM-A,B • XSD • PHYSICS, LIFE SCIENCES, GEOSCIENCE, MATERIALS SCIENCE • TOMOGRAPHY, PHASE CONTRAST IMAGING • 10-170 keV, 11-35 keV • ON-SITE • ACCEPTING GENERAL USERS

2-ID-D • XSD • LIFE SCIENCES, MATERIALS SCIENCE, ENVIRONMENTAL SCIENCE • MICROFLUORESCENCE (HARD X-RAY), MICRO X-RAY ABSORPTION FINE STRUCTURE, NANOIMAGING, PTYCHOGRAPHY • 5-30 keV • ON-SITE • ACCEPTING GENERAL USERS

2-ID-E • XSD • LIFE SCIENCES, ENVIRONMENTAL SCIENCE, MATERIALS SCIENCE • MICROFLUORESCENCE (HARD X-RAY), TOMOGRAPHY • 5-20 keV • ON-SITE • ACCEPTING GENERAL USERS

3-ID-B,C,D • XSD • PHYSICS, GEOSCIENCE, LIFE SCIENCES, CHEMISTRY, MATERIALS SCIENCE • NUCLEAR RESONANT SCATTERING, INELASTIC X-RAY SCATTERING, HIGH-PRESSURE DIAMOND ANVIL CELL • 7-27 keV, 14.41-14.42 keV • ON-SITE • ACCEPTING GENERAL USERS

4-ID-C • XSD • PHYSICS, MATERIALS SCIENCE • MAGNETIC CIRCULAR DICHROISM (SOFT X-RAY), X-RAY MAGNETIC LINEAR DICHROISM, X-RAY PHOTOEMISSION SPECTROSCOPY, ANOMALOUS AND RESONANT SCATTERING (SOFT X-RAY) • 400-2800 eV • ON-SITE • ACCEPTING GENERAL USERS

4-ID-D • XSD • PHYSICS, MATERIALS SCIENCE • ANOMALOUS AND RESONANT SCATTERING (HARD X-RAY), MAGNETIC X-RAY SCATTERING, MAGNETIC CIRCULAR DICHROISM (HARD X-RAY) HIGH-PRESSURE DIAMOND ANVIL CELL • 2.7-40 keV • REMOTE • ACCEPTING GENERAL USERS

4-ID-E • XSD • MATERIALS SCIENCE, PHYSICS • SYNCHROTRON X-RAY SCANNING TUNNELING MICROSCOPY • 500-1800 eV • ON-SITE • ACCEPTING GENERAL USERS

5-BM-C • **DUPONT-NORTHWESTERN-DOW COLLABORATIVE ACCESS TEAM (DND-CAT)** • MATERIALS SCIENCE, POLYMER SCIENCE • POWDER DIFFRACTION, TOMOGRAPHY, WIDE-ANGLE X-RAY SCATTERING • 10-42 keV • ON-SITE • ACCEPTING GENERAL USERS

5-BM-D • DND-CAT • MATERIALS SCIENCE, POLYMER SCIENCE, CHEMISTRY, ENVIRONMENTAL SCIENCE • X-RAY ABSORPTION FINE STRUCTURE, HIGH-ENERGY X-RAY DIFFRACTION, GENERAL DIFFRACTION • 4.5-25 keV, 4.5-80 keV • ON-SITE, MAIL-IN • ACCEPTING GENERAL USERS

5-ID-B,C,D • DND-CAT • MATERIALS SCIENCE, POLYMER SCIENCE, CHEMISTRY, LIFE SCIENCE • POWDER DIFFRACTION, X-RAY STANDING WAVES, X-RAY OPTICS DEVELOPMENT/TECHNIQUES, SMALL-ANGLE X-RAY SCATTERING, SURFACE DIFFRACTION, X-RAY REFLECTIVITY, WIDE-ANGLE X-RAY SCATTERING • 6-17.5 keV • ON-SITE • ACCEPTING GENERAL USERS

6-BM-A,B • **COMPRES/XSD** • MATERIALS SCIENCE, GEOSCIENCE • ENERGY DISPERSIVE X-RAY DIFFRACTION, HIGH-PRESSURE MULTI-ANVIL PRESS, RADIOGRAPHY, TOMOGRAPHY • 20-200 keV • ON-SITE • ACCEPTING GENERAL USERS

6-ID-B,C • XSD • PHYSICS, MATERIALS SCIENCE • MAGNETIC X-RAY SCATTERING, ANOMALOUS AND RESONANT SCATTERING (HARD X-RAY), GENERAL DIFFRACTION, GRAZING INCIDENCE DIFFRACTION • 4-38 keV • REMOTE • ACCEPTING GENERAL USERS

6-ID-D • XSD • PHYSICS, MATERIALS SCIENCE • HIGH-ENERGY X-RAY DIFFRACTION, POWDER DIFFRACTION, PAIR DISTRIBUTION FUNCTION • 50-100 keV, 70-130 keV • REMOTE • ACCEPTING GENERAL USERS

7-BM-B • XSD • PHYSICS • RADIOGRAPHY, TOMOGRAPHY, MICROFLUORESCENCE (HARD X-RAY) • 5-150 keV, 6-15 keV, 15-60 keV • ON-SITE • ACCEPTING GENERAL USERS

7-ID-B,C,D • XSD • MATERIALS SCIENCE, ATOMIC PHYSICS, CHEMISTRY • TIME-RESOLVED X-RAY SCATTERING, TIME-RESOLVED X-RAY ABSORPTION FINE STRUCTURE, PHASE CONTRAST IMAGING • 6-18 keV, 12-26 keV • ON-SITE, REMOTE • ACCEPTING GENERAL USERS

8-ID-E • XSD • MATERIALS SCIENCE, POLYMER SCIENCE, PHYSICS • GRAZING INCIDENCE SMALL-ANGLE SCATTERING, X-RAY PHOTON CORRELATION SPECTROSCOPY • 7.35-7.35 keV, 10.9-10.9 keV • ON-SITE, REMOTE • ACCEPTING GENERAL USERS

8-ID-I • XSD • POLYMER SCIENCE, MATERIALS SCIENCE, PHYSICS • X-RAY PHOTON CORRELATION SPECTROSCOPY, SMALL-ANGLE X-RAY SCATTERING • 7.35-7.35 keV, 10.9-10.9 keV • ON-SITE, REMOTE • ACCEPTING GENERAL USERS

9-BM-B,C • XSD • MATERIALS SCIENCE, CHEMISTRY, ENVIRONMENTAL SCIENCE • X-RAY ABSORPTION FINE STRUCTURE, X-RAY ABSORPTION NEAR-EDGE STRUCTURE • 2.1-22.5 keV • ON-SITE, REMOTE, MAIL-IN • ACCEPTING GENERAL USERS

9-ID-B,C • XSD • CHEMISTRY, MATERIALS SCIENCE, LIFE SCIENCES • NANO-IMAGING, MICROFLUORESCENCE (HARD X-RAY), ULTRA-SMALL-ANGLE X-RAY SCATTERING, TOMOGRAPHY, PTYCHOGRAPHY • 4.5-30 keV • ON-SITE • ACCEPTING GENERAL USERS

10-BM-A,B • **MATERIALS RESEARCH (MR)-CAT** • MATERIALS SCIENCE, CHEMISTRY, ENVIRONMENTAL SCIENCE, PHYSICS • X-RAY ABSORPTION FINE STRUCTURE, TIME-RESOLVED X-RAY ABSORPTION FINE STRUCTURE, MICROFLUORESCENCE (HARD X-RAY) • 4-32 keV • ON-SITE, REMOTE, MAIL-IN, OBSERVER, BEAMLINE SUPPORT • ACCEPTING GENERAL USERS

10-ID-B • MR-CAT • MATERIALS SCIENCE, ENVIRONMENTAL SCIENCE, CHEMISTRY, PHYSICS • X-RAY ABSORPTION FINE STRUCTURE, TIME-RESOLVED X-RAY ABSORPTION FINE STRUCTURE, MICROFLUORESCENCE (HARD X-RAY), X-RAY PHOTOEMISSION SPECTROSCOPY, X-RAY EMISSION SPECTROSCOPY • 4.8-32 keV, 15-65 keV, 15-65 keV • ON-SITE, REMOTE, MAIL-IN, OBSERVER, BEAMLINE SUPPORT • ACCEPTING GENERAL USERS

11-BM-B • XSD • CHEMISTRY, MATERIALS SCIENCE, PHYSICS • POWDER DIFFRACTION • 15-33 keV • ON-SITE, REMOTE, MAIL-IN • ACCEPTING GENERAL USERS

11-ID-B • XSD • CHEMISTRY, ENVIRONMENTAL SCIENCE, MATERIALS SCIENCE • PAIR DISTRIBUTION FUNCTION, HIGH-ENERGY X-RAY DIFFRACTION • 58.66 keV, 86.7 keV • ON-SITE • ACCEPTING GENERAL USERS

11-ID-C • XSD • MATERIALS SCIENCE, CHEMISTRY, PHYSICS • HIGH-ENERGY X-RAY DIFFRACTION, DIFFUSE X-RAY SCATTERING, PAIR DISTRIBUTION FUNCTION • 105.6 keV • ON-SITE, REMOTE • ACCEPTING GENERAL USERS

11-ID-D • XSD • CHEMISTRY, ENVIRONMENTAL SCIENCE, MATERIALS SCIENCE • TIME-RESOLVED X-RAY ABSORPTION FINE STRUCTURE, TIME-RESOLVED X-RAY SCATTERING • 6-25 keV • ON-SITE, REMOTE, MAIL-IN • ACCEPTING GENERAL USERS

12-BM-B • XSD • MATERIALS SCIENCE, POLYMER SCIENCE, CHEMISTRY, PHYSICS, ENVIRONMENTAL SCIENCE • X-RAY ABSORPTION FINE STRUCTURE, SMALL-ANGLE X-RAY SCATTERING, WIDE-ANGLE X-RAY SCATTERING • 4.5-30 keV, 10-40 keV • ON-SITE, REMOTE, MAIL-IN • ACCEPTING GENERAL USERS

12-ID-B • XSD • CHEMISTRY, MATERIALS SCIENCE, LIFE SCIENCES, POLYMER SCIENCE, PHYSICS • SMALL-ANGLE X-RAY SCATTERING, GRAZING INCIDENCE SMALL-ANGLE SCATTERING, WIDE-ANGLE X-RAY SCATTERING, GRAZING INCIDENCE DIFFRACTION • 7.9-14 keV • ON-SITE, REMOTE • ACCEPTING GENERAL USERS

12-ID-C,D • XSD • CHEMISTRY, PHYSICS, MATERIALS SCIENCE • SMALL-ANGLE X-RAY SCATTERING, GRAZING INCIDENCE SMALL-ANGLE SCATTERING, WIDE-ANGLE X-RAY SCATTERING, SURFACE DIFFRACTION • 4.5-40 keV • ON-SITE • ACCEPTING GENERAL USERS

13-BM-C • **GeoSoilEnviro Center for Advanced Radiation Sources (GSECARS)** • GEOSCIENCE, ENVIRONMENTAL SCIENCE • SURFACE DIFFRACTION, HIGH-PRESSURE DIAMOND ANVIL CELL, SINGLE-CRYSTAL DIFFRACTION • 15-15 keV, 28.6-28.6 keV • ON-SITE • ACCEPTING GENERAL USERS

13-BM-D • GSECARS • GEOSCIENCE, ENVIRONMENTAL SCIENCE • TOMOGRAPHY, HIGH-PRESSURE DIAMOND ANVIL CELL, HIGH-PRESSURE MULTI-ANVIL PRESS • 4.5-100 keV • ON-SITE • ACCEPTING GENERAL USERS

13-ID-C,D • GSECARS • GEOSCIENCE, ENVIRONMENTAL SCIENCE • SURFACE DIFFRACTION, MICRODIFFRACTION, X-RAY STANDING WAVES, X-RAY ABSORPTION FINE STRUCTURE, RESONANT INELASTIC X-RAY SCATTERING, X-RAY EMISSION SPECTROSCOPY, HIGH-PRESSURE DIAMOND ANVIL CELL, HIGH-PRESSURE MULTI-ANVIL PRESS • 4.9-45 keV, 10-75 keV • ON-SITE • ACCEPTING GENERAL USERS

13-ID-E • GSECARS • GEOSCIENCE, ENVIRONMENTAL SCIENCE • MICROFLUORESCENCE (HARD X-RAY), MICRO X-RAY ABSORPTION FINE STRUCTURE, MICRODIFFRACTION, FLUORESCENCE SPECTROSCOPY • 2.4-28 keV, 5.4-28 keV • ON-SITE • ACCEPTING GENERAL USERS

14-BM-C • **BioCARS** • LIFE SCIENCES • MACROMOLECULAR CRYSTALLOGRAPHY, FIBER DIFFRACTION, BIOHAZARDS AT THE BSL2/3 LEVEL • 8-14.9 keV • ON-SITE, REMOTE, BEAMLINE SUPPORT • ACCEPTING GENERAL USERS

14-ID-B • **BioCARS** • LIFE SCIENCES • TIME-RESOLVED CRYSTALLOGRAPHY, TIME-RESOLVED X-RAY SCATTERING, LAUE CRYSTALLOGRAPHY, WIDE-ANGLE X-RAY SCATTERING, BIOHAZARDS AT THE BSL2/3 LEVEL, MACROMOLECULAR CRYSTALLOGRAPHY, SERIAL CRYSTALLOGRAPHY • 7-19 keV • ON SITE, REMOTE, BEAMLINE SUPPORT • ACCEPTING GENERAL USERS

15-ID-B,C,D • **ChemMatCARS** • MATERIALS SCIENCE, CHEMISTRY • RESONANT DIFFRACTION (DAFS)-SINGLE-CRYSTAL, HIGH-PRESSURE DIAMOND ANVIL CELL, PHOTO-CRYSTALLOGRAPHY, SINGLE-CRYSTAL DIFFRACTION, LIQUID INTERFACE SCATTERING, LIQUID INTERFACE SPECTROSCOPY, ANOMALOUS SMALL-ANGLE SCATTERING • 5.5-32 keV, 10-70 keV • ON-SITE • ACCEPTING GENERAL USERS

16-BM-B • **High Pressure (HP)CAT-XSD** • MATERIALS SCIENCE, GEOSCIENCE, CHEMISTRY, PHYSICS • WHITE LAUE SINGLE-CRYSTAL DIFFRACTION, ENERGY DISPERSIVE X-RAY DIFFRACTION, PHASE CONTRAST IMAGING, RADIOGRAPHY, PAIR DISTRIBUTION FUNCTION • 10-120 keV • REMOTE • ACCEPTING GENERAL USERS

16-BM-D • **HPCAT-XSD** • MATERIALS SCIENCE, GEOSCIENCE, CHEMISTRY, PHYSICS • POWDER ANGULAR DISPERSIVE X-RAY DIFFRACTION, SINGLE-CRYSTAL DIFFRACTION, X-RAY ABSORPTION NEAR-EDGE STRUCTURE, X-RAY ABSORPTION FINE STRUCTURE, TOMOGRAPHY • 6-45 keV • REMOTE • ACCEPTING GENERAL USERS

16-ID-B • **HPCAT-XSD** • MATERIALS SCIENCE, GEOSCIENCE, CHEMISTRY, PHYSICS • MICRODIFFRACTION, SINGLE-CRYSTAL DIFFRACTION • 18-50 keV • REMOTE • ACCEPTING GENERAL USERS

16-ID-D • **HPCAT-XSD** • MATERIALS SCIENCE, GEOSCIENCE, CHEMISTRY, PHYSICS • NUCLEAR RESONANT SCATTERING, INELASTIC X-RAY SCATTERING (1-eV RESOLUTION), X-RAY EMISSION SPECTROSCOPY • 5-37 keV, 14.41-14.42 keV • REMOTE • ACCEPTING GENERAL USERS

17-BM-B • **XSD** • CHEMISTRY, MATERIALS SCIENCE • POWDER DIFFRACTION, PAIR DISTRIBUTION FUNCTION • 27-51 keV • ON-SITE, REMOTE, MAIL-IN • ACCEPTING GENERAL USERS

17-ID-B • **INDUSTRIAL MACROMOLECULAR CRYSTALLOGRAPHY ASSOCIATION (IMCA)-CAT** • LIFE SCIENCES • MACROMOLECULAR CRYSTALLOGRAPHY, MULTI-WAVELENGTH ANOMALOUS DISPERSION, MICROBEAM, SINGLE-WAVELENGTH ANOMALOUS DISPERSION, LARGE UNIT CELL CRYSTALLOGRAPHY • SUBATOMIC (<0.85 Å) RESOLUTION • 6-20 keV • ON-SITE, REMOTE, MAIL-IN • ACCEPTING GENERAL USERS

18-ID-D • **Biophysics (Bio)-CAT** • LIFE SCIENCES • FIBER DIFFRACTION, MICRO-DIFFRACTION, SMALL-ANGLE X-RAY SCATTERING, TIME-RESOLVED X-RAY SCATTERING • 3.5-35 keV • ON-SITE, REMOTE, MAIL-IN • ACCEPTING GENERAL USERS

19-BM-D • **STRUCTURAL BIOLOGY CENTER (SBC)-XSD** • LIFE SCIENCES • MULTI-WAVELENGTH ANOMALOUS DISPERSION, MACROMOLECULAR CRYSTALLOGRAPHY, SINGLE-WAVELENGTH ANOMALOUS DISPERSION • 6-18.5 keV • REMOTE, ON-SITE, MAIL-IN • ACCEPTING GENERAL USERS

19-ID-D • **SBC-XSD** • LIFE SCIENCES • MACROMOLECULAR CRYSTALLOGRAPHY, MULTI-WAVELENGTH ANOMALOUS DISPERSION, SUBATOMIC (<0.85 Å) RESOLUTION, LARGE UNIT CELL CRYSTALLOGRAPHY, SINGLE-WAVELENGTH ANOMALOUS DISPERSION, SERIAL CRYSTALLOGRAPHY • 6-19 keV • ON-SITE, REMOTE, MAIL-IN • ACCEPTING GENERAL USERS

20-BM-B • **XSD** • MATERIALS SCIENCE, ENVIRONMENTAL SCIENCE, CHEMISTRY • X-RAY ABSORPTION FINE STRUCTURE, MICROFLUORESCENCE (HARD X-RAY) • 2.7-32 keV, 2.7-35 keV • ON-SITE, REMOTE, MAIL-IN • ACCEPTING GENERAL USERS

20-ID-B,C • **XSD** • MATERIALS SCIENCE, ENVIRONMENTAL SCIENCE, CHEMISTRY • X-RAY ABSORPTION FINE STRUCTURE, X-RAY RAMAN SCATTERING, MICRO X-RAY ABSORPTION FINE STRUCTURE, MICROFLUORESCENCE (HARD X-RAY), X-RAY EMISSION SPECTROSCOPY • 4.3-27 keV, 7-52 keV • ON-SITE, REMOTE, MAIL-IN • ACCEPTING GENERAL USERS

21-ID-D • **LIFE SCIENCES (LS)-CAT** • LIFE SCIENCES • MACROMOLECULAR CRYSTALLOGRAPHY • 6.5-20 keV • ON-SITE, REMOTE, MAIL-IN • ACCEPTING GENERAL USERS

21-ID-F • **LS-CAT** • LIFE SCIENCES • MACROMOLECULAR CRYSTALLOGRAPHY • 12.7 keV • REMOTE, ON-SITE, MAIL-IN • ACCEPTING GENERAL USERS

21-ID-G • **LS-CAT** • LIFE SCIENCES • MACROMOLECULAR CRYSTALLOGRAPHY • 12.7 keV • REMOTE, ON-SITE, MAIL-IN • ACCEPTING GENERAL USERS

22-BM-D • **SOUTHEAST REGIONAL (SER)-CAT** • LIFE SCIENCES • MACROMOLECULAR CRYSTALLOGRAPHY, SINGLE-WAVELENGTH ANOMALOUS DISPERSION, MULTI-WAVELENGTH ANOMALOUS DISPERSION • 8-16 keV • ON-SITE, REMOTE • ACCEPTING GENERAL USERS

22-ID-D • **SER-CAT** • LIFE SCIENCES • MACROMOLECULAR CRYSTALLOGRAPHY, MULTI-WAVELENGTH ANOMALOUS DISPERSION, SINGLE-WAVELENGTH ANOMALOUS DISPERSION, MICROBEAM • 6-16 keV • ON-SITE, REMOTE • ACCEPTING GENERAL USERS

23-ID-B • **NATIONAL INSTITUTE OF GENERAL MEDICAL SCIENCES AND NATIONAL CANCER INSTITUTE (GM/CA)-XSD** • LIFE SCIENCES • MACROMOLECULAR CRYSTALLOGRAPHY, MICROBEAM, LARGE UNIT CELL CRYSTALLOGRAPHY, SUBATOMIC (<0.85 Å) RESOLUTION, MULTI-WAVELENGTH ANOMALOUS DISPERSION, SINGLE-WAVELENGTH ANOMALOUS DISPERSION • 3.5-20 keV • ON-SITE, REMOTE • ACCEPTING GENERAL USERS

23-ID-D • **GM/CA-XSD** • LIFE SCIENCES • MACROMOLECULAR CRYSTALLOGRAPHY, MICROBEAM, LARGE UNIT CELL CRYSTALLOGRAPHY, SUBATOMIC (<0.85 Å) RESOLUTION, MULTI-WAVELENGTH ANOMALOUS DISPERSION, SINGLE-WAVELENGTH ANOMALOUS DISPERSION, SERIAL CRYSTALLOGRAPHY • 11-13.5 keV • ON-SITE, REMOTE • ACCEPTING GENERAL USERS

24-ID-C • **NORTHEASTERN (NE)-CAT** • LIFE SCIENCES • MACROMOLECULAR CRYSTALLOGRAPHY, MICRODIFFRACTION, SINGLE-WAVELENGTH ANOMALOUS DISPERSION, SINGLE-CRYSTAL DIFFRACTION, MICROBEAM, MULTI-WAVELENGTH ANOMALOUS DISPERSION, SUBATOMIC (<0.85 Å) RESOLUTION • 6.5-20 keV • ON-SITE, REMOTE • ACCEPTING GENERAL USERS

24-ID-E • **NE-CAT** • LIFE SCIENCES • MACROMOLECULAR CRYSTALLOGRAPHY, MICROBEAM, MICRODIFFRACTION, SINGLE-WAVELENGTH ANOMALOUS DISPERSION, SINGLE-CRYSTAL DIFFRACTION • 12.68 keV • ON-SITE, REMOTE • ACCEPTING GENERAL USERS

26-ID-C • **CENTER FOR NANOSCALE MATERIALS (CNM)/XSD** • PHYSICS, MATERIALS SCIENCE • NANODIFFRACTION, NANO-IMAGING, COHERENT X-RAY SCATTERING, SYNCHROTRON X-RAY SCANNING TUNNELING MICROSCOPY • 7-12 keV • ON-SITE • ACCEPTING GENERAL USERS

27-ID-B • **XSD** • PHYSICS, MATERIALS SCIENCE, CHEMISTRY • RESONANT INELASTIC X-RAY SCATTERING • 5-14 keV • ON-SITE • ACCEPTING GENERAL USERS

29-ID-C,D • **XSD** • PHYSICS, MATERIALS SCIENCE • RESONANT SOFT X-RAY SCATTERING, ANGLE-RESOLVED PHOTOEMISSION SPECTROSCOPY • 250-2200 eV, 2200-3000 eV • REMOTE, MAIL-IN • ACCEPTING GENERAL USERS

30-ID-B,C • **XSD** • PHYSICS, MATERIALS SCIENCE, GEOSCIENCE, LIFE SCIENCES • INELASTIC X-RAY SCATTERING, NUCLEAR RESONANT SCATTERING • 23.7-23.9 keV • ON-SITE • ACCEPTING GENERAL USERS

31-ID-D • **LILY RESEARCH LABORATORIES (LRL)-CAT** • LIFE SCIENCES • MACROMOLECULAR CRYSTALLOGRAPHY, SINGLE-WAVELENGTH ANOMALOUS DISPERSION • 5-22 keV • MAIL-IN • ACCEPTING GENERAL USERS

32-ID-B,C • **XSD** • MATERIALS SCIENCE, LIFE SCIENCES, GEOSCIENCE • PHASE CONTRAST IMAGING, RADIOGRAPHY, TRANSMISSION X-RAY MICROSCOPY, TOMOGRAPHY • 7-40 keV • ON-SITE • ACCEPTING GENERAL USERS

33-BM-C • **XSD** • MATERIALS SCIENCE, PHYSICS, CHEMISTRY • DIFFUSE X-RAY SCATTERING, GENERAL DIFFRACTION, POWDER DIFFRACTION, X-RAY REFLECTIVITY, GRAZING INCIDENCE DIFFRACTION, ANOMALOUS AND RESONANT SCATTERING (HARD X-RAY) • 5-35 keV • ON-SITE • ACCEPTING GENERAL USERS

33-ID-D,E • **XSD** • MATERIALS SCIENCE, PHYSICS, CHEMISTRY, ENVIRONMENTAL SCIENCE • ANOMALOUS AND RESONANT SCATTERING (HARD X-RAY), DIFFUSE X-RAY SCATTERING, GENERAL DIFFRACTION, SURFACE DIFFRACTION, SURFACE DIFFRACTION (UHV), X-RAY REFLECTIVITY • 5-30 keV • ON-SITE • ACCEPTING GENERAL USERS

34-ID-C • **XSD** • MATERIALS SCIENCE, PHYSICS • COHERENT X-RAY SCATTERING • 5-15 keV • ON-SITE, REMOTE • ACCEPTING GENERAL USERS

34-ID-E • **XSD** • MATERIALS SCIENCE, PHYSICS, ENVIRONMENTAL SCIENCE, GEOSCIENCE • MICRODIFFRACTION, LAUE CRYSTALLOGRAPHY, MICROBEAM, MICROFLUORESCENCE (HARD X-RAY) • 7-30 keV • ON-SITE • ACCEPTING GENERAL USERS

35-ID-B,C,D,E • **DYNAMIC COMPRESSION SECTOR (DCS)** • PHYSICS, MATERIALS SCIENCE, GEOSCIENCE • TIME-RESOLVED X-RAY SCATTERING, PHASE CONTRAST IMAGING, RADIOGRAPHY • 7-35 keV, 7-100 keV, 24-24 keV • ON-SITE, REMOTE • ACCEPTING GENERAL USERS

Double-Safe in the Time of the Pandemic

Safety in an environment like the one found at the Advanced Photon Source (APS) in the Argonne National Laboratory Photon Sciences Directorate (PSC) is an exacting science in the best of times. Mix in a pandemic such as the one we're living through now and the degree of difficulty skyrockets.

X-ray light source research facilities such as the APS are among the most complex technical machines in the world. As complexity increases, safety risks scale accordingly. The safety experts assigned to PSC from the Argonne Environment, Safety, Health & Quality Directorate are tasked with keeping staff, visiting researchers, and visitors of any kind safe from potential electrical, mechanical, chemical, and radiological hazards, not to mention those old standbys: slips, trips, and falls, in good weather and bad. (There is the occasional hazardous biological sample studied at the APS; they are tightly regulated and monitored from shipment to receipt to study in a special Biohazard Level 2/3 enclosure to return shipment. These PSC safety folks have the responsibility for those materials while they are on site.)

The safety team at the APS comprises six safety professionals:

- **Paul Rossi**, PSC Safety Manager (which doesn't begin to describe the number of ESH roles he fills across PSC);
- **Elroy Chang**, ESH Coordinator for the APS user (researcher) program, Deployed ESH Coordinator for the PSC Engineering Support Division (AES) and Accelerator Systems Division (ASD), and specialized roles from environmental compliance through quality assurance;
- **Tiffany Freedman**, ESH Coordinator and Environmental Compliance Representative for PSC and the APS Upgrade Project;
- **Mike Fries**, ESH Coordinator for the PSC X-ray Science Division plus myriad other ESH roles at PSC;
- **Cassandra Hayden**, ESH Coordinator for AES and Deployed ESH Coordinator for ASD, among several other areas of ESH responsibility across PSC; and
- **Jeff McGhee**, ESH Coordinator for PSC with overall safety responsibility for the APS Upgrade Project and a number of other ESH roles requiring Expert or Competent Person qualifications.

These six dedicated people are responsible for assuring that environmental safeguards are followed, and for the safety of over 500 PSC employees, including a growing contingent working on the APS Upgrade Project; the more than 5,000 researchers who come to the APS in a normal (non-COVID) year; and the various outside contractors who carry out work on the APS physical plant.

Now add a global COVID pandemic. Even though Argonne and the APS have been in Limited Operations since June 15, 2020, and user research at the APS has been restricted primarily to mail-in and remote access with some exceptions, there is still a necessary number of APS personnel on-site at any given time. The PSC safety contingent has been responsible for assuring that all on-site workers follow strict and detailed COVID safety measures, and they have consulted with other Argonne safety professionals in developing those unique protocols.

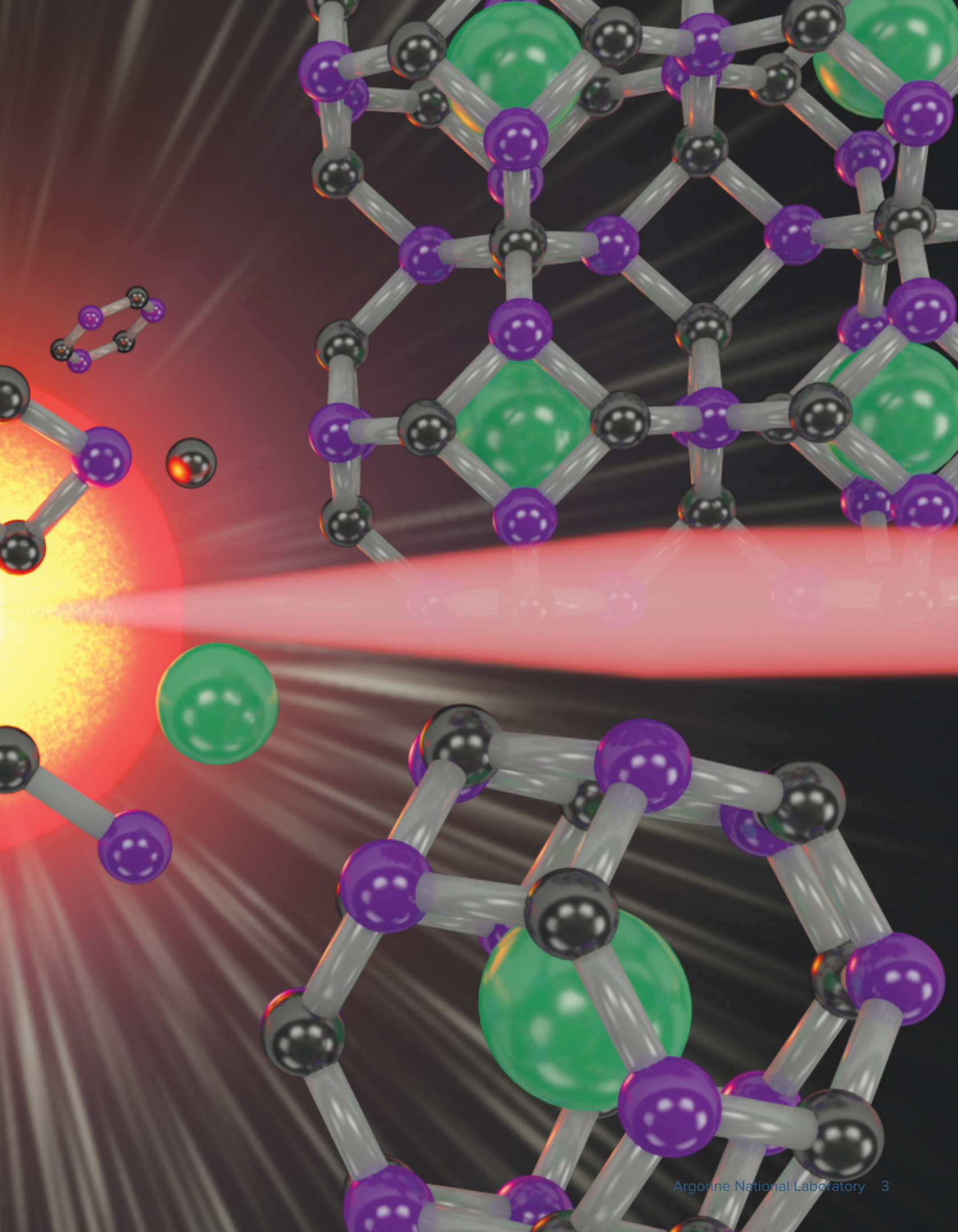
"Safety considerations are the first and primary ingredient in everything we do at the APS," said Stephen Streiffer, Deputy Laboratory Director for Science & Technology and Interim Associate Laboratory Director for PSC. "The tireless efforts of these extraordinary people make it possible for us to go about our jobs knowing that by paying close attention to what they tell us, we can carry out our mission safely."

Meet the ESHQ/PSC safety team on pages 44, 54, 68, 78, 118, and 128 :

Engineering Materials and Applications

Caging a New Class of Carbon-Boron Clathrates

Carbon's unparalleled ability to form complex stable molecules with many other atoms makes it perhaps the most versatile element in the universe. Not only is it the basis for all life as we know it, but its various forms and compounds comprise a nearly endless wealth of materials indispensable for human civilization in everything from pencils and diamond rings to battery electrodes and advanced nanomaterials. The specific properties of carbon-based materials depend on the types of bonds carbon atoms make, whether the two-dimensional sp^2 bonds in a soft and brittle material such as graphite or the three-dimensional sp^3 type in the incredibly hard and resistant structure of diamond. While two-dimensional carbon structures can be readily synthesized, creating three-dimensional structures featuring the sp^3 bonding of diamond has remained a challenge for more than 50 years. Now, a team of researchers has finally succeeded by constructing an extended cage structure of both carbon and boron enclosing guest atoms of strontium. This new class of clathrate materials, featuring the strength of diamond with tunable electronic properties for different applications, appears to finally realize the decades-long potential speculated for sp^3 -bonded carbon materials. Their work and the supporting studies were carried out at the APS. *"Caging" cont'd. on page 6*



Printing Ultrathin 2-D Polymer Electronics

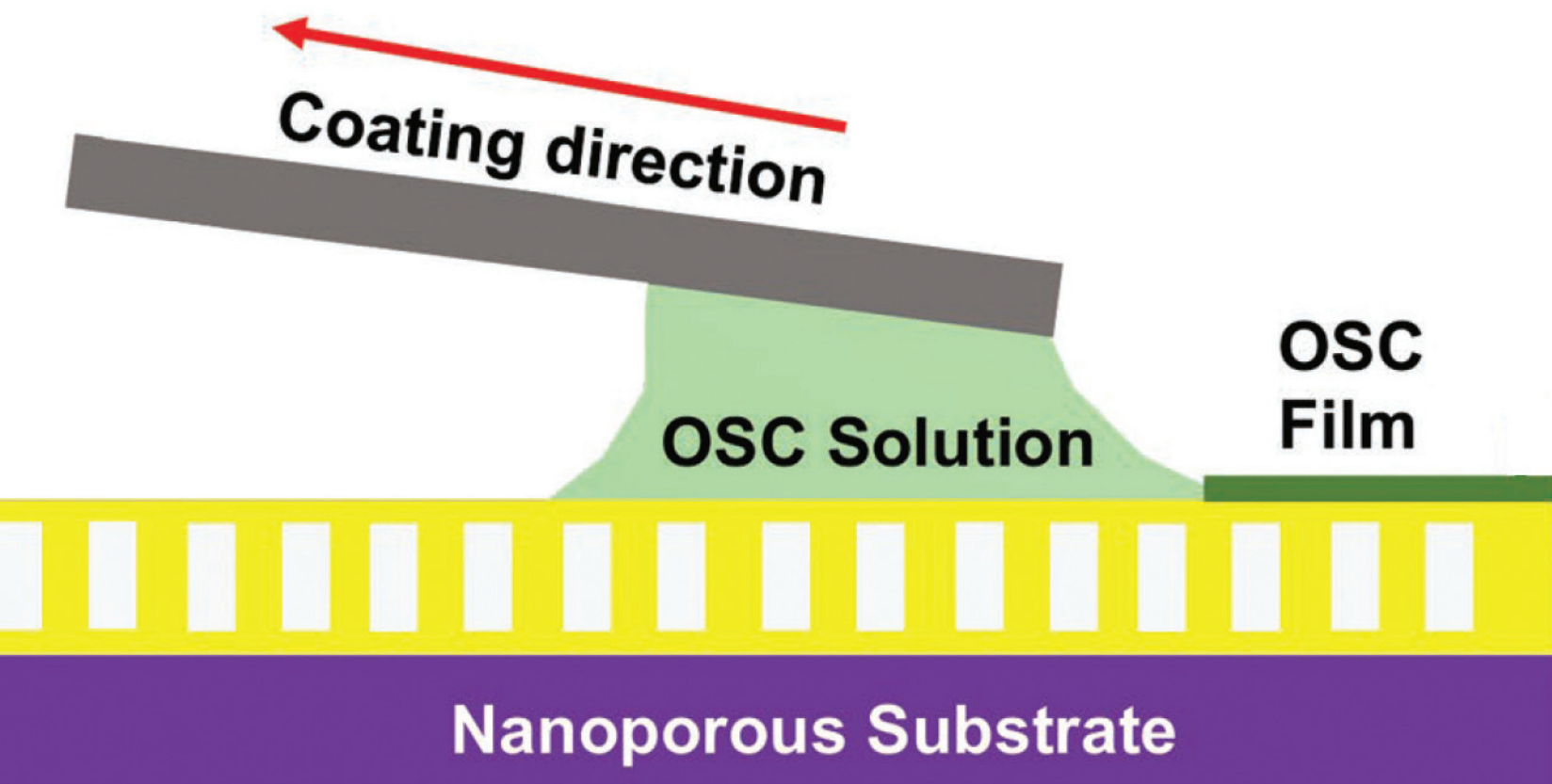


Fig. 1. Schematic of the meniscus-guided coating (MGC) technique. At top is the coating blade represented by a thin, flat gray bar. As the blade moves to the left (red arrow) it pulls along the liquid organic semiconductor (OSC) shown in light green. The OSC is a type of conjugated polymer. A solid thin film of polymer (dark green) forms from this motion. The dynamic-template technique guides the process, and consists of an ionic liquid (yellow) adhering to a nanoporous substrate. From P. Kafle et al., "Printing 2D Conjugated Polymer Monolayers and Their Distinct Electronic Properties," *Adv. Funct. Mater.* **30**, 1909787 (2020). © 2020 WILEY-VCH Verlag GmbH & Co. KGaA, Weinheim

Ultrathin films of electronic materials have been shown to exhibit remarkable physical properties. Some of these ultrathin films, known as monolayers, are only a single molecular layer thick. While such exceedingly thin films can be formed from a variety of layered compounds, it has proven difficult to coax organic polymers to reliably form highly-ordered, ultrathin sheets. Scientists would like to develop such polymer films because they consist of inexpensive and environmentally-friendly ingredients, are flexible, and their properties depend on their ordering, making them tunable. A team of researchers has now demonstrated a simple printing process that consistently yields high-quality ultrathin polymer films, with thicknesses ranging from several molecular layers down to monolayers, or about one ten-thousandth the diameter of a human hair. Controlling film thickness allowed the team to vary the film's properties. Moreover, the researchers successfully printed ultrathin films from different polymers, and transferred them to different substrates. The polymer chains in the ultrathin films were characterized using high-brightness x-rays at the APS. The relatively simple techniques demonstrated by the researchers may lead to the mass production of inexpensive, ultrathin polymer films down to monolayer thickness, with potential applications including photovoltaics, sensors, and wearable electronics.

Plastic consists of polymers, long chain molecules made up of many smaller, identical molecular units. Conjugated polymers, which played a key role in this study, are organic (carbon-based) polymers featuring a long molecular backbone with alternating single and double chemical bonds, a structure that allows these polymers to conduct charge, unlike most plastic materials, which are insulating. Conjugated polymers are known as organic (carbon-based) semiconductors (OSCs) because they have properties similar to silicon, and can also form the basis for transistors and other electronic devices. Previous studies have demonstrated the considerable potential of monolayer films of conjugated polymers, with unique optoelectronic and outstanding sensing properties. In spite of this considerable potential, efforts to develop a reliable and cost-effective technique for producing such monolayers have proven elusive. For instance, some fabrication methods yield monolayers composed of networks of one-dimensional polymer fibers instead of a truly uniform, two-dimensional (2-D) film.

The scientists conducting this study, from the University of Illinois at Urbana-Champaign, overcame these shortcomings and produced highly-ordered 2-D monolayers of conjugated polymers on various substrates. The first challenge involved selecting a method to rapidly lay down polymers over a large area. The team developed the meniscus-guided coating (MGC) method, which facilitates controlled deposition of polymers and provides direction-

ality for their ordering. The MGC technique is illustrated in Fig. 1. A liquid infused with conjugated polymers is sandwiched between a substrate and a coating blade. The liquid adheres to both surfaces, which are placed fractions of a millimeter apart. As the coating blade moves it drags the liquid over the substrate. As the film dries it leaves behind a sheet of conjugated polymers. Changing the blade's speed, its distance from the substrate, and the concentration of the solution varied the film's thickness, which in turn changed its structure and properties.

The other key technology is dynamic-template. It involves infusing a special ionic liquid (IL) into a substrate riddled with nanoscale voids (bottom of Fig. 1). The strong interaction between the polymer and the IL, along with the dynamic nature of the liquid surface, helped crystallize highly-ordered 2-D monolayer films. Another advantage of dynamic-template is the wide range of substrates that can be used for film transfer, including rigid and flexible materials.

Several ultrathin films were produced using two different conjugated polymers, abbreviated DPP2T-TT and PII-2T. Combining the dynamic-template and MGC techniques, the researchers created ultrathin films with varying thicknesses. These films were later transferred from the nanoporous substrate to both rigid and flexible substrates, thus illustrating the utility of the new approach. For comparison purposes, an ultrathin film formed on a static sub-

“Printing” cont’d. on page 7

“Caging” cont’d. from page 2

Fig. 1. The bipartite sodalite-type clathrate structure, which consists of truncated octahedral host cages that trap strontium guest atoms, was synthesized under high-pressure and high-temperature conditions using a laser heating technique at the APS.

One promising candidate for a three-dimensional carbon structure is a clathrate, in which a “cage” composed of host atoms encloses “guest” atoms of another element (Fig. 1). Such compounds have been identified or synthesized with many other elements. According to theoretical predictions and computer models, carbon-based clathrates could form highly useful materials that are not only lightweight and extremely strong but featuring properties that could be custom-tuned according to the type of guest atoms. A problem with the synthesis of clathrate structures composed solely of carbon atoms is that such sp^3 -bonded frameworks are thermodynamically unstable. To overcome this difficulty, the experimenters decided to examine a system incorporating boron atoms. An extensive search of predicted Sr-B-C structures revealed several promising candidates that could be stable at various pressures and temperatures.

The team of researchers from the Carnegie Institution for Science, the Warsaw University of Technology (Poland), The University of Chicago, the U.S. Naval Research Laboratory, the Ludwig Maximilians Universität (Germany), and University College London (UK) settled on a ternary compound with a composition of $2Sr@B_6C_6$ (SrB_3C_3), which is a type VII clathrate structure with a framework featuring 6 4-sided faces and 8 6-sided faces. Density functional theory calculations predicted this compound to remain stable from 50 GPa to at least 200 GPa at 0 K, far greater than a pure carbon version.

Samples of the SrB_3C_3 compound were synthesized and studied by a variety of techniques, including diamond anvil and x-ray diffraction experiments carried out with colleagues from the HPCAT-XSD 16-ID x-ray beamline and the GSECARS 13-ID beamline, both at the APS. The suite of experimental techniques was rounded out with scanning electron microscopy. Taken together, this provided good detail on the structure and properties of the compound and confirmed the theoretical predictions.

Due to the covalent sp^3 bonds of the carbon-boron framework, the SrB_3C_3 clathrate combines a light weight with great strength and resistance to pressure similar to diamond, while the strontium guest atoms give it metallic properties that make it an excellent electrical conductor.

The researchers note that encasing different elements within the clathrate structure would allow the compound to exhibit other properties. For example, the electronic band structure of the SrB_3C_3 clathrate makes it an excellent candidate for showing high-temperature superconductivity.

Although the SrB_3C_3 structure synthesized in these experiments is stable only at high pressure in an inert environment and degrades in several hours under ambient conditions, the research team is confident that this work will open fresh prospects for the discovery of similar compounds. Multiple possibilities remain to be explored with the substitution of atoms both in the clathrate framework and the guest atoms. The investigators also note that the concept of stabilizing carbon frameworks using boron could be extended to wholly different types of structures.

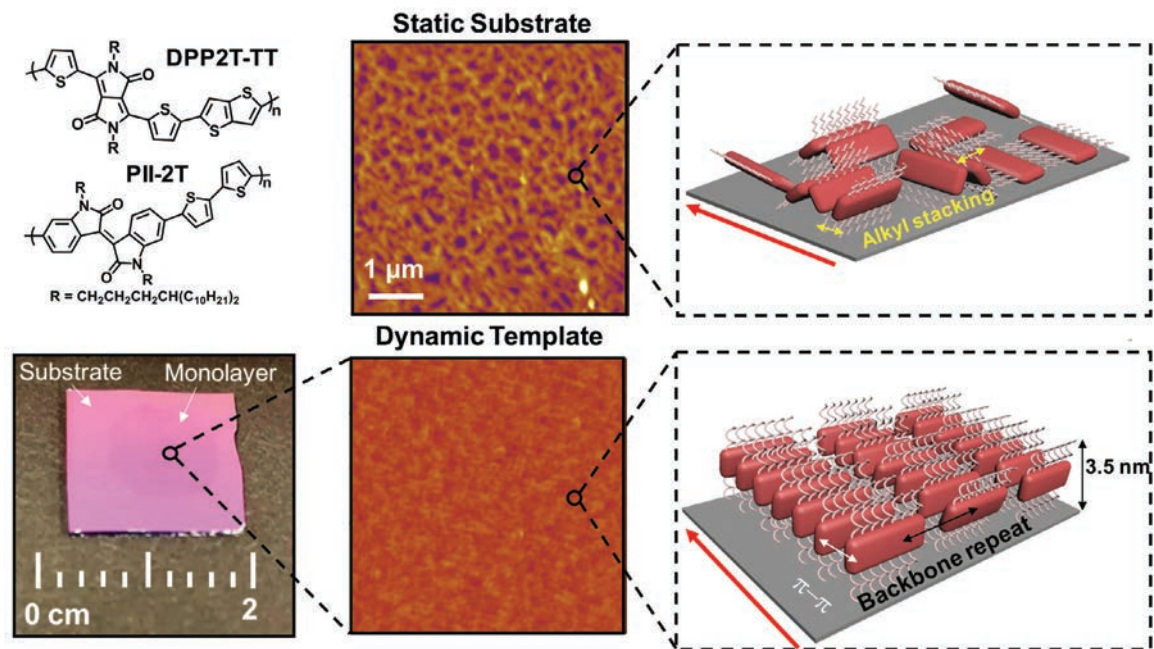
– Mark Wolverton

See: Li Zhu¹, Gustav M. Borstad^{1†}, Hanyu Liu^{1††}, Piotr A. Guřka^{1,2}, Michael Guerette¹, Juli-Anna Dolyniuk¹, Yue Meng^{1†††}, Eran Greenberg³, Vitali B. Prakapenka³, Brian L. Chaloux⁴, Albert Epshteyn⁴, Ronald E. Cohen^{1,5,6}, and Timothy A. Strobel¹, “Carbon-boron clathrates as a new class of sp^3 -bonded framework materials,” *Sci. Adv.* **6**, eaay8361 (10 January 2020).

DOI: 10.1126/sciadv.aay8361

Author affiliations: ¹Carnegie Institution for Science, ²Warsaw University of Technology, ³The University of Chicago, ⁴U.S. Naval Research Laboratory, ⁵Ludwig Maximilians Universität, ⁶University College London Present addresses: [†]University of Memphis, ^{††}Jilin University, ^{†††}Argonne National Laboratory Correspondence: * tstrobel@carnegiescience.edu

This work was supported by the Defense Advanced Research Projects Agency (DARPA) under grant no. W31P4Q1310005. Additional support was provided by the Energy Frontier Research in Extreme Environments (EFREE) Center, an Energy Frontier Research Center funded by the U.S. Department of Energy (DOE) Office of Science under award no. DE-SC0001057. P.A.G. thanks the Polish National Agency for Academic Exchange and the Warsaw University of Technology for financial support. R.E.C. was also supported by the European Research Council Advanced Grant ToMCoT. HPCAT-XSD operations are supported by the U.S. DOE National Nuclear Security Administration Office of Experimental Sciences. GeoSoilEnviroCARS is supported by the National Science Foundation-Earth Sciences (EAR-1634415) and DOE-GeoSciences (DE-FG02-94ER14466). This research used resources of the Advanced Photon Source, a U.S. DOE Office of Science User Facility operated for the DOE Office of Science by Argonne National Laboratory under Contract No. DE-AC02-06CH11357.



strate did not incorporate an ionic liquid or nanoporous substrate. The structures of all the ultrathin films were characterized by grazing incidence x-ray diffraction at APS beamline 8-ID-E, which is operated by the XSD Dynamics & Structure Group. The sensitivity of the technique is sufficient to detect crystallinity in even the thinnest films studied, and the versatility of the sample environment allowed the scientists to observe how the structure differed parallel and perpendicular to the MGC printing direction.

Figure 2 compares a monolayer film deposited on a static substrate with a monolayer film produced using the dynamic-template-assisted MGC approach. The static substrate film (upper half of Fig. 2) is riddled with voids that lead to poor conduction. By contrast, the dynamic-template film (lower half) appears smooth with a highly-ordered polymer structure and enhanced charge transport properties.

These results provide new insights into the morphological, electronic, and sensing performance of ultrathin conjugated polymer films, especially how these properties vary with thickness. A practical spin-off was also demonstrated. A 7-nm-thick film showed an ultrahigh sensitivity to gaseous ammonia, at a concentration of only one part per billion. The researchers speculate that such ultrathin films could serve as inexpensive, disposable ammonia detectors for spotting the early stages of kidney failure, when ammonia occurs in patients' breath. – Philip Koth

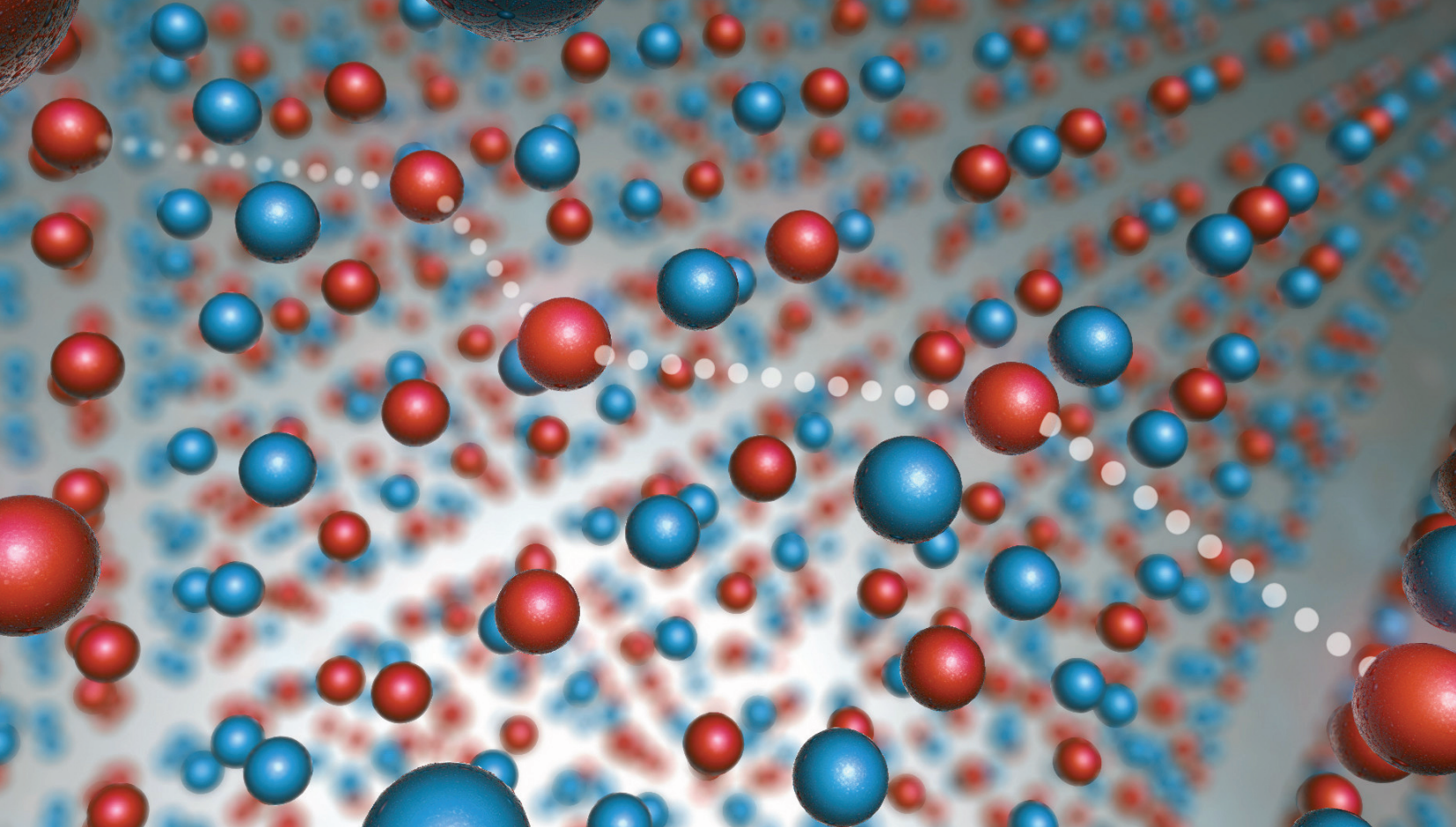
See: Prapti Kafle, Fengjiao Zhang, Noah B. Schorr, Kai-Yu

Fig. 2. Comparison of ultrathin polymer films formed on a static substrate, which is the conventional approach, and the dynamic template technique utilized for this study. Upper left corner shows the molecular structure of the two polymers, DPP2T-TT and PII-2T, used to form ultrathin films in the study. Two images of DPP2T-TT ultrathin films appear in the middle. The film created on the static substrate shows fiber-network-like morphology. In contrast, the film produced on the dynamic template exhibits continuous, void-less morphology with highly-ordered polymer chains. Illustrations at far right depict each film's structure based upon GIXD data.

Huang, Joaquín Rodríguez-López, and Ying Diao*, "Printing 2D Conjugated Polymer Monolayers and Their Distinct Electronic Properties," *Adv. Funct. Mater.* **30**, 1909787 (2020). DOI: 10.1002/adfm.201909787

Author affiliation: University of Illinois at Urbana-Champaign
Correspondence: * yingdiao@illinois.edu

This research was primarily supported by the National Science Foundation (NSF) Materials Research Science and Engineering Centers: Illinois Materials Research Center under grant number DMR 17-20633. P.K. acknowledges partial support from American Association of University Women (AAUW) International fellowship. Y.D. and K.-Y. H. were partially supported by NSF CAREER award under grant number NSF DMR 18-47828. Y.D. acknowledges partial support from the JITRI International Fellowship. The authors are grateful to beamline scientist Joseph Strzalka of the APS for facilitating the grazing incidence x-ray diffraction measurements. This research used the resources of the Advanced Photon Source, a U.S. Department of Energy (DOE) Office of Science User Facility operated for the DOE Office of Science by the Argonne National Laboratory under contract no. DE-AC02-06CH11357.



Obstacles to Sodium-Ion Battery Performance: When Too Much Order is a Bad Thing

A basic principle of rechargeable batteries is the reversible shuttling of ions (electrically-charged atoms or molecules) between their cathode and anode. The most popular rechargeable battery type is the lithium-ion (Li-ion) battery, which began development in the 1970s. Around the same time the sodium-ion (Na-ion) battery was also investigated, but the lithium type eventually prevailed. Interest in sodium-ion batteries has recently reemerged since they are cheaper, safer, and less reliant on strategically-important elements than are Li-ion batteries. The performance of both battery types is affected by how efficiently lithium (or sodium) ions move into and out of the positively-charged cathode during charging and discharging. To gain greater insight into this process, researchers probed sodium ions packed into a layered vanadium oxide compound to observe their short-range ordering, a domain that has proven difficult to examine. Short-range ion order was observed at different temperatures using diffuse x-ray scattering performed at the APS, complimented by measurements at the Cornell University's Cornell High Energy Synchrotron Source (CHESS) facility. The pioneering x-ray methods developed by this research team could lead to new strategies for improving rechargeable battery performance. More generally, these x-ray techniques offer an entirely new avenue for studying structural order in crystalline compounds.

The cathode of a Na-ion battery is packed with numerous microscopic layers. When the battery is powering a device (discharging), sodium ions travel from the battery's anode to its cathode, where the ions migrate into the cathode's layers in a process called intercalation. Previous research had shown that a highly-ordered ion arrangement within a cathode's layers makes it harder for the ions to quickly move in and out, reducing battery performance.

X-ray diffraction has been extensively used to study long-range ionic order in cathodes. Standard x-ray diffraction, also known as Bragg diffraction, involves bouncing an x-ray beam off a crystalline compound at a range of angles. Sharp peaks in the resulting Bragg patterns are then used to deduce the crystal's structure. While the analysis of Bragg peaks is good at determining long-range crystalline order, it is poor at detecting short-range order. This is a major shortcoming since overall performance depends upon optimizing both long-range and short-range ionic order in cathodes. To reveal short-range ionic order the researchers in this study from Argonne National Laboratory turned to the diffuse x-ray scattering technique, which requires detailed measurements of the scattering intensity between the Bragg peaks.

Diffuse scattering arises from distortions in a crystal's lattice, such as lattice vacancies or misaligned atoms. As the name implies, diffuse scattering involves x-rays scattered over a continuous distribution of angles, which seem haphazard in comparison to the orderly reflections associated with Bragg diffraction. In comparing the two phenomena, Bragg diffraction excels at revealing the overall lattice structure of a crystalline material while diffuse scattering reveals its atomic arrangements over spans as little as a nanometer.

In spite of its unique value for revealing short-range order, exploiting the potential of diffuse scattering has always been challenging. Several recent developments, however, enabled the research team to successfully generate data of unprecedented quality. First, by employing high-energy synchrotron x-rays together with improved fast area x-ray detectors at the XSD Magnetic Materials

< Fig. 1. Illustration of ion ordering within a layered vanadium oxide (V_2O_5) crystal. Diffuse x-ray scattering revealed an ordered pattern of sodium ions (red spheres) among vacant sites (blue spheres). The white dotted lines emphasize how the ions zig-zag between the vacancies. Revealing the degree of ion ordering in layered materials is important for improving lithium-ion and sodium-ion battery performance.

Group's 6-ID-D beamline at the APS and at the CHESS A2 beamline, sufficient experimental data could be gathered in a reasonable time (20 min). Additionally, the researchers developed the algorithms necessary to interpret the diffuse scattering data as probability maps indicating different ionic locations. Finally, they obtained the computer resources necessary to perform the complex computations required to process the large amount of diffuse scattering data generated by the experiments.

Armed with these tools, the research team probed a single crystal of vanadium oxide (V_2O_5) that was partially filled (intercalated) with sodium ions. The same approach could also be applied to lithium ions. Since ion ordering within a real-world cathode is temperature-dependent, diffuse scattering measurements were obtained at temperatures ranging from room temperature to nearly absolute zero. The diffuse scattering data demonstrated that the short-range ion order followed a zig-zag configuration (Fig. 1). Lowering the temperature extended the range of ion ordering, until eventually the sodium ions were frozen and unable to diffuse through the crystal.

Revealing the short-range order of ions in layered materials is critical to developing strategies to disrupt that order and increase ionic mobility. Hopefully such strategies can be applied to actual lithium-ion and sodium-ion cathodes for improved battery performance. Beyond layered materials, the diffuse scattering techniques demonstrated in this research can also be used to investigate a large variety of disordered crystalline compounds. – Philip Koth

See: Matthew J. Krogstad¹, Stephan Rosenkranz¹, Justin M. Wozniak¹, Guy Jennings¹, Jacob P. C. Ruff², John T. Vaughey¹, and Raymond Osborn^{1*}, "Reciprocal space imaging of ionic correlations in intercalation compounds," *Nat. Mater.* **19**, 63 (January 2020). DOI: 10.1038/s41563-019-0500-7

Author affiliations: ¹Argonne National Laboratory, ²Cornell University

Correspondence: * ROsborn@anl.gov

This work was supported by the U.S. Department of Energy (DOE) Office of Science-Basic Energy Sciences, Materials Sciences and Engineering Division and Scientific User Facilities Division. CHESS is supported by the National Science Foundation (NSF) and National Institutes of Health/National Institute of General Medical Sciences via NSF award DMR-1332208. Computational developments were supported by the Exascale Computing Project (17-SC-20-SC), a collaborative effort of the U.S. DOE Office of Science, and the National Nuclear Security Administration. We thank D. Robinson and X. Zhang for technical support during the experiments. This research used resources of the Advanced Photon Source, a U.S. DOE Office of Science User Facility operated for the DOE Office of Science by Argonne National Laboratory under Contract No. DE-AC02-06CH11357.

For Lithium-Ion Cathodes, Partial Order Up

Given the unending interest in portable electronics of all kinds, there's been an upsurge in research on high-energy-density cathode materials for rechargeable lithium-ion (L-ion) batteries. State-of-the-art layered $\text{Li}(\text{Ni},\text{Mn},\text{Co})\text{O}_2$ cathode materials provide good energy and power density for many applications; however, potential further improvement in these materials is limited. Additionally, as the lithium-ion industry continues to grow, so does the use of cobalt or nickel, straining scarce metal resources. To sustain this continued growth, development of new cathodes with high energy densities made from Earth-abundant elements will be necessary. Recent research has identified some promising energy-dense materials, such as Li-rich layered oxides and cation-disordered rock-salt-type cathodes; however, these materials don't have the rate capability (the rate for charge/discharge) high enough to make rechargeable batteries practical. To create both dense and fast energy storage will require an overhaul of the cathode material's makeup and structure. Toward that end, users of the APS report two new lithium-ion cathode materials with a structure that shares features with those of gemstones known as spinels but with a significant amount of disorder. These inexpensive materials exhibit both high energy density and high rate capability, giving them extraordinary potential as cathodes in lithium-ion batteries.

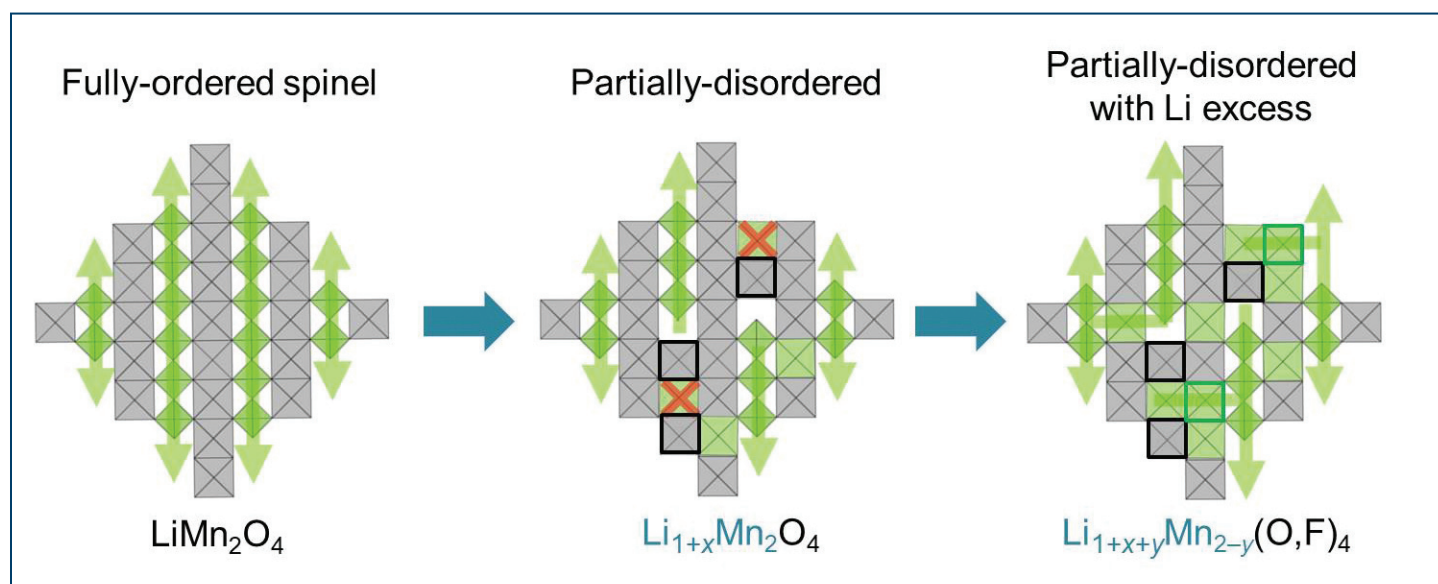


Fig. 1. Combining partial cation disorder with substantial lithium excess leads to exceptionally high energy and power in a new class of cathode materials based on Earth-abundant manganese.

The research team, including members from the University of California Berkeley, Lawrence Berkeley National Laboratory, Oak Ridge National Laboratory, and the University of California, Santa Barbara, and Argonne National Laboratory sought a face-centered-cubic anion framework for achieving dense energy storage because it's a close-packed crystalline arrangement. For high power density, the cations—including lithium and transition metal ions—need to be optimally positioned within this anion framework.

Previous work has suggested that a spinel-like cation order—which follows the structure of spinel gemstones and places divalent and trivalent cations in some or all of the octahedral or tetrahedral sites in the crystal lattice—can help lithium ions move efficiently in the framework. This arrangement promotes lower electrostatic repulsion between lithium and other cations compared to alternate structures. However, other spinel-like materials have been unsuitable for cathodes because they couldn't reliably cycle over low-voltage plateaus between discharged and charged states.

To overcome this issue, the researchers created two oxyfluorides with partial spinel-like order: $\text{Li}_{1.68}\text{Mn}_{1.6}\text{O}_{3.7}\text{F}_{0.3}$ (LMOF_{0.3}) and $\text{Li}_{1.68}\text{Mn}_{1.3}\text{O}_{3.4}\text{F}_{0.6}$ (LMOF_{0.6}) (Fig. 1).

After synthesis of these materials through mechanochemical alloying, the scientists characterized their structures by performing *ex situ* synchrotron diffraction using the XSD Structural Science Group's 11-ID-B beamline at the APS; *operando* x-ray absorption near edge spectroscopy experiments on the XSD Spectroscopy Group's 20-BM beamline at the APS; mapping of resonant inelastic x-ray scattering measurements at the iRIXS end station on beamline 8.0.1 of the DOE's Advanced Light Source (ALS) at Lawrence Berkeley National Laboratory; and neutron powder diffraction using the DOE's Spallation Neutron Source (SNS) at Oak Ridge National Laboratory on the Nanoscale Ordered Materials Diffractometer.

Their results showed a spinel-like structure with a pseudo face-centered-cubic anion framework. Both materials also displayed very high specific energies (energy per unit mass) and discharge rates—for example, samples of LMOF_{0.3} showed specific energies greater than 1,100 Wh kg⁻¹ and discharge rates up to 20 A g⁻¹.

These qualities are possible, the authors explain, because of the materials' unusual stoichiometry. Unlike ordered spinels, which have a 3:4 ratio of cations to anions, the new materials' ratio is 3.28:4. They also have a lithium excess compared to the ideal stoichiometry of LiM^2O^4 , where M is a non-lithium metal ion, because Li is partially

substituted for Mn. The excess lithium decreases electrostatic repulsion for a larger capacity and better lithium transport kinetics. The positive charges from this lithium excess are balanced by negatively charged fluorine, which in turn improves the ability of the material to cycle between charge and discharge. In addition, this cation overstoichiometry induces partial disorder in the metal ions, which overcomes the problems other spinel-like structures had with cycling over low-voltage plateaus.

Interestingly, further experiments show that half of the capacity in LMOF_{0.3} comes from reversible oxygen redox, a phenomenon observed in lithium-rich layered Ni-Mn-Co oxides and disordered rock-salts but is uncommon in spinel-like cathodes.

The authors suggest that these findings highlight the potential for designing high-performance and resource-efficient cathode materials that lie somewhere between fully ordered and disordered compounds. – [Christen Brownlee](#)

See: Huiwen Ji^{1,2}, Jinpeng Wu², Zijian Cai^{1,2}, Jue Liu³, Deok-Hwang Kwon^{1,2}, Hyunchul Kim², Alexander Urban⁴, Joseph K. Papp¹, Emily Foley⁵, Yaosen Tian^{1,2}, Mahalingam Balasubramanian⁶, Haegyeom Kim², Raphaële J. Clément⁵, Bryan D. McCloskey^{1,2}, Wanli Yang², and Gerbrand Ceder^{1,2*}, “Ultrahigh power and energy density in partially ordered lithium-ion cathode materials,” *Nat. Ener.* **5**, 213 (March 2020). DOI: 10.1038/s41560-020-0573-1

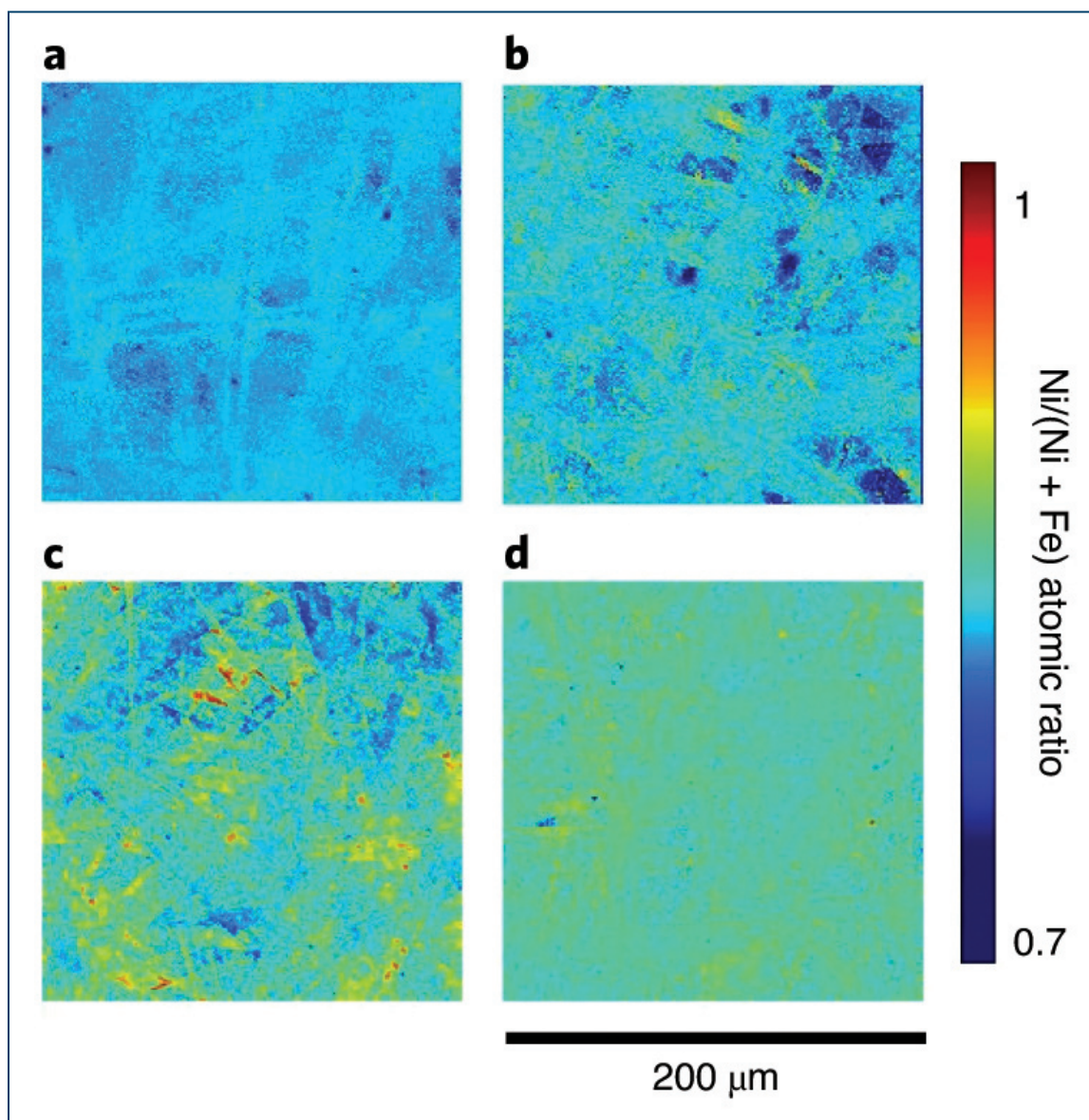
Author affiliations: ¹University of California, Berkeley, ²Lawrence Berkeley National Laboratory, ³Oak Ridge National Laboratory, ⁴Columbia University, ⁵University of California, Santa Barbara, ⁶Argonne National Laboratory

Correspondence: * gceder@berkeley.edu

This work is supported by the Umicore Specialty Oxides and Chemicals and the Assistant Secretary of Energy Efficiency and Renewable Energy, Vehicle Technologies Office of the U.S. Department of Energy (DOE) under contract no. DE-AC02-05CH11231 under the Advanced Battery Materials Research (BMR) Program. Recent characterization work was supported by the Assistant Secretary for Energy Efficiency and Renewable Energy, Vehicle Technologies Office, under the Applied Battery Materials Program, of the U.S. DOE under contract no. DE-AC02-05CH11231. Work at the ALS is supported by the Director, Office of Science-Basic Energy Sciences, of the U.S. DOE under contract no. DE-AC02-05CH11231. Research conducted at the Nanoscale Ordered Materials Diffractometer Beamline at Oak Ridge National Laboratory's Spallation Neutron Source is sponsored by the Scientific User Facilities Division-Basic Sciences of the U.S. DOE. Work at the Molecular Foundry at Lawrence Berkeley National Laboratory is supported by the Office of Science-Basic Energy Sciences of the U.S. DOE under contract no. DE-AC02-05CH11231. H.J. acknowledges support from the Assistant Secretary of Energy Efficiency and Renewable Energy, Vehicle Technologies Office of the U.S. DOE, under contract no. DE-AC02-05CH11231. J.K.P. also acknowledges support from the National Science Foundation Graduate Research Fellowship under contract no. DGE-1106400. This research used resources of the Advanced Photon Source, a U.S. DOE Office of Science User Facility operated for the U.S. DOE Office of Science by Argonne National Laboratory under contract no. DE-AC02-06CH11357.

A New Lease on Life for Electrocatalysts

Nothing lasts forever, including electrochemical devices such as batteries and fuel cells. But sometimes a new lease on life can be granted by partially reversing the inevitable structural degradation that causes loss of function. A research team carrying out studies at the APS and another DOE x-ray light source developed a way of revivifying mixed Ni-Fe hydroxide (MNF) electrocatalysts by reversing phase segregation at the electrocatalyst-electrolyte interface. The ability to reverse the degradation of oxygen evolution reaction (OER) electrocatalysts under operating conditions and at room temperature demonstrated in this work should be a major step in extending the usable lifetime of various electrochemical devices. The present work also provides important insights into the structural evolution and restoration of these OER electrocatalysts to enhance the development of new and longer-lasting materials.



A major cause of degradation in MNFs is the phase segregation that arises as various metal cations react in different ways with the electrolyte. Phase segregation, studied mostly under high-temperature rather than low- and room-temperature conditions, is widely reported to reduce catalytic activity. The experimenters in this study, from Virginia Tech, Argonne National Laboratory, Tianjin University (China), the SLAC National Accelerator Laboratory, and the University of Adelaide (Australia) focused on the OER in water oxidation catalysis, for which MNF electrocatalysts are used, first studying the chemical and structural changes of thin film and bulk MNF catalysts *ex situ* and *operando* during OER, and then testing a means of reversing those changes based on their analysis.

Observations used a variety of techniques, including synchrotron x-ray fluorescence microscopy (XFM) at the XSD Microscopy Group's 2-ID-E beamline and the Surface Scattering & Microdiffraction Group's 34-ID-E beamline at the APS, and x-ray absorption near-edge structure (XANES) and extended x-ray absorption fine structure (EXAFS) measurements at the Spectroscopy Group's 20-ID beamline also at the APS. Mixed Ni-Fe hydroxide data were obtained at beamline 4-1 of the DOE's Stanford Synchrotron Radiation Light Source.

Reversible phase segregation has been seen in high-temperature electrocatalysts but not in the low-temperature variety, which the investigators attribute to lower ion mobility and on the surface of catalytic materials. For this reason, they hypothesize that a thin two-dimensional electrocatalyst material will improve metal ion mobility and thus better enable reversible low-temperature phase segregation. Because electrochemical reactions occur at the catalyst and electrolyte interface, surface structure is the main factor in determining stability.

Stability and structural studies, also including chronoamperometry (CA) and cyclic voltammetry (CV) measurements, demonstrated that phase segregation is strongly associated with changes in structure. Under OER conditions, Fe atoms become segregated from the Ni-Fe lattice, and a FeOOH secondary phase forms, resulting in deactivation of the electrocatalyst. During recovery, Fe is again incorporated into the Ni hydroxide matrix.

< Fig. 1. Phase segregation and structural evolution of the water oxidation catalyst. a–d, Ni/(Ni + Fe) atomic ratio mapping of pristine thin MNF (a), thin MNF after 12 h of CA measurement at 1.6 V versus RHE (b), thin MNF after 18 h of CA measurement at 1.6 V versus RHE (c) and thin MNF after 450 CV cycles in the range 1.2–1.8 V versus RHE (d). These figures were generated by a pixel-by-pixel analysis of synchrotron XFM images of Ni and Fe.

To obtain a more direct picture of the evolution of this phase segregation process, the investigators conducted *operando* studies of an electrode using XFM and XAS. This confirmed the earlier results indicating a reversible metal dissolution and phase segregation after a resting period. The MNF lattice shows considerable distortion under OER because of the different properties of Fe and Ni which drive the metal dissolution and phase segregation. The experimenters used DFT calculations to model energy levels for different MNF lattice configurations, which show that the deposition of dissolved Fe onto NiOOH edge sites during OER reduction leads to phase segregation. The segregation and catalyst deactivation could therefore be reduced and reversed by increasing the surface area of the electrocatalyst to allow rapid cation redistribution and more uniform redeposition of metal ions during the reduction process.

The researchers suggest that an intermittent electrochemical reduction process to change the pH environment at the MNF surface would reverse phase segregation and accelerate and revive the catalytic properties. When this process was applied to thin and bulk MNF catalysts, both types showed definite performance revivification, to partial degree in the bulk MNF and full capacity in the thin MNF. In this work, the reduction process was applied to the anode, but a catalyst could also be designed that could be used in both the cathode and anode.

– Mark Wolverton

See: Chunguang Kuai^{1,2}, Zhengrui Xu¹, Cong Xi², Anyang Hu¹, Zhijie Yang¹, Yan Zhang^{2,3}, Cheng-Jun Sun⁴, Luxi Li^{4*}, Dimosthenis Sokaras³, Cunku Dong², Shi-Zhang Qiao⁵, Xi-Wen Du^{2**}, and Feng Lin^{1***}, "Phase segregation reversibility in mixed-metal hydroxide water oxidation catalysts," *Nat. Catal.* **3**, 743 (September 2020). DOI: /10.1038/s41929-020-0496-z

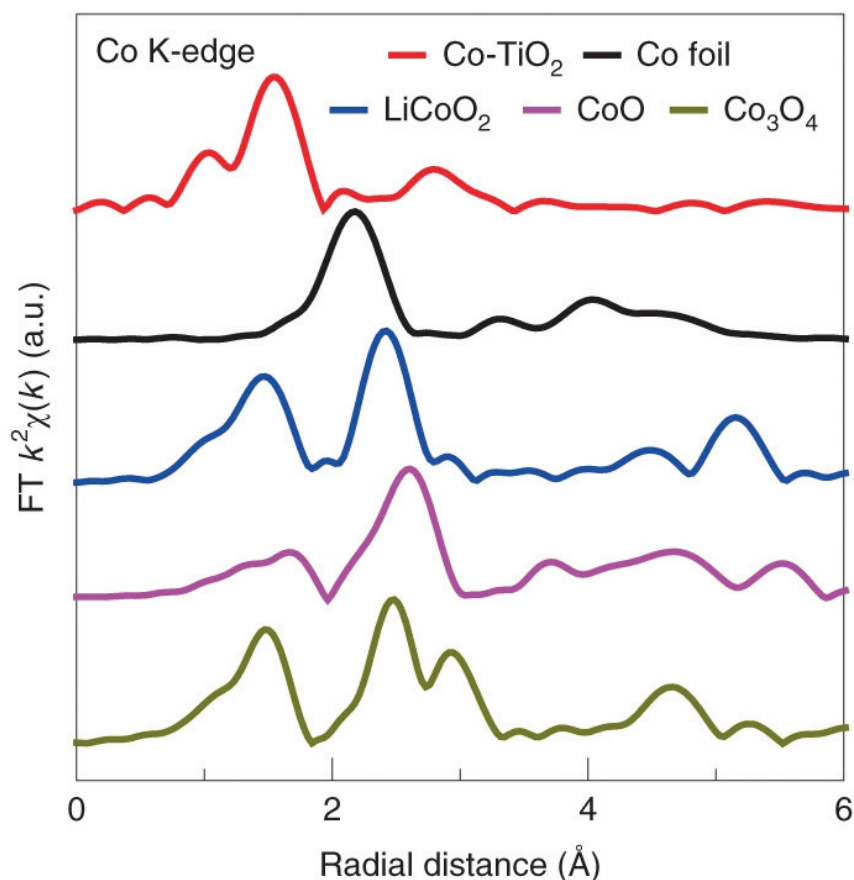
Author affiliations: ¹Virginia Tech, ²Tianjin University, ³SLAC National Accelerator Laboratory, ⁴Argonne National Laboratory, ⁵The University of Adelaide

Correspondence: * luxili@anl.gov, ** xwdu@tju.edu.cn, *** fenglin@vt.edu

This work was supported by the Department of Chemistry Startup Funds and the Institute for Critical Technology and Applied Science at Virginia Tech. The work at Tianjin university was supported by the Natural Science Foundation of China (grant nos. 51871160, 51671141 and 51471115). Use of the Stanford Synchrotron Radiation Lightsource, SLAC National Accelerator Laboratory, was supported by the U.S. Department of Energy (DOE) Office of Science-Basic Energy Sciences under contract no. DE-AC02-76SF00515. The authors thank S. Li and Y. Liu of SLAC for assisting the development of the synchrotron *operando* cells, and W. Liu for assisting the XFM measurements at APS 34-ID-E. This research used the resources of the Advanced Photon Source, a U.S. DOE Office of Science User Facility operated for the DOE Office of Science by Argonne National Laboratory under contract no. DE-AC02-06CH11357.

Single-Site Electrocatalyst Synthesis and Model Validation Increases Green Energy Options

Rechargeable batteries in electric cars and water electrolyzers for producing hydrogen fuel represent just a few electrochemical devices being optimized today, which could help green up our future energy options. These devices use electricity to power chemical reactions and often depend on materials which act as catalysts for those reactions. Many heterogeneous materials show promise as electrocatalysts. One of the challenges in working with these materials is determining the surface structure of their catalytic sites as well as the atomistic reaction mechanisms which occur during the catalyzed reaction. Modeling the structures and reaction mechanisms prior to synthesis would allow materials scientists to focus on only synthesizing the most promising electrocatalysts. Such a modeling process depends on validation of the model prior to use, through comparison with measurements from a straightforward heterogeneous catalyst. Research at the APS demonstrates such validation of a new method while also emphasizing a heterogeneous material with excellent electrocatalytic characteristics.



Collaborators from the University of Virginia, the California Institute of Technology, and three U.S. DOE national laboratories, including Argonne, worked together to develop a new method for simulating atomistic reaction mechanisms, called grand canonical QM, which is based on full solvent quantum mechanics. The new method differs from its predecessor in that it is applicable at a constant applied voltage. To validate this method, the team synthesized cobalt-doped brookite phase (orthorhombic) titanium-oxide nanorods with a specific (210) surface using single-site Co substitution.

The team analyzed the nanorods' structural characteristics using various types of electron microscopy. When the team assessed the nanorods as catalysts for the oxygen evolution reaction (the key reaction which occurs in electrochemical devices) they discovered the nanorods were highly efficient catalysts because of their high turnover frequencies. The intrinsic activity of each single-site Co catalytic centers, as assessed by the turnover frequencies (TOFs), is among the highest for Co-based heterogeneous catalysts reported to date.

To determine the atomic structure of Co single-site during the oxygen evolution reaction, the team applied multiple spectroscopic probes that were coupled with electrochemistry. They confirmed that high potentials do not cause cobalt phase segregation or titanium oxide phase transition using synchrotron radiation x-ray diffraction at the XSD Structural Science Group's 17-BM beamline at the APS. Also, they verified that the cobalt single-site dopant structure is stable using extended x-ray absorption fine structure probing at the XSD Spectroscopy Group's 20-BM beamline, also at the APS. They found that the choice of single-site substitution of the cobalt created a clear and well-defined structure, which enabled them to precisely assess the catalytic site's activity.

Next, the team compared their experimentally-measured activity values to the simulated results from their grand canonical QM method. Modeling three double-layer slabs with the validated Co-TiO₂ (210) surface, the team established a full description of oxygen evolution

< Fig.1. *In situ* Co K-edge Fourier-transformed extended x-ray absorption fine structure (FT-EXAFS) spectra of Co-TiO₂ nanorods under the oxygen evolution reaction conditions, as measured at beamline 20-BM of the APS.

reaction kinetics as a function of applied potential. To assess the results of the model, they compared two values: the electrochemical reaction's rate at different overpotentials (TOFs) and the reaction's Tafel slopes. The simulated results were in good agreement with the measured values. Because the clear structure of the electrocatalyst gave the team high confidence in their measured values, agreement between the measured and simulated results implies the more favorable reaction mechanism in the model (adsorbate evolution mechanism) occurs during the electrocatalytic reaction.

The strong agreement between measured and simulated results means that the grand canonical QM method will allow material scientists to simulate the capabilities of possibly heterogeneous electrocatalysts prior to synthesis, allowing them to concentrate their design and synthesis efforts more effectively and increase our sustainable energy choices for the future. – [Mary Alexandra Agner](#)

See: Chang Liu¹, Jin Qian², Yifan Ye³, Hua Zhou⁴, Cheng-Jun Sun⁴, Colton Sheehan¹, Zhiyong Zhang¹, Gang Wan⁴, Yi-Sheng Liu³, Jinghua Guo³, Shuang Li⁵, Hyeyoung Shin^{2†}, Sooyeon Hwang⁵, T. Brent Gunnoe¹, William A. Goddard III^{2*} and Sen Zhang^{1**}, “Oxygen evolution reaction over catalytic single-site Co in a well-defined brookite TiO₂ nanorod surface,” *Nat. Catal.*, published on line 14 December 2020. DOI: 10.1038/s41929-020-00550-5

Author affiliations: ¹University of Virginia, ²California Institute of Technology, ³Lawrence Berkeley National Laboratory, ⁴Argonne National Laboratory, ⁵Brookhaven National Laboratory [†]Present address: Chungnam National University

Correspondence: ** wag@caltech.edu, * sz3t@virginia.edu

This work was supported by the U.S. National Science Foundation (CBET-1805022, CBET-2004808 and CBET-2005250). This research used the resources of the Center for Functional Nanomaterials, which is a U.S. Department of Energy (DOE) Office of Science Facility at Brookhaven National Laboratory under contract no. DE-SC0012704. This research used the resources of the Advanced Light Source, a U.S. DOE Office of Science User Facility under contract no. DE-AC02-05CH11231. This research used the resources of the Advanced Photon Source, an Office of Science User Facility operated for the U.S. DOE Office of Science by the Argonne National Laboratory, and was supported by the U.S. DOE under contract no. DE-AC02-06CH11357 and the Canadian Light Source and its funding partners.

Water Adsorption in Metal-Organic Frameworks

Most metal-organic frameworks (MOFs) are unstable in the presence of water, limiting their application, but some can adsorb water into active sites and remain stable. Although their bonds may rearrange, there is no irreversible structural change or degradation. Researchers using the APS revealed crystallographic evidence of the importance of water loading effects on a metal-organic framework that does not experience large-scale structural changes. By obtaining a better understanding of these substances, their usefulness in important industrial and even medical applications can be increased.

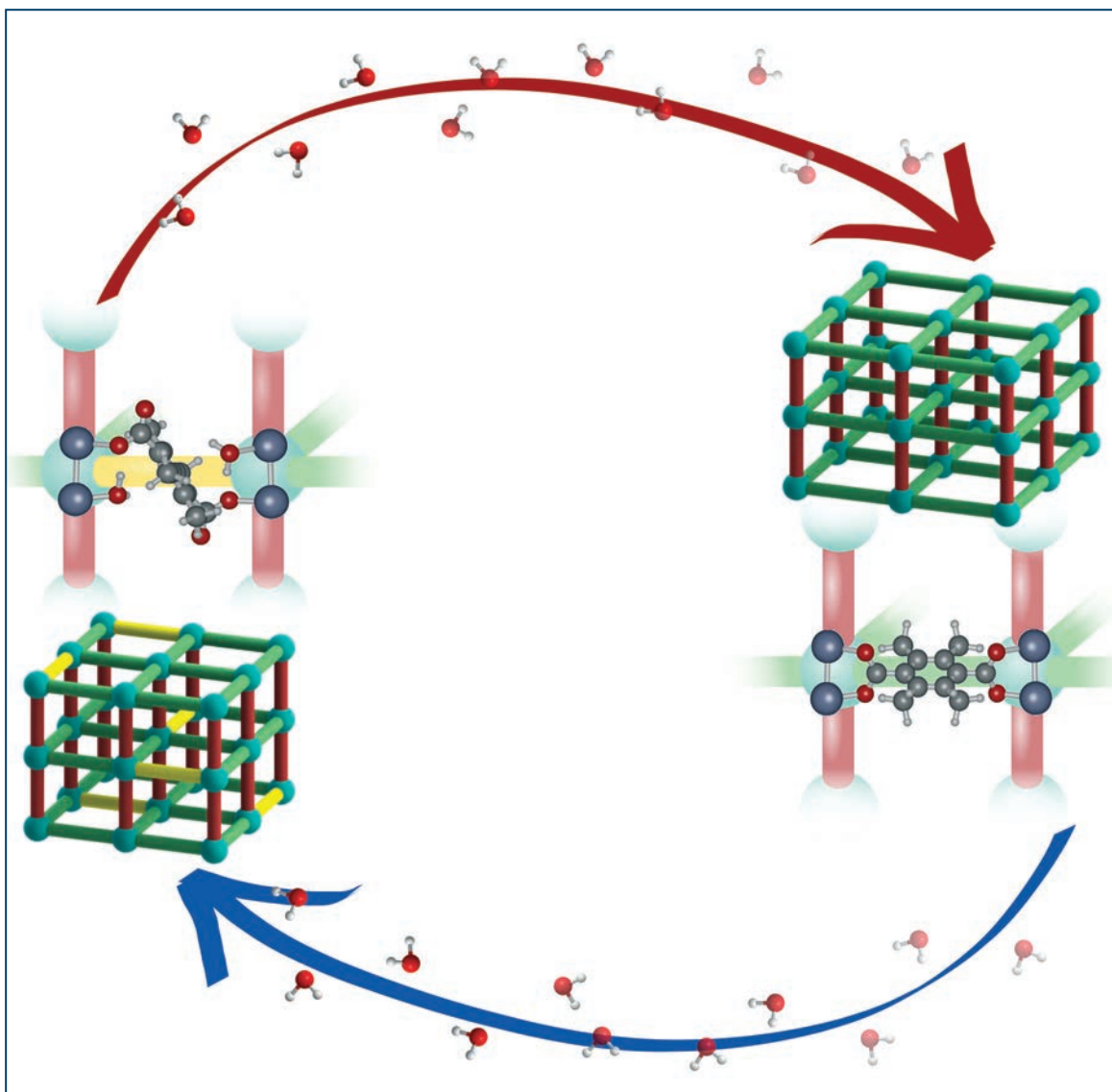


Fig. 1. Water-induced structural changes in a metal-organic framework.

MOFs are crystalline, nanoporous materials formed by the assembly of inorganic nodes and multitopic organic linkers. MOF structures are tunable; they can be altered to match their properties to the purpose of the application, such as gas separation and storage to catalysis, chemical sensing, and drug delivery. A better understanding of the chemical stability and guest-host interactions in MOFs will help researchers expand their applications.

Studies of some guest-host interactions of water on MOFs reveal their stability and adsorptive properties. Water guests in MOF hosts can have a wide variety of interactions due to the highly directional bonding behavior of water. The dynamic structural response to the water molecules are the proposed source of stability in some MOFs; they induce bond rearrangement in the MOF lattice without causing irreversible structural changes.

The directionality of hydrogen bonding in water leads to guest-host interactions within the MOF framework that affects the stability and absorption of the material. Competitive water adsorption changes the properties of the MOF. Water can occupy active sites to encourage catalytic reactions or can co-adsorb at some adsorption sites during gas separation and storage.

For this study, researchers from the Georgia Institute of Technology, The University of Amsterdam (the Netherlands), The University of Chicago, and Argonne synthesized a MOF framework with methyl groups on the terephthalate ligand. This MOF was chosen because the methyl groups give the framework the ability to adsorb relatively large amounts of water and retain stability and low-pressure CO₂ affinity. The material also can release water without altering its structure. The researchers performed three separate water adsorption experiments on three different crystalline structures. The synthesized MOF was exposed to moisture to test each structure's equilibrium water loading and to determine how water adsorption causes reversible changes in the structure.

The researchers obtained information on crystallographic lattice parameters, water siting, and water-induced defect structure. *In situ* powder diffraction experiments were performed at the XSD Structural Science Group's 17-BM-B beamline at the APS. *In situ* single-crystal x-ray diffraction experiments were performed at the ChemMatCARS beamline 15-ID-D at the APS. They determined the quantitative structural response of each lattice in the three regimes.

While each MOF maintained its porosity and crystallinity after exposure to water, water adsorption caused still structural changes at the molecular level due to guest-host interactions such as water-induced bond rearrangements. This work suggests a potential source of stability in some MOFs. However, in the experiments, water guests caused dynamic and reversible structural changes even at low guest loading in the unit cell parameters, microstrain, vibrational spectra and atomic structure. Structural changes continued with guest loading, although a static simulated framework may not be appropriate for understanding the structural stability.

This research highlights the need to investigate stable MOFs to understand the dynamic structural response as source of their stability. Such an understanding can help guide the design of stable MOFs. In the future, researchers will sample the coordination of water within the MOF framework to understand the energy barrier. Although this work did not shed light on the ligand functionality and coordination environment of many MOFs, it reveals many of the factors that affect MOF performance and stability. – Dana Desonie

See: Nicholas C. Burtch¹, Ian M. Walton¹, Julian T. Hungerford¹, Cody R. Morelock¹, Yang Jiao¹, Jurn Heinen², Yu-Sheng Chen³, Andrey A. Yakovenko⁴, Wenqian Xu⁴, David Dubbeldam², and Krista S. Walton^{1*}, "In situ visualization of loading-dependent water effects in a stable metal-organic framework," *Nat. Chem.* **12**, 186 (February 2020). DOI: 10.1038/s41557-019-0374-y
Author affiliations: ¹Georgia Institute of Technology, ²University of Amsterdam, ³The University of Chicago, ⁴Argonne National Laboratory
Correspondence: * krista.walton@chbe.gatech.edu

This work was supported as a part of the Center for Understanding and Control of Acid Gas-Induced Evolution of Materials for Energy, an Energy Frontier Research Center funded by the U.S. Department of Energy (DOE) Office of Science-Basic Energy Sciences under award no. DE-SC0012577. N.C.B. acknowledges support from the National Science Foundation (NSF) Graduate Research Fellowship and the Graduate Research Opportunities Worldwide (GROW) award under grant no. DGE-1148903. D.D. acknowledges support from the Netherlands Research Council for Chemical Sciences through a VIDI grant and the Dutch Research Council (NWO) Exacte Wetenschappen (Physical Sciences) for the use of supercomputer facilities with financial support from the NWO. ChemMatCARS is supported by the Divisions of Chemistry (CHE) and Materials Research (DMR), NSF, under grant no. NSF/CHE-1834750. This research used resources of the Advanced Photon Source, a U.S. DOE Office of Science User Facility operated for the DOE Office of Science by Argonne National Laboratory.

Slow Flow and Sudden Avalanches Relax Stress in Glasses

When familiar solids like metal, wood, or rubber are deformed, a consistent restoring force appears that pushes back against the deformation. Such materials are called elastic solids. In contrast, amorphous solids respond quite differently when deformed. Amorphous solids are substances like pastes, gels, and glasses that lack any long-range crystalline structure. When these materials are subjected to deformation (strain) the restoring force (stress) does not remain constant but slowly decreases over time, a process called stress relaxation. Although such behavior has been extensively studied at the macroscopic scale, investigations of the microscopic phenomena driving the large-scale behavior have lagged behind. In response, scientists recently performed first-of-their-kind experiments that tracked particle motion in a soft glass using x-ray photon correlation spectroscopy (XPCS) performed at the APS, while simultaneously observing how stress and strain varied with time. These complementary measurements revealed that following deformation of the soft glass, a persistent, microscopic backward flow was observed along with intermittent surges of particle motion perpendicular to the back flow. These experimental results may guide new strategies for processing amorphous solids and could also provide new theoretical insights into the factors underlying their dynamic behavior.

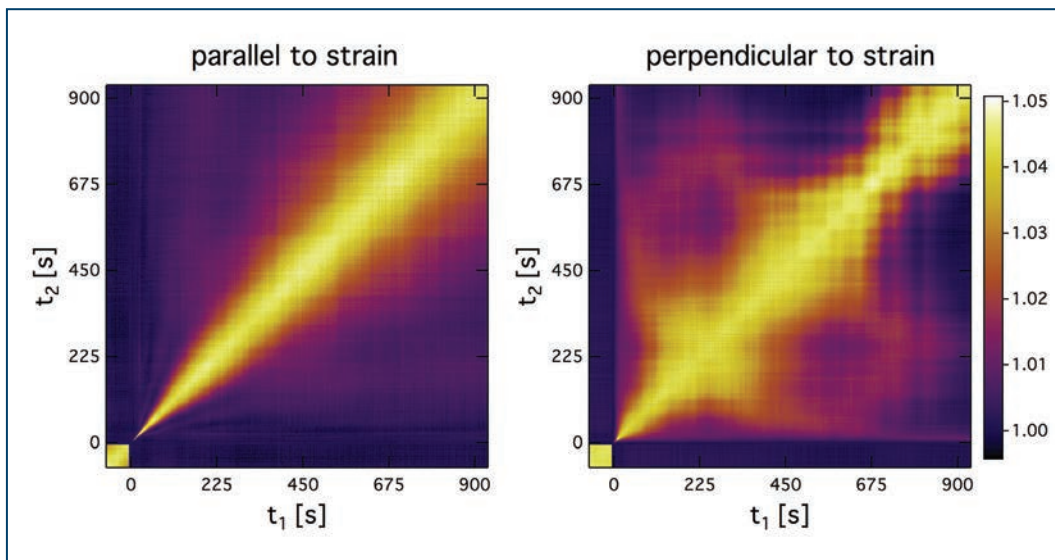


Fig. 1. Two graphs indicating particle motion in the soft glass over time. The left panel reveals particle motion along the strain (deformation) direction. The smoothness of the bright line indicates that motion is relatively steady along the strain direction. The right panel, by contrast, indicates particle motion perpendicular to the strain. The bulges in the bright pattern indicate sudden surges in particle motion, which move away from the strain direction. The data were derived from the XPCS measurements obtained at the APS. Adapted from Y. Chen et al., “Microscopic dynamics of stress relaxation in a nanocolloidal soft glass,” *Phys. Rev. Mater.* **4**, 035602 (2020). ©2020 American Physical Society. All rights reserved.

The amorphous solid examined in this research was a model system referred to as a “soft glass,” which consisted of densely packed silica (silicon dioxide) nanospheres in water. The surfaces of the nanospheres were charged, causing them to repel one another and become jammed in a static, disordered configuration. Macroscopically, the soft glass had a consistency similar to mayonnaise.

To examine the deformation and flow behavior of liquids and amorphous solids, scientists typically employ specialized laboratory equipment such as rheometers. This study, by researchers from Johns Hopkins University, the University of Illinois Urbana-Champaign, and the University of Ottawa (Canada) utilized a rheometer that incorporated a device called a Couette cell, which consisted of two coaxial cylinders. In a Couette cell a sample is placed in the gap between the walls of the cylinders and then the inner cylinder is rotated at precise speeds. The rotation introduces a tangential stress, or shearing force, across the sample's surface, which deforms it.

The soft glass was placed in the Couette cell and subjected to sudden deformations after which the torque needed to maintain the deformation was monitored as a function of time. More specifically, the strain (deformation) in the soft glass was increased stepwise from zero up to a maximum predetermined value and then held constant, and the resulting stress (force) needed to maintain that maximum strain was measured. The required stress was initially large but slowly decreased over time.

The innovative aspect of this study entailed using the highly-intense synchrotron x-rays produced at the APS to view the motion of the glassy nanospheres during simultaneous operation of the rheometer. A series of experiments was performed by the team and a colleague from Argonne over two days, employing the XSD Dynamics & Structure Group's 8-ID-I x-ray beamline at the APS. Each experiment lasted 1000 sec, or nearly 17 min. To track movement in the soft glass, XPCS images in the form of time varying speckle patterns were captured 10 times per sec, resulting in a total of 10,000 x-ray images per experiment.

The XPCS measured two types of motion in the soft glass during stress relaxation. One component to the mo-

tion was parallel to the cylinder wall and in the direction opposite to the initial deformation, hence its description as a back flow. This motion was captured by smoothly-varying XPCS correlation functions, as illustrated in the left panel of Fig. 1. The researchers were surprised at the persistent nature of the back flow, which steadily slowed over time but lasted throughout the entire duration of the experiments. The back flow was intimately linked with the rate of stress relaxation in the soft glass, and its detailed behavior was unexpected in light of previous computer simulations used to predict soft glass dynamics.

The other observed motion consisted of intermittent surges, or avalanches, perpendicular to the back flow. This perpendicular orientation is called the vorticity direction. Irregular changes in the XPCS correlation functions can highlight such intermittent motion, as illustrated in the right panel of Fig. 1. The researchers attributed these surges to coordinated motion of the jammed nanospheres in the vorticity direction to accommodate the back flow. The researchers suspect that the perpendicular flow observed in the soft glass may likewise occur in many amorphous solids.

The unique experimental setup utilized in this study will undoubtedly prove useful in future studies to uncover the microscopic mechanisms of deformation and flow in a wide variety of soft materials. The APS Upgrade would boost the coherent flux by 100 times and further enable the imaging of speckles to yield transformational insight into such studies. – Philip Koth

See: Yihao Chen¹, Simon A. Rogers², Suresh Narayanan³, James L. Harden⁴, and Robert L. Leheny^{1*}, “Microscopic dynamics of stress relaxation in a nanocolloidal soft glass,” *Phys. Rev. Mater.* **4**, 035602 (2020). DOI: 10.1103/PhysRevMaterials.4.035602

Author affiliations: ¹Johns Hopkins University, ²University of Illinois Urbana-Champaign, ³Argonne National Laboratory, ⁴University of Ottawa

Correspondence: * leheny@jhu.edu

Funding was provided by the National Science Foundation (CBET-1804721) and the Natural Sciences and Engineering Research Council of Canada Discovery grant program. This research used resources of the Advanced Photon Source and the Center for Nanoscale Materials, U.S. Department of Energy (DOE) Office of Science User Facilities operated for the DOE Office of Science by Argonne National Laboratory under Contract No. DE-AC02-06CH11357.

Putting a Shine on Metal 3-D Printing

The promise of metal three-dimensional (3-D) printing is hard to overstate, with the opportunity to revolutionize the manufacturing of a vast array of components, from the automotive to the medical industries. However, the technology has yet to mature to a point where metal 3-D printers reliably churn out consistently high-quality products at high volumes. One common approach to metal 3-D printing is called laser powder bed fusion additive manufacturing. In this method, a laser melts a metal powder, fusing the particles together. However, controlling the process dynamics can be tricky, and instability can cause defects in the printed material. To capture metal 3-D printing dynamics, a team of researchers combined high-fidelity simulations with x-ray imaging data collected at the APS. Using this information, the researchers came up with a set of criteria to stabilize the melted metal and reduce defects in the finished product.

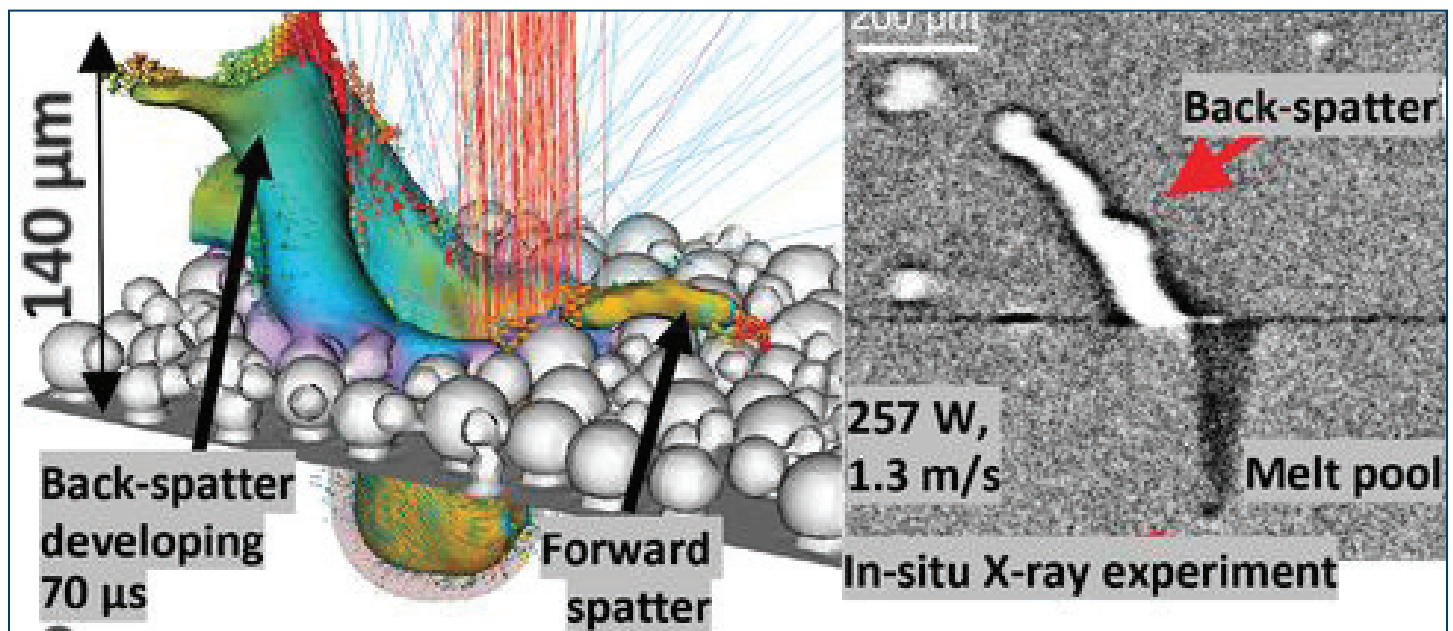


Fig. 1. Stability criterion to control start of track spatter, pores, and end of track frozen depression. Simulation (left) and *in situ* x-ray experiments show oversized ($\sim 200\ \mu\text{m}$) back-spatter at the start of the track during a skywriting scan of Ti-6Al-4V. From S. A. Khairallah et al., “Controlling interdependent meso-nanosecond dynamics and defect generation in metal 3D printing,” *Science* **368**, 660, (8 May 2020). Copyright © 2020 The Authors, some rights reserved; exclusive licensee American Association for the Advancement of Science.

In laser powder bed fusion additive manufacturing, a laser scans over a flat pattern of metal powder, melting and fusing the microscopic particles together bit by bit. This layer then forms a melt pool that trickles down a track to join with previous layers. The process is repeated thousands of times until the 3-D metal object is fully formed. But the accumulation of pores and other randomly generated defects leads to variability in the finished product, and variability is the enemy of high manufacturing standards, leading to quality and safety issues.

Combining the high-fidelity simulation and x-ray data collected at the DCS facility located at Sector 35 at the APS using transmission x-ray imaging, the researchers in this study, from Lawrence Livermore National Laboratory, the Air Force Research Laboratory, UES, Inc., and The Barnes Group Advisors came up with a strategy for reducing spatter and other sources of variability. They used a physics-based stability criterion to set critical stability limits on the laser scan strategy (laser power and scan speed). They called this approach the “power map strategy,” which is essentially a way to modulate the laser’s power level to stabilize the melt pool dynamics and thus reduce spatter. This study demonstrates how the combination of simulation and experiment may help usher in the metal 3-D printing revolution.

The team realized that understanding and controlling the interdependency between the laser, the powder, and the melt pool may help address the metal 3-D printing variability issue. They turned to a powerful simulation algorithm to capture the underlying physics of the laser powder bed fusion additive manufacturing process. The researchers conducted virtual experiments, on a microscale, to look for the source of defects under various conditions. Through these virtual experiments, the team discovered a new way that spatter is produced as part of the metal 3-D printing process.

Spatter consists of bits of metal that are ejected from the laser beam and can be a source of defects in the final product. The researchers observed spatter in their simulation that was related to the particulars of the laser scanning strategy, among other factors.

To anchor the simulation’s findings to the real world, the researchers also performed ultra-fast x-ray experiments at the XSD Imaging Group’s 32-ID beamline, also at the APS, using Ti-6Al-4V, a grade-5 titanium alloy. The x-ray experiments imaged the surface of the metal particles and melt pools, as well as beneath the surface, on a time scale that allowed the researchers to track structural changes on the fast time scale of a laser. Thus, they could observe spatter and other defect-related phenomena in the x-ray experiments. – Erika Gebel Berg

See: Saad A. Khairallah^{1*}, Aiden A. Martin¹, Jonathan R. I. Lee¹, Gabe Guss¹, Nicholas P. Calta¹, Joshua A. Hammons¹, Michael H. Nielsen¹, Kevin Chaput², Edwin Schwalbach², Megna N. Shah², Michael G. Chapman^{2,3}, Trevor M. Willey¹, Alexander M. Rubenchik¹, Andrew T. Anderson¹, Y. Morris Wang¹, Manyalibo J. Matthews¹, and Wayne E. King⁴, “Controlling interdependent meso-nanosecond dynamics and defect generation in metal 3D printing,” *Science* **368**, 660, (8 May 2020).

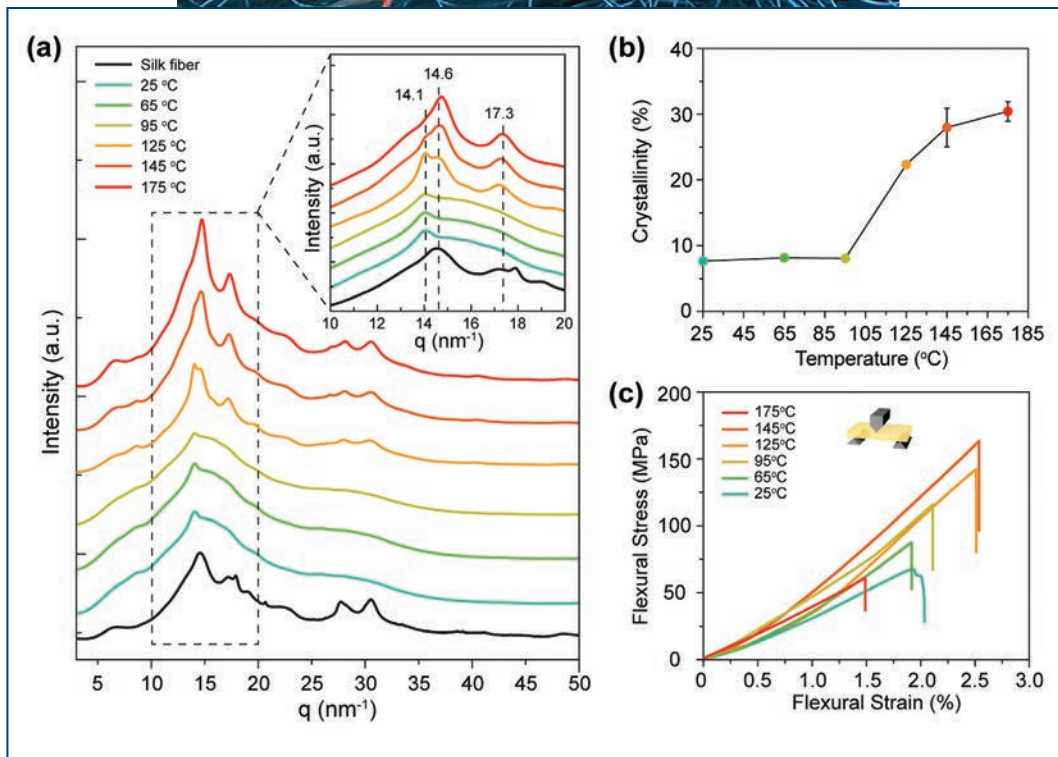
DOI: 10.1126/science.aay7830

Author affiliations: ¹Lawrence Livermore National Laboratory, ²Air Force Research Laboratory, ³UES, Inc., ⁴The Barnes Group Advisors

Correspondence: * khairallah1@llnl.gov

We thank N. Sinclair, P. Rigg, and D. Rickerson (x-ray imaging at DCS); and K. Fezzaa and A. Deriy (beamline 32-ID). Work was performed under the auspices of the U.S. Department of Energy (DOE) by Lawrence Livermore National Laboratory (LLNL) contract DE-AC52-07NA27344. Lawrence Livermore National Laboratory directed research and development, project 17-ERD-042, 18-SI-003. The Dynamic Compression Sector is operated by Washington State University under (DOE)/National Nuclear Security Administration award no. DE-NA0002442. This research used resources of the Advanced Photon Source, a U.S. DOE Office of Science User Facility operated for the DOE Office of Science by Argonne National Laboratory under contract no. DE-AC02-06CH11357.

Making Strong Plastics from Silk



Silk is an attractive material for all sorts of applications, particularly in the biomedical field, because of its mechanical toughness and biocompatibility. Solution-based processing, however, yields a product that is expensive to ship and changes properties over time. Now researchers using the APS have shown they can create an intermediate form of silk-based polymer that can be stored and shipped easily and processed into other items with tunable mechanical properties.

Silk is a semi-crystalline, protein-based polymer. As a source material, it is environmentally sustainable. Bioactive materials, such as antibiotics and monoclonal antibodies, can be mixed in with it, and it will protect them during processing and for long-term storage. It can be used for medical implants that eventually degrade within the human body, without causing an immunological response.

Solution-based procedures for processing silk, however, have drawbacks, including steps that involve water and salts that must be removed. Another drawback is that manufacturers wind up shipping products that are a mostly water, which adds weight and costs them money. Yet another is that in an aqueous solution, the proteins tend to slowly self-assemble, rendering the polymer less usable.

To solve those problems, an international team of scientists first produced a solution containing the silk protein, fibroin, then freeze-dried it to remove most of the water. That left them with amorphous silk nanomaterials—pellets of silk measuring between 30 and 1,000 nm in diameter. Those pellets can be stored indefinitely without any degradation.

Once heated above 97° C, the pellets begin to melt, and putting them under pressure causes them to fuse into a continuous material. Compressing the material in a mold at high temperatures and pressure leaves behind a hard, solid bar of silk. The researchers put silk bars into a lathe and carved them into bone screws, which can be implanted into a fractured bone to help it heal. They also machined the material into ear tubes, which are used to drain infected ear canals.

To understand changes to the silk's molecular structure caused by the process, researchers performed wide-angle x-ray scattering measurements at the BioCARS 14-BM-C beamline at APS, as well as spectroscopic studies. They looked at traditional silk fibers, the amorphous silk nanomaterials, and the fully processed material to see how the crystalline structure of the materials had changed.

< Fig. 1. X-ray profiles of silk plates prepared at a pressure of 632 MPA vary with temperature (a). The crystallinity of the material (b) and its tensile strength (c) also vary with temperature.

They found that one type of crystalline structure that was prevalent in the silk fibers was significantly reduced in the pellets, but increased again under high-temperature processing.

The researchers also found they could fine-tune the flexibility, tensile strength, and compression strength of the final product by varying the temperature and pressure at which they processed the material, with maximum strength at a processing temperature of 145° C and a decrease at 175° C.

The team added antibiotics to their pellets and found that the silk stabilized those drugs, allowing them to survive processing temperatures that would normally render them inactive. They doped the material they used to make ear tubes with an enzyme that caused the tubes to degrade faster than undoped ones, showing that the time for biodegradation can be tuned as well. They also found that their silk-based bone screws took up some water and swelled slightly to fit the space they'd been inserted into, and softened a bit to match the mechanical properties of the bone.

Future studies will examine how the material works in living tissue and how it can be further fine-tuned.

– Neil Savage

See: Chengchen Guo¹, Chunmei Li^{1*}, Hiep V. Vu¹, Philip Hanna³, Aron Lechtig³ Yimin Qiu¹, Xuan Mu¹, Shengjie Ling^{1,3}, Ara Nazarian^{3,4}, Samuel J. Lin², and David L. Kaplan^{1,**}, “Thermoplastic moulding of regenerated silk,” *Nat. Mater.* **19**, 102 (January 2020). DOI: 10.1038/s41563-019-0560-8

Author affiliations: ¹Tufts University, ²Harvard Medical School, ³ShanghaiTech University, ⁴Yerevan State Medical University

Correspondence: * chunmei.li@tufts.edu,

** david.kaplan@tufts.edu

This work was supported by grants from the National Institutes of Health (R01AR068048, R01DE016525), the Air Force Office of Scientific Research (FA9550-17-1-0333), and the Stepping Strong Foundation, Brigham and Women's Hospital (A. Nazarian and G. Dyer). Use of BioCARS was supported by the National Institutes of Health, National Institute of General Medical Sciences grant P41 GM118217. This research used resources of the Advanced Photon Source, a U.S. Department of Energy (DOE) Office of Science User Facility operated for the DOE Office of Science by Argonne National Laboratory under Contract No. DE-AC02-06CH11357.

A Short, Sharp Shock to Gold Structure

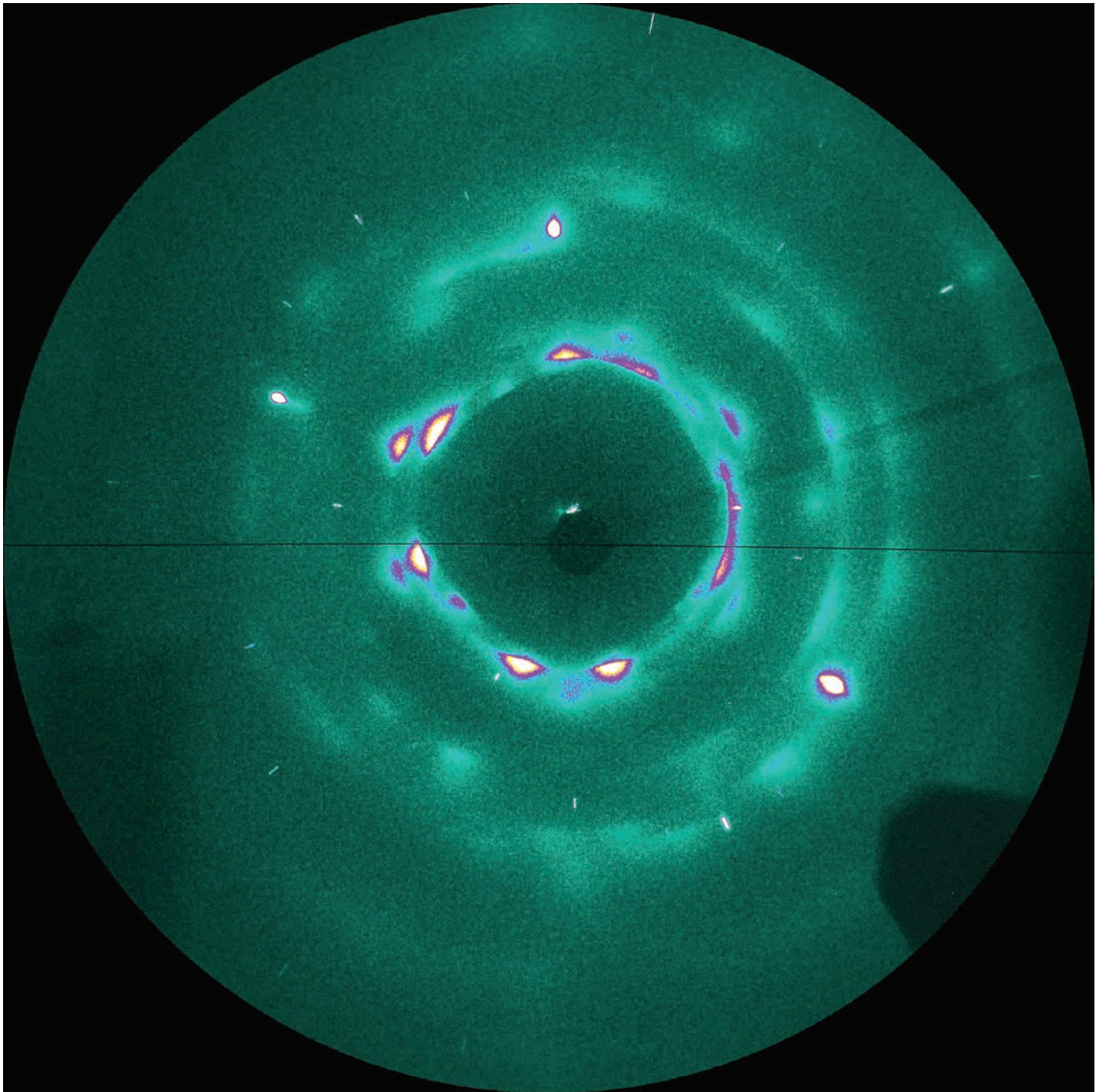


Fig. 1. X-ray diffraction image of shock-compressed gold (1.3 Mbar).

Put any solid material under enough pressure and its structure will be changed, either temporarily or permanently. But pressure comes in different forms: it can be a steady, even force that induces gradual and predictable alterations in atomic structure, or a short, sudden shock that causes abrupt and unpredictable change. Studying how a material responds to all types of pressure under different thermodynamic conditions is vital to understanding its properties at the microscopic scale and determining its equation-of-state data. The nanosecond time scale of shock compression phenomena makes them difficult to observe, compared to static compression studies. To overcome such challenges, a research team utilized high-brightness x-rays from the APS to achieve the first real-time, *in situ* experimental observations of shock-induced stacking faults in gold using x-ray diffraction (XRD) studies (Fig. 1).

Gold is a well-studied representative monatomic cubic metal, used as a pressure standard with an established equation-of-state, so it was an excellent candidate for this work. Its face-centered-cubic (fcc) structure provides a good window into shock-induced changes that can be observed through the shifting of Bragg peaks in XRD experiments. The Washington State University research team conducted its work at the DCS beamline 35-ID of the APS, creating shock waves, which propagated into a gold-foil sample and were observed via XRD, using laser pulses to ablate a thin Kapton® film (Fig. 2), .

Unlike static pressure, which produces isotropic compression, shock waves create uniaxial compression resulting in significant shear strains which produce lattice defects. Such shock-induced lattice defects have not as yet been adequately studied in experimental results. These defects in the form of dislocations and stacking faults also change XRD patterns through both broadening and shifting of Bragg peaks. The research team took these phenomena into account by computing simulated diffraction profiles and using them in the analysis of their experimental results.

The series of experiments demonstrated that stacking faults (and partial dislocations) contribute significantly to plastic deformation under high-pressure shock compression. Previous experiments and molecular dynamics (MD) simulations have claimed to observe or predict the same effects in aluminum and copper, but those findings were ambiguous and not confirmed. Although no MD simulations of shock compression in gold are as yet available for a quantitative comparison with these experimental obser-

ventions, characteristics of the shock-induced stacking faults seen here are qualitatively similar to other MD studies. The present work is the first confirmed, real-time, *in situ* experimental observation of stacking faults caused by shock-wave compression in a fcc material.

Because the XRD peak shifting due to shock-induced stacking faults in fcc metals is *hkl* dependent, determining volume compression in the shock-compressed gold samples based solely on analyzing a single XRD line can lead to inaccurate results. Instead, the experimenters suggest that analysis using multiple peaks better accounts for the XRD effects induced by the presence of a significant number of stacking faults. Comparison between different high-pressure XRD studies should also consider the differences in the observed diffraction patterns arising from the absence of these structural defects in static compression and their marked presence in shock-compressed samples.

The findings seen in this work confirm that density and pressure results are not enough to detect the plastic deformation in shock-compressed fcc metals. X-ray diffraction studies are needed to fully characterize the shocked state of these materials at the microscopic level. For example, these experiments reveal that the state of shock-compressed gold is not isotropic as previously speculated, and that high-temperature annealing of possible structural defects is not likely, at least on a nanosecond timescale. Such findings may have important implications for the use of gold as a diamond anvil cell pressure standard, or in applications for other similarly structured metals.

Using a variety of experimental methods to comple-

“Structure” cont’d. on page 28

Shocking Cerium into a New Phase

A material's equation of state (EOS) – which indicates its state under various conditions of pressure, temperature, volume, and energy, and relates them to various phases – is a vital part of understanding the material's behavior and response in different environments and applications. However, determining the EOS and complete phase diagrams of some materials can pose daunting challenges. One of these materials is cerium, for which some regions of the phase diagram have proven elusive. Investigators from the U.S. Department of Energy's (DOE's) Los Alamos National Laboratory (LANL) employed the APS to probe the high-pressure solid phase of cerium through shock-wave experiments that provided a detailed look at the cerium's transition from the α - ϵ phases. Their work provides the first evidence that an α - ϵ phase transition can be shock-induced in cerium.

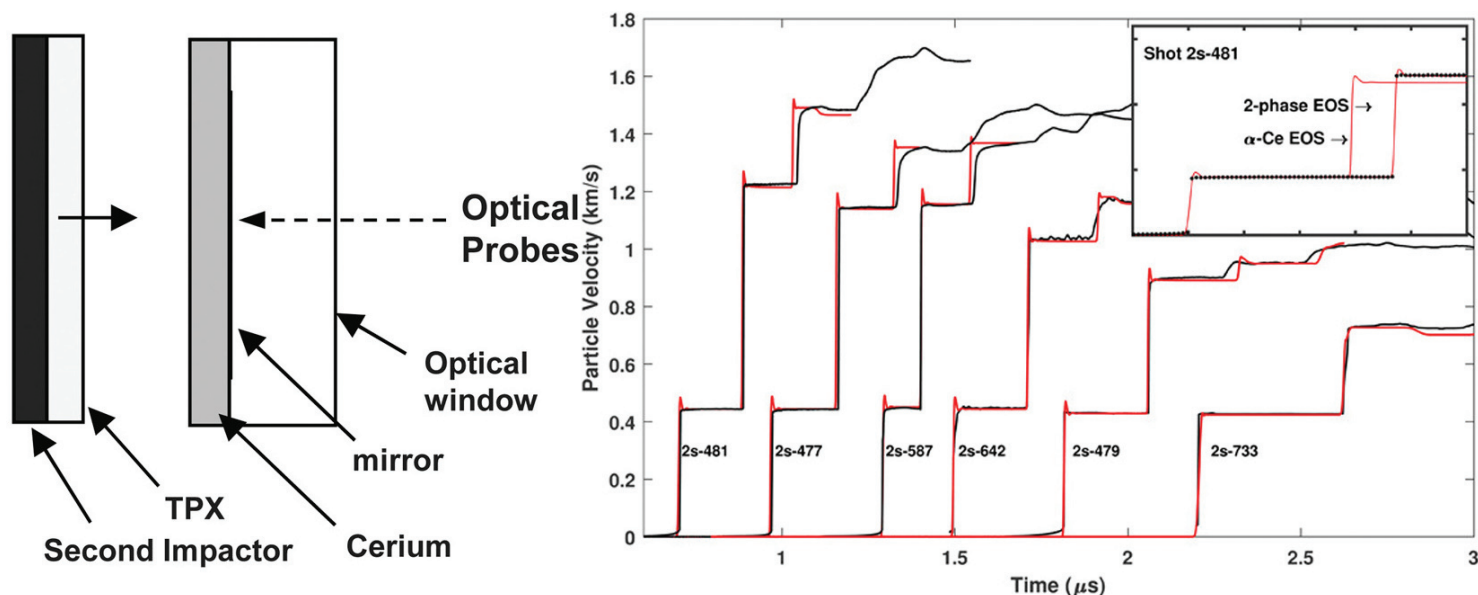
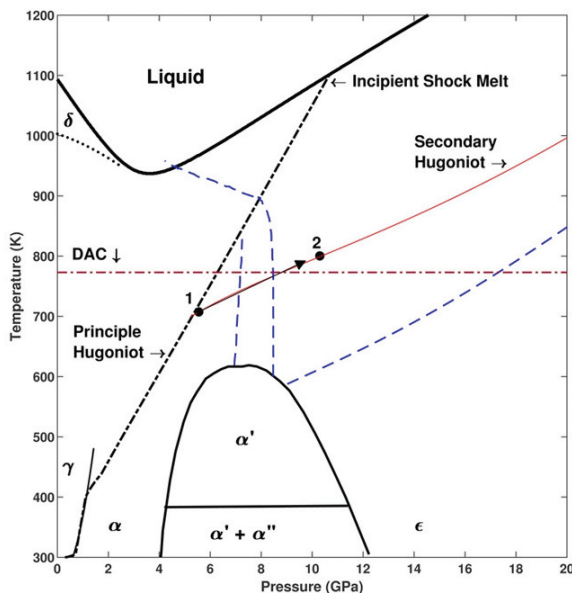


Fig. 1. High-performance gun systems at Los Alamos National Laboratory along with state-of-the-art DACs at HPCAT-XSD at the APS were used to study the complex phase diagram of metallic cerium. Left: Schematic of the experimental configurations for transmission experiment configurations used to generate double-shock loading in the cerium sample. The front-surface-impact (FSI) configuration was used to achieve second stress states (state 2) up to 12–13 GPa, whereas the transmission configuration was used to achieve higher stress states in excess of 25 GPa. Center: Shock wave profiles measured at the Ce–LiF interface for transmission configuration. Data are plotted as particle velocity (km/s) vs time (μ s) shown as black curves. Calculated wave profiles (red curves) obtained from the α -phase EOS are also shown for comparison. (Inset) Comparison between predicted and experimental (Shot No. 2S-481) wave profiles illustrating the need for the two-phase model for the higher-pressure experiments. A significant decrease in shock velocity of the second wave was observed in the data as compared to the simulated profile that used a single-phase EOS for α -Ce. Right: Example schematic of the cerium phase diagram showing the relevant phases. The Hugoniot is indicated along with states 1 and 2 which were achieved in a single experiment using a double-shock method. The red curve is a secondary Hugoniot, calculated using our multiphase EOS, centered about a shocked state (state 1) of 5.2 GPa. The blue dashed curves represent three of the reported locations for the ϵ -phase boundary. State 2 is varied by changing the second impactor on the projectile, while keeping the projectile velocity constant.

The principal Hugoniot (which defines conditions on both sides of a shock wave) of cerium has already been measured through traditional shock-wave techniques, but to go beyond it to find the secondary Hugoniot that marks the boundary of the ϵ -Ce phase requires a more complex approach that uses multiple shock loading. Data from regions beyond the principal Hugoniot are needed to determine multiphase equations of state. Toward this end, diamond anvil cell (DAC) experiments were conducted at the HPCAT-XSD 16-BM-D x-ray beamline at the APS, while



double-shock experiments were conducted at Los Alamos National Laboratory (Fig. 1).

In the shock impact work, two different experimental configurations were performed: front surface impact experiments (FSI), which used a cerium impactor; and double-shock transmission experiments, which used a cerium target and a complex projectile launched using high-performance gun systems. The researchers also performed static high-pressure DAC experiments at HPCAT-XSD to complement the dynamic measurements. Together, these different configurations allowed the researchers to study cerium using very different loading paths and time scales.

The dynamic studies showed that a secondary Hugo-

niot centered around 5.2-5.7 GPa and extends with the second shock to a peak stress of 25-30 GPa and beyond. DAC data were obtained along an isotherm of 773 K and shows that a gradual transition from α -Ce to ϵ -Ce begins at about 6 GPa. This mixed phase completely changes to ϵ -Ce at 12.1 GPa for both static and dynamic experiments.

The experimental team obtained simulated shock wave profiles for comparison with the experimental data, using a one-dimensional hydrodynamic code and a two-phase model to separately account for both the α -Ce to ϵ -Ce phases. The simulations generally showed good agreement with the experimental profiles, although some discrepancies were seen with the α -Ce phase model and the second high-pressure shock state above 12 GPa.

The necessity of a two-phase model to accommodate the disagreement in measured shock velocities of the second shock wave between the experimental data and the predictions from simulated profiles strongly supports a α -Ce to ϵ -Ce phase transition at a peak stress of about 12.25 GPa.

The complete transition to the ϵ phase is similar to the DAC experiments performed in this work, though the DAC data show a gradual transition from one phase to another. The research team next plans to repeat similar experiments under x-ray diffraction observation to study the evolution of the cerium microstructure across the phase transition. – Mark Wolverton

See: B. J. Jensen*, F. J. Cherne, and N. Velisavljevic†, “Dynamic experiments to study the α - ϵ phase transition in cerium,” *J. Appl. Phys.* **127**, 095901 (2020). DOI: 10.1063/1.5142508

Author affiliation: Los Alamos National Laboratory †Present address: Lawrence Livermore National Laboratory

Correspondence: * bjjensen@lanl.gov

This work was supported by the U.S. Department of Energy (DOE) through the Los Alamos National Laboratory’s Science Campaign C2. The Los Alamos National Laboratory is operated by Triad National Security, LLC, for the National Nuclear Security Administration (NNSA) of the U.S. DOE (Contract No. 89233218CNA000001). HPCAT-XSD operations are supported by the DOE-NNSA Office of Experimental Sciences. This research used resources of the Advanced Photon Source, a U.S. Department of Energy (DOE) Office of Science User Facility operated for the DOE Office of Science by Argonne National Laboratory under Contract No. DE-AC02-06CH11357.

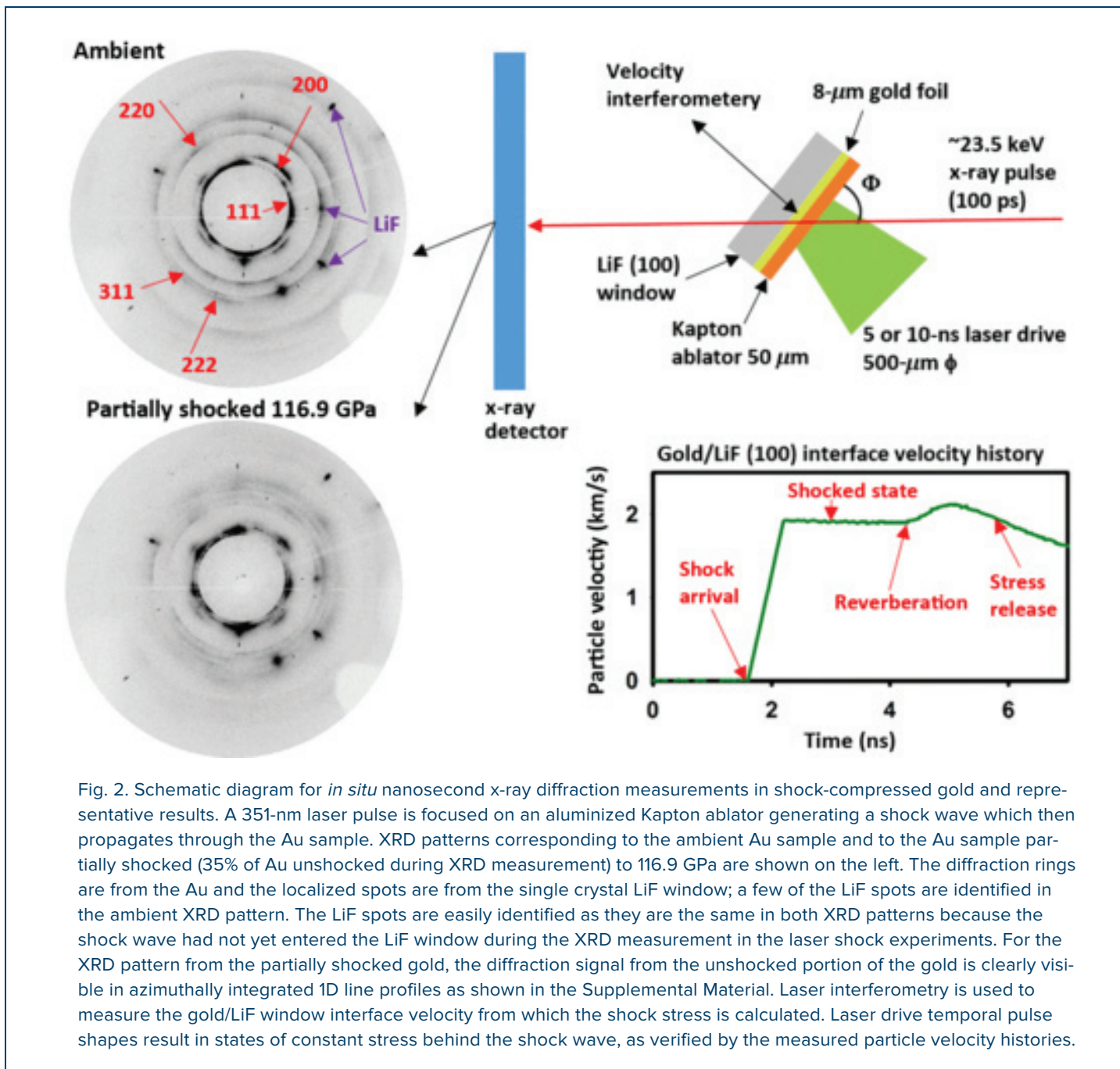


Fig. 2. Schematic diagram for *in situ* nanosecond x-ray diffraction measurements in shock-compressed gold and representative results. A 351-nm laser pulse is focused on an aluminized Kapton ablator generating a shock wave which then propagates through the Au sample. XRD patterns corresponding to the ambient Au sample and to the Au sample partially shocked (35% of Au unshocked during XRD measurement) to 116.9 GPa are shown on the left. The diffraction rings are from the Au and the localized spots are from the single crystal LiF window; a few of the LiF spots are identified in the ambient XRD pattern. The LiF spots are easily identified as they are the same in both XRD patterns because the shock wave had not yet entered the LiF window during the XRD measurement in the laser shock experiments. For the XRD pattern from the partially shocked gold, the diffraction signal from the unshocked portion of the gold is clearly visible in azimuthally integrated 1D line profiles as shown in the Supplemental Material. Laser interferometry is used to measure the gold/LiF window interface velocity from which the shock stress is calculated. Laser drive temporal pulse shapes result in states of constant stress behind the shock wave, as verified by the measured particle velocity histories.

ment and supplement each other assures the most complete understanding of such a complex phenomenon as the effects of pressure on solid materials. As the present work shows, it can also provide fresh perspectives that lead to new and important questions. – Mark Wolverton

See: Surinder M. Sharma, Stefan J. Turneaure, J. M. Winey, P. A. Rigg, N. Sinclair, Xiaoming Wang, Y. Toyoda, and Y. M. Gupta*. "Real-Time Observation of Stacking Faults in Gold Shock Compressed to 150 GPa," *Phys. Rev. X* **10**, 011010 (2020). DOI: 10.1103/PhysRevX.10.011010

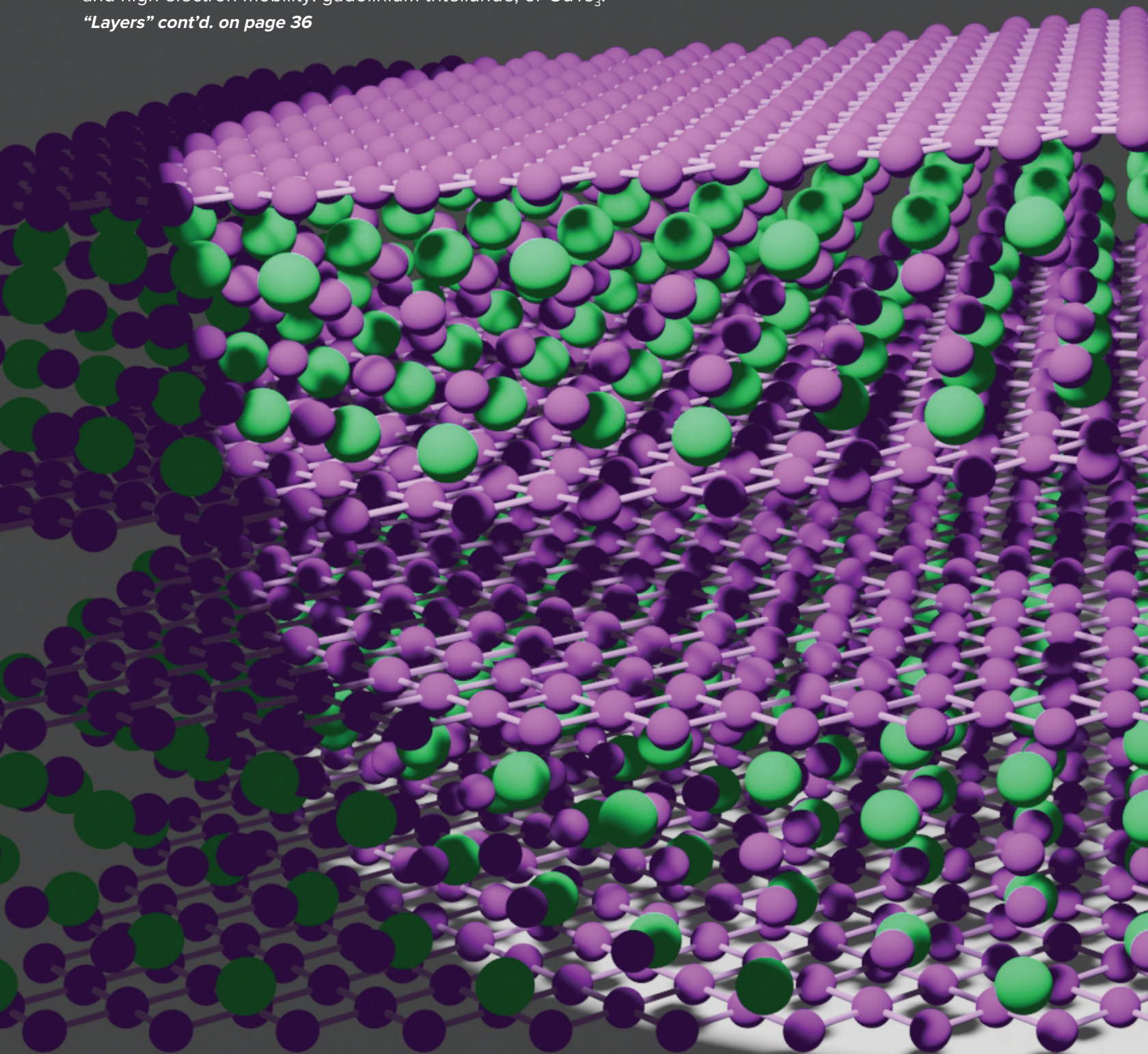
Author affiliation: Washington State University
Correspondence: * ymgupta@wsu.edu

Yuelin Li, Adam Schuman, Nicholas Weir, and Jun Zhang at the Dynamic Compression Sector are gratefully acknowledged for their expert assistance with the experiments. This publication is based upon work supported by the U.S. Department of Energy (DOE), National Nuclear Security Administration (NNSA) under Award No. DE-NA0002007. The Dynamic Compression Sector is operated by Washington State University under DOE/NNSA Award No. DE-NA0002442. This research used resources of the Advanced Photon Source, a U.S. DOE Office of Science User Facility operated for the U. S. DOE Office of Science by Argonne National Laboratory under Contract No. DE-AC02-06CH11357.

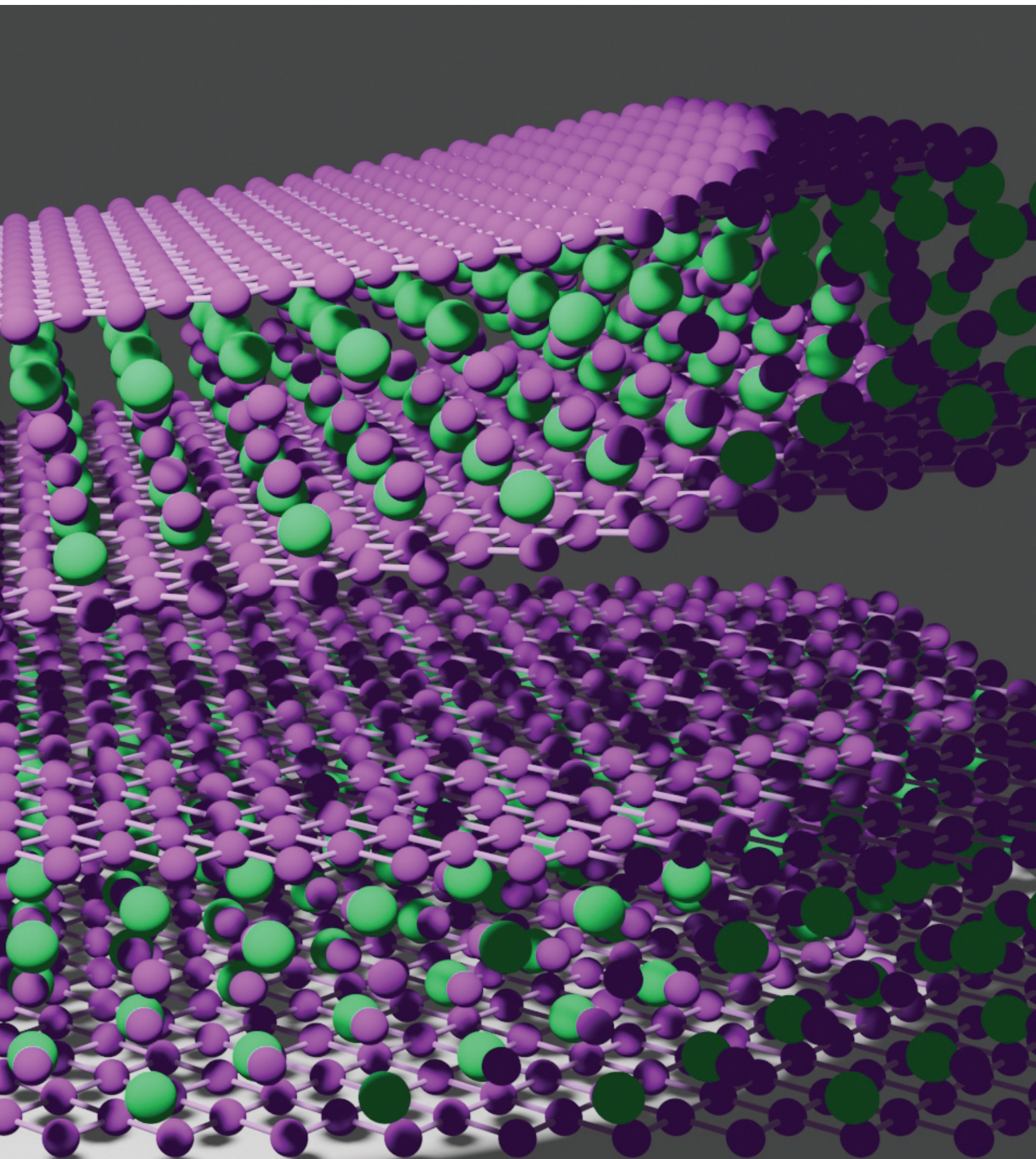
Electronic and Magnetic Materials

Van der Waals materials—layered materials held together through weak van der Waals attractions (a distance-dependent interaction between atoms or molecules)—have attracted significant attention since the discovery of graphene in 2004. Often grown or exfoliated into atomically thin, two-layer sheets, these materials have made their mark in applications including photovoltaics, semiconductors, electrodes, and water purification. However, although more than 2500 van der Waals materials have been discovered thus far, the vast majority are insulating or semiconducting rather than metals, and few exhibit magnetic order. Additionally, none of the magnetic van der Waals materials discovered thus far have high electron mobility, a quality that is rare in van der Waals materials in general. Finding a high-mobility van der Waals material that also exhibits magnetic order could open the possibility of using this class of materials for novel devices that harness the intrinsic spin of electrons and their associated magnetic moment, a field known as spintronics, or devices that take advantage of how the angle between layers of van der Waals materials affect their electrical properties, a field known as twistrionics. A study by users of the APS has identified a van der Waals material that shares both magnetic order and high electron mobility: gadolinium tritelluride, or GdTe_3 .

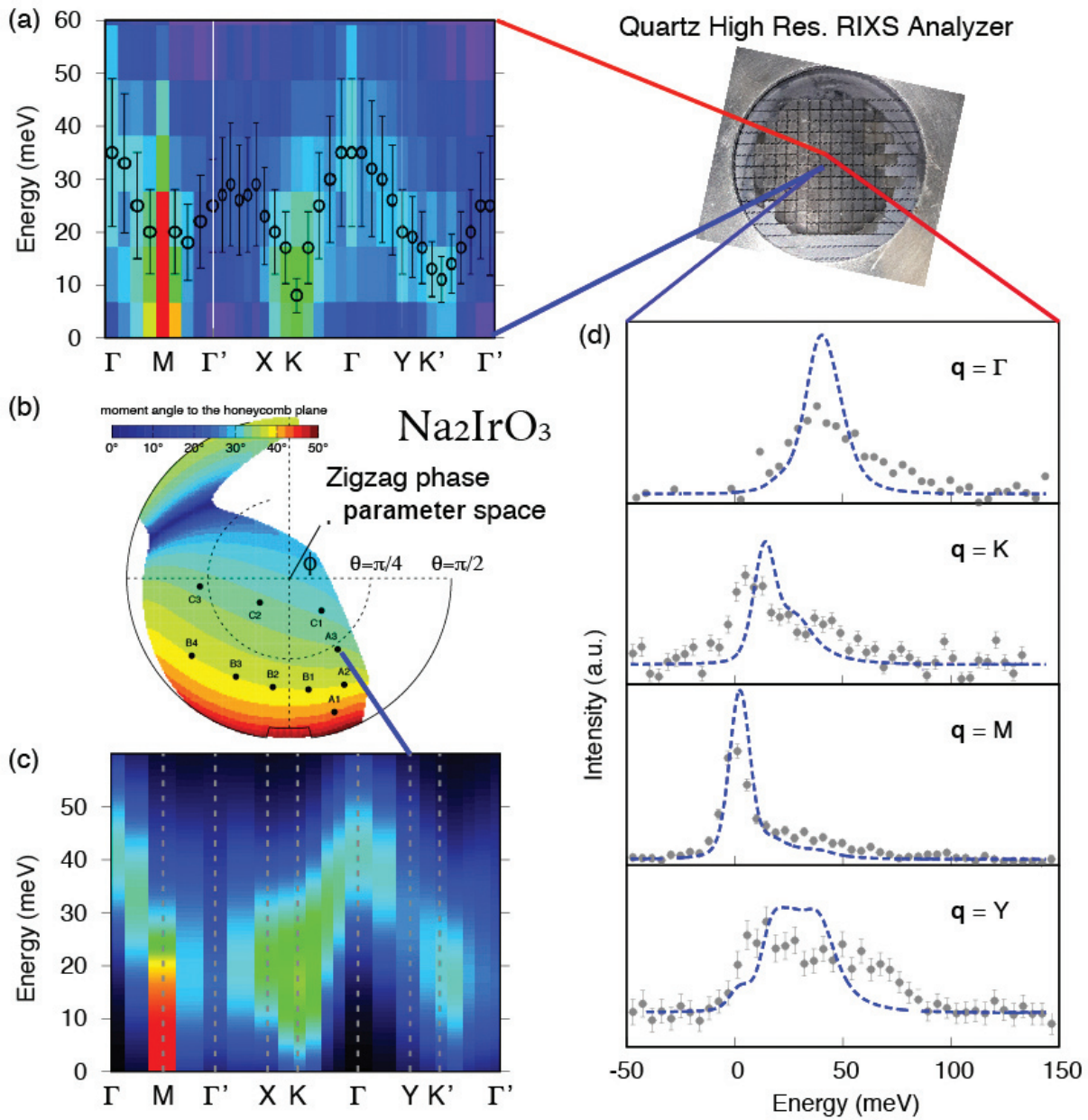
“Layers” cont’d. on page 36



Peeling Back the Layers on GdTe_3



High-Resolution RIXS System Reveals Dynamic Spin Correlations in Na_2IrO_3



Buoyed by the experimental finding that bond-directional pseudospin- $\frac{1}{2}$ interactions occur in the spin-orbit entangled Mott insulator Na_2IrO_3 , the principal investigators responsible for that discovery joined with colleagues in a detailed follow-up study of the dynamic spin correlations in this highly frustrated magnetic material using high-brightness x-ray beams from the APS. Bond-directional interactions of this form are the essential building blocks for unconventional magnetism in the celebrated Kitaev model hosting the Kitaev quantum spin liquid (KQSL). The long-range quantum entanglement and topologically protected fractional excitations are of particular interest for potential quantum computing applications. The possibility of Majorana-mediated spin transport through a KQSL has been shown recently as well.

In principle, measurement of the dynamical structure factor using resonant inelastic x-ray scattering (RIXS) should yield direct access to the Hamiltonian describing all of the magnetic interactions in Na_2IrO_3 . However, until recently, RIXS lacked the energy resolution to provide detailed information about the magnetic ground state.

In the present study, magnetic excitation spectra in Na_2IrO_3 were measured by a state-of-the-art RIXS spectrometer using a quartz analyzer, thereby providing an unprecedented energy resolution of 12 meV. The measurements at the XSD Inelastic X-ray & Nuclear Resonant Scattering Group's 27-ID beamline of the APS were carried out along all high-symmetry paths including the second Brillouin zone center. The international team of researchers followed the temperature evolution of the RIXS dynamic response from 7 K, which is below the antiferromagnetic (AFM) order temperature of Na_2IrO_3 , up to 280 K. The 12-meV measurements could identify a low-energy sharp magnon peak below the AFM order temperature and verify the broad widths of the magnetic excitations. These sets of data allowed for detailed comparisons with theoretical calculations (Fig. 1).

In Na_2IrO_3 , iridium⁴⁺ ions with pseudospin- $\frac{1}{2}$ moments form a quasi-two-dimensional honeycomb network that is sandwiched between two layers of oxygen ions that frame edge-shared octahedra around the magnetic ions and mediate superexchange interactions between neighboring pseudospins. This configuration gives rise to an AFM insulating ground state with a zigzag spin alignment.

RIXS measurements were taken at the Ir L_3 edge at two energy resolutions, 25 meV and 12 meV, with an eye to parameterizing an extended Kitaev-Heisenberg model that captured the highly frustrated nature of the magnetic interactions. Accordingly, the model consisted of terms corresponding to Kitaev interactions, Heisenberg exchange interactions, and two kinds of off-diagonal exchange interactions between the spins.

The measured spectra at low temperature showed that the dynamic response lacked resolution-limited coherent spin waves in most parts of the Brillouin zone but had a discernible dispersion and spectral weight distribution within the energy window of 60 meV. A systematic investigation using the exact diagonalization method and direct comparison of the high-resolution experimental spectra and theoretical sim-

"RIXS" cont'd. on page 37

< Fig. 1. (a) Experimental RIXS intensity map. (b) Zigzag phase in the parameter space of the extended Kitaev Heisenberg model. The color indicates the angle of the zigzag-ordered moments to the honeycomb plane. (c) Theoretical RIXS intensity map which mimics the experimental geometry and energy and momentum-transfer resolutions. (d) High-resolution RIXS spectra at representative wave vectors from the quartz analyzer compared with the theoretical spectra.

Ferroelectric Domain Wall Movement in a Complex Oxide Thin Film

Complex oxides are compounds that contain oxygen and at least two other elements. These materials exhibit the unusual electric and magnetic properties needed for next-generation electronic devices. Because silicon is the dominant electronic material, any promising complex oxide should be capable of interfacing with it. However, achieving this interface is challenging. For instance, lead zirconium titanate (PZT) is a well-known complex oxide that is strongly ferroelectric, but it fails to properly “grow” on silicon. One solution is to form thin-film PZT on a compatible substrate and then transfer it to silicon. While conceptually straightforward, the effects of such transfers on thin films are largely unknown. In order to resolve this mystery a research team investigated the properties of a transferred thin film using several techniques, including scanning probe microscopy and charge-voltage relationship measurement performed at the Argonne Material Science Division (MSD), and x-ray nanodiffraction experimentation carried out at the APS and the Argonne Center for Nanoscale Materials (CNM). The researchers found that the static ferroelectric surface charge and structural properties of the transferred PZT film were more-or-less preserved. However, the ferroelectric’s dynamic electromechanical response changed substantially. Taken together, these findings demonstrate the feasibility of transferring thin-film PZT and other complex oxides to silicon, thereby promoting their use for applications including non-volatile computer memory and quantum computing.

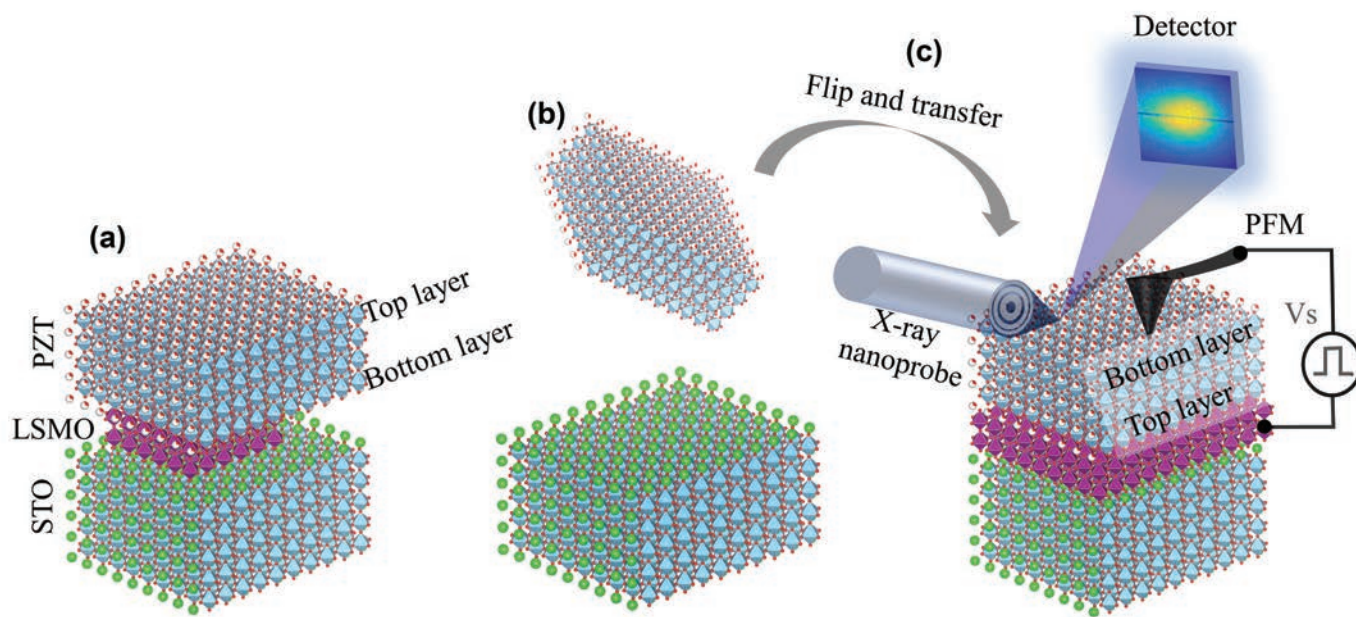


Fig. 1. The transfer of thin-film PZT is shown in (a) through (c). In (a) the original PZT film is deposited on a layer of lanthanum strontium manganite (LSMO), highlighted in magenta. The greenish-colored underlying substrate is strontium titanate (STO). Removing the LSMO layer releases the PZT film, as shown in (b). The PZT film is then flipped upside-down onto another LSMO/STO substrate, shown in (c), where it was examined via scanning probe microscopy, charge-voltage relationship measurement and x-ray nanodiffraction. Figures adapted from S. R. Bakaul et al., “Ferroelectric Domain Wall Motion in Freestanding Single-Crystal Complex Oxide Thin Film,” *Adv. Mater.* **32**, 1907036 (2020). © 2019 WILEY-VCH Verlag GmbH & Co. KGaA, Weinheim

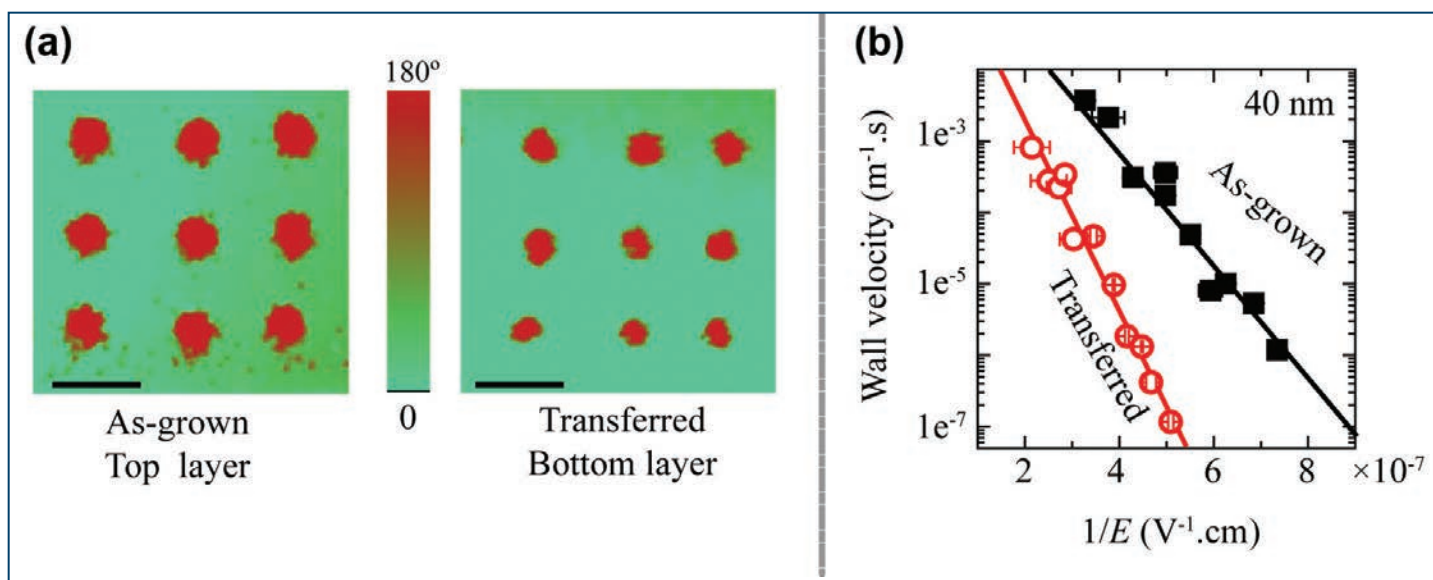


Fig. 2. Panel (a) shows a side-by-side comparison of reverse-polarized regions (red circles) induced in the original (as-grown) PZT film shown on the left side, versus reverse-polarized regions in the transferred PZT film on the right. The circular reverse-polarized regions arise from 2-msec electrostatic pulses emitted by the tip in scanning probe microscope. Note the smaller reverse-polarized regions in the transferred film. The boundary lines between the reverse-polarized circles and surrounding unipolar matrix (green areas) are domain walls. As electric field intensifies, the domain walls move. Wall movement was up to 1,000 times slower in the transferred film, as demonstrated by the graph in panel (b).

PZT was developed in the 1950s as a piezoelectric compound, meaning it produces electricity when deformed, and changes shape in response to an electric field. Due to its excellent piezoelectric properties, PZT is widely used in ultrasound transducers and actuators. This widely-used material is also ferroelectric, meaning that positive and negative charge separation spontaneously arises. Interest in ferroelectrics has increased due to their potential use in computational, switching, and sensor applications. But the advantages offered by ferroelectrics depend upon integration with silicon. Due to their mismatched crystalline structures, PZT will not correctly form on silicon. Fortunately, the lead author of this work previously (while doing postdoctoral research at UC Berkeley) developed an alternative approach known as layer transfer technique (LTT). Using LTT allows scientists to form a thin-film complex oxide on a highly-compatible substrate and then transfer the film to another substrate.

For this study, the researchers from Argonne, the Korea Advanced Institute of Science and Technology (KAIST), and the University of California, Berkeley used pulsed

laser deposition to form a crystalline layer of PZT on one substrate and then moved it to another substrate. The researchers were interested in resolving several issues, including whether LTT could transfer a PZT film without destroying it; to provide the first-ever look at the underside of a complex oxide thin-film; and to determine how the transfer affected the film's properties.

Figure 1 illustrates the experimental concept. Thin-film PZT (Fig. 1a) is extracted from the substrate (Fig. 1b) and placed upside-down on a similar substrate (Fig. 1c). This LTT procedure, performed in the CNM cleanroom facility, releases the molecular bonds between the PZT and its original substrate, resulting in a freestanding film resting on the second substrate. Scanning probe microscopy experiments and charge-voltage relationship measurement, performed at MSD, revealed drastically reduced dynamic ferroelectric properties in freestanding film. X-ray nanoprobe data, gathered at the joint CNM/XSD 26-ID beamline at the APS, confirmed that the transferred film's crystalline structure remained intact.

"Domain" cont'd. on page 37

“Layers” cont’d. from page 30

Fig. 1 from page 30. Antiferromagnet GdTe_3 with exceptional high-mobility and easy exfoliation down to a few atomic layers. Figure illustrates an exfoliation from the van der Waals gap located between two neighboring tellurium square-net planes (shown in purple). A puckered GdTe bilayer is sandwiched between two exterior tellurium layers.

The research team—with members from Princeton University, Boston College, the Max-Planck-Institut für Festkörperforschung (Germany), and Argonne National Laboratory—started by growing high-quality, plate-like GdTe_3 crystals that stretched out in approximately 8 mm x 8 mm planes, using a technique called “self-flux,” which allows crystals to precipitate from solution. Initial tests showed excellent metallicity with few defects in the crystal structure. In addition, the researchers confirmed that this material exhibits antiferromagnetism.

For use in high-speed devices, it’s important to determine the electron transport mobility, or how quickly an electron can move through a material when pulled by an electric field. Tests showed that GdTe_3 has an electron mobility greater than $60,000 \text{ cm}^2\text{V}^{-1}\text{s}^{-1}$. Although this value is low compared to some nonmagnetic compounds, it is the highest ever reported for any magnetically ordered compound and stands out even among van der Waals compounds—its mobility is second only to graphite among van der Waals materials and is about as high as black phosphorous, a van der Waals material that has been explored for optoelectric, semiconductor, and photovoltaic applications.

High mobility in magnetically ordered materials is a product of both a long scattering time (how long an electron can be accelerated by an external electric field before it collides with something that changes its direction and/or energy) and a low effective mass (how quickly an electron can be accelerated by internal forces created by other charges in the material). While the long scattering time in GdTe_3 is a product of its high crystal quality, the effective mass was unknown. To measure this parameter, the researchers used the XSD Magnetic Materials Group’s 29-ID x-ray beamline at the APS to perform angle-resolved photoemission spectroscopy, a technique that uses soft x-rays to measure the distribution in energy and momentum of electrons ejected from a solid through a process known as the photoelectric effect. Their results show values similar to graphene, another high mobility material.

Lastly, the researchers demonstrated that bulk GdTe_3 can be exfoliated into thin flakes composed of only a few

atomic layers. The researchers peeled off layers of this material using Scotch® Tape, a type of micromechanical exfoliation used to collect layers of van der Waals materials. In one such flake, about 22-nm thick, they confirmed that the exfoliated material retained magnetic order and an electron mobility of $5700 \text{ cm}^2\text{V}^{-1}\text{s}^{-1}$ —a value significantly lower than the bulk material, but still higher than black phosphorous of similar thickness. This lower mobility might result from sample degradation due to air exposure, they posit, a scenario that could be prevented through encapsulation.

By optimizing their micromechanical exfoliation, they achieved GdTe_3 flakes as thin as 3.8 nm, about as thick as three monolayers—thus, the researchers say, they’re confident that mono- or bilayer devices of GdTe_3 will be accessible by perfecting their exfoliation technique, enhancing the variety of applications this material could be used for. The researchers add that discovering GdTe_3 ’s magnetic order and high mobility opens numerous exciting opportunities for future studies. — [Christen Brownlee](#)

See: Shiming Lei¹, Jingjing Lin¹, Yanyu Jia¹, Mason Gray², Andreas Topp³, Gelareh Farahi¹, Sebastian Klemenz¹, Tong Gao¹, Fanny Rodolakis⁴, Jessica L. McChesney⁴, Christian R. Ast³, Ali Yazdani¹, Kenneth S. Burch², Sanfeng Wu¹, Nai Phuan Ong¹, and Leslie M. Schoop^{1*}, “High mobility in a van der Waals layered antiferromagnetic metal,” *Sci. Adv.* **6**, eaay6407 (7 February 2020). DOI: 10.1126/sciadv.aay6407

Author affiliations: ¹Princeton University, ²Boston College, ³Max-Planck-Institut für Festkörperforschung, ⁴Argonne National Laboratory

Correspondence: * lschoop@princeton.edu

This work was supported by the National Science Foundation (NSF) through the Princeton Center for Complex Materials, a Materials Research Science and Engineering Center (DMR-1420541). L.M.S. was supported by a Beckman Young Investigator award from the Arnold and Mabel Beckman foundation. L.M.S. and S.L. were additionally supported by a MURI grant on Topological Insulators from the Army Research Office (grant number ARO W911NF-12-1-0461). J.L., T.G., and N.P.O. acknowledge the support from the U.S. Department of Energy (DOE) (contract DE SC0017863). G.F. and A.Y. acknowledge the support of ExxonMobil through the Andlinger Center for Energy and the Environment. M.G. and K.S.B. acknowledge support from the NSF under grant DMR-1709987. A.T. was supported by the DFG (proposal no. SCHO 1730/1-1). Additional support was given by the NSF under grant no. DMR-0703406. A.Y. received funding from DOE-Basic Energy Sciences grant DE-FG02-07ER46419, NSF-MRSEC programs through the Princeton Center for Complex Materials DMR-142054, and NSF-DMR-1904442. This research used resources of the Advanced Photon Source, a U.S. DOE Office of Science User Facility operated for the DOE Office of Science by Argonne National Laboratory under contract no. DE-AC02-06CH11357.

“RIXS” cont’d. from page 33

ulations allowed the researchers to confine a parameter regime in which the extended Kitaev-Heisenberg model reasonably reproduced the main features of the observed magnetic excitations. Hidden Kitaev quantum spin-liquid and Heisenberg phases found in the complex parameter space were used as references in proposing a picture of renormalized magnons as explaining the incoherent nature of the magnetic excitations.

Magnetic excitation spectra were taken at elevated temperatures to follow the temperature evolution of the RIXS dynamic response in the paramagnetic state. Whereas the low-energy excitation progressively diminished as the zigzag order disappeared, the broad high-energy excitation maintained its spectral weight up to a much higher temperature of 160 K. The researchers conjectured that dominant nearest-neighbor interactions kept short-range correlations up to quite high temperatures with a specific short-range dynamics that has a possible connection to a proximate spin-liquid phase. It has been suggested on theoretical grounds that the full continuum of the Majorana fermions of the KQSL can be mapped without interference with flux excitations using spin-conserving RIXS. However, such spin-conserving measurements require two instrumental capabilities that cannot be achieved using a standard (spherical analyzer-based) RIXS spectrometer, as they require high-energy resolution and an efficient scattered x-ray polarization analysis. Recently, a novel flat-crystal RIXS analyzer system was developed at the APS, which provides efficient polarization analysis without compromising its sub-10-meV energy resolution. If successful, spin-conserving RIXS measurements using this system will yield a transparent description of the existence of a proximate KQSL in Na_2IrO_3 . – Vic Comello

See: Jung-ho Kim^{1*}, Jiří Chaloupka^{2,3**}, Yogesh Singh⁴, J. W. Kim¹, B. J. Kim^{5,6}, D. Casa¹, A. Said¹, X. Huang¹, and T. Gog¹, “Dynamic Spin Correlations in the Honeycomb Lattice Na_2IrO_3 Measured by Resonant Inelastic x-Ray Scattering,” *Phys. Rev. X* **10**, 021034 (2020). DOI: 10.1103/PhysRevX.10.021034

Author affiliations: ¹Argonne National Laboratory, ²Masaryk University, ³Indian Institute of Science Education and Research Mohali, ⁴Pohang University of Science and Technology, ⁵Institute for Basic Science

Correspondence: * jhkim@aps.anl.gov,
** chaloupka@physics.muni.cz

J. C. acknowledges support by Czech Science Foundation (GAČR) under Project No. 19-16937S and MŠMT ČR under NPU II Project No. CEITEC 2020(LQ1601). This research used resources of the Advanced Photon Source, a U.S. Department of Energy (DOE) Office of Science User Facility operated for the DOE Office of Science by Argonne National Laboratory under Contract DE-AC02-06CH11357.

“Domain” cont’d. from page 35

Polarized regions are created using a scanning probe microscope in ferroelectric films. The nanoscale spaces between two oppositely polarized areas are called domain walls. Upon applying an electric field, the intervening domain walls can rapidly shift. Taking snapshots of the position of a particular domain wall after applying pulsed electric fields revealed that domain wall movement was 100 to 1000 times slower in the freestanding film versus the originally deposited form (Fig. 2a). The reduction of domain wall speed was unexpected since theory indicated it should actually increase in a strain-free, freestanding film. The researchers attributed the dramatic reduction in wall speed to the induced flexoelectric fields within the film that altered its polarization landscape. The presence of such flexoelectric fields was confirmed by capacitance measurements and numerical simulations. The induced flexoelectric field arose from the pronounced crystallographic tilts caused by thin-film separation, as revealed by the contact mode scanning probe microscopy and x-ray data.

Although wall speed was lowered in the freestanding film, its polarization strength was little changed. The fact that the crystallographic structure and important ferroelectric properties (polarization strength, etc.) were largely preserved in the freestanding PZT film indicates that integrating thin films of complex oxides with silicon is entirely feasible using LTT. However, the researchers note that effects arising from the flexoelectric fields will require additional investigation. – Philip Koth

See: Saidur R. Bakaul^{1*}, Jaegyu Kim², Seungbum Hong², Mathew J. Cherukara¹, Tao Zhou¹, Lilianna Stan¹, Claudy R. Serrao³, Say-eef Salahuddin³, Amanda K. Petford-Long¹, Dillon D. Fong¹, and Martin V. Holt¹, “Ferroelectric Domain Wall Motion in Freestanding Single-Crystal Complex Oxide Thin Film,” *Adv. Mater.* **32**, 1907036 (2020). DOI: 10.1002/adma.201907036

Author affiliations: ¹Argonne National Laboratory, ²Korea Advanced Institute of Science and Technology (KAIST), ³University of California, Berkeley

Correspondence: * sbakaul@anl.gov

Scanning probe microscopy, electronic transport, and sample fabrication carried out at Argonne National Laboratory were supported by the U.S. Department of Energy (DOE) Office of Science-Basic Energy Sciences, Materials Sciences and Engineering Division. Use of the Center for Nanoscale Materials was supported by the U.S. DOE Office of Science-Basic Energy Sciences, under contract No. DE-AC02-06CH11357. Materials growth carried out at the University of California Berkeley was supported by Office of Naval Research Contract No: N00014-14-1-0654. J.K. and S.H. acknowledge support from Brain Korea 21 Plus and KAIST. This research used resources of the Advanced Photon Source, a U.S. DOE Office of Science User Facility operated for the DOE Office of Science by Argonne National Laboratory under Contract No. DE-AC02-06CH11357.

Nematoelastic Coupling Reveals the Nematic Correlation Lengths of Three Fe-Based Superconductors

A growing body of evidence suggests an intimate connection between electronic nematic phases and high-temperature (high- T_c) superconductivity. Actually, nematicity (liquid crystal-like behavior in the form of large quantum fluctuations) is ubiquitous in the electronic phases of high- T_c superconductors, particularly in iron (Fe)-based systems. However, the extent to which there is a causal relationship between nematic fluctuations and superconductivity is currently unclear. Previous research [1] by the principal investigators of the present study showed that transverse acoustic phonons can serve as efficient probes of spatial nematic correlations. The research also went on to show that quantitative analysis of the softening that takes place as the temperature approaches that of the onset of the nematic phase (T_s) can lead to a determination of the nematic correlation length. The present study, based upon research carried out at the APS, extends that previous work.

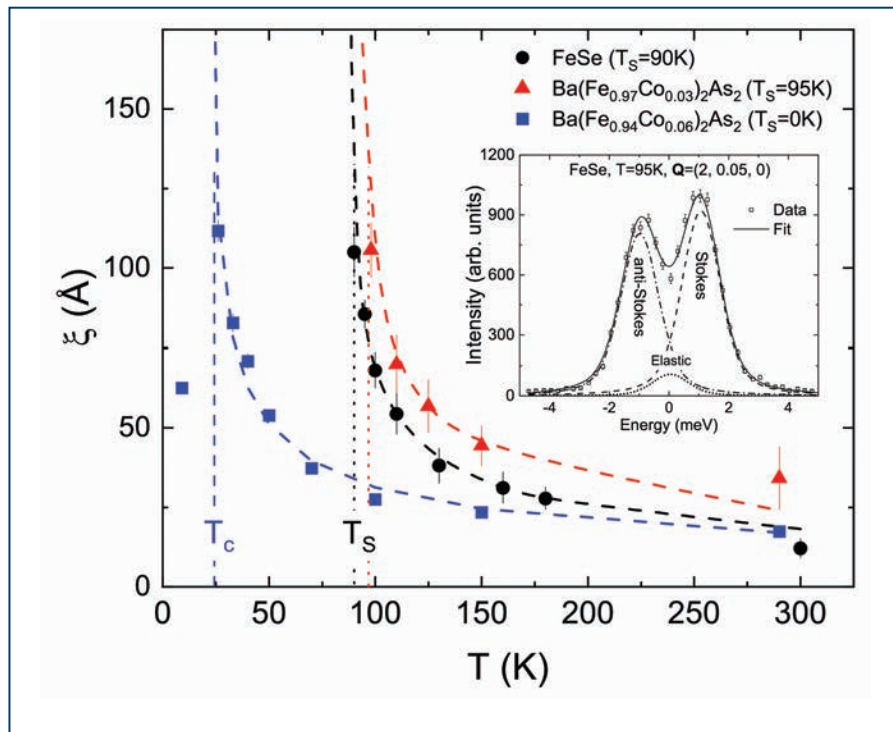


Fig. 1. Nematic correlation length ξ as a function of temperature for FeSe (black circles), for UD Ba-122 (red triangles), and for OP Ba-122 (blue squares). The curved dashed lines are power-law fits of the form $\xi = \xi_0 / (T - T_0)^{1/2}$. Inset: Raw data with fit, and Stokes, anti-Stokes, and elastic peak fits separated.

In the present study, the investigators from the University of Colorado at Boulder, Karlsruhe Institute of Technology (Germany), Laboratoire Léon Brillouin (France), and the University of Minnesota collaborated with scientists from Argonne and the RIKEN SPring-8 Center (Japan) to employ high-brightness x-ray beams in order to broaden their investigation to include a comparison of the temperature dependence of the nematic correlation length ξ for three Fe-based compounds. They used high-resolution inelastic x-ray scattering to extract the temperature-dependent nematic correlation length ξ from the anomalous softening of acoustic phonon modes in FeSe, underdoped Ba(Fe_{0.97}Co_{0.03})₂As₂ (UD Ba-122), and optimally doped Ba(Fe_{0.94}Co_{0.06})₂As₂ (OP Ba-122). The data were gathered on the XSD Inelastic X-ray & Nuclear Resonant Scattering Group's 30-ID-C x-ray beamline at the APS, and the RIKEN BL43LXU beamline at SPring-8.

The researchers found a striking similarity in the behavior of all three compounds, despite their rather different ground states. The values for the nematic correlation length ξ above the superconducting transition temperature T_c were analyzed with a power law fit for ξ versus T using $\xi = \xi_0(T - T_0)^{-\nu}$. The fit allowed the exponent ν to vary freely, yielding values of $\nu = 0.58 \pm 0.06$ for FeSe, $\nu = 0.40 \pm 0.04$ for UD Ba-122, and $\nu = 0.57 \pm 0.07$ for OP Ba-122, with no significant effect on the fit quality or values of T_0 . The values of ν were all close to $1/2$ considering the experimental uncertainty. Thus, the researchers fixed ν at $\nu = 1/2$. In this way, the researchers found that the T dependence of the nematic correlation length ξ in two different families of iron-based compounds and at different regimes (underdoped and optimally doped) was very well described by $(T - T_0)^{-1/2}$ (Fig. 1). In each case, T_0 was found to be very close to the structural transition temperature T_s , which is the temperature at which nematic electronic self-organization prompts a lattice transition to an orthorhombic configuration. Combined with the previously reported Curie-Weiss behavior observed in the nematic susceptibility, the results point to mean-field behavior with fluctuations extending to high temperatures above T_s . The researchers attribute this mean-field behavior to electronic coupling to the lattice—more specifically, to the acoustic phonons.

The observations highlighted the key role played by nematoelastic coupling, which not only changed the character of the nematic transition, but also extended the impact of nematic fluctuations to rather high temperatures above T_s . Such a coupling has been proposed to be detrimental to the enhancement of T_c by quantum critical nematic fluctuations. Whether this explains the observed behavior of T_c across the phase diagram of chemically substituted FeSe_{1-x}S_x, which shows no sizable enhancement upon crossing the nematic quantum critical point, is an interesting topic for future investigation. Moreover, the similarity in nematic correlation length that was observed in FeSe and Ba-122 raises important questions about the interplay between nematicity and magnetism. Although FeSe displays no long-range magnetic order, a strong fluctuating magnetic moment, comparable to that of Ba-122, has been observed experimentally. Whether this is enough to explain the similar behavior of ξ in both compounds is an issue that deserves further study.

– Vic Comello

REFERENCE

- [1] F. Weber, D. Parshall, L. Pintschovius, J.-P. Castellan, M. Kauth, M. Merz, Th. Wolf, M. Schütt, J. Schmalian, R. M. Fernandes, and D. Reznik, "Soft phonons reveal the nematic correlation length in Ba(Fe_{0.94}Co_{0.06})₂As₂," *Phys. Rev. B* **98**, 014516 (2018). DOI: <https://doi.org/10.1103/PhysRevB.98.014516>

See: A. M. Merritt¹, F. Weber², J.-P. Castellan^{2,3}, Th. Wolf², D. Ishikawa⁴, A. H. Said⁵, A. Alatas⁵, R. M. Fernandes⁵, A. Q. R. Baron⁴, and D. Reznik^{1*}, "Nematic Correlation Length in Iron-Based Superconductors Probed by Inelastic X-Ray Scattering," *Phys. Rev. Lett.* **124**, 157001 (2020).

DOI: [10.1103/PhysRevLett.124.157001](https://doi.org/10.1103/PhysRevLett.124.157001)

Author affiliations: ¹University of Colorado at Boulder, ²Karlsruhe Institute of Technology, ³Laboratoire Léon Brillouin, ⁴RIKEN SPring-8 Center, ⁵Argonne National Laboratory, ⁶University of Minnesota

Correspondence: * Dmitry.Reznik@colorado.edu

A. M. M. and D. R. were supported by the U.S. Department of Energy (DOE) Office of Science-Basic Energy Sciences, under Contract No. DE-SC0006939. Theory work (RMF) was supported by the DOE Office of Science-Basic Energy Sciences, under Award No. DE-SC0020045. This research used resources of the Advanced Photon Source, a U.S. DOE Office of Science User Facility operated for the DOE Office of Science by Argonne National Laboratory under Contract No. DE-AC02-06CH11357.

How Tantalum Clustering Leads to Charge Density Wave Lattice Distortions in $2H\text{-TaSe}_2$

The $2H$ (H : hexagonal) polytype of tantalum diselenide ($2H\text{-TaSe}_2$) is an important material, not only because it is an archetypical charge density wave (CDW) system, but also because it may enable future superconducting, optoelectronic, and ultrafast electronic devices. As with any CDW system (an ordered quantum fluid of electrons in a linear chain compound or layered crystal that form a standing wave pattern and can carry an electric current) coupled periodic crystal lattice distortions (PLDs) form as conduction electrons spontaneously configure themselves into standing waves called charge density waves. Although the lattice distortions have received much study at temperatures below the CDW/PLD critical ordering temperature (T_{CDW}), little was known about possible precursor clustering of Ta atoms at higher temperatures that may lead to the PLDs as temperatures drop toward T_{CDW} until researchers using the APS took a detailed look at high-temperature Ta behavior.

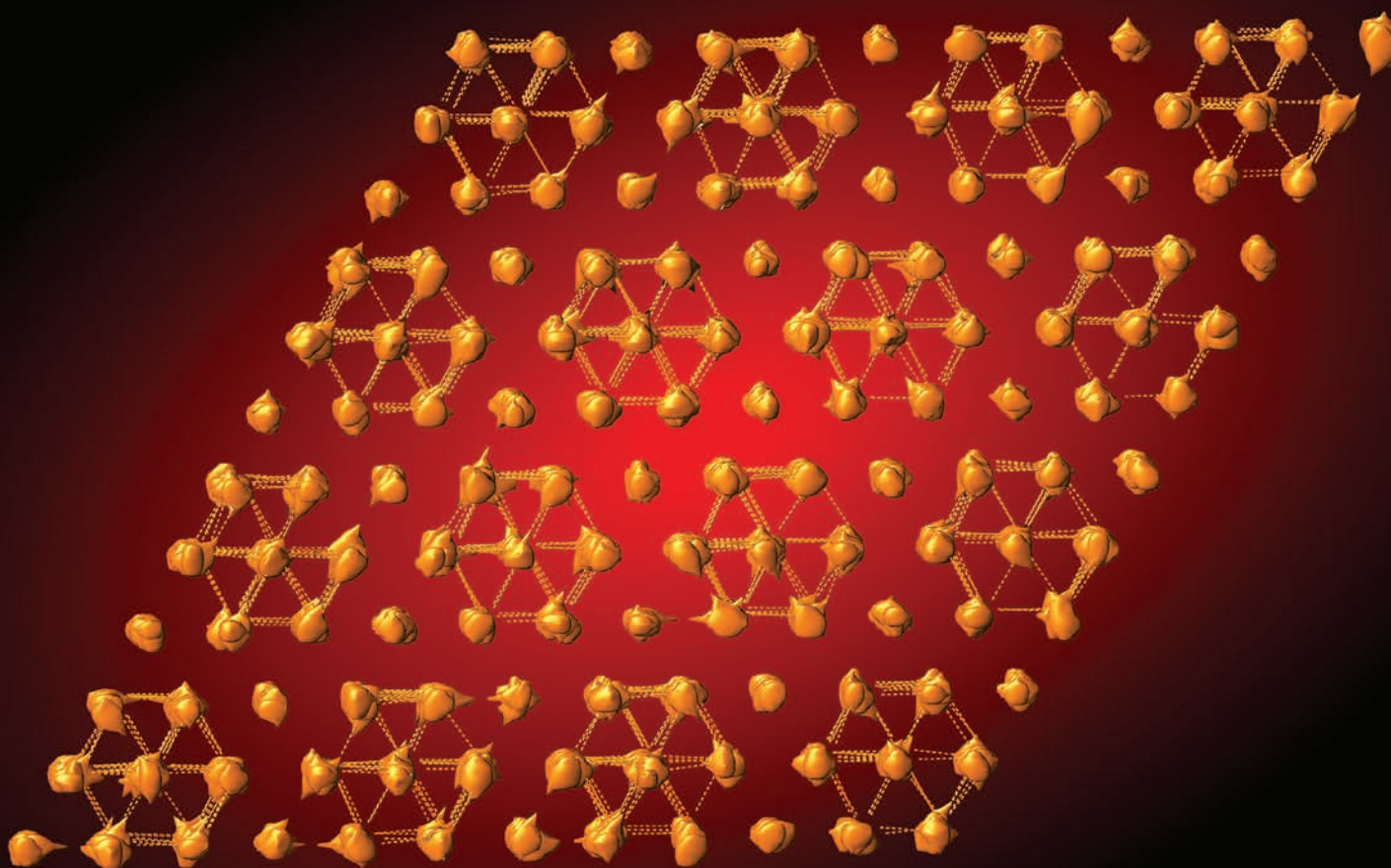


Fig. 1. Spatial density distribution of Ta atoms in the first CDW phase of $2H\text{-TaSe}_2$ obtained by mapping a $120 \text{ \AA} \times 120 \text{ \AA} \times 120 \text{ \AA}$ RMC-refined model (80500 Ta and Se atoms) onto a single Ta plane.

$2H\text{-TaSe}_2$ consists of stacked Ta-Se layers, each consisting of Ta atomic planes sandwiched between two hexagonal Se atomic planes. In a CDW/PLD state of $2H\text{-TaSe}_2$, Ta atoms become displaced from their positions in the undistorted hexagonal lattice, forming a repetitive pattern of small planar clusters. The researchers from Central Michigan University and Argonne studied how these displacements multiplied and grew with decreasing temperature using both conventional and resonant high-energy x-ray diffraction (XRD) as a basis for atomic pair distribution function (PDF) analysis and reverse Monte Carlo (RMC) simulations over the temperatures 400 K to 100 K, concentrating on fine details of the local arrangements of Ta atoms throughout this temperature range.

Two sets of XRD patterns were collected at each temperature. One set of patterns was measured at XSD Materials Physics & Engineering Group's x-ray beamline 1-ID-C at the APS with the detector positioned 1000 mm away from the sample to achieve high wave vector resolution. These patterns were used to perform Rietveld analysis, which indicated the presence of significant positional disorder of the Ta and Se atoms within and between the Ta-Se layers, respectively. The other diffraction patterns were collected with the detector positioned 300 mm away from the sample to reach wave vector values as high as 30 \AA^{-1} . These XRD patterns were used to obtain atomic PDFs having high real-space resolution.

Analysis of the total atomic PDFs derived from the high-energy XRD patterns showed that unusually short Ta-Ta or Se-Se distances already emerged in $2H\text{-TaSe}_2$ near room temperature. To better study these distances, the researchers conducted a resonant high-energy XRD experiment at the K edge of Ta, again at the XSD 1-ID-C beamline. The resulting Ta-differential atomic PDFs doubled the experimental sensitivity to Ta positions, revealing that upon cooling below room temperature, some nearby Ta atoms in $2H\text{-TaSe}_2$ came closer together than their average separation distances in the undistorted crystal structure. To provide a detailed understanding of the character of the apparent clustering of Ta atoms, the researchers built large-scale three-dimensional (3-D) structure models using RMC.

The experimental atomic PDF analysis and large-scale 3-D structure simulations allowed the researchers to uncover fine details of the genesis of the PLDs in the CDW phase of $2H\text{-TaSe}_2$. They found that Ta atoms underwent significant in-plane displacements that brought about un-

usually short Ta-Ta distances already near room temperature. The amplitude and direction of the displacements above T_{CDW} were close to those of the static distortions of Ta planes observed below T_{CDW} . The difference was that the latter formed a 3-D periodic pattern, whereas the former were correlated only over short-range distances, with the correlation length gradually increasing with decreasing temperature. The correlations remained local with decreasing temperature, leading to the formation of small-size Ta clusters at about 200 K. The clusters became distinct and clearly separated from each other at about 150 K. Finally, at 100 K, i.e., below the first T_{CDW} , the clusters were arranged in a periodic superstructure (Fig. 1). Because the bonding distances between atoms in the clusters remained somewhat different, the clusters were not completely aligned with each other, leading to the incommensurability of the emerged first CDW/PLD phase. Upon further cooling, the clusters became nearly perfectly aligned, enabling them to lock into a commensurate superstructure to minimize the elastic energy, leading to the commensurate CDW/PLD phase. Thus, the transition between the normal and CDW/PLD state of $2H\text{-TaSe}_2$ appeared gradual with locally correlated displacements of Ta atoms above T_{CDW} serving as precursors of the PLDs below T_{CDW} .

This result may well explain the emergence of a “precursor” CDW pseudogap in the normal state near room temperature and its smooth evolution into a band gap below T_{CDW} . Specifically, the pseudogap may be due to the locally correlated Ta displacements, and the band gap may be understood as being a consequence of the complete alignment of these displacements into a periodic superstructure. – Vic Comello

See: Valeri Petkov^{1*}, Kamal Chapagain¹, Sarvjit Shastri², and Yang Ren², “Genesis of the periodic lattice distortions in the charge density wave state of $2H\text{-TaSe}_2$,” *Phys. Rev. B* **101**, 121114(R) (2020). DOI: 10.1103/PhysRevB.101.121114

Author affiliations: ¹Central Michigan University, ²Argonne National Laboratory

Correspondence: * petko1vg@cmich.edu

Thanks are due to O. Shovon for the help with the synchrotron XRD experiment. This work was supported by the U.S. Department of Energy (DOE) Office of Science-Basic Energy Sciences under Award No. DE-SC0006877 and used resources of the Advanced Photon Source, a U.S. DOE Office of Science User Facility operated for the DOE Office of Science by Argonne National Laboratory under Contract No. DE-AC02-06CH11357.

Growing the Skinniest Magnets

Iron, nickel, and cobalt are the classic magnetic elements. From them we make everything from the magnets that stick to your fridge to the computer chips in your phone. But in all these familiar applications, the metals are in their bulk, three-dimensional (3-D) forms. A group of researchers used porous metal-organic frameworks to coax nickel, iron, and cobalt to join with the halogens bromine and chlorine in single hexagonal sheets. Experiments performed at the APS helped confirm that these sheets were, indeed, two-dimensional (2-D) molecules of metal halides. The work could lead to much smaller, more powerful computers and other magnetic devices.

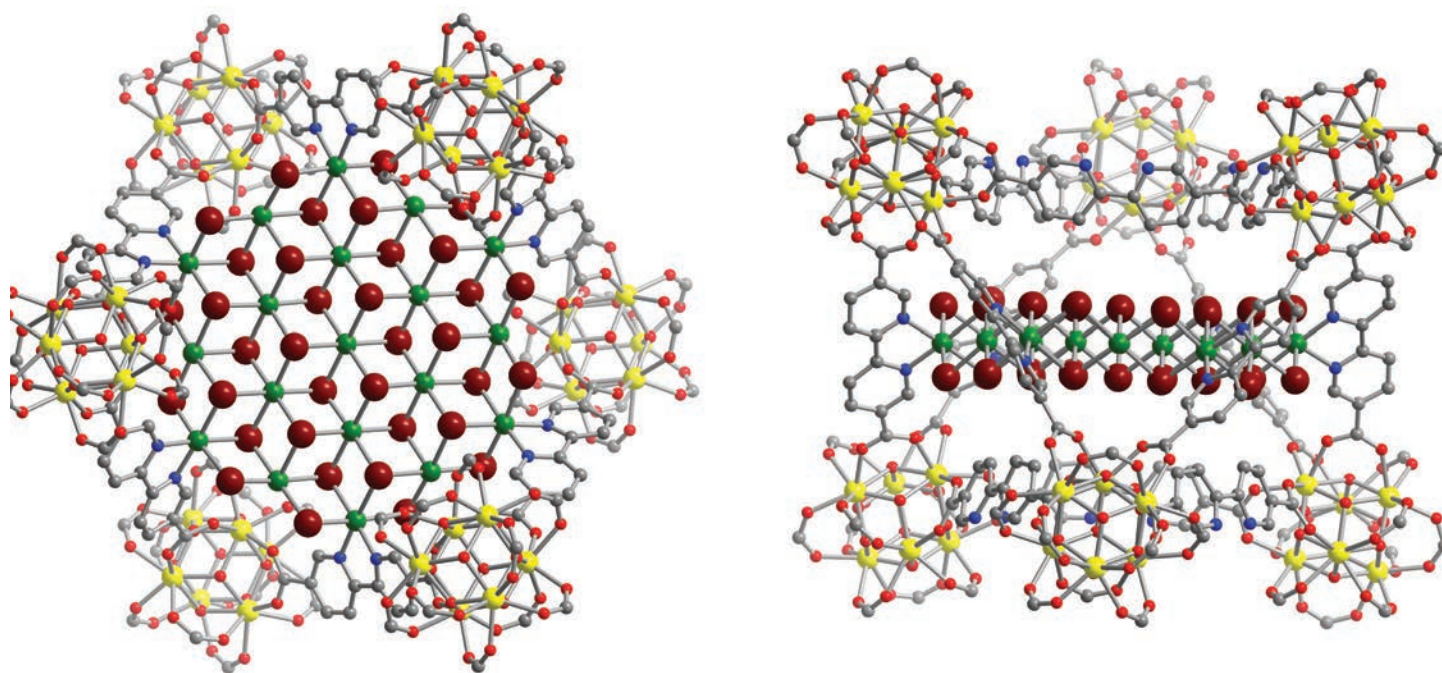


Fig. 1. Atomic structure of $\text{Zr}_6\text{O}_4(\text{OH})_4(\text{bpydc})_6(\text{NiBr}_2)_{15}$ as determined by single-crystal x-ray diffraction. Yellow, green, dark red, red, blue, and grey spheres represent Zr, Ni, Br, O, N and C atoms, respectively. H atoms are omitted for clarity. From M.I. Gonzalez et al., “Confinement of atomically defined metal halide sheets in a metal–organic framework,” *Nature* **577**, 64 (2 January 2020). ©2020 Springer Nature Limited

Many scientists would like to study 2-D transition metal salts such as iron chloride (FeCl_2) and nickel bromide (NiBr_2). But producing these materials has been a challenge. Researchers from the University of California, Berkeley, Lawrence Berkeley National Laboratory, and the Missouri University of Science and Technology invented a novel way of making them. They used metal-organic frameworks made of zirconium bipyridine dicarboxylate as a template for the transition metal halide crystals. The pores of the metal-organic framework had regularly spaced pairs of nitrogen atoms, referred to as pyridine anchoring sites. Nickel, cobalt, or iron atoms attach to those anchoring sites and the sheets of metal halide grow outward from there. The researchers calculated the spacing of the pyridine attachment sites to grow nearly perfect sheets without defects (Fig. 1).

The first metal-halide compound the team grew successfully in this way was the NiBr_2 . The average distance between two nickel atoms in these 2-D sheets, 3.723 Å, matches the average distance between two nickels in the 3-D material, suggesting the structure is very similar.

Nickel chloride (NiCl_2) sheets formed just as well in the bipyridine framework as the NiBr_2 , even though the bond lengths between nickel and chlorine are shorter than those between nickel and bromine. The researchers believe this is because the metal-organic framework is flexible enough to allow the initial metal attachment spots to move and accommodate the tighter lattice. Cobalt and iron chloride also grew using the same framework.

The team used multiple techniques to characterize these 2-D sheets and ensure they'd really made two dimensional sheets of transition metal halides. First, they used beamline 11.3.1 at the DOE's Advanced Light Source to take single-crystal x-ray diffraction snapshots of 2-D crystals of metal halide as they formed. They were able to discern differences in crystal growth between the chlorides and the bromides, but the basic structure was the same: a single layer of metal and halide in a pore.

The team then turned to the XSD Structural Science Group's beamline 17-BM-B of the APS. The extreme brightness of the APS x-rays enable high-quality data, and the beamline scientists have set up 17-BM-B to make it easy to collect high-quality powder diffraction data from diverse materials, according to the research team. This allowed the team to collect x-ray diffraction patterns from the bulk powdered material. The APS data were essential for con-

firming that the same tiny, 2-D hexagonal sheets of metal halide had formed throughout.

The researchers were initially surprised that the metal-organic frameworks with pyridine anchoring sites worked so well. They had planned on testing and tweaking many different crystalline structures to find one that worked.

They were also surprised that the 2-D metal halide sheets had large magnetic moments. The normal, 3-D bulk materials usually need to be polarized with a large magnetic field to have a discernible magnetic moment, otherwise the many layers of metal orient in various directions to cancel each other out. But the lone sheets formed in the nanopores have nothing with which to cancel themselves out.

These tiny molecular magnets could someday store information at a very small scale, leading to faster computing in a smaller device footprint. Currently, most magnetic computer memories operate at scales on the many tens of nanometers, at least an order of magnitude larger than what these two-dimensional sheets of metal halides could do. The next steps will involve exploring how to engineer computer memories at these tiny, molecular sizes.

The APS upgrade will enhance the beamline 11-ID-D to a high-energy x-ray beamline working in the photon energy range between 26 to 120 keV. It will enable fast measurements and extend the range of structural distances measured simultaneously. – Kim Krieger

See: Miguel I. Gonzalez¹, Ari B. Turkiewicz¹, Lucy E. Darago¹, Julia Oktawiec¹, Karen Bustillo², Fernande Grandjean³, Gary J. Long³, and Jeffrey R. Long^{1,2*}, "Confinement of atomically defined metal halide sheets in a metal-organic framework," *Nature* **577**, 64 (2 January 2020). DOI: 10.1038/s41586-019-1776-0

Author affiliations: ¹University of California, Berkeley, ²Lawrence Berkeley National Laboratory, ³Missouri University of Science and Technology

Correspondence: * jrlong@berkeley.edu

This research was supported through a Multidisciplinary University Research Initiatives Program funded by the U.S. Department of Defense, Office of Naval Research, under award N00014-15-1-2681. We thank the U.S. National Science Foundation for providing graduate fellowship support for A.B.T, L.E.D. and J.O. The Advanced Light Source is supported by the Director, Office of Science-Basic Energy Sciences, of the U.S. Department of Energy (DOE) under contract no. DE-AC02-05CH11231. Work at the Molecular Foundry was supported by the Office of Science-Basic Energy Sciences, of the U.S. DOE under contract no. DE-AC02-05CH11231. This research used resources of the Advanced Photon Source, a U.S. DOE Office of Science User Facility operated for the DOE Office of Science by Argonne National Laboratory under Contract No. DE-AC02-06CH11357.

Double-Safe in the Time of the Pandemic: **Paul Rossi**

“It has been a very challenging year as the pandemic has put us in situations that no one ever considered when we created the process for working safely at the APS. We needed to develop, often on the fly, new methods and processes that allowed vital work to happen while putting in the necessary controls that would hopefully prevent the spread of COVID throughout our workforce. The ESH team appreciates all the patience and assistance from staff (both PSC and collaborative access team) as we tackled each new challenge to returning our operational posture while keeping everyone safe.” **Paul Rossi**



Soft Materials and Liquids

Crystals Could Reveal a New Spin on Quantum Physics

Physicists would like to know whether a theorized new state of matter, called a quantum spin liquid, actually exists. They believe the state, which arises at temperatures close to absolute zero, may occur in the mineral herbertsmithite, and are trying to synthesize new materials to look for this ground state. One multi-institution group of researchers using the APS thinks they may have found a rare state very similar to a quantum spin liquid.

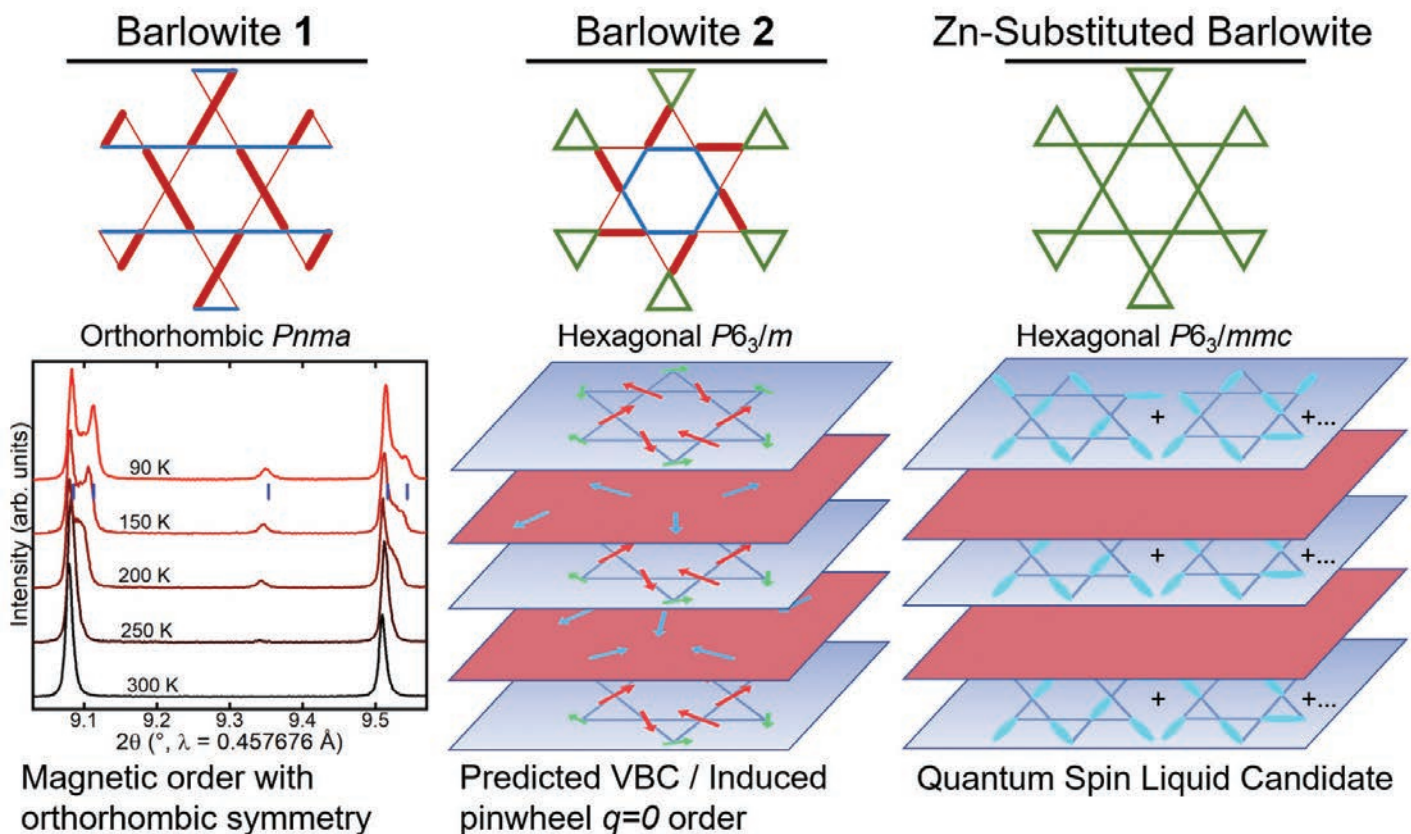


Fig. 1. One version of barlowite with the least symmetrical lattice as shown by x-ray diffraction also has an ordered magnetic structure at extremely low temperatures (left). A second version with only a slight lattice distortion appears to have a valence bond crystal ground state (center), while a third version with zinc added could be a quantum spin liquid (right).

Spin is a quantum mechanical property of electrons, and can be visualized as a pole sticking through a globe. In most ordinary materials, the spins are oriented at random, but in magnetic materials, the spins all align either parallel or antiparallel to each other. In a quantum spin liquid, however, the spins of neighboring electrons line up in opposite directions—one pointing north, the next south—but instead of being frozen in place as in other materials, those spins can continually flip in a correlated manner. Though the material itself isn't a liquid in the traditional sense, the spin correlations can flow back and forth like a liquid.

To investigate, the researchers created four different versions of another copper-containing mineral, barlowite. Two of the versions have almost the same crystalline lattice with just minor distortions, which should result in different low-temperature ground states. Introducing different amounts of zinc into the mix in the other two versions yields a crystalline structure that the scientists believe should result in a quantum spin liquid.

Once they'd synthesized the crystals, the researchers performed single-crystal x-ray diffraction measurements at the ChemMatCARS beamline 15-ID at the APS, which gives detailed information on the position of atoms in the crystalline lattice (Fig. 1). They also did powder x-ray diffraction measurements on powdered crystals at XSD beamline 11-BM at the APS, which is operated by the XSD Structural Science Group. Both beamlines have helium cryostats that allow samples to be reduced to extremely low temperatures, where the magnetic phenomena the researchers are interested in take place.

Combining the measurements, along with similar data gathered at the DOE's Advanced Light Source at Lawrence Berkeley National Laboratory allowed them to draw a picture of structural phase transitions in the compounds. Neutron diffraction measurements at the High Flux Isotope Reactor (HFIR) at the DOE's Oak Ridge National Laboratory and at the Center for Neutron Research at the U.S. Department of Commerce's National Institute of Standards and Technology provided information about the materials' magnetic states, which the researchers then combined with the APS data to see how structure was affecting magnetism.

In one of the two distorted compounds, the researchers think they've found a valence bond crystal, which has a ground state energy very close to that of the spin liquid. Instead of constantly fluctuating magnetic moments like the spin liquid, such crystals have their spins

frozen in place. The zinc-containing versions give hints of having a quantum spin liquid state, although it will take more study to confirm that.

Finding quantum spin liquid materials could lead to other possibilities. If crystals with quantum spin liquid physics are doped with charge carriers, they might become high-temperature superconductors. They also exhibit long-range entanglement, in which the spins of electrons at far ends of the sample can share information with one another. Such distant interaction is very unusual; generally when an electron inside a material is linked to another, it's only with the ones closest to it. Spin liquid crystals also have properties that might make them useful as bits in future quantum computers. Such applications lie many years or decades in the future. – Neil Savage

See: Rebecca W. Smaha^{1,2*}, Wei He^{1,2}, Jack Mingde Jiang^{1,2}, Jiajia Wen¹, Yi-Fan Jiang¹, John P. Sheckelton¹, Charles J. Titus², Suyin Grass Wang³, Yu-Sheng Chen³, Simon J. Teat⁴, Adam A. Aczel^{5,6}, Yang Zhao^{7,8}, Guangyong Xu⁷, Jeffrey W. Lynn⁷, Hong-Chen Jiang¹, and Young S. Lee^{1,2**}, "Materializing rival ground states in the barlowite family of kagome magnets: quantum spin liquid, spin ordered, and valence bond crystal states," *Quantum Mater.* **5**, 23 (2020). DOI: 10.1038/s41535-020-0222-8

Author affiliations: ¹SLAC National Accelerator Laboratory, ²Stanford University, ³The University of Chicago, ⁴Lawrence Berkeley National Laboratory, ⁵Oak Ridge National Laboratory, ⁶University of Tennessee, ⁷National Institute of Standards and Technology, ⁸University of Maryland

Correspondence: * rsmaha@stanford.edu,
** youngsl@stanford.edu

The work at Stanford and SLAC was supported by the U.S. Department of Energy (DOE) Office of Science-Basic Energy Sciences, Materials Sciences and Engineering Division, under contract no. DE-AC02-76SF00515; this includes the synthesis, physical property measurements, neutron scattering, x-ray scattering, and numerical simulations. A portion of this research used resources at the HFIR, a DOE Office of Science User Facility operated by the Oak Ridge National Laboratory. We acknowledge the support of the National Institute of Standards and Technology, U. S. Department of Commerce, in providing the neutron research facilities used in this work. The Advanced Light Source is a DOE Office of Science User Facility under contract no. DE-AC02-05CH11231. ChemMatCARS is supported by the Divisions of Chemistry (CHE) and Materials Research (DMR), National Science Foundation (NSF), under grant number NSF/CHE-1834750. Use of the PILATUS3 X CdTe 1M detector is supported by the NSF under grant number NSF/DMR-1531283. Part of this work was performed at the Stanford Nano Shared Facilities, supported by the NSF under award ECCS-1542152. R.W.S. was supported by the Department of Defense through the NDSEG Fellowship Program and by an NSF Graduate Research Fellowship (DGE- 1656518). This research used resources of the Advanced Photon Source, a U.S. DOE Office of Science User Facility operated for the DOE Office of Science by Argonne National Laboratory under Contract DE-AC02-06CH11357.

Putting the Starch in Tissue-Like Materials

Biological tissues have amazing properties. They can self-heal, identify chemicals, choose which chemicals to allow inside a barrier and which to exclude, they are flexible, and they often have strength that varies depending on the direction of the force applied. Replicating all of these properties in a single synthetic material has proven very difficult. But now, researchers have shown that hydrated starch granules mixed into conventional hydrogels can create tissue-like materials that behave in ways very similar to the extra-cellular matrices in biological tissues. These tissue-like materials can produce unique mechanical properties such as mechanical heterogeneity, trainability, memory, and impact absorption, which are not observed in traditional materials. The scientists in this study used the APS to illuminate the mechanical performance attributed to the synergistic effect at multiple length scales. Materials designed along the same lines as the starch-hydrogel could someday be used to create soft robots and biomedical implants with functionality beyond that of natural systems.

Extracellular matrices are critical to our body's functioning. The fate of a young cell is often determined by the extra cellular matrix supporting it. The matrix that creates the heart is very different from the matrices that creates the brain or a bone, for example. The mechanical properties, chemical transfer and surface functionalities of biological extracellular matrices are complex and difficult to mimic artificially. Many previous attempts to create artificial matrices have failed. In the past, the multiscale characterization for the composite materials usually happens on battery materials.

To better mimic the mechanical properties of biological tissue instead of conventional biomaterials, the team of researchers from the University of Chicago, Northwestern University, Brookhaven National Laboratory, and Argonne report their success at making a remarkable artificial tissue-like material with properties similar to an extracellular matrix with cells, using hydrogel and wheat starch.

Starch is a polymer carbohydrate, essentially a chain of sugar molecules strung together. Polysaccharides ("many sugars"), as starch molecules are often called, are good at bonding to many other molecules, especially water. To make their material, the researchers mixed round granules of starch around 11 μm in diameter into water and then added acrylamide and alginate, two common ingredients of hydrogels. They let the mixture gel, and then began to study its properties. They found that the hydrogel acted like an extracellular matrix supporting "cells" of wheat starch (Fig. 1.)

The hydrogel-starch material has several advantages compared to other polymers that have been tried in the

quest to replicate biological materials. The scale of the starch granules is similar to the scale of living cells. Starch (polysaccharide) chemistry has similarities to the chemistry on the surface of biological cells, which can reach out and grab chemicals of many different sorts, and then either pull them into the cell or exclude them. And most importantly for the researcher's project, the starch-hydrogel's mechanical properties are very similar to living extracellular matrices.

The structure of biological tissue consists of cell granular and extracellular matrix (ECM). The interface between cell and ECM form a strong focal adhesion. Due to the synergistic cooperation between cell and ECM, biological systems show promising dynamic responsiveness, such as impact absorption, mechanical heterogeneity, and trainability. In this work, the researchers investigated the roles of granules and the surround matrix on the dynamic response of hybrid systems. To probe this, the team incorporated the starch granules in synthetic hydrogels to mimic the biological tissues. Interestingly, the scale of the starch granule is like that of the cell; the starch granules could also form strong interactions with the synthetic hydrogels due to the unique surface chemistry of the starch granule.

First, it was possible to coax the starch granules to align in a preferred direction, much like muscle tissue. Alignment makes the material tougher in response to stress from one direction than from others. Besides that, the researchers also discovered the starch hybrid materials can be trained under loading the various strains, which is also similar to muscle tissue. The material was also self-healing, thanks to the ease with which hydrogen bonds pull apart and then reform. The team also found that all

the transitions happened at strain=100% for the first stretch, including modulus jumping, energy dissipation, separation, and mesoscale mechanical heterogeneity, indicating a training threshold of mechanical strain=100% for the first stretch. This training phenomenon is also observed in the microtube system.

But the starch-hydrogel also had a surprising feature—even after it had been stretched to align the starch

granules in a preferred direction, the granules still “remembered” their former random alignment, and would snap back into it if the material was stretched perpendicularly to the alignment direction. This type of memory has rarely been observed in conventional designed biomaterials, but it does happen in natural biological materials such as the actin filaments in muscles.

To ensure that memory property was really acting the way they thought it was, the team used the XSD Time Resolved Research Group's x-ray beamline 7-ID-B at the APS to perform x-ray speckle correlation spectroscopy. Beamline 7-ID-B allowed them to watch the starch-hydrogel as it moved, allowing them to see dynamically how the particles realigned under various different stresses. The instantaneous images allowed the researchers to see exactly how fast, or how slow, the particles froze in certain states. The ability to study dynamic effects in the material was very valuable in understanding this soft substance. The team also used the XSD Imaging Group's beamline 2-BM at the APS to perform x-ray tomography and do three-dimensional reconstructions of the distribution of starch granules while stretching. This allowed the researchers to precisely characterize the relationship between the mesoscale alignment of starch and the macroscale mechanical performance of the material. Nano-computed to-

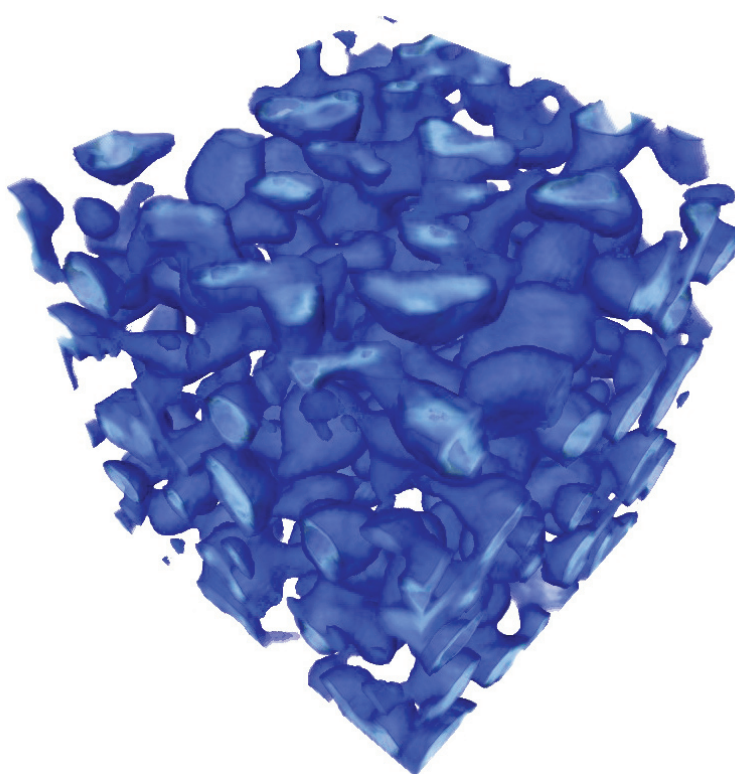


Fig. 1. Reconstructed x-ray tomography data from APS beamline 2-BM showing the irregularly shaped particle contacts within a tissue-like hydrogel-starch material.

mography measurements were carried out with the transmission x-ray microscope at the FXI 18-ID beamline of the National Synchrotron Light Source II at Brookhaven National Laboratory.

Although starch and hydrogels are both relatively common materials, combining them into a system has rarely been done before, and there is much to explore. The team intends to test the material's capabilities next by building a soft, humanized robots.

– Kim Krieger

See: Yin Fang^{1*}, Endao Han¹, Xin-Xing Zhang¹, Yuanwen Jiang¹, Yiliang Lin¹, Jiuyun Shi¹, Jiangbo Wu¹, Lingyuan Meng¹, Xiang Gao¹, Philip J. Griffin¹, Xianghui Xiao^{2,3}, Hsiu-Ming Tsai¹, Hua Zhou², Xiaobing Zuo², Qing Zhang², Miaoqi Chu², Qingteng Zhang², Ya Gao²,

Leah K. Roth¹, Reiner Bleher⁴, Zhiyuan Ma², Zhang Jiang², Jiping Yue¹, Chien-Min Kao¹, Chin-Tu Chen¹, Andrei Tokmakoff¹, Jin Wang², Heinrich M. Jaeger^{1**}, and Bozhi Tian^{1***}, "Dynamic and Programmable Cellular-Scale Granules Enable Tissue-like Materials," *Matter* **2**, 948 (April 1, 2020).

DOI: 10.1016/j.matt.2020.01.008

Author affiliations: ¹The University of Chicago, ²Argonne National Laboratory, ³Brookhaven National Laboratory, ⁴Northwestern University,

Correspondence: * fangyin123@uchicago.edu

** jaeger@uchicago.edu, *** btian@uchicago.edu

This work was supported by the U.S. Office of Naval Research (ONR YIP, N000141612530; PECASE, N000141612958) and the National Science Foundation (NSF MRSEC, DMR 1420709). The work made use of the BioCryo facility of Northwestern University's NUANCE Center, which received support from the Soft and Hybrid Nanotechnology Experimental Resource (NSF ECCS-1542205); the Materials Research Science and Engineering Centers (MRSEC) program (NSF DMR-1720139) at the Materials Research Center; the International Institute for Nanotechnology (IIN); and the State of Illinois, through the IIN. It also made use of the CryoCluster equipment, which received support from the Major Research Instrumentation program (NSF DMR-1229693). This research used resources at the National Synchrotron Light Source II, a U.S. Department of Energy (DOE) Office of Science User Facility operated for the DOE Office of Science by Brookhaven National Laboratory under contract no. DE-AC02-98CH10886. This research used resources of the Advanced Photon Source, a U.S. DOE Office of Science User Facility operated for the DOE Office of Science by Argonne National Laboratory under contract no. DE-AC02-06CH11357.

X-rays Paint a “Grainy” Portrait of Coarsening Soft Materials

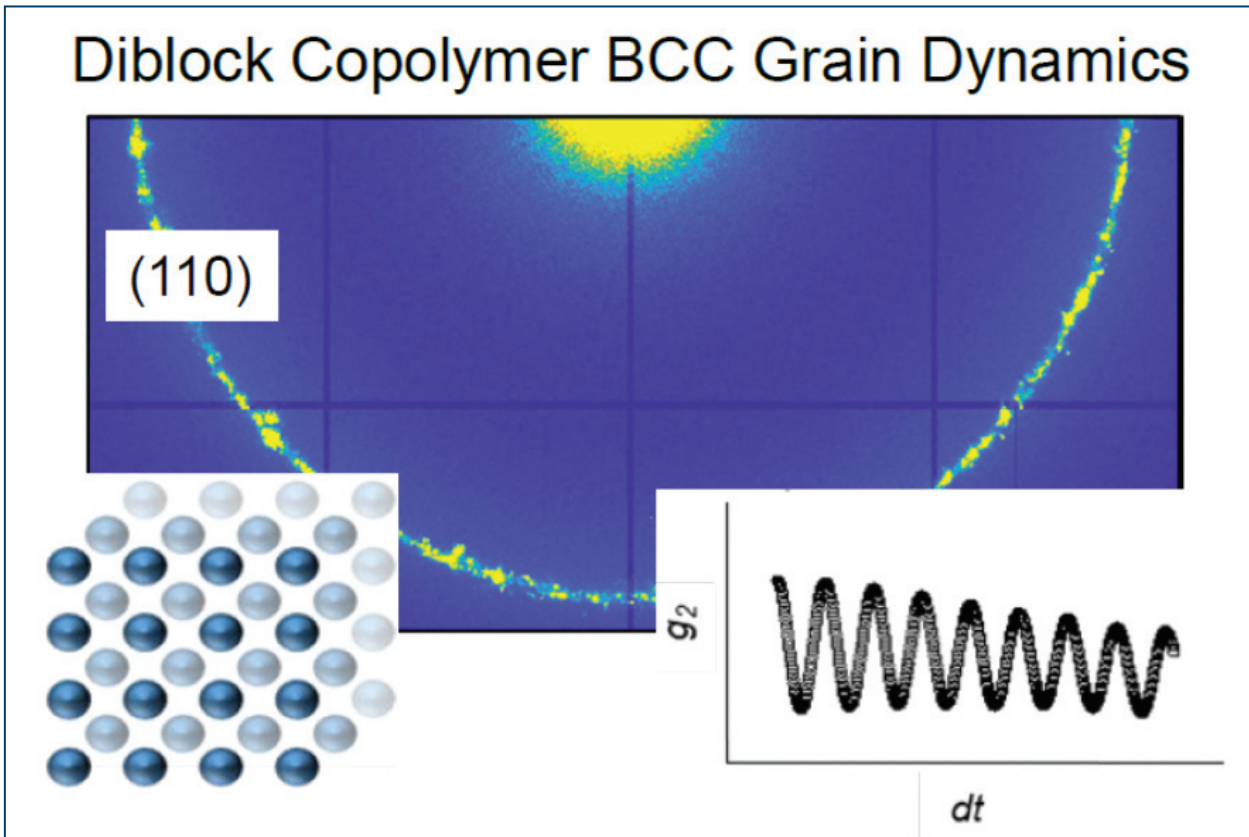


Fig. 1. Background. SAXS powder pattern obtained from BCC phase highlighting the (110) reflection of a PS-PB diblock copolymer. Lower right inset. Heterodyne correlation function obtained at 130° C after annealing sample for approximately 8 h following quench from $T > T_{ODT}$.

Block copolymers are a ubiquitous form of soft matter, with applications as pressure sensitive adhesives, thermoplastics, templating agents in the production of microelectronics, and as drug eluting coatings on cardiovascular stents. A defining feature of this class of polymers is their ability to spontaneously form exquisitely ordered structures with nanoscale periodicities, including micelles in compositionally asymmetric diblock copolymers that pack on a body-centered cubic (BCC) lattice. Elucidating the molecular scale dynamics that govern the properties of these materials is necessary for commercial applications, but challenging due to spatiotemporal limitations of conventional instrumentation. A model poly(styrene)-block-poly(1,4-butadiene) (PS-PB) diblock copolymer was prepared by anionic polymerization and shown by synchrotron small-angle x-ray scattering (SAXS) carried out at the APS to comprise spherical micelles ordered on a BCC lattice with an order-disorder transition temperature (T_{ODT}) of 153° C, at which the supramolecular crystal melts. These findings are critical to our understanding of nucleation and growth dynamics, which underlie the desired properties and use of soft and hard materials in a variety of applications, including those mentioned above.

The team used the XSD Dynamics & Structure Group's 8-ID-I beamline at the APS. They employed x-ray photon correlation spectroscopy (XPCS) to assess the particle scale dynamics associated with scattering from (110) planes during grain growth following rapid quenches in temperature from $T > T_{\text{ODT}}$ to a series of temperatures between 120° C and 145° C (Fig 1). A new analytical framework was used to azimuthally split the primary scattering arc into 750 bins of detector pixels, and each bin was correlated through time. The autocorrelation functions were categorized, and dynamic information was extracted according to corresponding mathematical routines. Individual experiments were conducted in this way many times over the course of nucleation and growth of the BCC polycrystal, thus enabling a time-resolved perspective of this process. Long after the nucleation and initial growth of the polycrystalline BCC structure, we observed a temperature-independent structural relaxation mode that is associated with grain rotation during coarsening. Additionally, definitive evidence of internally referenced heterodyne correlations (see illustration inset) enabled quantitative extraction of particle speeds in these samples, ranging from 0.001 nm/s to 1.5 nm/s, which are attributed to grain boundary migration and cooperative particle movement.

The XPCS setup enabled high spatial resolution at wavevectors that were commensurate with the BCC lattice

constant while providing precise temperature control, features that were specifically beneficial to this study. This work highlights the power of XPCS at the APS in revealing nanoscale dynamics in block copolymers and other ordered and disordered soft materials, while highlighting potential microstructural analogies to metallic materials with related crystalline order.

The upgrade of the APS source will enhance coherent flux by 2 orders of magnitude resulting in a concomitant increase in the XPCS capabilities for studying dynamics in soft and hard condensed matter. – Frank Bates

See: Ronald M. Lewis, III¹, Grayson L. Jackson², Michael J. Maher¹, Kyungtae Kim¹, Suresh Narayanan³, Timothy P. Lodge¹, Mahesh K. Mahanthappa^{1*}, and Frank S. Bates^{1**}, "Grain Growth and Coarsening Dynamics in a Compositionally Asymmetric Block Copolymer Revealed by X-ray Photon Correlation Spectroscopy," *Macromol* **53**, 8233 (September 17, 2020). DOI: 10.1021/acs.macromol.0c01676

Author affiliations: ¹University of Minnesota, ²University of Wisconsin–Madison, ³Argonne National Laboratory

Correspondence: ** bates001@umn.edu, * maheshkm@umn.edu

Support for this work was provided by the National Science Foundation under Grants DMR-1801993 (R.M.L., M.J.M., K.K., and F.S.B.), CHE-1608115 and CHE-1807330 (G.L.J. and M.K.M.). This research used resources of the Advanced Photon Source, a U.S. Department of Energy (DOE) Office of Science User Facility operated for the DOE Office of Science by Argonne National Laboratory under Contract No. DE-AC02-06CH11357.

Finding the Recipe for Protein-Based Drugs

Pharmaceutical companies are increasingly using monoclonal antibodies (a type of protein made in the laboratory that can bind to substances in the body, including cancer cells) and other proteins instead of the more traditional small molecules to make drugs. Such drugs are usually stored in solutions and administered from a bag for an intravenous drip or in a preloaded syringe. That presents an opportunity for the proteins to accumulate at the air-water interface, where they can form films and lose therapeutic efficacy. Drug manufacturers often add surfactants to the solution to create a barrier between air and water, preventing the proteins from adsorbing to the interface, but they have no good way to know just how much surfactant is necessary. Now researchers using the APS have shown that they can define the lowest concentration of surfactant needed to protect the antibodies.

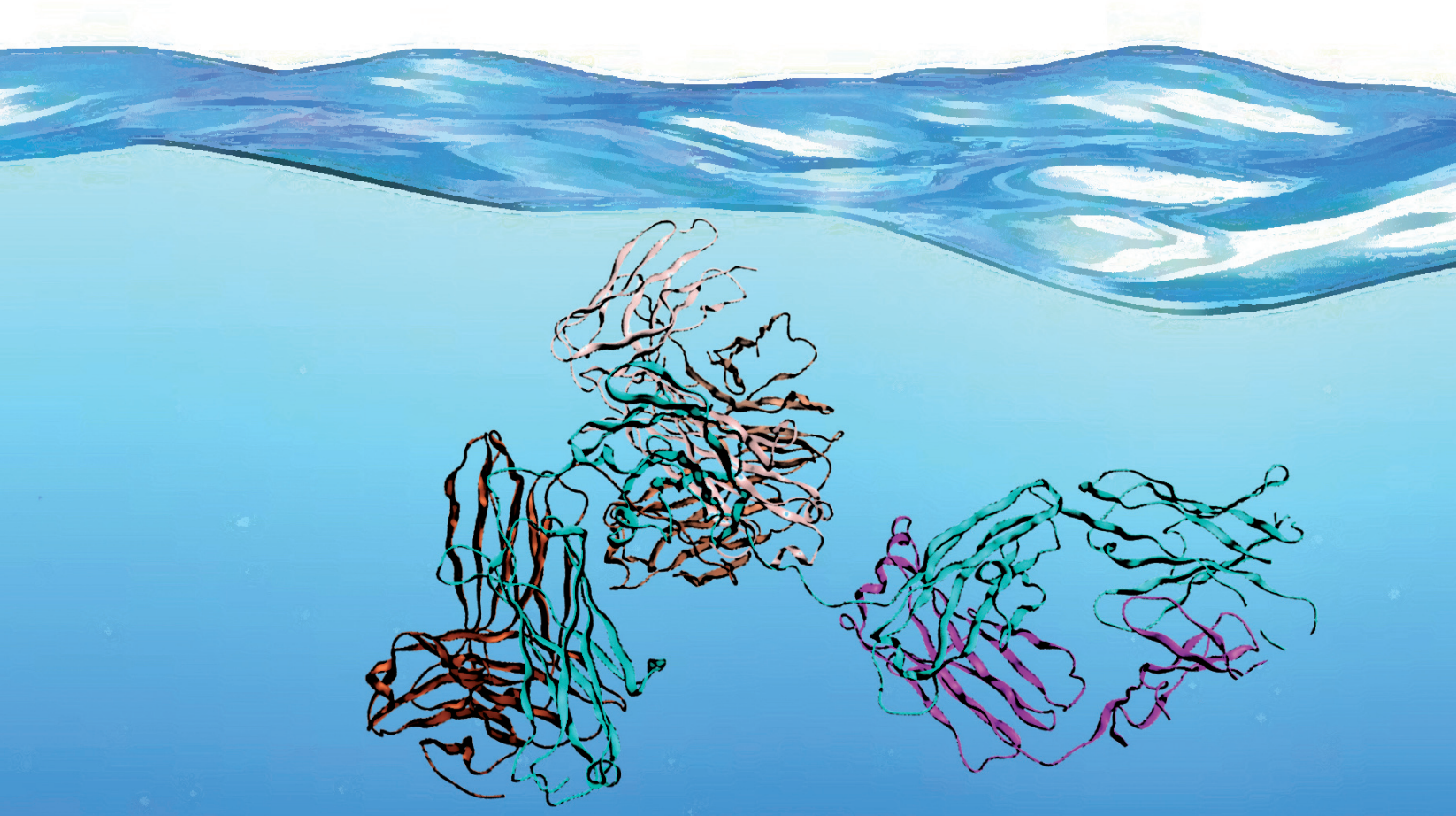


Fig. 1. Antibodies, with four domains represented by different colors, can move to the interface between air and water.

Different antibodies have different amounts and arrangements of amino acids resulting in different aversions to combining with, or dissolving in, water. Those differences make some antibodies accumulate at the surface of the liquid faster than others. They also affect how the molecules behave on the surface—often unfolding, and then sometimes aggregating with others to form a film. As it turns out, those differences also lead to a variation in the minimum concentration of surfactant required.

The team of researchers from The City College of New York and Bristol-Myers Squibb used two types of antibodies, labeled 1 and 2 (Fig. 1). For the surfactant they chose polysorbate-80, which is commonly used by the pharmaceutical industry. In separate trials, they added only surfactant to the water, each of the proteins alone, or both surfactant and protein at varying concentrations. They measured the surface tension of the mixtures over time to define a general picture of how fast the various molecules made it to the surface, but couldn't identify whether antibodies or surfactant dominated at the interface.

To get a deeper understanding, the researchers, with colleagues from The University of Chicago, performed x-ray reflectivity measurements at the ChemMatCARS x-ray beamline 15-ID-C at the APS. Each type of molecule at the surface reflects the x-rays differently with changing angles, allowing researchers to distinguish which component is at the interface. This is one of the few x-ray beamlines in the world that has a liquid-air reflectometer with a high-power x-ray. Once again, the team measured the antibodies and the surfactant separately, and then mixtures of both at varying concentrations.

It turned out that, for antibody 1, the concentration of polysorbate-80 had to be high enough for it to form micelles—aggregates of surfactant molecules—to prevent the antibody from collecting on the surface. For antibody 2, however, the concentration of surfactant had to be only one fifth that amount to be effective. The difference lies in the spatial aggregation propensity of each antibody, a measure of the antibody's hydrophobicity. In other words,

the researchers found that knowing the structure of a protein allows them to predict the minimum concentration of surfactant they need.

Whether too high a concentration of surfactant in formulations for drug delivery would be a problem is an open question, but it could be that an overabundance could block the antibody's binding sites and render it ineffective.

The scientists were concerned that the proteins might form multiple layers at the surface, creating a thick film, but the experiments showed that wasn't the case. They also discovered that even if the proteins reached the surface first, the surfactant could displace them if it were at a high enough concentrations.

Further studies will look at other surfactants and other proteins to understand how general the results are. Scientists would also like to learn more about how the protein molecules unfold at the air-water interface, what characteristics of the protein or solvent drives that unfolding, and how long it takes for the unfolding to become irreversible.

– Neil Savage

See: Ankit D. Kanthe¹, Mary Krause², Songyan Zheng², Andrew Ilott², Jinjiang Li², Wei Bu³, Mrinal K. Bera³, Binhua Lin³, Charles Maldarelli^{1*}, and Raymond S. Tu^{1**}, “Armoring the Interface with Surfactants to Prevent the Adsorption of Monoclonal Antibodies,” *ACS Appl. Mater. Interfaces* **12**, 9977 (2020).

DOI: 10.1021/acsami.9b21979

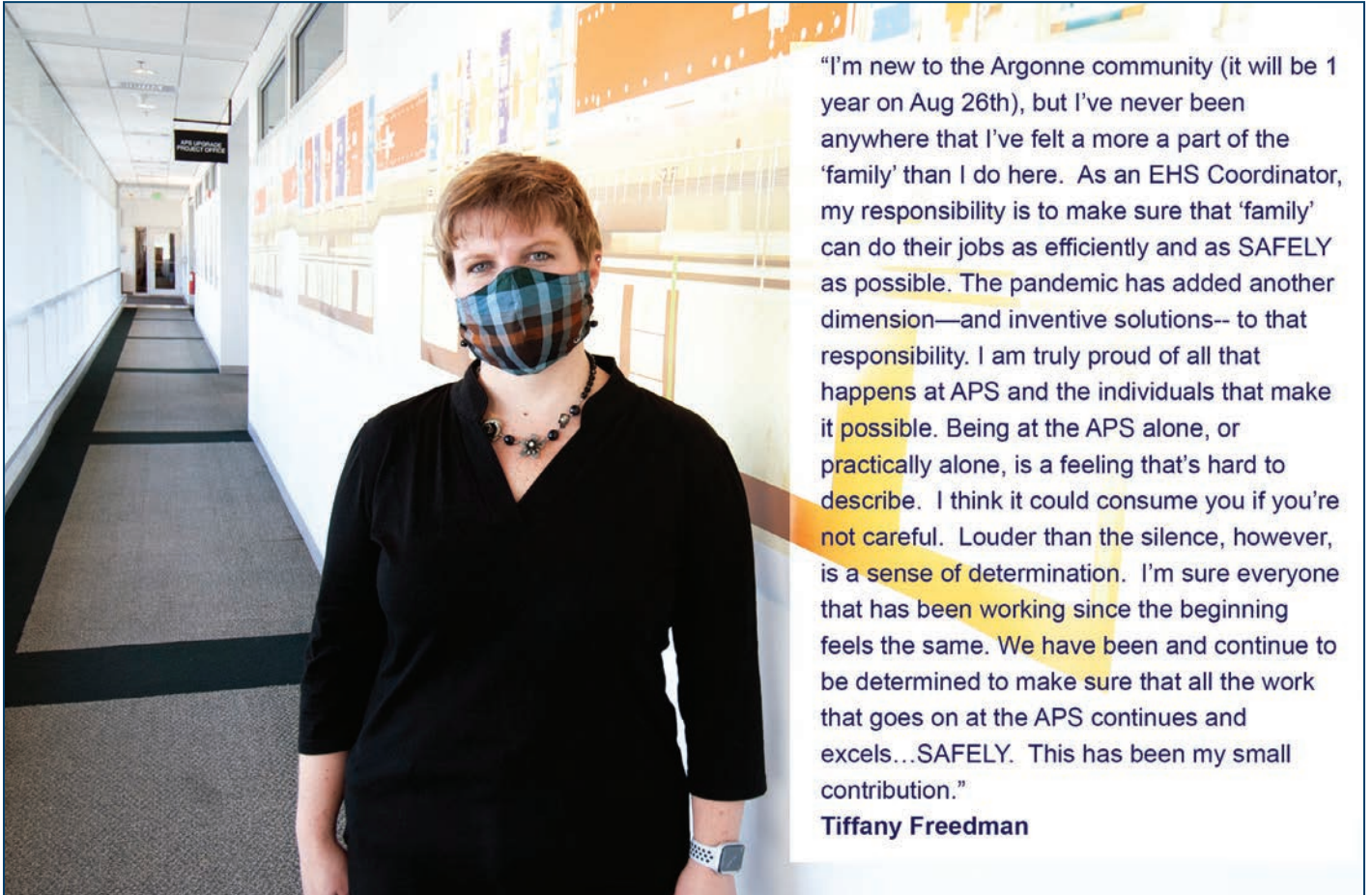
Author affiliations: ¹The City College of New York, ²Bristol-Myers Squibb, ³The University of Chicago

Correspondence: * cmaldarelli@ccny.cuny.edu,

** tu@ccny.cuny.edu

We acknowledge the financial support from Bristol Myers Squibb Co. ChemMatCARS is principally supported by the Divisions of Chemistry (CHE) and Materials Research (DMR), National Science Foundation (NSF), under grant number NSF/CHE-1834750. C.M. and R.S.T. thank Dr. Joe Strzalka, Beamline Scientist, Sector 8, APS, for his insights on the modeling of the x-ray reflectivity data. R.S.T. thanks the support of the NSF under Grant No. 1605904. This research used resources of the Advanced Photon Source, a U.S. Department of Energy (DOE) Office of Science User Facility operated for the DOE Office of Science by Argonne National Laboratory under Contract DE-AC02-06CH11357.

Double-Safe in the Time of the Pandemic: Tiffany Freedman



"I'm new to the Argonne community (it will be 1 year on Aug 26th), but I've never been anywhere that I've felt a more a part of the 'family' than I do here. As an EHS Coordinator, my responsibility is to make sure that 'family' can do their jobs as efficiently and as SAFELY as possible. The pandemic has added another dimension—and inventive solutions-- to that responsibility. I am truly proud of all that happens at APS and the individuals that make it possible. Being at the APS alone, or practically alone, is a feeling that's hard to describe. I think it could consume you if you're not careful. Louder than the silence, however, is a sense of determination. I'm sure everyone that has been working since the beginning feels the same. We have been and continue to be determined to make sure that all the work that goes on at the APS continues and excels...SAFELY. This has been my small contribution."

Tiffany Freedman

Chemical Science

Catalytic Magic

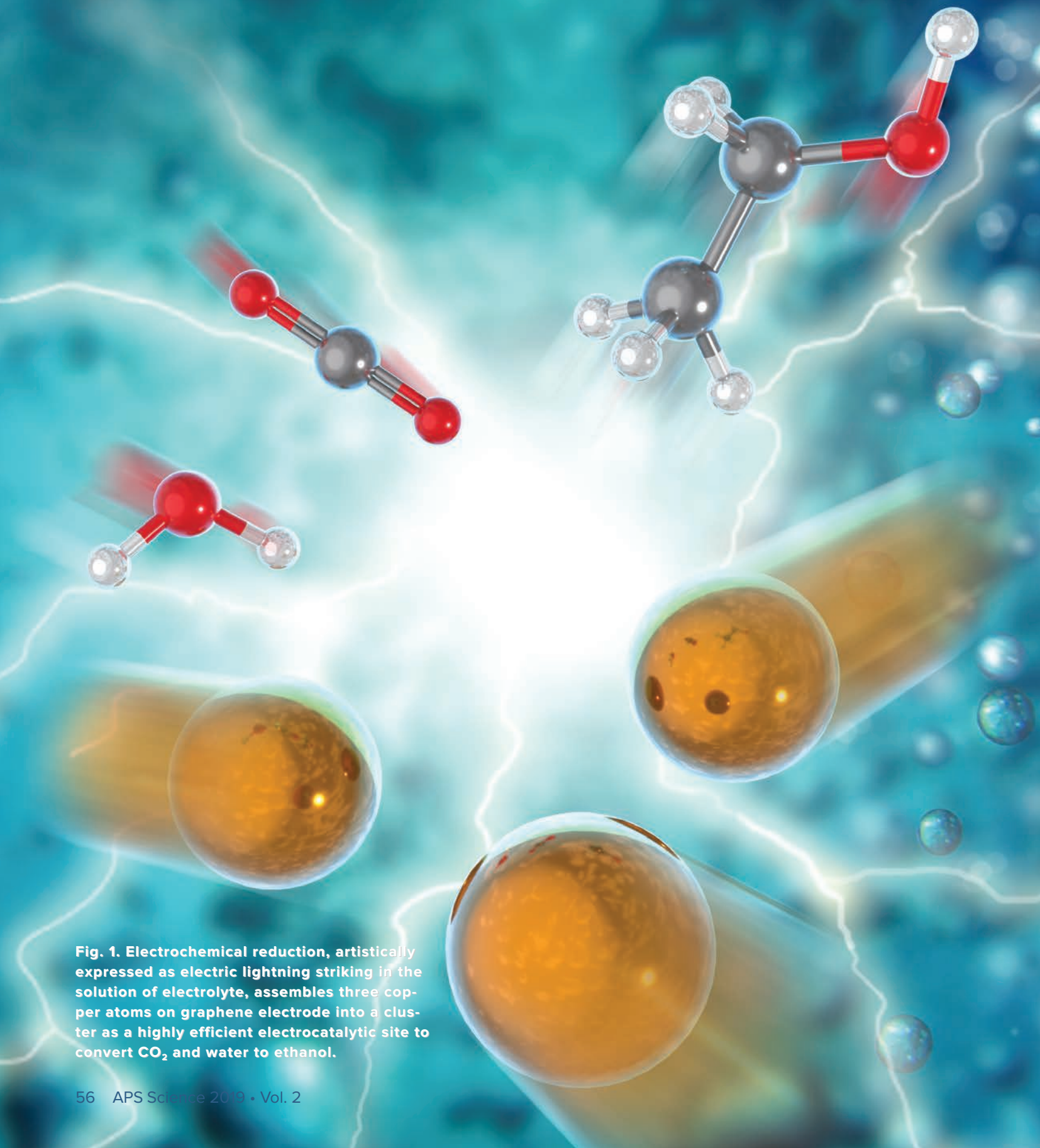


Fig. 1. Electrochemical reduction, artistically expressed as electric lightning striking in the solution of electrolyte, assembles three copper atoms on graphene electrode into a cluster as a highly efficient electrocatalytic site to convert CO_2 and water to ethanol.

Converting carbon dioxide and water into ethanol efficiently and cheaply could reduce the amount of CO₂ that is released into the atmosphere. So researchers seek to develop new electrocatalysts to assist with this chemical reaction, a technological leap that could lead to new methods for converting CO₂ into a wide array of value-added chemicals. By using renewable energy sources to power the reactions, this technology will reduce atmospheric greenhouse gas emissions and bring us one big step closer to a circular economy. For this work, the researchers designed a novel catalyst to break down CO₂ with maximum efficiency. These catalysts have a supporting structure of carbon with a group of copper atoms. The structural characterization was performed using the APS and the Argonne Center for Nanoscale Materials (CNM).

Carbon dioxide is abundant and, as an atmospheric greenhouse gas, helps to keep Earth warm. One goal of forward thinkers is creating a circular economy, in which waste is turned into useful products and the use of new resources is minimal. Instead of being lost to the atmosphere, where it will increase warming, CO₂ can be transformed into other hydrocarbons, such as ethanol, which in the U.S. is mixed with gasoline to raise the octane rating and reduce carbon emissions. Ethanol also is an important intermediate product in the chemical, pharmaceutical, and cosmetics industries. However, CO₂ molecules are extremely stable, so breaking them apart is energy intensive and costly. For CO₂ breakdown to be more efficient, researchers are searching for new catalysts, which increase the rate of chemical reactions with no permanent change to its own chemistry and are commonly used in industrial processes, including in the manufacture of more than 80% of products.

In these experiments, which were designed to investigate the local environment around the copper atoms in the carbon-supported copper samples, the catalyst was stable over an extended operation at low voltage. Using the high photon flux of the x-ray beams at the XSD Chemical & Materials Science Group's 12-BM and XSD Spectroscopy Group's 20-BM bending magnet beamlines of the APS to perform x-ray absorption spectroscopy with *operando* x-ray absorption near-edge structure and extended x-ray absorption fine structure experiments, the researchers observed structural changes in the catalyst. The dispersed copper atoms became energized and formed tiny clusters of three copper atoms under the electrochemical potential, a reaction that was reversible. The carbon-supported copper catalysts broke down the CO₂ and water molecules, then reassembled them into ethanol (CH₃CH₂OH) (Fig. 1). The catalyst structure was confirmed by scanning transmission electron microscopy (STEM) studies at the CNM.

This reaction had very high energy efficiency and low cost. Indeed, the Faradaic efficiency—the efficiency with which electrons are transferred in a system facilitating an

electrochemical reaction—was extremely high at more than 90%. The efficiency of the process decreased when CuO and the large Cu clusters became dominant.

These researchers have found a path to electrochemically convert the CO₂ emitted from industrial processes, such as fossil fuel power plants or alcohol fermentation plants, into valuable commodities at reasonable cost. Most ethanol currently comes from corn, which is extremely inefficient and produces large amount of CO₂. The technique described here will make ethanol production more efficient and less costly.

Although further research is needed to determine how to scale-up the reaction, this catalyst is the first of what likely will become a long series of catalysts developed to turn CO₂ into useful chemicals. Researchers have already used this approach to create different catalysts that are all were highly efficient at converting CO₂ to other hydrocarbons. The team plans to work with industry partners to advance this promising technology.

– Dana Desonie

See: Haiping Xu^{1,2}, Dominic Rebollar^{1,2}, Haiying He³, Lina Chong¹, Yuzi Liu¹, Cong Liu^{1*}, Cheng-Jun Sun¹, Tao Li^{1,2**}, John V. Muntean¹, Randall E. Winans¹, Di-Jia Liu^{1,4***}, and Tao Xu^{2****}, “Highly selective electrocatalytic CO₂ reduction to ethanol by metallic clusters dynamically formed from atomically dispersed copper,” *Nat. Ener.* **5**, 623 (August 2020).

DOI: 10.1038/s41560-020-0666-x

Author affiliations: ¹Argonne National Laboratory, ²Northern Illinois University, ³Valparaiso University, ⁴The University of Chicago

Correspondence: * congliu@anl.gov, ** taoli@aps.anl.gov, *** djliu@anl.gov, **** txu@niu.edu

This material is based on work supported by Laboratory Directed Research and Development funding from Argonne National Laboratory, provided by the Director, Office of Science, of the U.S. Department of Energy (DOE) under contract no. DE-AC02-06CH11357. The works performed at Argonne National Laboratory's Center for Nanoscale Materials and APS, U.S. DOE Office of Science User Facilities, are supported by Office of Science, U.S. DOE, under contract no. DE-AC02-06CH11357. Part of the DFT calculations were also performed using the computational resources provided by the Laboratory Computing Resource Center at the Argonne National Laboratory. T.X. acknowledges the financial support from the X-ray Science Division visiting scientist program at the APS. C.L.'s work is supported by the U.S. DOE Office of Science-Basic Energy Sciences, Division of Chemical Sciences, Geosciences and Biosciences, under contract no. DE-AC02-06CH11357.

A Deeper Look into Bio-Inspired Catalysts

Developing hydrogen as a fuel is important for both economic and environmental reasons. This work studied the sulfur-rich environment in active hydrogenase enzymes by synthesizing nickel (Ni)-based proton reduction catalysts bearing sulfur-rich tetradentate ligands and pentadentate ligands (ligands that bind with four and five donor atoms to a central atom to form four and five chemical bonds, respectively). Photocatalytic studies with a variety of research techniques—including time-resolved ultraviolet-visible spectroscopy and time-resolved x-ray absorption spectroscopy at the APS—revealed electronic and structural changes in the photocatalytic system. Kinetic analyses of the photo-reduced Ni species revealed differences in charge-separation dynamics; complementary techniques paved the way to a mechanistic pathway for the photocatalytic cycle. This work, published as a “Hot Paper” in *Chemistry—A European Journal*, advances our understanding of the charge-separation dynamics that occur in bio-inspired photocatalytic systems for the hydrogen evolution reaction. While it sheds light on the fundamental implications of catalyst-design strategies for more efficient water reduction processes, more in-depth investigations will unravel the rate-limiting steps of this artificial catalytic system and also of natural enzymatic processes.

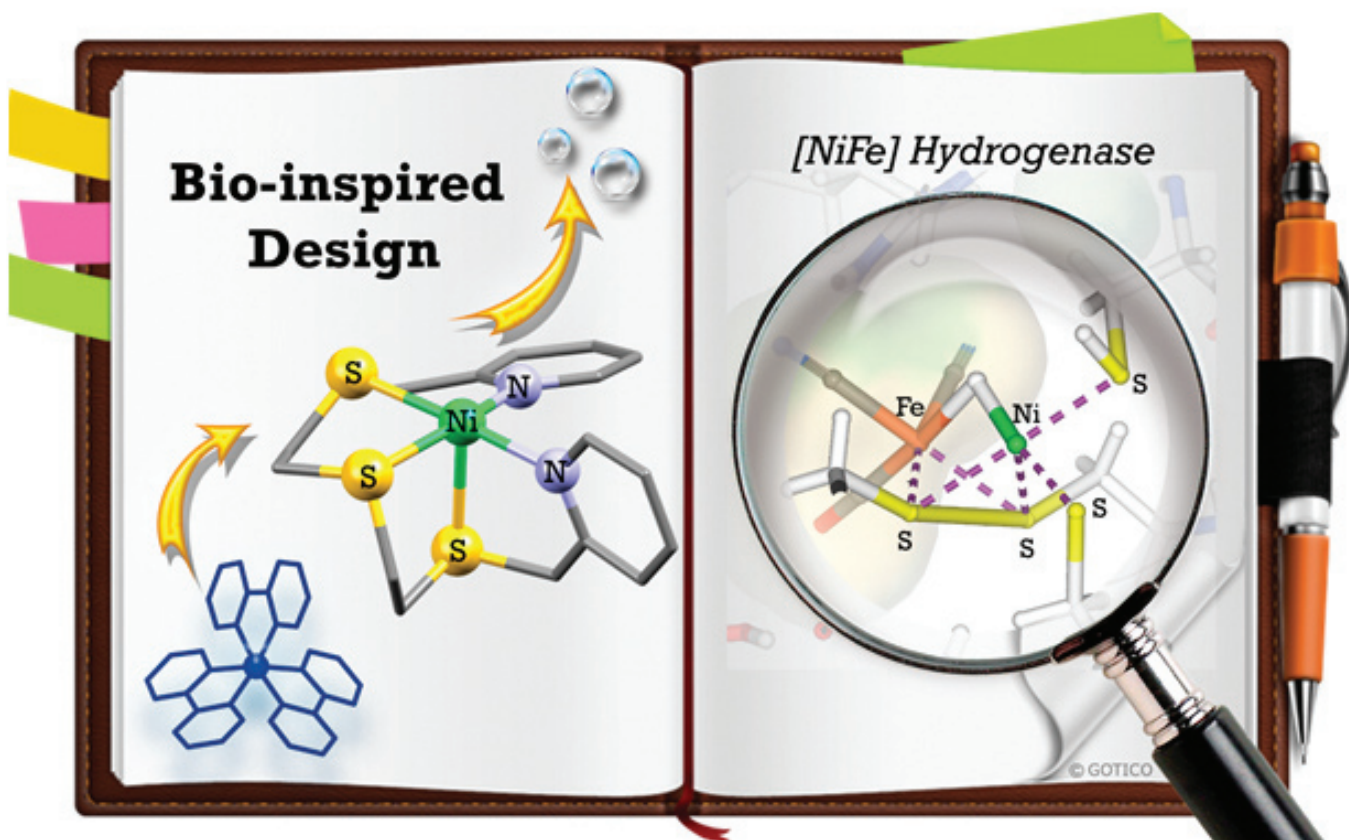


Fig. 1. Bio-inspired, Ni-based proton reduction catalyst with a pentadentate ligand improved photocatalytic activity.

Hydrogen is abundant, and can be produced, stored, and distributed cleanly. While traditionally CO₂-intensive processes are used to extract hydrogen from fossil fuels, solar power can cleanly extract hydrogen from water. A catalyst will boost the reaction while lowering its energy requirements. The challenge is to develop catalysts that are efficient, selective, stable, and also inexpensive.

Bio-mimetic and bio-inspired catalysts imitate active enzyme sites. Hydrogenases are enzymes that can transform protons from water into molecular hydrogen efficiently. However, the use of hydrogenases is hindered because they are unstable. Artificial-enzyme mimics are easier to produce and control.

These enzymes are made of a nickel atom (cheap and abundant) surrounded by sulfur atoms, which stabilize the low oxidation states of the metal needed for hydrogen production. To mimic these characteristics, the researchers in this study synthesized artificial catalysts containing a central nickel atom surrounded by a differing number of sulfur atoms: one with two sulfur atoms and another with three. Because the number of atoms attached to the nickel are different, their coordination spheres and geometries are also different.

The researchers studied these differences to determine how they affect the enzymes' catalytic performances. They were particularly interested in the mechanisms of photo-induced electron-transfer under catalytic conditions to determine how best to maintain efficient catalytic activity for proton reduction. To understand the rate-determining step, they studied the photocatalytic route by capturing the spectral features of the intermediate species that are transiently formed. Photo-irradiation induces important electronic and structural changes in Ni species, which can be described using x-ray-based spectroscopic techniques. The researchers used time-resolved x-ray absorption spectroscopy to collect data at the XSD Time Resolved Research Group's 11 ID-D x-ray beamline at the APS, together with x-ray absorption near edge structure and extended x-ray absorption fine structure analysis at the XSD Spectroscopy Group's beamline 9-BM, also at the APS.

The photocatalytic investigation of the system composed of the Ni catalyst, ruthenium photosensitizer, and

ascorbate electron donor showed that the pentadentate ligand was critical for the improved efficiencies of proton reduction. This is in accordance with optical transient absorption studies that show distinct kinetic differences in the charge-separation dynamics between the pentadentate and tetradentate forms. For the pentadentate catalyst, complementary spectroscopic and density functional theory analyses revealed the transformation of the Ni (II) catalyst to a metal-centered reduced form of Ni (I) species with a distorted square-bipyramidal geometry (Fig. 1).

This first photo-induced electron transfer may not be the rate-determining step. Electrochemical characterization showed that the catalytic activity begins with the formation of a doubly reduced Ni species. This second electron transfer is likely coupled to proton transfer for the proton reduction activity. The pyridine donor in the ligand can be knocked off the metal center, providing a free base to dock a proton. Further protonation leads to a Ni (II) hydride species, which may react intramolecularly with the proton on the pyridine unit to form molecular hydrogen.

– Dana Desonie

See: Philipp Gotico¹, Dooshaye Moonshiram^{2**}, Cunming Liu³, Xiaoyi Zhang³, Régis Guillot⁴, Annamaria Quaranta¹, Zakaria Halime⁴, Winfried Leibl¹, and Ally Aukauloo^{1,4*}, "Spectroscopic Characterisation of a Bio-Inspired Ni-Based Proton Reduction Catalyst Bearing a Pentadentate N2S3 Ligand with Improved Photocatalytic Activity," *Chem. Eur. J.* **26**,285 (2020).

DOI:10.1002/chem.201904934

Author affiliations: ¹Institut des Sciences du Vivant Frédéric-Joliot, ²Instituto Madrilenio de Estudios Avanzados en Nanociencia, ³Argonne National Laboratory, ⁴Institut de Chimie Moleculaire et des Materiaux d'Orsay

Correspondence: * ally.aukauloo@u-psud.fr, ** dooshaye.moonshiram@imdea.org

This work was supported by the CEA IRTTELIS Ph.D. fellowship program (for P.G.), LabEx CHARMMMAT; and by the French Infrastructure for Integrated Structural Biology (FRISBI) ANR-10-INSB-05-01. D.M. acknowledges funding from the Severo Ochoa Excellence program (SEV-2016-0686) from the Instituto IMDEA Nanociencia. This research used resources of the Advanced Photon Source, a U.S. Department of Energy (DOE) Office of Science User Facility operated for the DOE Office of Science by Argonne National Laboratory under Contract No. DE-AC02-06CH11357. Beamline 9-BM-B operations were also supported by the Canadian Light Source and its funding partners.

Reversible Isomerization Reaction Drives a COF-Based Humidity Sensor

Covalent organic frameworks (COFs) are coveted for their porosity. This feature makes the polymeric compounds useful systems for detecting volatile analytes such as water vapor. Researchers have reported COF films that sense humidity via a color change, but the optical response is modest. Now a team of scientists, with results from investigations at the APS, have demonstrated that a diiminol-based COF can act as a rapid humidity sensor with an easily visible color change. These findings provide an important proof-of-concept for using tautomerization-induced changes in COFs to design rapid and reversible sensing systems. The team expects that demonstrating the viability of practical tautomeric sensing will inspire engineered devices capable of complex sensing responses, and that these materials might be of interest as components in internet-of-things systems where passive and long-term-stable sensors are a necessity.

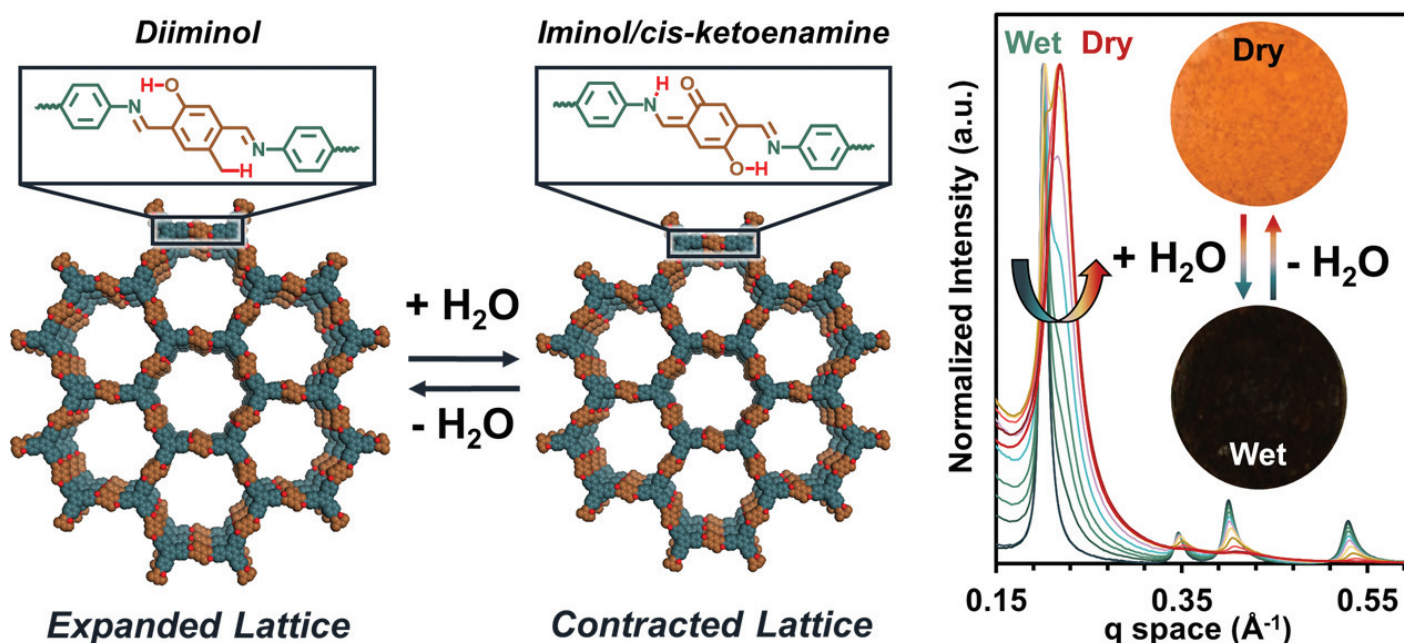


Fig. 1. Researchers have developed a diiminol-based COF that can act as a colorimetric humidity sensor. Through synchrotron x-ray diffraction, the team observed the COF's "breathing" behavior as the structure expands and contracts in the presence or absence of water.

To detect water vapor, the diiminol-based COF undergoes a tautomerization reaction, whereby a proton shifts from one atom in the compound to another, to change from an isomer that appears orange to an isomer that appears black when wet. Notably, this structural rearrangement is reversible, which the team observed through x-ray diffraction experiments as they watched the COF expand and contract as water molecules were added or removed from the atmosphere. The team demonstrated that the diiminol-based COF film was stable up to two months and was responsive even to slight changes in humidity, such as that produced by breathing on the film.

Switching between isomers in tautomerization reactions often takes place quickly and in response to changes in the surrounding environment. For this reason, many tautomeric compounds have been explored as sensing agents, including tautomeric COFs.

One such well-known tautomeric COF is TAPB-TFP, made from the condensation between 2,4,6-triformylphloroglucinol and 1,3,5-tris(4-aminophenyl)benzene). In the presence of water, TAPB-TFP completely tautomerizes from a triiminol compound to a β -ketoenamine compound. However, the β -ketoenamine isomer is highly stable, which means the reaction is only reversible at raised temperatures.

Now, the researchers in this study from the Georgia Institute of Technology and Northwestern University have found that a similar compound, which swaps 2,4,6-triformylphloroglucinol for 2,5-dihydroxyterephthaldehyde (PDA-OH) to form the diiminol TAPB-PDA-OH, also undergoes a water-induced tautomerization reaction but reversibly. Based on the molecule's resonance structure, TAPB-PDA-OH would only tautomerize partially on one side of the molecule, to form a ketoenamine that exists in dynamic equilibrium with the diiminol. In the diiminol form, the compound is an orange powder while the ketoenamine appears black, which makes TAPB-PDA-OH an attractive material for colorimetric sensors. A previously reported tautomeric COF that was used to sense humidity changes did so through solvatochromatism, which relies on a limited optical response that came from water stabilizing an intermediate.

The team synthesized a model compound to confirm their proposed mechanism and found that the compound indeed exhibited the water-dependent equilibrium between iminol and ketoenamine forms, which display distinct absorption patterns. In control experiments, the scientists synthesized analogs of TAPB-PDA-OH that were incapable of tautomerization and confirmed that these

analogues did not display optical changes. Data from computational DFT studies further supported that COF's color change was attributable to tautomerization and not solvatochromatism.

To study the structural changes to the polymer during tautomerization, the researchers turned to synchrotron x-ray diffraction analysis. Small- and wide-angle x-ray scattering diffraction patterns were collected at the DND-CAT 5-ID-D x-ray beamline at the APS, and grazing incidence diffraction patterns were obtained at the XSD Dynamics & Structure Group's 8-ID-E beamline also at the APS. The x-ray diffraction data revealed that the local tautomerization induced a larger structural change to the COF, essentially letting the researchers watch the COF "breathe" as it became wet or dry (Fig. 1).

To test TAPB-PDA-OH's ability to sense humidity, the team made a detector using a thin film of the COF, which was monitored using UV-vis spectroscopy. They found that when the environment was switched from dry to humid, the sensor responded in 9 sec and even as fast as 1 sec when conditions were reversed. After multiple cycles and more than a month of storage, the sensors demonstrated the same level of performance, suggesting that these materials could be valuable long-term sensors.

– Tien Nguyen

See: Samik Jhulki¹, Austin M. Evans², Xue-Li Hao¹, Matthew W. Cooper¹, Cameron H. Feriante¹, Johannes Leisen¹, Hong Li¹, David Lam², Mark C. Hersam², Stephen Barlow¹, Jean-Luc Brédas, William R. Dichtel^{2*}, and Seth R. Marder^{1**}, "Humidity Sensing through Reversible Isomerization of a Covalent Organic Framework," *J. Am. Chem. Soc.* **142**, 783 (2020).

DOI: 10.1021/jacs.9b08628

Author affiliations: ¹Georgia Institute of Technology, ²Northwestern University

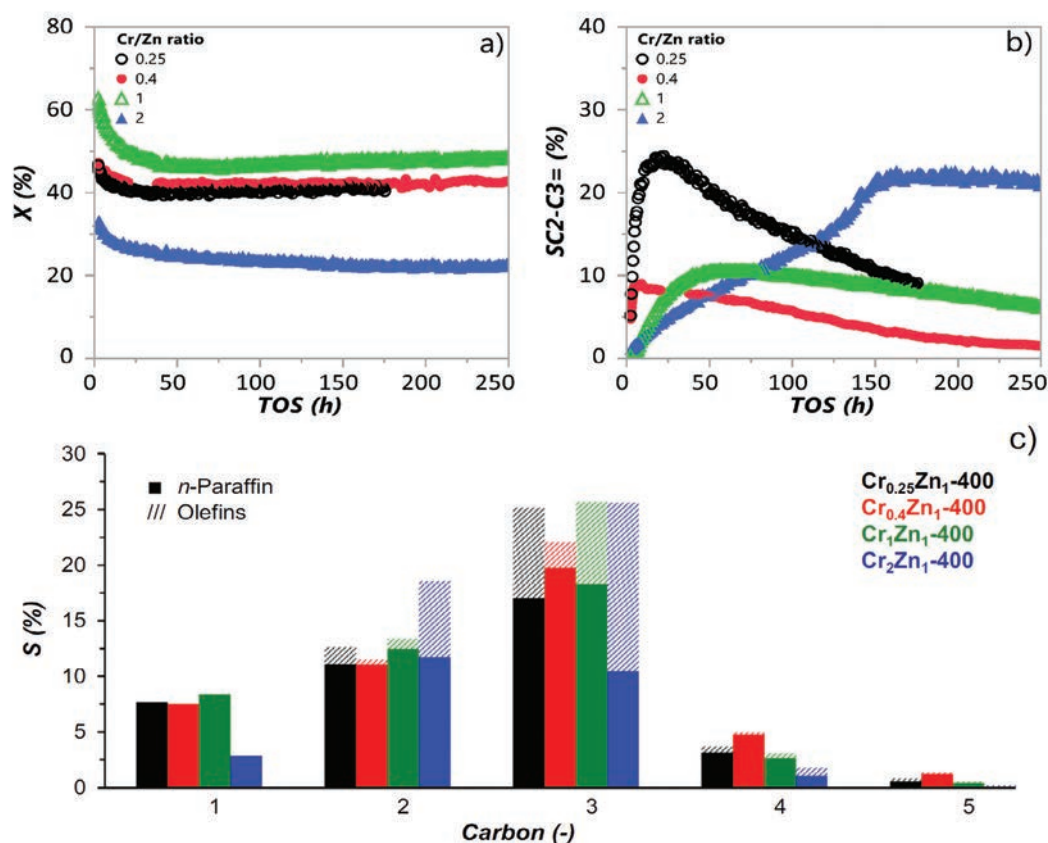
Correspondence: * wdichtel@northwestern.edu,

** seth.marder@chemistry.gatech.edu

We thank the United States Army Research Office for a Multidisciplinary University Research Initiative (MURI) award under grant number W911NF-15-1-0447. S.J. thanks the United States-India Educational Foundation (USIEF, India) and the Institute of International Education (IIE, USA) for a Fulbright-Nehru Postdoctoral Fellowship (grant no. 2266/FNPDR/2017). A.M.E. is supported by the National Science Foundation Graduate Research Fellowship under grant no.(DGE-1324585). H.L. and J.-L.B. acknowledge funding of this work by the United States Army Research Office under award W911NF-17-10339. D.L. and M.C.H. acknowledge the U.S. Department of Energy (DOE) (grant DE-SC0019356) for support of the Raman spectroscopy characterization. The DuPont-Northwestern-Dow Collaborative Access Team is supported by Northwestern University, The Dow Chemical Company, and DuPont de Nemours, Inc. This research used resources of the Advanced Photon Source, a U.S. DOE Office of Science User Facility operated for the DOE Office of Science by Argonne National Laboratory under contract no. DE-AC02-06CH11357.

Chromium-Zinc Catalysts Expand Potential for Synthetic Gas and Non-Petroleum-Based Manufacturing

Synthesis gas, also known as “syngas,” is a chemical fuel mixture that contains hydrogen, carbon monoxide, and carbon dioxide. Syngas can be used to produce diesel, methanol, and other high-value chemicals and can be used as an alternative fuel source to produce electricity. Since the availability of crude oil varies from one geographical region to another, syngas is an important non-petroleum resource. A highly desirable application is the utilization of syngas to produce chemical materials referred to as light olefins, which are in high demand and are critically important in industrial manufacturing. Many technical challenges have, however, made it difficult to directly convert syngas to light olefins. Research efforts spearheaded by the team in this study can enhance the ability of a chemical reaction to occur; the authors were able to successfully convert syngas to light olefins and affect the conversion process by tweaking various parameters. The researchers used CrZn–SAPO-34 catalysts to accomplish this goal and found that olefin production was sensitive to the catalyst ratio of chromium to zinc as well as the heating temperature. These findings, based upon research at the APS, have momentous implications for the industrial manufacturing field and help expand the usage potential of syngas.



Although petroleum is a globally prevalent fuel source, it presents complications. Crude oil is not ubiquitously available and can only be found in certain geographical regions. Moreover, crude oil is subject to significant price fluctuations that impact its commercial reliability. Given these undesirables, the alternative fuel resource syngas is invaluable. Syngas is comprised of the molecules hydrogen, carbon monoxide, and carbon dioxide.

One paramount application of syngas is in the production of molecules referred to as olefins. Olefins are also known as alkenes in chemistry and represent compounds that 1) exclusively contain hydrogen and carbon and 2) contain a carbon-carbon double or triple bond. The presence of this double or triple bond makes the hydrocarbon unsaturated, as it is not saturated with hydrogen atoms. Olefins are incredibly important in the industrial manufacturing sector and are pervasive in our society. Examples of light olefins are ethylene and propylene, both of which are important chemical building blocks that are prevalent in the manufacturing of everyday products, for instance apparel designed for athletic use.

Unfortunately, technical challenges have made it difficult to use syngas to produce light olefins with a high selectivity. Fischer-Tropsch synthesis (the process by syngas can be converted into ultra-clean fuels and value added chemicals) can hydrogenate carbon dioxide into light olefins, but selectivity is low. Despite this selectivity hindrance, the Fischer-Tropsch process has been used for the production of diesel and other significant resources.

Very recently, this conversion obstacle was directly addressed by this team of researchers from Dow Benelux B.V. (The Netherlands) and The Dow Chemical Company. The authors assessed the ability of chromium-zinc catalysts to directly convert syngas to light olefins. Using a combination of electron microscopy, x-ray photoelectron

and absorption spectroscopy, and x-ray diffraction techniques they were able to evaluate how the heating temperature and the ratio of chromium and affect the conversion process.

They found that CrZn–SAPO-34 catalysts can selectively convert syngas to light olefins. The production stability was sensitive to the chromium/zinc ratio as well as the heating temperature. For example, increasing the ratio of chromium to zinc improved the stability of olefin selectivity, while lowering the heating temperature was preferable in regards to catalyst activity. These results are displayed in Fig. 1. The x-ray absorption spectroscopy studies were carried out at the DND-CAT beamline 5-BM-D at the APS.

Light olefins hold a massive market demand due to the vital roles they play in the global industrial manufacturing chain. Therefore, these recent findings are tangibly beneficial and further elevate syngas as a useful resource. In fact, it would be unsurprising to see syngas become an even more desirable gas mixture in the near future.

– Alicia Surrao

See: Vera P. Santos^{1*}, Glenn Pollefeyt¹, David F. Yancey², Aysegul Ciftci Sandikci¹, Britt Vanchura², Davy L.S. Nieskens², Martine de Kok-Kleiberg², Alexey Kirilin¹, Adam Chojecki¹, and Andrzej Malek², “Direct conversion of syngas to light olefins (C2–C3) over a tandem catalyst CrZn–SAPO-34: Tailoring activity and stability by varying the Cr/Zn ratio and calcination temperature,” *J. Catal.* **381**, 108 (2020).

DOI: 10.1016/j.jcat.2019.08.027

Author affiliations: ¹Dow Benelux B.V., ²The Dow Chemical Company

Correspondence: * vpsantos@dow.com

DND-CAT is supported by Northwestern University, the Dow Chemical Company, and DuPont de Nemours, Inc. This research used resources of the Advanced Photon Source, a U.S. Department of Energy (DOE) Office of Science User Facility operated for the DOE Office of Science by Argonne National Laboratory under Contract DE-AC02-06CH11357.

< Fig. 1. At a heating temperature of 400° C, (a) the conversion of carbon monoxide, and (b) olefin selectivity are sensitive to the ratio of chromium to zinc in the catalyst. There is a correlation between this ratio and olefin selectivity, with the greatest selectivity being observed with the highest Cr/Zn ratio. From V.P. Santos et al., “Direct conversion of syngas to light olefins (C2–C3) over a tandem catalyst CrZn–SAPO-34: Tailoring activity and stability by varying the Cr/Zn ratio and calcination temperature,” *J. Catal.* **381**, 108 (2020). © 2019 Published by Elsevier Inc.

Designing a Catalyst

Metals play an important role in human health with functions in enzyme catalysis, bone health, cellular respiration, and immune function. However, too much metal or the wrong type of metal can be poisonous to our cells by causing DNA damage or disruption of normal functions, or simply by overwhelming our organs' ability to detoxify them. Researchers have developed models designed to study the details of protein-metal interactions with the hope that increased understanding of these complex systems may facilitate the development of enzymes with new catalytic abilities or peptides that can detoxify heavy metal exposures. Work conducted at the APS highlights one research group's big step toward *de novo* enzyme design. This work paves the way for the design of novel catalytic and metal-binding peptides with unique properties for a variety of applications in heavy-metal biochemistry.

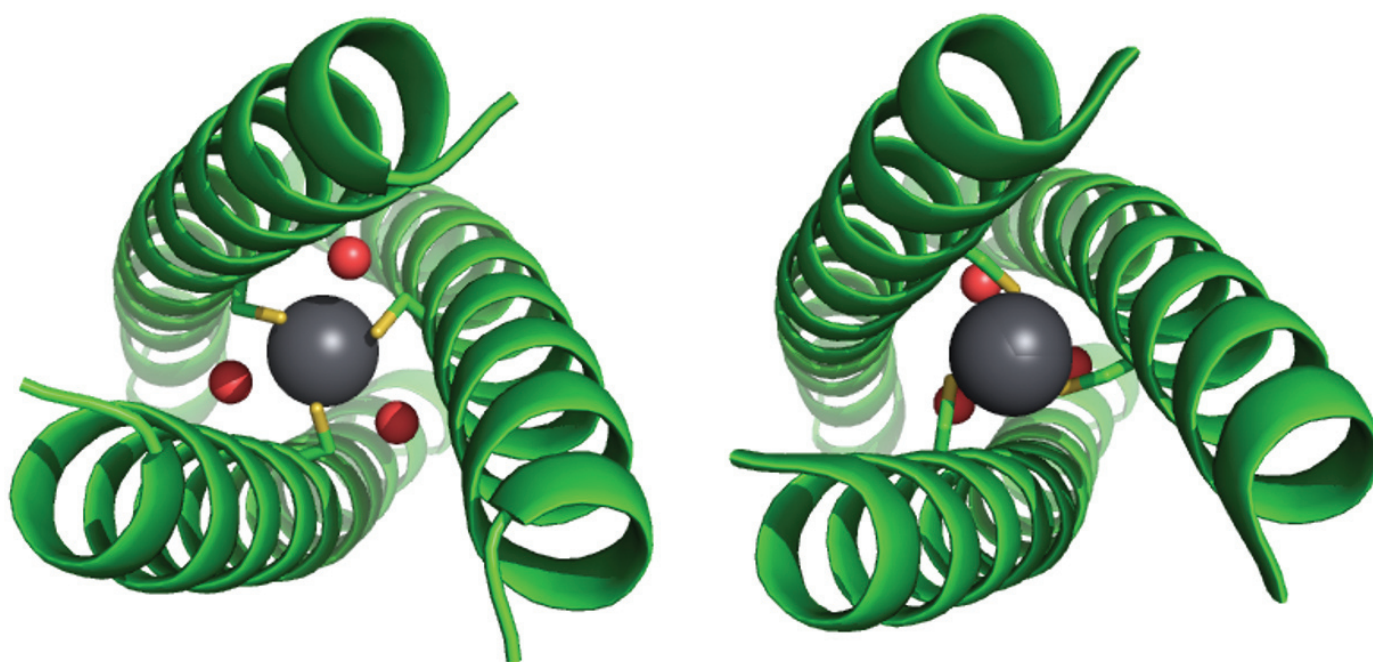


Fig. 1. Top-down view of 6EGP (left) and 6MCD (right) with Pb(II) as a large grey sphere illustrating how changing the position of Cys and Ala residues changes water coordination.

The work was part of a collaboration between researchers at the University of Michigan, the University of Miami, and King Mongkut's University of Technology (Thailand). Previous work from this group had shown that short peptides consisting of 4 or 5 7-amino acid repeats could be designed to form three-stranded coiled-coil scaffolds that could bind a metal ion. Although the scaffold oriented the metal ion near a catalytic histidine, as is observed in many enzyme active sites, the symmetry in the three-stranded coil inhibited critical chemical interactions. The designed enzyme performed well but was still 300-fold less efficient than the enzymes they were modeling. The group hypothesized that if they could generate coiled coils using two different types of peptides rather than three of the same peptide, they might make an asymmetric site in their enzyme for the needed chemistry to occur.

The group started by designing peptides based on the previously successful version but with some changes that would hopefully bias the three-stranded coiled-coil structures to fold with two different types of peptides. The main design for the peptides was to have the same basic 7-amino acid sequence for 4 or 5 repeats but vary a hydrophobic amino acid at positions 1 and 4 to a metal-binding amino acid at critical locations. For example, in the 7-amino acid sequence, two paired peptides would have the same basic sequence, including a cysteine amino acid to bind to a lead ion, but one would have a leucine at the fourth position while the other would have an alanine at that position, creating a little more space in the coil for differential packing of water molecules. The team also varied whether one or both peptides would have a hydrogen bonding residue in addition to the catalytic histidine at a critical location. After developing over a dozen versions of the peptides, the group set about testing which combinations would form mixed coiled-coil structures and whether they had the correct orientation of all of the important catalytic players.

The first step was to mix the peptides and confirm that

they formed the correct three-stranded coiled-coil structures. The team used x-ray crystallography at the LS-CAT 21-ID-F x-ray beamline at the APS to confirm that they could indeed form three-stranded coiled coils (Fig. 1). Quantum mechanics/molecular mechanics analyses identified two versions that had the most favorable complexation energies, forming the most stable structures. In order to be sure that they had a homogeneous solution of only one type of coil (for example, A2B only and not A2B plus A3 and B3) they performed ²⁰⁷Pb nuclear magnetic resonance spectroscopy on the samples. The samples generated one peak, suggesting that the sample was purely one type of coil. Finally, in an important first step towards testing the ability of their three-stranded coils to mimic enzymatic catalysis, the team was able to bind zinc to the catalytic histidine without disrupting the coiled structure.

These results show that it is possible to design three-stranded coiled-coil protein structures that can mimic the metal-binding active sites of known enzymes using a combination of two different types of peptides, providing for variability in functional uses. – Sandy Field

See: Audrey E. Tolbert¹, Catherine S. Ervin¹, Leela Ruckthong², Thomas J. Paul³, Vindi M. Jayasinghe-Arachchige³, Kosh P. Neupane¹, Jeanne A. Stuckey¹, Rajeev Prabhakar³, and Vincent L. Pecoraro^{1*}, "Heteromeric three-stranded coiled coils designed using a Pb(II)(Cys)₃ template mediated strategy," *Nat. Chem.* **12**, 405 (April 2020). DOI: 10.1038/s41557-020-0423-6

Author affiliations: ¹University of Michigan, ²King Mongkut's University of Technology, ³University of Miami
Correspondence: * vlpec@umich.edu

The authors acknowledge funding from National Institutes of Health grant no. R01 ES012236, National Science Foundation grant no. CHE-1664926, and the Skill Development Grant from King Mongkut's University of Technology, Thonburi, Thailand. Use of the Life Sciences Collaborative Access Team x-ray facility was supported by the Michigan Economic Development Corporation and the Michigan Technology Tri-Corridor (grant no. 085P1000817). This research used resources of the Advanced Photon Source, a U.S. Department of Energy (DOE) Office of Science User Facility operated for the DOE Office of Science by Argonne National Laboratory under Contract No. DE-AC02-06CH11357.

New Pathways to Advance Adsorbent Technologies for Alkene Purification

The separation and purification of chemicals remains a significant challenge. On a global scale, processes used in chemical separations account for 10–15% of the world's total energy consumption. In the United States alone, improvements in separation technology in the petroleum, chemical, and paper manufacturing sectors could save up to 100 million metric tons of CO₂ emissions per year and \$4 billion in annual energy costs. Despite the obvious need to develop alternative processes and materials aimed at improving energy efficiency and lowering the overall carbon footprint for industrial separation processes, the development of alternative, commercially viable routes have shown limited success. In a new study by an international team of scientists, the researchers show that taking a new approach to the development of chemical adsorbents may pave the way to novel materials that can compete with traditional industrial distillation processes. The study, completed in collaboration with beamline scientists at the APS, describes the structure and reactivity of two new copper(I) complexes that exhibit a unique combination of low heat adsorption, high selectivity, good uptake capacity, and rapid kinetics for the separation of gaseous alkenes (i.e., ethene and propene) from alkanes. These findings have exciting implications for the development of new adsorbent materials that can significantly improve the energy efficiency and carbon footprint of industrial-scale alkene purification processes.

Ethene and propene are vitally important to the global economy. Both are among the top five most produced chemicals in the world—combined annual production of around 230 million tons—with primary applications focused on the production of polymer and chemical products. However, 75% of alkene production costs come from the capital and energy-intensive cryogenic distillation process. Alternative separation techniques such as membrane, adsorption, molecular sieving, or hybrid processes all face road blocks for industrial-scale implementation. Specifically, traditional approaches to improve adsorbing materials (e.g., increased capacity, increased selectivity) for alkene purification require the tradeoff of desirable properties. For example, increasing the capacity of adsorbents by increasing surface area results in a decrease in selectivity.

To overcome these challenges, the researchers developed two new olefin-responsive copper(I) complexes: $[[4\text{-Br-}3,5\text{-(CF}_3)_2\text{Pz}]\text{Cu}]_3$ (**[Cu-Br]**₃) and $[[3,5\text{-(CF}_3)_2\text{Pz}]\text{Cu}]_3$ (**[Cu-H]**₃). The unique aspect of these materials, as opposed to traditional porous adsorbent materials, is that

they undergo a reversible structural rearrangement upon exposure to ethene and propene, resulting in dimeric copper(I)-alkene analogues: **[Cu-Br·(alkene)]**₂ and **[Cu-H·(alkene)]**₂. The alkene is released from the complex upon removal of the alkene source, and the complexes convert back to their original trimeric structure. **[Cu-H]**₃ is a highly attractive candidate for commercial applications because the complex undergoes ethene adsorption above 1 bar at near ambient temperature and rapid desorption when exposed to the atmosphere. These attributes would allow for operation conditions near atmospheric pressure and avoid complicated adsorption process designs.

Two of the most remarkable pieces of data demonstrating the unique reversibility of this material were collected at the high-energy x-ray diffraction beamline 17-BM operated by the XSD Structural Science Group (SRS) at the APS. The team of scientists from The University of Texas at Arlington, the University of Canterbury (New Zealand), and Massey University (New Zealand), together with colleagues from the SRS, utilized x-ray powder dif-

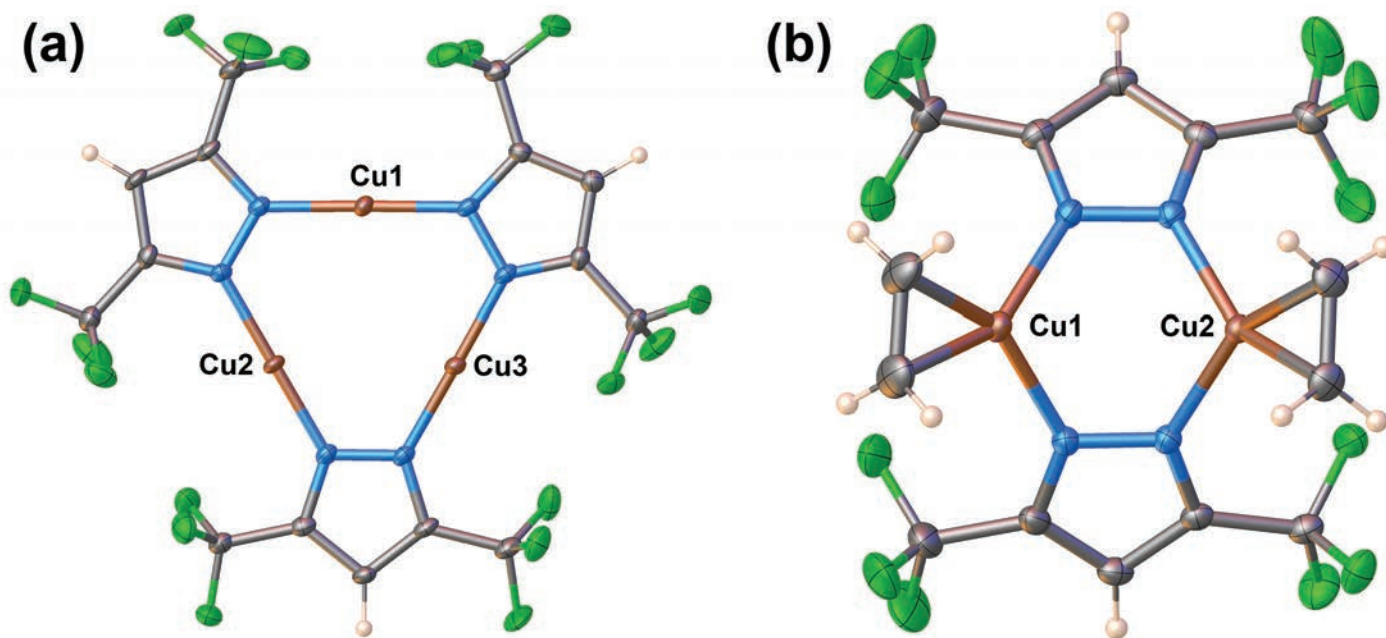


Fig. 1. Molecular structures of (a) $[\text{Cu-H}]_3$ and (b) $[\text{Cu-H}\cdot(\text{C}_2\text{H}_4)]_2$. From D. Parasar et al., "Overcoming Fundamental Limitations in Adsorbent Design: Alkene Adsorption by Non-porous Copper(I) Complexes," *Angew. Chem. Int. Ed.* **59**, 21001 (2020). © 2020 Wiley-VCH GmbH

fraction under high-pressure ethene flow to confirm stoichiometric ethene coordination by $[\text{Cu-H}]_3$ and the formation and breaking of several bonds in the solid-state to form $[\text{Cu-H}\cdot(\text{C}_2\text{H}_4)]_2$ (Fig. 1). Based on crystal structures of the final product, the team were able to confirm that greater than 95% of the starting material $[\text{Cu-H}]_3$ converted into the dimeric-alkene derivative within 2 minutes at 10 bar. Furthermore, complete removal of ethene under helium flow accompanied by recovery of the original trimeric starting material occurred within 1 hour with most of the transformation occurring within the first 15 minutes.

These promising results illustrate the potential to use this approach to develop new adsorbent materials capable of separating high-value chemical targets like alkenes from alkanes. Specifically, $[\text{Cu-H}]_3$ is an attractive target for alkene-alkane separation due to its ability to rapidly adsorb ethene at near atmospheric conditions. Furthermore, $[\text{Cu-H}]_3$ is air-stable and can be prepared using commercially available raw materials which will lower the barrier for commercial manufacturing. These new complexes represent the "tip of the iceberg" when it

comes to the potential for this new approach to the development of adsorbent materials. – Alicia Surrao

See: Devaborning Parasar¹, Ahmed H. Elashkar², Andrey A. Yakovenko³, Naleen B. Jayaratna¹, Brian L. Edwards¹, Shane G. Telfer⁴, H. V. Rasika Dias^{1*} and Matthew G. Cowan^{2**,} "Overcoming Fundamental Limitations in Adsorbent Design: Alkene Adsorption by Non-porous Copper(I) Complexes," *Angew. Chem. Int. Ed.* **59**, 21001 (2020). DOI: 10.1002/anie.202010405

Author affiliations: ¹The University of Texas at Arlington, ²University of Canterbury, ³Argonne National Laboratory, ⁴Massey University

Correspondence: * dias@uta.edu,

** matthew.cowan@canterbury.ac.nz

M.G.C. thanks the Royal Society of New Zealand for awarding a Rutherford Fellowship to support this research (RFT-UOC1601-PD) and the Marsden Fund (MFP-19-UOC-072), and acknowledges the support of the MacDiarmid Institute. H.V.R.D. acknowledges the Robert A. Welch Foundation (Y-1289) for the funding of this research. A.H.E. thanks the New Zealand Ministry of Foreign Affairs and Trade for provision of a New Zealand Aid Scholarship. This research used the resources of the Advanced Photon Source, a U.S. Department of Energy (DOE) Office of Science User Facility operated for the DOE Office of Science by Argonne National Laboratory under contract no. DE-AC02-06CH11357.

Double-Safe in the Time of the Pandemic: **Mike Fries**

“Communication has become more important than ever at the APS to ensure personnel are conducting their work safely. We must all do our part in making sure that employees are prepared and able to perform their tasks in a more independent work environment with the limited personnel onsite.”
Mike Fries



Life Science

Key Insights into an Inherited Muscle Disease

The gene *NEB* encodes for the skeletal muscle protein nebulin. Mutations in *NEB* cause the disease nemaline myopathy, which is one of the more common inherited myopathies. Patients with this muscle disorder have muscle weakness in multiple different parts of their body and can also experience difficulties with feeding or breathing. Currently, there is no cure for nemaline myopathy and treatment options are limited. Therefore, there is a need to better understand this disease and design new therapeutics that can improve patient quality of life. A team of researchers working to provide new insights into the pathogenesis of this skeletal muscle disorder report a new mouse model of nemaline myopathy that exhibits similar symptoms to those identified in human patients. An important part of this work utilized x-ray diffraction data collected at the APS. The diffraction data provide new insights into how mutations of *NEB* alter the molecular structure of skeletal muscles. The findings from the study are highly impactful because they significantly increase our understanding of how mutations in the gene *NEB* cause nemaline myopathy. Importantly, the new mouse model of this disease can be used to test future therapeutics. Future studies are warranted to determine if interventions can relieve disease symptoms in these mice. If successful, such therapeutics could be used for improving the quality of life in human patients.

Nemaline myopathy is a rare muscle disease that can be caused by mutations in the gene *NEB*. Over 240 different disease-causing mutations in *NEB* have been identified in conjunction with nemaline myopathy, with the majority of patients having two different mutations in the gene *NEB*. Patients experience symptoms ranging from muscle weakness in the arms, legs, face, and neck to difficulties with feeding or breathing. Despite these serious symptoms, there is currently no cure and the available treatment options are limited.

From a functional standpoint, *NEB* encodes for the protein Nebulin, which is found in the sarcomere of skeletal muscle. Unlike cardiac and smooth muscle which undergo involuntary muscle contractions, skeletal muscles are under voluntary control and are responsible for carrying out bodily movements. For example, someone performing bicep curls in the gym is actively controlling and exercising their biceps using skeletal muscles.

To gain more insight into the molecular structures and mechanisms underlying the disease nemaline myopathy, the researchers from the University of Arizona developed a novel animal model to study this skeletal muscle disorder. To do this, they created genetically modified mice harboring two different mutations in *NEB*. One of these mutations is a missense mutation (resulting in a single amino acid change) and the other mutation is a deletion mutation (meaning that a portion of the gene has been removed). The result of these two mutations is a class of genetically modified mice that exhibit similar symptoms as humans with nemaline myopathy. These genetically modified mice also weighed less and have a shorter tibia bone compared to genetically normal controls.

Using the new mouse model, the team examined how these two mutations impacted the structure of the muscle on a molecular level. A key part of this work was performed in collaboration with Illinois Institute of Technology scientists at the Bio-CAT 18-ID-D beamline at the APS. X-ray diffraction patterns collected at beamline 18-ID-D were used to identify molecular structures altered in the mice (Fig. 1). The research team found that the sarcomeres in the new strain

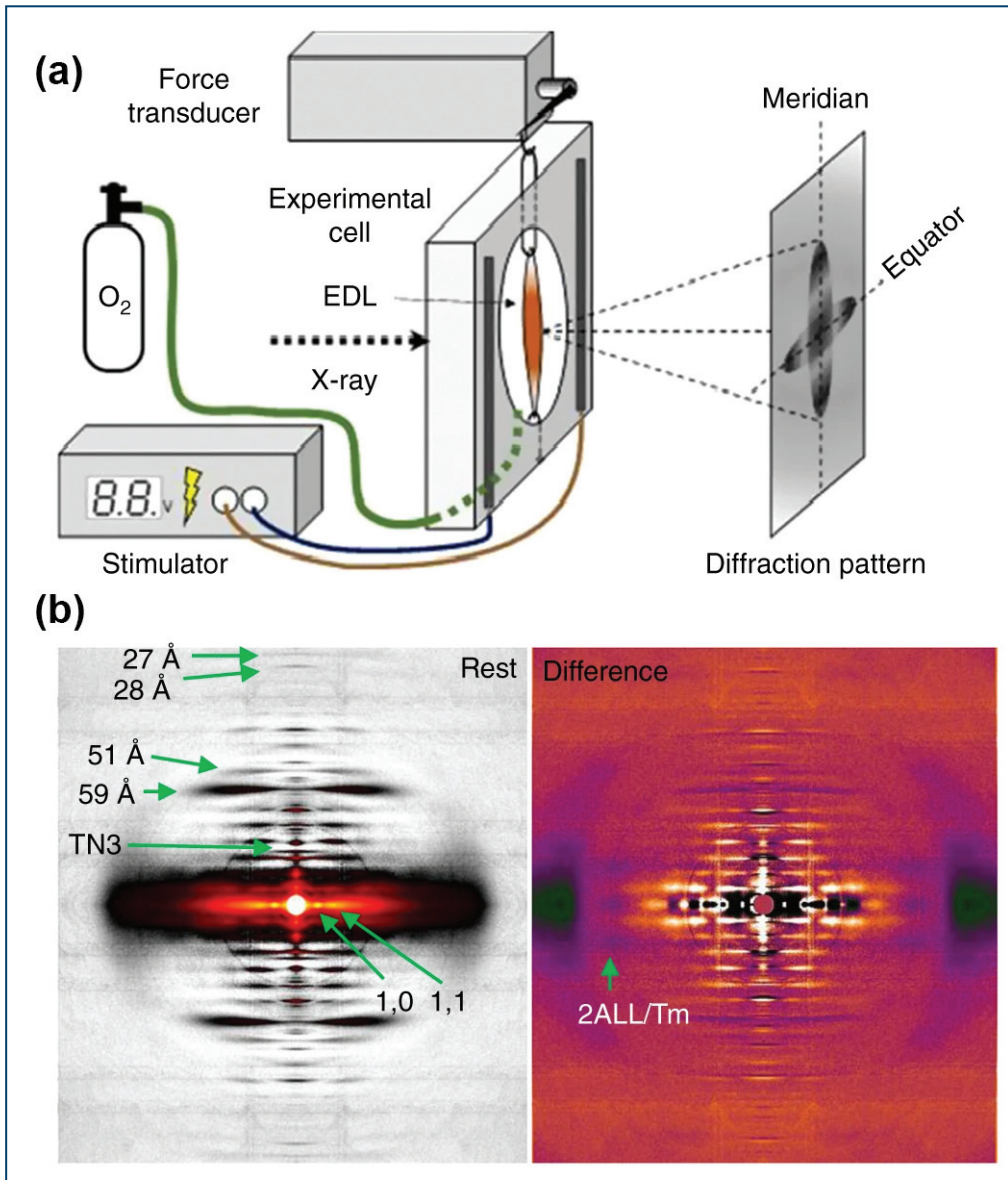


Fig. 1. (a) Experimental setup. (b) X-ray diffraction images with examined reflections indicated. Left image taken during rest and Right image is the difference between active and passive muscle. From J. Lindqvist et al., “Triggering typical nemaline myopathy with compound heterozygous nebulin mutations reveals myofilament structural changes as pathomechanism,” *Nat. Commun.* **11**, 2699 (2020). © 2020 Springer Nature Limited

of genetically modified mice were disorganized. One prominent finding was that actin filaments—which play an important role in muscle contraction—were twisted and have a larger radius when compared to the control.

– Stephen Taylor

See: Johan Lindqvist¹, Weikang Ma², Frank Li¹, Yaeren Hernandez¹, Justin Kolb¹, Balazs Kiss¹, Paola Tonino¹, Robbert van der Pijl¹, Esmat Karimi¹, Henry Gong², Josh Strom¹, Zaynab Hourani¹, John E. Smith III¹, Coen Ottenheijm¹, Thomas Irving², and Henk Granzier*, “Triggering typical nemaline myopathy with compound heterozygous nebulin mutations reveals myofilament structural changes as pathomechanism,” *Nat. Commun.* **11**, 2699

(2020). DOI: 10.1038/s41467-020-16526-9

Author affiliations: ¹University of Arizona, ²Illinois Institute of Technology

Correspondence: * granzier@email.arizona.edu

This work was supported by grants from A Foundation Building Strength, and National Institute of Arthritis and Musculoskeletal and Skin Disease grant R01AR053897. Bio-CAT is supported by grant 9 P41 GM103622 and 1S10OD018090-01 from the National Institute of General Medical Sciences of the National Institutes of Health. This research used the resources of the Advanced Photon Source, an Office of Science User Facility operated for the U.S. Department of Energy (DOE) Office of Science by Argonne National Laboratory under contract no. DE-AC02-06CH11357.

Developing Tiny Sensors to Test Oxygen Passage in Lung Membranes

When sickened with pneumonia, the lungs become flooded with fluid and pus, making it difficult to breathe. Yet, in some cases, too much oxygen (hyperoxia) is thought to contribute to the pathology of bacterial pneumonia. To understand how pneumonia impacts oxygen penetration in the lungs, scientists are looking closely at the membranes that serve as an interface between air and the bloodstream. A team of researchers developed a graphene-based sensor to measure oxygen transport in lung membranes. That work, combined with structural data collected at the APS, provided key mechanistic insights regarding how pneumonia may modify lung tissues to enhance oxygen permeation. The findings may spur innovations in clinical research on how oxygen diffusion is related to lung health.

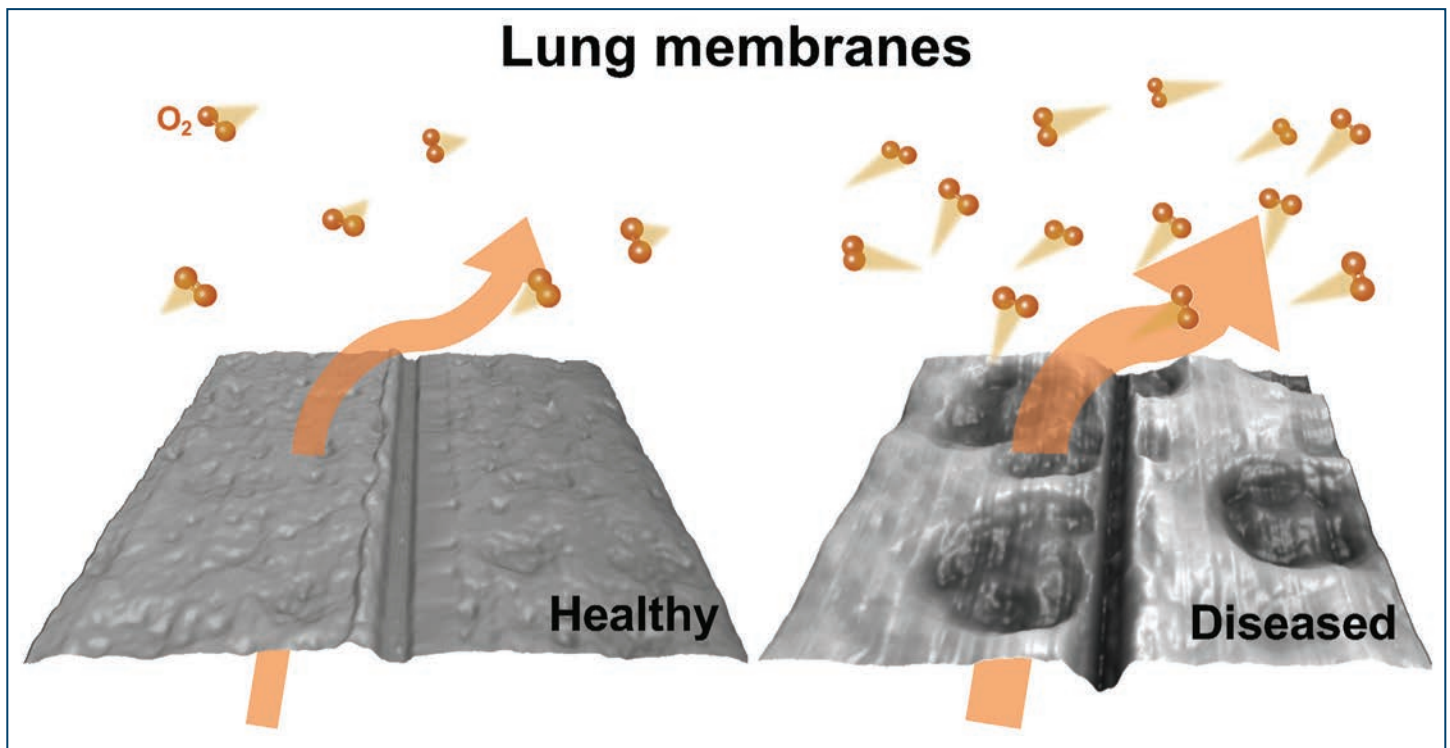


Fig. 1. A schematic showing differences in oxygen passage through AFM images of healthy and diseased lung membranes.

As a first step, the team of researchers from the University of Illinois at Urbana-Champaign needed to construct a lung membrane model atop an oxygen sensing system. The lung membrane proxy consisted of a stack of several lipid bilayers. For the sensor, they looked to graphene. This handy carbon molecule forms two-dimensional sheets that can be spread into thin layers on a surface and is compatible with a high-humidity environment—a key requirement of lung membrane studies. Plus, when mounted between two electrodes with a gate contact to modulate the electronic response of the channel, graphene becomes a field-effect transistor capable of sensing oxygen. The researchers built a 1-cm x 1-cm chip with a grid of 50 graphene sensors; the chip served as a solid support for the stack of lipid bilayers.

Sensing platform in hand, the researchers took a series of baseline measurements, assessing the thickness and morphology of their lung membrane proxy using atomic force microscopy (AFM). They assessed two model systems, one designed to mimic healthy tissue and the other an imitation of diseased tissue (Fig. 1). The healthy lung mimetic included only lipids, while the diseased lung membranes included lipids as well as two additional substances that have been associated with pneumonia: cardiolipin and calcium. Cardiolipin is a mitochondrial phospholipid that is elevated in the lung fluid from people with pneumonia, suggesting a role in the disease's pathology. This molecule is thought to be involved with calcium transport, and high levels of calcium have been detected in lung disease. Compared to the healthy membranes, the AFM revealed that the diseased membranes showed greater surface roughness.

Next, the researchers investigated the atomic structure of the healthy and diseased lung lipid films using grazing-incidence small-angle x-ray scattering (GISAXS) experiments at the XSD Chemical & Materials Science Group's x-ray beamline 12-ID-B at the APS (Fig. 2). In the diseased model, they observed inter-membrane hydrophobic contacts at regular intervals across the stack of lipid bilayers. These inter-membrane “stalks” were not present in the healthy model and represent membrane defects. Also, they were associated with an increase in oxygen penetration, as measured with the graphene sensor on the exact same samples. AFM images suggested that disease models had greater pore structures, suggesting a potential mechanism for the increase in oxygen permeation.

The team also looked at the structure and oxygen permeability of lipid-protein extract surfactants from healthy

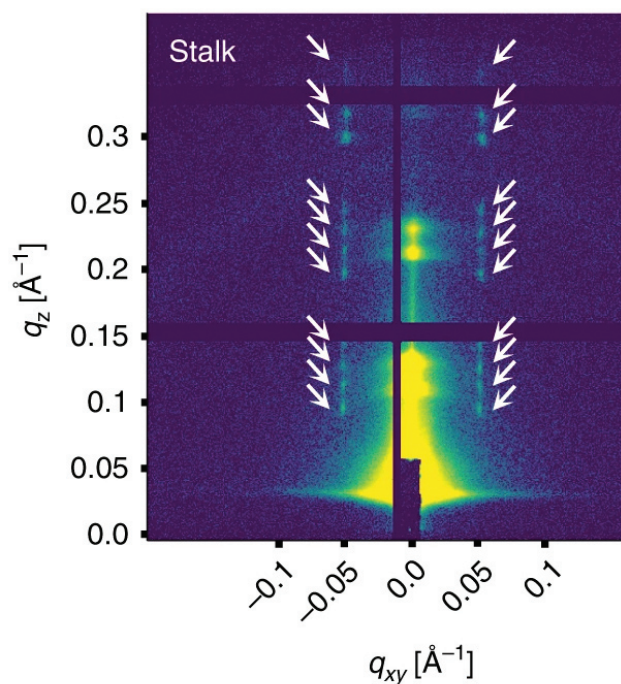


Fig. 2. Synchrotron GISAXS of the diseased lung membrane model system. White arrows indicate stalk phase peaks.

and diseased lungs. These extracts include hydrophobic lung membrane surfactant proteins, SP-B and SP-C, which are thought to play a role stabilizing the formation of membrane contacts that promote membrane permeability. Again, the diseased state had different structural features and increased oxygen permeability relative to the healthy state. This observation is consistent with the idea that surfactant proteins stabilize the inter-bilayer contacts that act as pathways for oxygen transport.

To further explore the relationship between lung membranes and stalk defects, the researchers propose a study of structure and oxygen permeability of intact lung membranes extracted from healthy and diseased mammalian lungs. – Erika Gebel Berg

See: Mijung Kim, Marilyn Porras-Gomez, and Cecilia Leal*, “Graphene-based sensing of oxygen transport through pulmonary membranes,” *Nat. Commun.* **11**, 1103 (2020). DOI: 10.1038/s41467-020-14825-9

Author affiliation: University of Illinois at Urbana-Champaign
Correspondence: * cecilia@illinois.edu

This work is funded by the Office of Naval Research (ONR) grant numbers N000141612886 and N000141812087 (DURIP-Defense University Research Instrumentation Program) and in part by the National Institutes of Health, grant number: 1DP2EB024377 (non-lamellar lipid structures). This research was carried out in part at the Materials Research Laboratory, University of Illinois. This work used resources of the Advanced Photon Source, a U.S. Department of Energy (DOE) Office of Science User Facility operated for the DOE Office of Science by Argonne National Laboratory under contract no. DE-AC02-06CH11357.

Effects of Gravity on the Open Circulatory Systems of Invertebrates

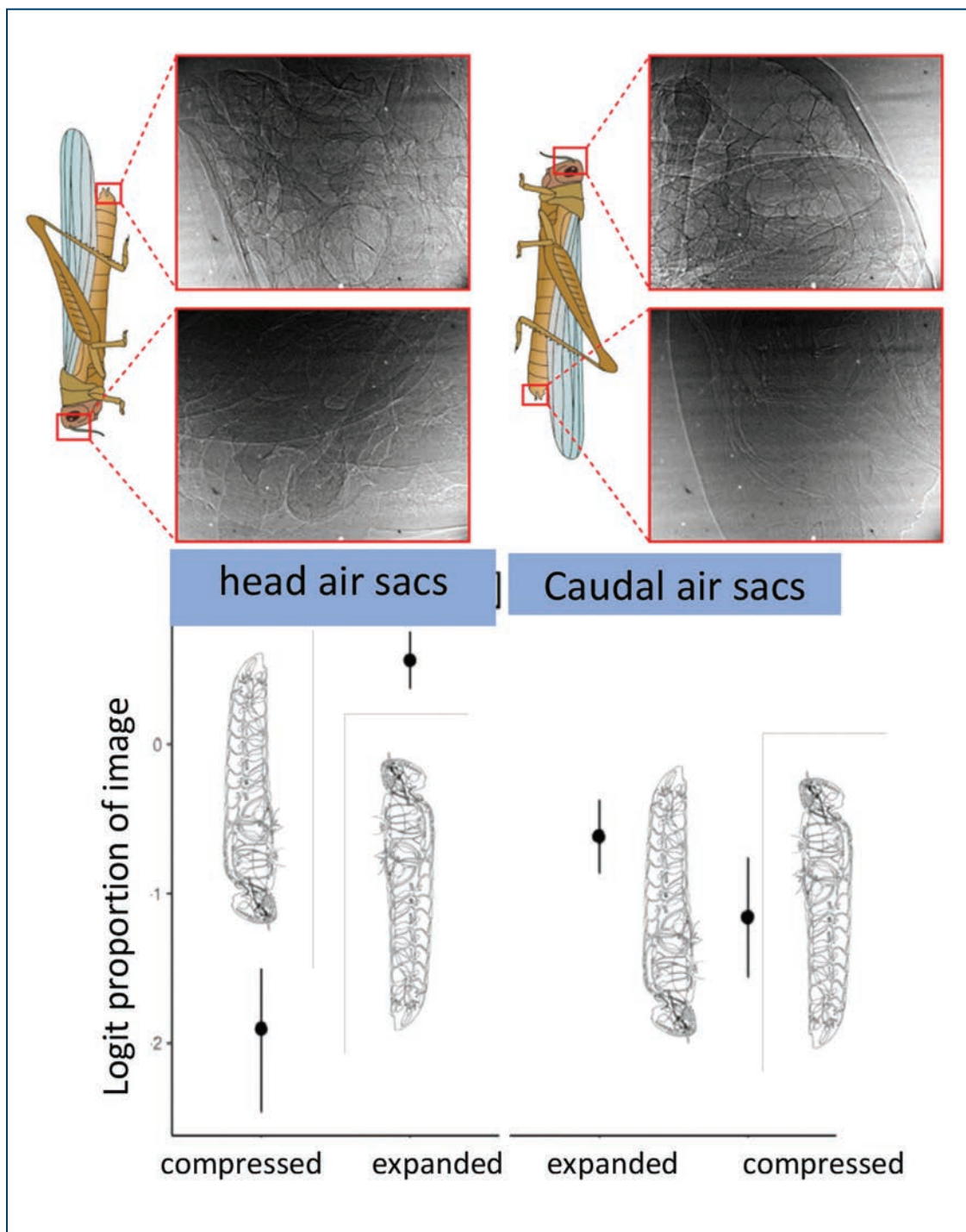


Fig. 1. Effect of body orientation on gravitational effects in grasshoppers.

Humans and other vertebrates have strong physiological reactions to gravity, but the effects of gravity on respiration and circulation in invertebrates are not well known. For this work, researchers flipped live American grasshoppers (*Schistocerca americana*) upside down and right-side up and imaged them at the APS to see the effects of gravity on blood and air within their bodies. Grasshoppers have flexible air sacs throughout their bodies that can easily be seen and quantified by x-rays. The results show that insects have sophisticated physiological responses to gravity, such as changes in ventilation and heart rate, and even show some type of functional valving to maintain fluid pressure through their body. These findings suggest that responses to gravity are ancient and widely shared among animals. Such widespread traits suggest that responses to gravity evolved early in animal cardiovascular systems, and that invertebrates can be used as model systems for investigating some mechanistic responses to gravity.

Everyone has felt the effects of gravity on their body, such as when you stand on your head or stand up too quickly. Humans and other vertebrates have closed circulatory systems, with veins, arteries and a heart working together to regulate fluid pressure. Blood vessels open or restrict blood flow to various parts of the body, as needed. The heart quickly accelerates when you move from a prone to a standing position. In general, the physiological reactions on larger bodies are more pronounced than on smaller bodies.

Invertebrates have an open circulatory system, mostly without closed arteries or veins. In such an open system, pressures inside an invertebrate's body should all be similar. Invertebrate blood has been thought to flow freely around the animal's body, which should make it vulnerable to the effects of gravity. Yet we know that many insects, including grasshoppers, spend much of their time upside down or sideways, with no apparent negative effects. The question becomes: How do insects adjust their cardiovascular and respiratory activity in response to changes in body position?

The researchers in this study, from Arizona State University and Virginia Tech along with a colleague from Argonne, imaged the live grasshoppers using extreme-brightness x-rays at the XSD Imaging Group's beamline 32-ID at the APS, while movements of invertebrate blood, called hemolymph, were tracked with a radioactive tracer. The images revealed that the grasshoppers had acute physiological responses to gravity, seen in air and hemolymph distribution. When the grasshoppers were head-up, the air sacs in their heads expanded. There was very little hemolymph in the head, but the air sacs in their abdomens were compressed by hemolymph moving downward. When the grasshoppers were flipped, the reverse was true: the air sacs in their heads were

compressed and surrounded by fluid, but the air-sacs in their abdomens were expanded with hemolymph draining downward (Fig. 1).

When the grasshoppers were anesthetized, blocking heart and muscular function, the gravitational effects were much larger, showing that the insects actively resist the effects of gravity. The researchers discovered that grasshoppers combat the effects of gravity by varying their heart and breathing rates. Grasshopper heart rates change with the orientation of their body. When upside down, the heart slows to reduce fluid pooling in the brain, but the ventilation rate increases, possibly because the compressed air sacs around the brain reduce oxygen delivery. When the heads are up, the heart rate speeds up. Also, unlike the old idea of an open circulatory system, blood pressures in the grasshopper's thorax and abdomen are not always the same, providing evidence of a functional valve within the grasshopper's body. This valve system is a third way that grasshoppers control the effects of gravity. – Dana Desonie

See: Jon F. Harrison^{1*}, Khaled Adjerid², Anelia Kassi¹, C. Jacob KloK¹, John M. VandenBrooks¹, Meghan E. Duell¹, Jacob B. Campbell¹, Stav Talal¹, Christopher D. Abdo¹, Kamel Fezzaa³, Hodjat Pendar², and John J. Socha², "Physiological responses to gravity in an insect," *Proc. Natl. Acad. Sci. U.S.A.* **117**(4), 2180 (January 28, 2020). DOI: 10.1073/pnas.1915424117

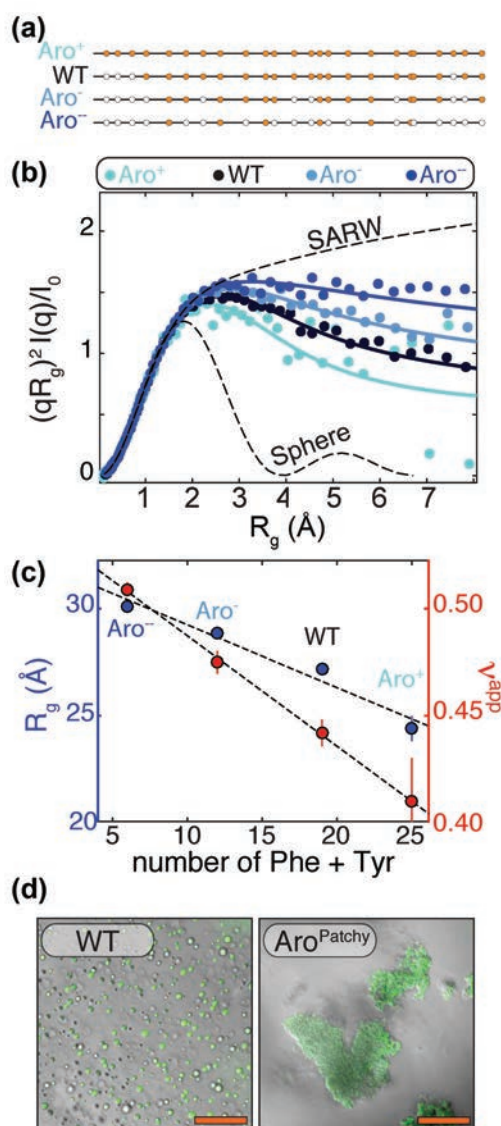
Author affiliations: ¹Arizona State University, ²Virginia Tech, ³Argonne National Laboratory

Correspondence: * j.harrison@asu.edu

This research was supported by National Science Foundation (NSF) Integrative Organismal Systems (IOS) 1558052 and NSF Emerging Frontiers in Research and Innovation (EFRI) 0938047. This research used resources of the Advanced Photon Source, a U.S. Department of Energy (DOE) Office of Science User Facility operated for the DOE Office of Science by Argonne National Laboratory under Contract No. DE-AC02-06CH11357.

Uncovering Unique Structural Features in Protein Regions Associated with ALS

Many of us are familiar with mad cow disease—the neurodegenerative disease caused by prions. Although they have a similar name, the less familiar prion-like domains (PLDs) refer to something different—unique, low-complexity regions of proteins that are capable of regulating gene expression and affecting important cellular processes. Prion-like domains have become a topic of interest because of their connection with a variety of debilitating brain diseases, such as amyotrophic lateral sclerosis (ALS) and frontotemporal dementia. In fact, mutations in PLDs of some genes have been shown to cause neurodegenerative disease. For example, mutations in PLDs of the genes hnRNPA2B1 and hnRNPA1 can cause the neurodegenerative disorders ALS and multisystem proteinopathy. A recent study using data obtained at the APS completed a comprehensive biophysical investigation of PLDs in the protein hnRNPA1 to uncover the major behavioral and structural features of these domains. This meaningful work may lead to discoveries that can help individuals living with such neurodegenerative diseases.



Amyotrophic lateral sclerosis is a devastating disease of the nervous system that affects the brain and spinal cord. Patients often present with symptoms such as slurred speech, muscle twitching, and muscle weakness. Patients lose total control of muscle function as the disease progresses, resulting in a fatal inability to perform everyday tasks such as eating, breathing, moving, and speaking. Age of onset tends to occur later in adult life; at present, there is no cure.

Although the cause of ALS is largely unknown, genetic mutations in PLDs is known to be involved. PLDs have been shown to impact a variety of important cellular processes, such as cell division and understanding how cells respond to stress. The proteins hnRNPA2B1 and hnRNPA1 serve important functions in the processing and stabilization of mRNA. More broadly, PLDs can drive the aggregation of proteins within cells.

Since PLDs have such a palpable relevance to medicine and brain health, investigations into their behavior and structure are highly valuable. Seeking to better understand how PLDs behave and affect molecular aggregation, the authors in this study, from St. Jude Children's Research Hospital, Washington University in St. Louis, and Washington University School of Medicine, found that the temperature-dependent compaction of molecules within a liquid solution is determined by the number of aromatic residues in PLDs. The uniform patterning of these aromatic residues promotes a phenomenon known as liquid-liquid phase separation while preventing aggregation. Liq-

< Fig. 1. The number of adhesive aromatic residues in the PLD of hnRNPA1 determines its compactness. (a) Schematic showing the position of aromatic residues (orange circles) and mutations to other residues (white circles). (b) size exclusion chromatography-coupled small-angle x-ray scattering data (measured at the Bio-CAT x-ray beamline at the APS) in normalized Kratky representation where solid-lines are fits to an empirical molecular form factor (MFF). The MFFs for a self-avoiding random walk (SARW) and a solid sphere are overlaid as dashed lines for comparison. (c) Values of R_g (blue) and v^{app} (red) derived from the MFF fits in (b). (d) Segregation of aromatic residues into patches drives aggregation rather than liquid-liquid phase separation. Overlaid differential interference contrast (DIC) and fluorescence images of wild-type (WT) and Aro^{Patchy} LCDs at identical solution conditions. Adapted from E.W. Martin et al., "Valence and patterning of aromatic residues determine the phase behavior of prion-like domains," *Science* **367**, 694 (7 February 2020). Copyright © 2020 The American Association for the Advancement of Science.

uid-liquid phase separation is a physical process that leads to the formation of two co-existing liquid phases (a dilute and a dense phase), which is the underlying process for the formation of many non-membrane bound cellular compartments. The authors additionally put forth an impressive stickers-and-spacers model (adapted from the associative polymer field) that can be used to make predictions regarding the behavior of PLDs. This study utilized multiscale simulations, nuclear magnetic resonance spectroscopy, and small-angle x-ray scattering (SAXS) to uncover behavioral and structural features of PLDs (Fig. 1). The SAXS research was carried out using high-brightness x-rays at the Bio-CAT 18-ID beamline at the APS. The high brightness x-rays were essential to characterize small differences between structural features of different mutants of the PLD.

The data generated from this work will enable more precise characterization of PLDs within cells, which will in turn provide the ability to predict how PLDs form and dissolve condensates in response to different circumstances (e.g., protein concentration, conditions in cells). Given that PLDs appear to have an important role in the maintenance of brain health, the significant insights into how phase behavior and structure of PLDs are coupled may allow for the development of PLD-targeted therapeutics that can help patients with ALS and other debilitating neurodegenerative disorders. – [Stephen Taylor](#)

See: Erik W. Martin¹, Alex S. Holehouse², Ivan Peran¹, Mina Farag², J. Jeremias Incicco³, Anne Bremer¹, Christy R. Grace¹, Andrea Soranno^{2,3}, Rohit V. Pappu^{2*}, and Tanja Mittag^{1**}, "Valence and patterning of aromatic residues determine the phase behavior of prion-like domains," *Science* **367**, 694 (7 February 2020). DOI: 10.1126/science.aaw8653

Author affiliations: ¹St. Jude Children's Research Hospital, ²Washington University in St. Louis, ³Washington University School of Medicine

Correspondence: * pappu@wustl.edu, ** tanja.mittag@stjude.org

This work was funded by the St. Jude Children's Research Hospital Research Collaborative on Membraneless Organelles in Health and Disease (to T.M. and R.V.P.), the U.S. National Science Foundation (MCB1614766 to R.V.P.), the Human Frontier Science Program (RGP0034/2017 to R.V.P.), the American Federation for Aging Research (to A.S.), and the American Lebanese Syrian Associated Charities (to T.M.). The Biophysics Collaborative Access Team is supported by grant 9 P41 GM103622 from the National Institute of General Medical Sciences of the National Institutes of Health. This research used resources of the Advanced Photon Source, a U.S. Department of Energy (DOE) Office of Science User Facility operated for the DOE Office of Science by Argonne National Laboratory under contract no. DE-AC02-06CH11357.

Double-Safe in the Time of the Pandemic: **Cassandra Hayden**



Structural Biology

Discoveries from First SARS Outbreak Jump-Start COVID-19 Treatment Development

Science can be a capricious endeavor. Research can make unexpected leaps or come to a screeching halt when new information becomes available. This was the case with research into inhibitors for the 3C-like cysteine protease (3CLPRO) of severe acute respiratory syndrome coronavirus 1 (SARS-CoV-1), the coronavirus that caused the outbreak of sudden acute respiratory syndrome in 2002 that killed 799 people. When the current pandemic started and the SARS-CoV-2 virus was identified as the cause, comparison of the new virus to known viruses showed that the 3CLPRO proteins from SARS-CoV-1 and SARS-CoV-2 have 96% sequence identity and are 100% identical with regard to amino acids in the active site. This was incentive for the research team in this study to solve the structure of PF-00835231 (a particularly promising variant of a SARS-CoV-1 protease inhibitor they had been working on) in complex with the 3CLPRO from both coronaviruses in the hope that PF-00835231 would also inhibit the SARS-CoV-2 protease. This study was carried out using the APS.

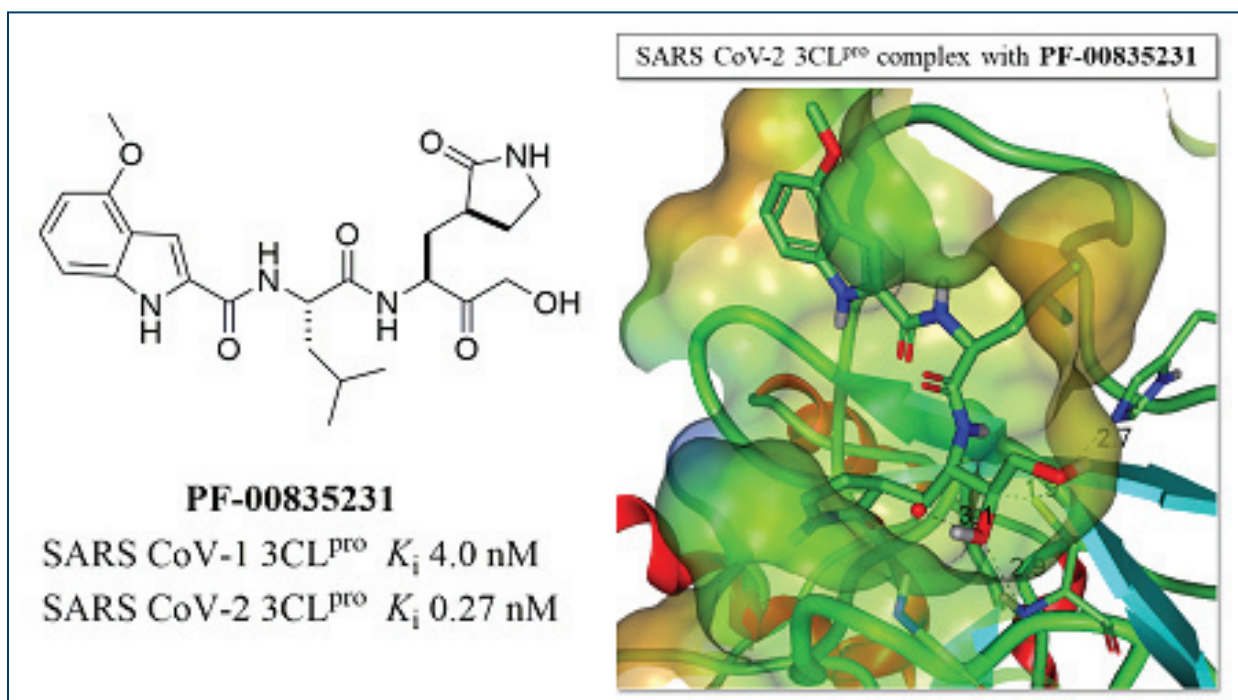


Fig. 1. PF-00835231, a protease inhibitor that is a potential treatment for COVID-19, alone and in complex with the active site of the SARS-CoV-2 3CL protease.

In 2002, researchers hoped to develop a treatment for SARS using PF-00835231. This molecule was one of a series of inhibitors developed based on careful chemical modification of a starting “warhead” that had been successful in development of an inhibitor for a similar protease from another virus. Using structure activity relationships and x-ray co-crystal structural data of inhibitors in complex with the SARS-CoV-1 3CLPRO to modify the warhead and design portions to mimic the viral protein substrates that specifically interact with the protease, PF-00835231 was the most promising candidate against the SARS protease. However, in the case of SARS, the public health response was successful, and the research program was suspended as it was no longer needed.

Fast-forward 18 years and PF-00835231 is back in the limelight as the focus of research into treatments to block the spread of SARS-CoV-2, the coronavirus that is the cause of COVID-19 and the 2020 pandemic.

The initial research project in 2002 focused on the development of compounds designed to inhibit the SARS-CoV-1 protease, 3CLPRO. The 3CLPRO protein acts at the start of viral entry into the host cell to cleave two SARS-CoV-1 polyproteins into multiple active proteins needed for viral infection and replication. This is why researchers hypothesized that inhibiting this step could inhibit viral replication and spread. PF-00835231 had been chosen because it strongly inhibited the SARS-CoV-1 3CLPRO, had excellent stability, and had solubility characteristics that suggested it would be appropriate for intravenous administration.

The x-ray diffraction data in the current study were collected at the IMCA-CAT 17-ID beamline of the APS by a team of researchers from Pfizer Worldwide Research and the Southern Research Institute. The crystal structures (Fig. 1) show that the two proteases are almost identical with conserved catalytic residues in their ligand binding sites and nearly identical structures. PF-00835231 binds in the same way to both proteases, forming a covalent bond to an active site cysteine (Cys 145) and forming hy-

drogen bonds with a number of other key active site amino acids.

Evaluation of the inhibitory activity of number PF-00835231 against the SARS-CoV-2 3CLPRO demonstrated that it is a very potent inhibitor of the enzyme that showed selectivity for coronavirus enzymes among a panel of other viral and human proteases. PF-00835231 had potent and selective antiviral activity against both SARS-CoV-1 and another coronavirus but not other viruses in the panel. Further preclinical evaluation of PF-00835231 demonstrated that this molecule displays potent anti-viral inhibition of SARS CoV-2 which has led to the development of the phosphate prodrug PF-07304814 that has entered clinical trials as a potential treatment for COVID-19.

– Sandy Field

See: Robert L. Hoffman^{1*}, Robert S. Kania¹, Mary A. Brothers, Jay F. Davies¹, Rose A. Ferre¹, Ketan S. Gajiwala¹, Mingying He¹, Robert J. Hogan¹, Kirk Kozminski¹, Lilian Y. Li¹, Jonathan W. Lockner¹, Jihong Lou¹, Michelle T. Marra¹, Lennert J. Mitchell, Jr.¹, Brion W. Murray¹, James A. Nieman¹, Stephen Noell¹, Simon P. Planken¹, Thomas Rowe², Kevin Ryan¹, George J. Smith, III¹, James E. Solowiej¹, Claire M. Stepan¹, and Barbara Taggart², “Discovery of Ketone-Based Covalent Inhibitors of Coronavirus 3CL Proteases for the Potential Therapeutic Treatment of COVID-19,” *J. Med. Chem.* **63**(21), 12725 (2020). DOI: 10.1021/acs.jmedchem.0c01063

Author affiliation: ¹Pfizer Worldwide Research and Development, ²Southern Research Institute

Correspondence: * robert.l.hoffman@pfizer.com

This research used resources at the Industrial Macromolecular Crystallography Association Collaborative Access Team beamline 17-ID, supported by the companies of the Industrial Macromolecular Crystallography Association through a contract with Hauptman-Woodward Medical Research Institute. This research used resources of the Advanced Photon Source, a U.S. Department of Energy (DOE) Office of Science User Facility, operated for the DOE Office of Science by Argonne National Laboratory under Contract No. DE-AC02-06CH11357. Extraordinary facility operations were supported in part by the DOE Office of Science through the National Virtual Biotechnology Laboratory, a consortium of DOE national laboratories focused on the response to COVID-19, with funding provided by the Coronavirus CARES Act.

Viral Life Cycle Inspires New Approaches to Drug Design for SARS-CoV-2

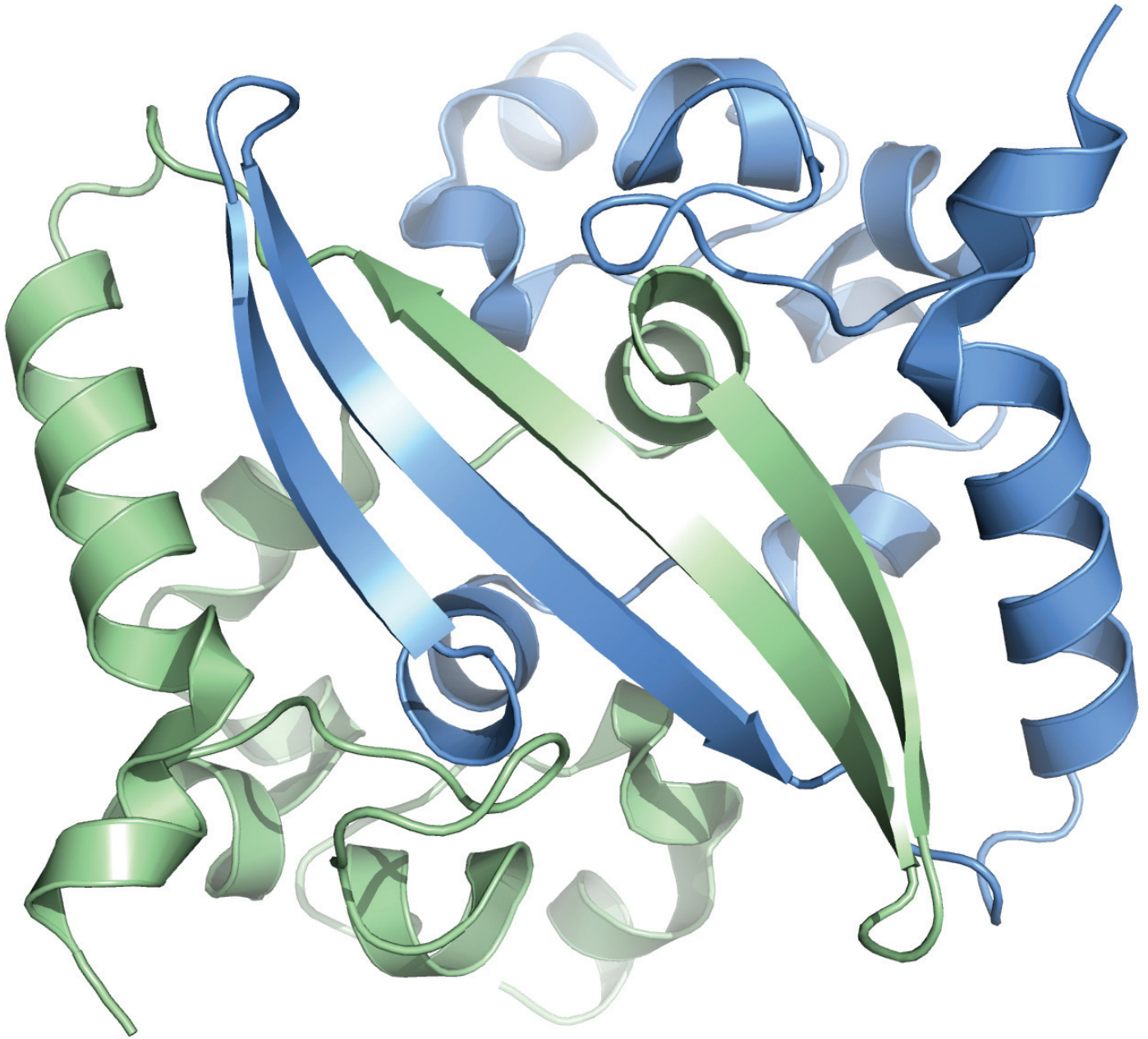


Fig. 1. Structure of the SARS-CoV-2 N protein N2b domain, PDB ID 6WZQ.

Since the year 2000, the world has witnessed three coronavirus outbreaks. The first two outbreaks were SARS (severe acute respiratory syndrome) in 2003 and MERS (Middle East respiratory syndrome) in 2012 that accounted for 774 and 858 deaths worldwide, respectively. Today, we are enduring the third coronavirus outbreak in 20 years. Severe acute respiratory syndrome coronavirus 2 (SARS-CoV-2) has infected more than 23 million people and resulted in over 800,000 deaths worldwide, at the time of writing. Despite advances in science and medicine, we find that we are not immune to these types of global outbreaks. Our best path forward is to continue to learn as much as we can from these viruses, so that we can prevent their rapid transmission in the future. To this end, a team of researchers is making strides in developing a better understanding of an often-overlooked component of SARS-CoV-2, the nucleocapsid (N) protein. The N protein plays vital roles in the replication of SARS-CoV-2 in the cell, and for the packaging of new infectious virus particles (virions). With the help of diffraction data collected at the APS, a research team is developing a better understanding of the protein's structure and self-assembly mechanisms, which could contribute to new therapeutics targeting this protein.

Current approaches to vaccine development have mostly focused on antibodies for the well-known spike proteins on the surface of the virus, which play a critical role in receptor binding and endocytosis. This approach works well for preventing coronavirus infection and has shown some potential in decreasing infection severity. But the researchers in this study, from the University of California, San Diego, are looking beyond the point of cell entry and into the entire viral life cycle of SARS-CoV-2 for inspiration on potential pathways to limit the devastating effect that this disease has on the human body.

This work reports new high-resolution structures of the SARS-CoV-2 N protein determined at the NE-CAT 24-ID-E x-ray beamline at the APS. The structures provide new insights about its self-assembly in solution (Fig. 1). Combining crystallography and hydrogen-deuterium exchange mass spectrometry, they show that the N protein's N2b and C-terminal spacer B/N3 regions self-associate in solution to form a robust N-protein tetramer that facilitates binding of viral RNA for packaging into virions. The group postulates that designing drugs to target and disrupt this self-assembly process may limit virion production, thereby reducing a patient's viral load and ultimately lowering the severity and infectivity of the disease.

Combining their new structures of the SARS-CoV-2 N protein with a set of over 38,000 genome sequencing datasets available on the virus, the team was able to identify approximately 650 sites where amino acid substitutions occur within the structured N1b and N2b domains of this protein. They find that the sites of amino acid substitu-

tion are clustered away from the RNA binding and dimerization interfaces of the N-protein. The fact that these surfaces are highly conserved across numerous genome sequences of SARS-CoV-2 and among coronavirus variants like SARS and MERS, shows the importance of these regions to critical viral functions and also the potential to exploit these regions for the development of life-saving drugs.

Understanding how viruses like SARS-CoV-2 evolve is critical for the design of highly effective medications and tests for the current pandemic, and for future ones to come. – Stephen Taylor

See: Qiaozhen Ye, Alan M. V. West, Steve Silletti, and Kevin D. Corbett*, "Architecture and self-assembly of the SARS-CoV-2 nucleocapsid protein," *Prot. Sci.* **29**(9), 1890 (2020). DOI: 10.1002/pro.3909

Author affiliation: University of California, San Diego

Correspondence: * kcorbett@ucsd.edu

The authors thank the staff of NE-CAT beamline for assistance with diffraction data collection. K. D. C. acknowledges generous institutional support from UC San Diego. NE-CAT is funded by the National Institute of General Medical Sciences from the National Institutes of Health (P30 GM124165). The Eiger 16M detector on the 24-ID-E beam line is funded by a NIH-ORIP HEI grant (S10OD021527). This research used resources of the Advanced Photon Source, a U.S. Department of Energy (DOE) Office of Science User Facility operated for the DOE Office of Science by Argonne National Laboratory under Contract No. DE-AC02-06CH11357. Extraordinary Advanced Photon Source operations were supported in part by the DOE Office of Science through the National Virtual Biotechnology Laboratory, a consortium of DOE national laboratories focused on response to COVID-19, with funding provided by the Coronavirus CARES Act.

Deciphering Coronavirus Protein Behavior

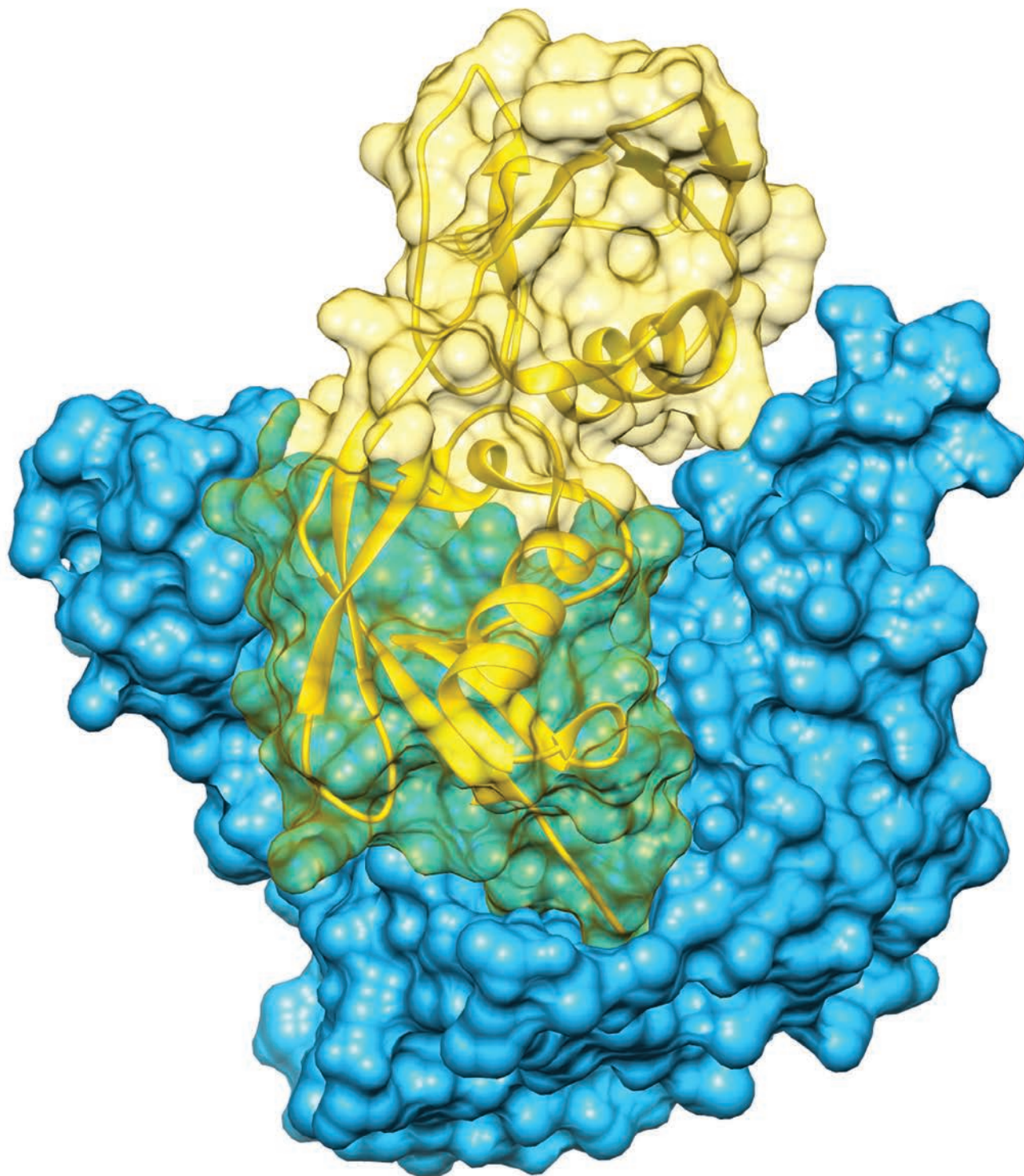


Fig. 1. X-ray structure of the MERS Papain-like protease (PLpro) bound to human ISG15 as determined to 2.3 Å from x-ray data collected at the LS-CAT beamline. MERS PLpro is colored in blue and ISG15 is colored in gold. The solvent-accessible surfaces of both are shown along with a ribbon representation of ISG15.

Before there was severe acute respiratory syndrome 2 (SARS-CoV-2), the coronavirus responsible for the COVID-19 global pandemic, there was MERS-CoV, the Middle East Respiratory Syndrome coronavirus. MERS-CoV, also known as camel flu, is fatal in about a third of humans with co-morbidities who contract it. It is still in circulation and there is no vaccine. A team of scientists, in research that predated the current coronavirus outbreak, targeted a particular protein from the MERS virus called the papain-like protease (PLpro) as part of a potential strategy for vaccine development. Using x-ray data collected at the APS, the researchers solved a high-resolution structure of the viral protein in complex with the human protein interferon-stimulated gene 15 (ISG-15). This information allowed the team to develop a series of PLpro variants to help unravel how the virus suppresses innate immunity.

ISG-15 is a small antiviral protein that looks a bit like ubiquitin, a ubiquitous regulatory protein in eukaryotes. Upon viral infection, interferons promote the rapid production of ISG-15 to combat the pathogen. Its mechanism is still under investigation, but scientists suggest that, in a process called ISGylation, ISG-15 is attached to newly synthesized viral proteins, gumming up the works and blocking viral activity. But coronaviruses and other viruses have their own countermeasures, enlisting deISGylating enzymes to remove the ISG tags. PLpro is one such protease, but the enzyme has other activities as well, such as deubiquitination, as well as its normal function, which is to cleave the viral polyprotein. Due to its multifunctional nature, scientists have struggled to disentangle the role of PLpro in the suppression of the immune response.

To better understand the structural basis for how the PLpro recognizes and cleaves ISG-15 versus ubiquitin, the research team from Purdue University co-crystallized the viral protein with the ISG-15 protein and solved the structure to a resolution of 2.3 angstroms (Fig. 1) using high-brightness APS x-rays at beamline 21-ID-D of LS-CAT. They found that the MERS-CoV PLpro only interacts with the C-terminal domain of ISG-15. The researchers superimposed the PLpro-ISG-15 structure to one previously solved of PLpro in complex with ubiquitin. They found a number of differences, and used this information in the next phase of their experiment: the production of mutant PLpro variants.

Based on a comparison of the PLpro-ISG-15 structure and the PLpro-ubiquitin structures, the team selected 13 different sites on PLpro to mutate, with the goal of disrupting either PLpro's deISGylation or deubiquitination functions, or both. The researchers found that by mutating PLpro at positions 1649 and 1653, they could knock out the deubiquitination activity. By mutating amino acids at positions 1691 or 1652, they could impair both deISGylation and deubiquitination.

These mutants will provide critical information to help scientists figure out the importance of PLpro's various enzymatic roles on MERS-CoV pathogenesis and replication.

This study is just the first step, though. The hope is that these mutants will facilitate studies that allow scientists to infect cells with the mutant viruses in the laboratory and see what happens when a MERS virus loses its ability to deISGylate or deubiquitinate or both. The idea is that if one of these mutant strains has lost its ability to be dangerous, then it becomes a live attenuated vaccine candidate. Such vaccines consist of a weakened form of a virus that, because they are so similar to the natural virus, trigger a strong and lasting immune response.

This general approach is applicable beyond MERS-CoV, and may hold promise in the fight against other members of the coronavirus family, including SARS-CoV-2, which causes COVID-19. – Erika Gebel Berg

See: Jozlyn R. Clasman, Renata K. Everett, Karthik Srinivasan, and Andrew D. Mesecar*, “Decoupling deISGylating and deubiquitinating activities of the MERS virus papain-like protease,” *Antivir. Res.* **174**, 104661 (2020).

DOI: 10.1016/j.antiviral.2019.104661

Author affiliation: Purdue University

Correspondence: * amesecar@purdue.edu

This research was supported by the National Institute of Allergy and Infectious Disease (NIAID) of the National Institutes of Health (NIH) under award number R01AI085089. A.D.M. also wishes to also acknowledge partial support from the Center for Structural Genomics of Infectious Disease (NIH-NIAID Contract HHSN272201700060C) and the Walther Cancer Foundation. Use of the Life Sciences Collaborative Access Team was supported by the Michigan Economic Development Corporation and the Michigan Technology Tri-Corridor (Grant 085P1000817). This research used resources of the Advanced Photon Source, a U.S. Department of Energy (DOE) Office of Science User Facility operated for the DOE Office of Science by Argonne National Laboratory under Contract No. DE-AC02-06CH11357. Extraordinary Advanced Photon Source operations were supported in part by the DOE Office of Science through the National Virtual Biotechnology Laboratory, a consortium of DOE national laboratories focused on response to COVID-19, with funding provided by the Coronavirus CARES Act.

Dexamethasone and COVID-19: All Patients Are Not Alike

While healthcare workers and public health officials have been fighting on the front lines against the severe acute respiratory syndrome coronavirus 2 (SARS-CoV-2) infections that cause the devastating symptoms of COVID-19, researchers have been working to understand how the virus causes the symptoms of the disease and to identify the best treatments. Recent research based on x-ray data collected at the APS has provided important insights into how dexamethasone, a drug used to treat COVID-19 patients, is transported within the body and the factors that may determine whether it helps or harms these vulnerable patients. Their results were the cover article in the *IUCr Journal*.

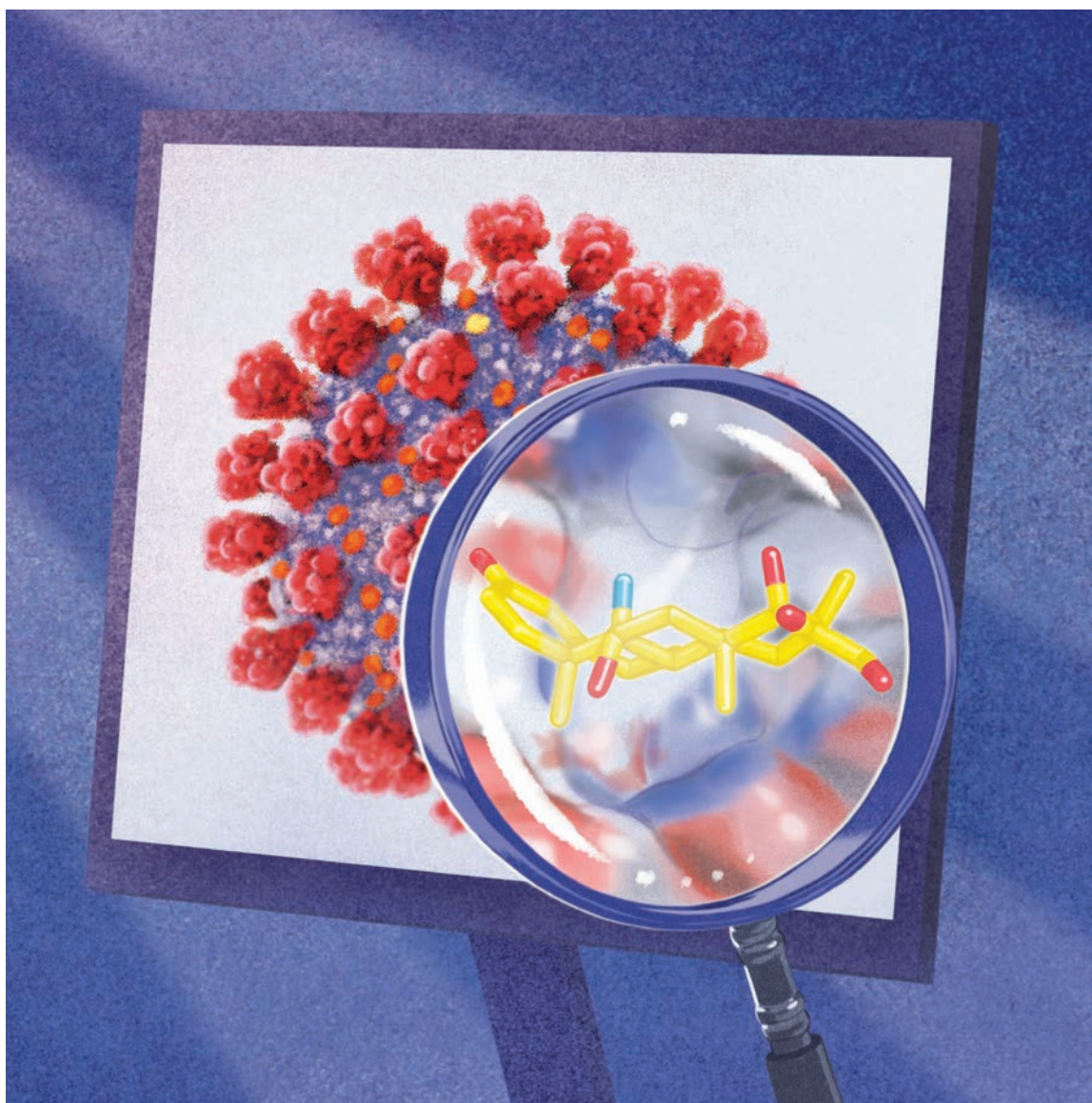


Fig. 1. Dexamethasone (foreground) was recently shown to reduce mortality in patients with serious SARS CoV-2 infections. Image: Marcin Minor.

Dexamethasone is a commonly used corticosteroid drug that gained global attention in June, 2020, when it was reported to reduce death rates by 20%-30% in COVID-19 patients who have respiratory symptoms that require them to be on ventilation or oxygen. However, although the therapeutic actions of dexamethasone are quite well understood, what is less well studied is the way the drug gets to its targets via the bloodstream. This is important because, like most drugs, dexamethasone works within a “window” of therapeutic efficacy and can have off-target side effects if too high a dose is administered. In the blood, dexamethasone is transported by a very abundant protein called albumin. The drug exists in an equilibrium between the albumin-bound form and a pharmacologically active “free” form. Factors that affect this equilibrium can change how much active dexamethasone is in the bloodstream and make the difference between helpful efficacy and harmful side effects.

In an international collaboration led by a team from the University of Virginia, scientists from the United States and Poland conducted experiments at the APS. Their study focused on learning more about the interactions between serum albumin and dexamethasone by solving the crystal structure for this drug-protein complex to 2.4-Å resolution at the LS-CAT 21-ID-F beamline at the APS. The structure (Fig. 1) showed that dexamethasone binds between two subdomains of albumin, which is known to have 10 drug binding sites. The dexamethasone binding site (drug site 7) is already known to bind non-steroidal anti-inflammatory drugs (like ibuprofen), the hormone testosterone, and anesthetics. This highlights the fact that other albumin cargoes could affect dexamethasone levels in the blood. Many of the drugs that are commonly used for COVID-19 patients are known to bind to serum albumin, but their binding sites are not necessarily known. If they compete for dexamethasone binding at site 7, this could impact the therapeutic effects of dexamethasone. Also, the impact of testosterone binding to the same site is interesting as low testosterone levels are a predictor of poor outcomes in COVID-19 and this is suspected to be a contributing factor in why more men die of COVID-19 than women. Dexamethasone in too high a dose could compete with testosterone for albumin binding and affect its transport, further exacerbating the impact of low testosterone.

The team extended their structural findings by analyzing data from patients admitted to the hospital for COVID-

19 in Wuhan, China, early in 2020 to understand the role of albumin transport in determining outcomes in COVID-19 patients. Their first observation was that patients who died of COVID-19 had lower than normal albumin levels and also lower albumin levels compared to those who survived. Although low albumin is a well-recognized risk factor during critical disease, it is important to be aware of this possibility when treating COVID-19 patients with dexamethasone. The Wuhan patients who died also had higher blood glucose levels than those who survived. This finding supports public health advice that patients with diabetes are at higher risk for serious COVID-19 disease. The high blood sugar could also result in modifications of albumin at site 7 and affect its ability to bind dexamethasone and other cargoes.

Dexamethasone is certainly an important treatment for COVID-19, but this study suggests that its administration should potentially be adjusted according to patient risk factors such as albumin levels and diabetes to be sure they achieve the benefits of treatment and not the harms of excess dosing. – [Sandy Field](#)

See: Ivan G. Shabalin¹, Mateusz P. Czub¹, Karolina A. Majorek^{1†}, Dariusz Brzezinski^{1,2,3}, Marek Grabowski¹, David R. Cooper¹, Mateusz Panasiuk⁴, Maksymilian Chruszcz⁵, and Wlodek Minor^{1*}, “Molecular determinants of vascular transport of dexamethasone in COVID-19 therapy,” *IUCrJ* **7**(6), 1048 (November 2020). DOI: 10.1107/S2052252520012944

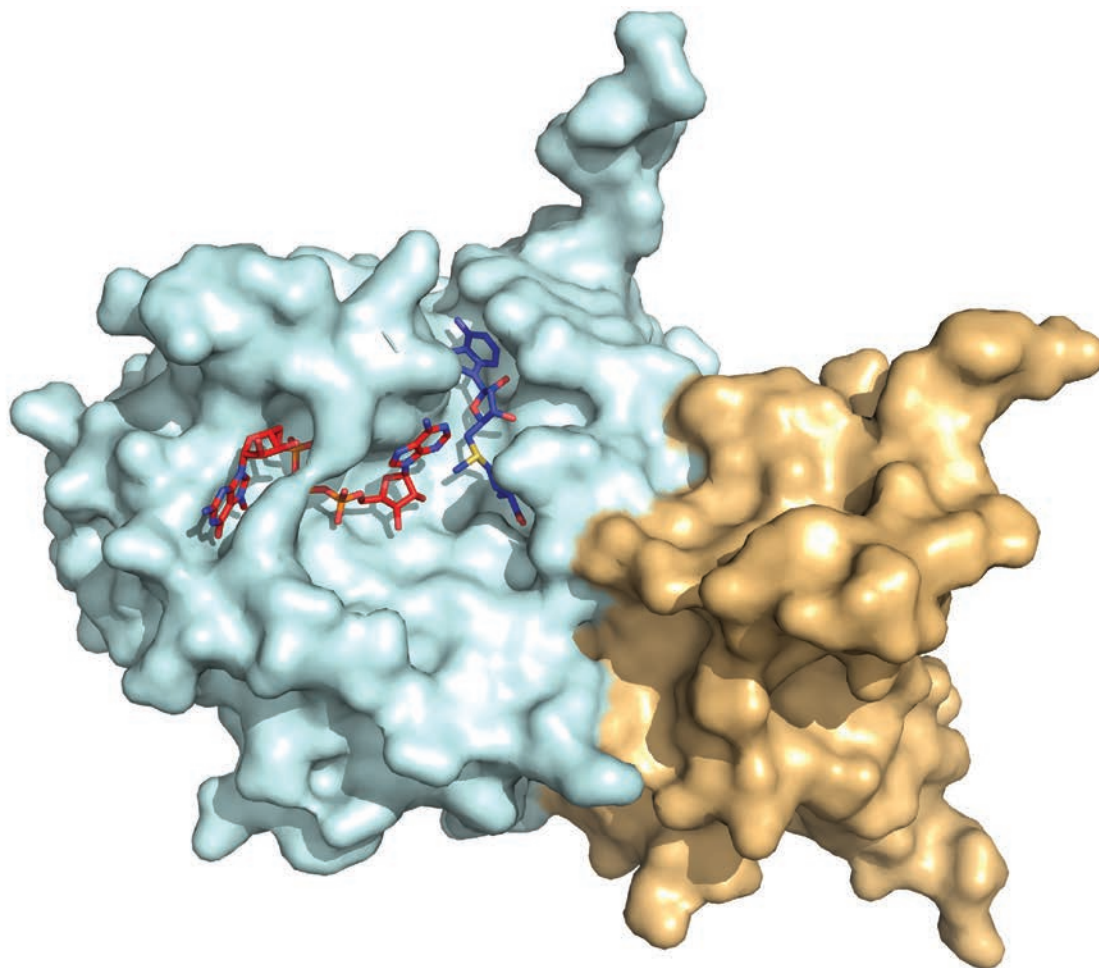
Author affiliations: ¹University of Virginia, ²Polish Academy of Sciences, ³Poznan University of Technology, ⁴Medical University of Bialystok, ⁵University of South Carolina [†]Present address: The Beatson Institute for Cancer Research

Correspondence: * wladek@iwonka.med.virginia.edu

We thank Keith Brister, Zdzislaw Wawrzak, Spencer Anderson, and Joseph Brunzelle at LS-CAT Sector 21 for their assistance in data collection. This work was supported by the National Institute of General Medical Sciences grants R01-GM132595 and U54-GM094662. D.B. acknowledges the support of the Polish National Agency for Academic Exchange (grant No. PPN/BEK/2018/1/00058/U/00001) and Polish National Science Center (grant No. 2020/ 01/0/NZ1/00134). M.P.C. acknowledges the support of the Robert R. Wagner Fellowship at the University of Virginia. M.C. was partially supported by a COVID-19 Research Initiative grant from the Office of the Vice President for Research at the University of South Carolina. Use of the LS-CAT Sector 21 was supported by the Michigan Economic Development Corporation and the Michigan Technology Tri-Corridor (Grant 085P1000817). Extraordinary facility operations were supported in part by the DOE Office of Science through the National Virtual Biotechnology Laboratory, a consortium of DOE national laboratories focused on response to COVID-19, with funding provided by the Coronavirus CARES Act. This research used resources of the Advanced Photon Source, a U.S. Department of Energy (DOE) Office of Science User Facility operated for the DOE Office of Science by Argonne National Laboratory.

How SARS-CoV-2 RNA Evades Host Immune Responses

As we all know too well, the virus severe acute respiratory syndrome 2 (SARS-CoV-2) causes the severe respiratory illness COVID-19. In parallel with the critical search for a cure, scientists are working diligently to develop effective treatments that can help lower the morbidity of this deadly virus. To develop these therapeutics, we must understand how the virus is able to invade a host's cells and dodge detection. A report based on research carried out at the APS reveals key details about how SARS-CoV-2 modifies its messenger RNA and evades immune responses in its host. Using high-resolution x-ray crystallography, the researchers determined a high-resolution structure of the ternary SARS-CoV-2 RNA cap/nsp16/nsp10 complex and the conformational changes that catalytic nsp16 undergoes during RNA cap-binding. The researchers also discovered a distantly located ligand-binding site that allows nsp16 to bind small molecules outside the catalytic pocket. These findings improve our understanding of mRNA capping in coronaviruses and provide a strategy by which scientists could develop small-molecule drugs that will fight and treat the diseases caused by coronaviruses like SARS-CoV-2.



Coronaviruses are enveloped positive-sense RNA viruses that are notorious for causing a variety of diseases from enteritis to respiratory illnesses in both animals and humans. The latest SARS-CoV-2 pandemic illustrates how CoVs can jump between species, gain access to host cells, and propagate with little inhibition. But, in order to design vaccines and treatments that will reduce the burden of the diseases caused by coronaviruses, we must understand their immunopathology.

SARS-CoV-2 is a β -coronavirus that virally encodes mRNAs to mimic host cellular mRNA. To do this, the non-structural protein 16 (nsp16), together with nsp10, methylates the 5'-end of virally encoded mRNAs. Then, nsp16/nsp10 complex converts the mRNA species to the cap-1 form via 2'-O methylation of the ribose sugar of the first nucleotide. So, what information is missing? In short, the catalytic mechanism of mRNA capping is still unclear. Previous reports have presented crystal structures for SARS-CoV nsp16/nsp10 in complex with the methyl donor S-adenosyl methionine (SAM) without an RNA cap. However, no high-resolution structures had been reported for SARS-CoV-2 nsp16/nsp10 in complex with SAM, the methyl donor, and RNA cap m7GpppA. That is, until recently.

The researchers in this study, from University of Texas Health at San Antonio, New England Biolabs, and the Texas Biomedical Research Institute, employed high-brightness x-rays from the APS at the NE-CAT 24-ID-C beamline to collect the high-resolution x-ray crystallography data on crystals of the nsp16/nsp10/SAM/Cap-O/adenosine complex. With the data collected at NE-CAT, the researchers were able to determine the high-resolution structure of the ternary complex of SARS-CoV-2 RNA cap/nsp16/nsp10 complex captured just before ribose 2'-O methylation. A representation of this structure is shown in Fig. 1. They observed that during RNA cap-binding, the catalytic nsp16 undergoes a conformational change from a binary to ternary state. This transition facilitates the addi-

< Fig. 1. Structure of the ternary complex of SARS-CoV-2 RNA nsp16 (cyan)/nsp10 (beige) in complex with RNA cap (red) and S-adenosyl methionine or SAM (blue). (Illustration courtesy of Yogesh Gupta)

tion of a cap-1 structure, m7GpppNm, which acts as a camouflage for the viral mRNA. As a result, the host cells are tricked into recognizing the viral mRNA as their own. This discovery is especially important because it demonstrates how SARS-CoV-2 can avoid detection by the host's immune system.

The researchers also discovered a distantly located ligand-binding site in nsp16/10 where small molecules can bind outside the catalytic pocket. The findings may help to guide the development of SARS-CoV-2 therapies. In essence, if scientists are able to design small-molecule drugs that prohibit cap-1 structure addition by nsp16, they can eliminate the "camouflage" effect and expose the virus to host immune restriction.

The structural details gleaned from this research provide a clearer picture of mRNA capping in coronaviruses. These findings improve our collective understanding of how SARSCoV-2 replicates and avoids detection.

– Alicia Surrao

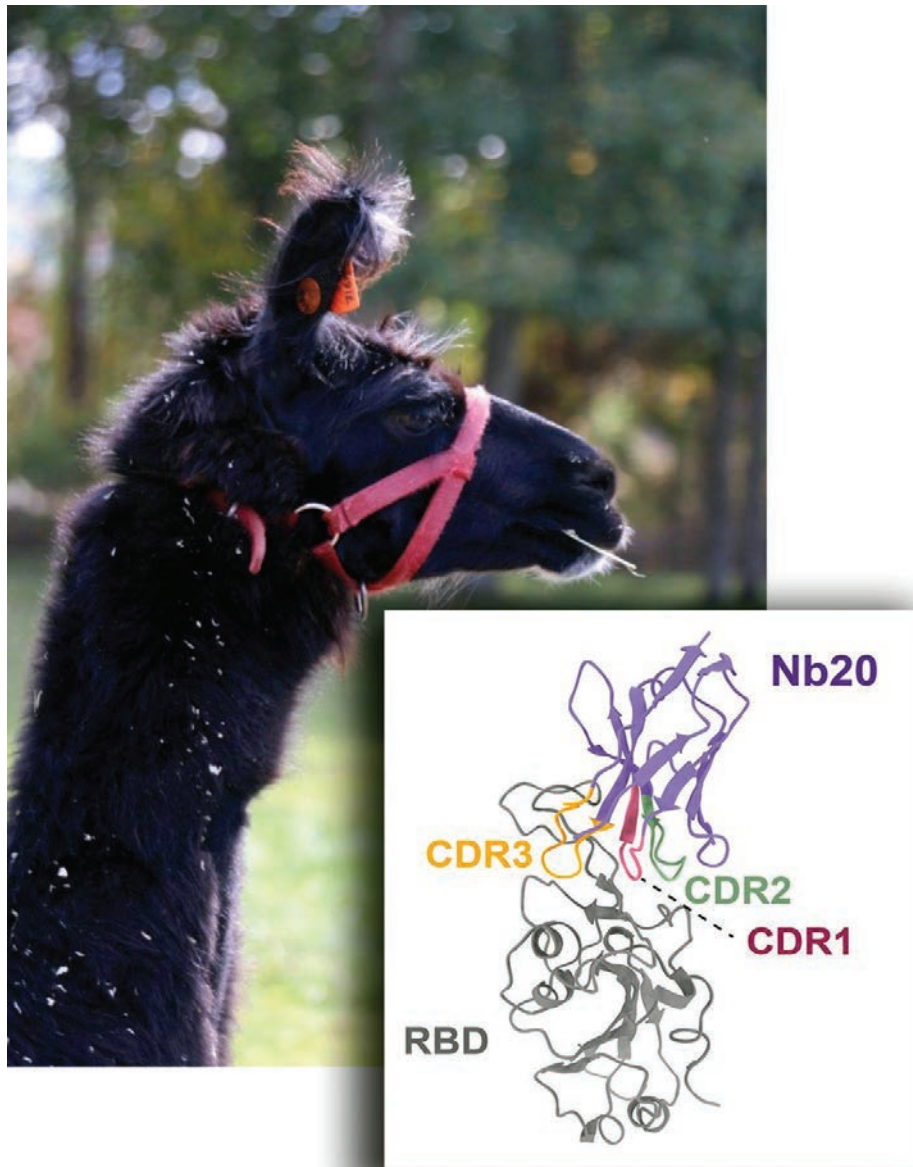
See: Thiruselvam Viswanathan¹, Shailee Arya¹, Siu-Hong Chan², Shan Qi¹, Nan Dai², Anurag Misra¹, Jun-Gyu Park³, Fatai Oladunni³, Dmytro Kovalskyi¹, Robert A. Hromas¹, Luis Martinez-Sobrido³, and Yogesh K. Gupta^{1*}, "Structural basis of RNA cap modification by SARS-CoV-2," *Nat. Commun.* **11**, 3718 (2020). DOI: 10.1038/s41467-020-17496-8

Author affiliations: ¹University of Texas Health at San Antonio, ²New England Biolabs, ³Texas Biomedical Research Institute
Correspondence: * guptay@uthscsa.edu

We are grateful to beamline scientists at NE-CAT for providing synchrotron beam time and facilitating data collection. This work was supported by funding from the Max and Minnie Tomerlin Voelcker Foundation, San Antonio Area Foundation, a Pilot award from the University of Texas (UT) Health San Antonio (UTHSA), and laboratory startup funds from the Greehey Children's Cancer Research Institute of UTHSA to Y.K.G. R. A.H. is supported by National Institutes of Health CA205224. T.V. is supported by a Research Training Award (RP170345) from the Cancer Prevention Research Institute of Texas (CPRIT). We also thank the x-ray core of UTHSA. Y.K.G. is also supported by a high-impact/high-risk award from the CPRIT (RP190534), and a Rising STARS award from the UT System. NE-CAT is funded by the National Institute of General Medical Sciences from the National Institutes of Health (P30 GM124165). This research used resources of the Advanced Photon Source, a U.S. Department of Energy (DOE) Office of Science User Facility operated for the DOE Office of Science by Argonne National Laboratory under Contract No. DE-AC02-06CH11357.

Compact Llama Antibody Combats Coronavirus

Treatments for COVID-19, the illness caused by the novel coronavirus, are urgently needed. Recently, antibody-based COVID-19 treatments have received emergency approval, but questions remain about their effectiveness, particularly in people with the most severe illness. In groundbreaking studies by researchers using the APS, llamas were enlisted to produce small antibodies—or “nanobodies”—that appear to neutralize the coronavirus more potently than anything else scientists have yet identified. The researchers solved the structure of one of these nanobodies in complex with a portion of the coronavirus using diffraction data collected at the APS. Though further research is needed, this work potentially translates into an effective treatment for COVID-19.



Severe acute respiratory syndrome 2 (SARS-CoV-2) invades human cells using its surface spike glycoprotein, a common target for treatments and vaccines to the coronavirus. Spike contains a receptor binding domain (RBD) that sticks to the human ACE-2 receptor, allowing the virus to gain entry to the cell. Scientists have already developed treatments that include antibodies to bind to the spike protein, often to the RBD region, crippling the virus. However, this approach has drawbacks; for example, antibodies are large proteins with multiple subunits, which can be cumbersome and expensive to produce. Another concern is antibody-associated enhancement, in which a virus is actually strengthened through its suboptimal interactions with an antibody.

Nanobodies may be a way around these limitations. These small single-domain antibodies produced naturally by camelids, a family that includes camels, alpacas, and llamas, may offer an alternative approach to coronavirus treatment. Compared to conventional antibodies, nanobodies, at about 15 kilodaltons, are about a tenth as large, yet they maintain similar specificity and selectivity when binding a target. A research team from the University of Pittsburgh, the Pitt/CMU Program, and The Hebrew University of Jerusalem wanted to know whether nanobodies could be targeted to SARS-CoV-2 to block infection as well as, or better than, their larger antibody counterparts.

As a first step, the researchers injected a llama with recombinant RBD, triggering the llama's immune system to produce antibodies that recognize the foreign particle. They then sifted through the llama's serum for RBD-binding nanobodies and found thousands, prompting a series of experiments to whittle the candidates down to only the tightest-binding species. One of the star nanobodies, called Nb20, had an affinity for RBD of 10.4 pM and achieved 100% neutralization of SARS-CoV-2 in a dose-dependent manner, with 50% neutralization (IC50) at 0.048 nM.

To learn more about how the Nb20 achieved such antiviral effectiveness, Zhang's team from Pittsburgh co-crystallized Nb20 with RBD and headed to the National Institute of GM/CA-XSD beamline 23-ID-B at the APS. There, they employed a 10- μ m-diameter microbeam to solve the

< Fig. 1. This llama, named Wally, generated small antibodies that specifically target the SARS-CoV-2 spike protein, neutralizing the virus. Inset: Cartoon presentation of Nb20 in complex with the RBD. CDR1, 2, and 3 are in red, green, and orange, respectively.

structure to a resolution of 3.3 Å and gained useful mechanistic insights for structural studies. Nb20 showed remarkable shape complementarity to RBD, hugging the molecule through extensive hydrophobic and polar interactions (Fig. 1).

The structure also offered some additional insights. The spike glycoprotein actually exists as a trimer on the viral surface, and the researchers realized, through computational modeling, that three molecules of Nb20 could simultaneously grip all three RBD surfaces of the trimer at the same time, potentially offering a boost in binding. They created a genetic construct that threaded together three Nb20 molecules to form a homotrimer and tested it against the virus. The homotrimeric Nb20 construct boasted a 30-fold improvement in viral neutralization as compared to the monomer, in an additive binding phenomenon known as avidity. These are the most potent SARS-CoV-2 neutralizers known to date. They have also designed a plethora of heterodimeric nanobody constructs that cover different epitopes on the viral spike that may efficiently block mutational escape of the virus. The findings could herald a new type of viral treatment to help stem this pandemic, and potentially the next one as well.

– Erika Gebel Berg

See: Yufei Xiang¹, Sham Nambulli^{1*}, Zhengyun Xiao^{1*}, Heng¹Liu^{1*}, Zhe Sang^{1,2}, W. Paul Duprex¹, Dina Schneidman-Duhovny^{3*}, Cheng Zhang^{1**}, and Yi Shi^{1,2***}, “Versatile and multivalent nanobodies efficiently neutralize SARS-CoV-2,” *Science* **370**(6523), 1479 (18 December 2020). DOI: 10.1126/science.abe4747

Author affiliations: ¹University of Pittsburgh, ²Pitt/CMU Program for Computational Biology, ³The Hebrew University of Jerusalem

Correspondence: * dina.schneidman@mail.huji.ac.il, **chengzh@pitt.edu, ***yi.shi@pitt.edu

We thank the staff at the GM/CA-XSD for their assistance with x-ray diffraction data collection. This work was supported by The University of Pittsburgh School of Medicine (Y.S.), a CTSI pilot fund (Y.S.), National Institute of Health (NIH) grant R35GM137905 (Y.S.), The University of Pittsburgh and the Center for Vaccine Research (WPD), NIH grant R35GM128641 (C.Z.), ISF 1466/18 (D.S.), and Israeli Ministry of Science and Technology (D.S.). GM/CA-XSD has been funded in whole or in part with Federal funds from the National Cancer Institute (ACB-12002) and the National Institute of General Medical Sciences (AGM-12006). The Eiger 16M detector at GM/CA-XSD was funded by NIH grant S10 OD012289. This research used resources of the Advanced Photon Source, a U.S. Department of Energy (DOE) Office of Science User Facility operated for the DOE Office of Science by Argonne National Laboratory under Contract No. DE-AC02-06CH11357. Extraordinary Advanced Photon Source operations were supported in part by the DOE Office of Science through the National Virtual Biotechnology Laboratory, a consortium of DOE national laboratories focused on response to COVID-19, with funding provided by the Coronavirus CARES Act.

3-D Structure of SARS-CoV-2 Explains High Infectivity vs. Other Coronaviruses

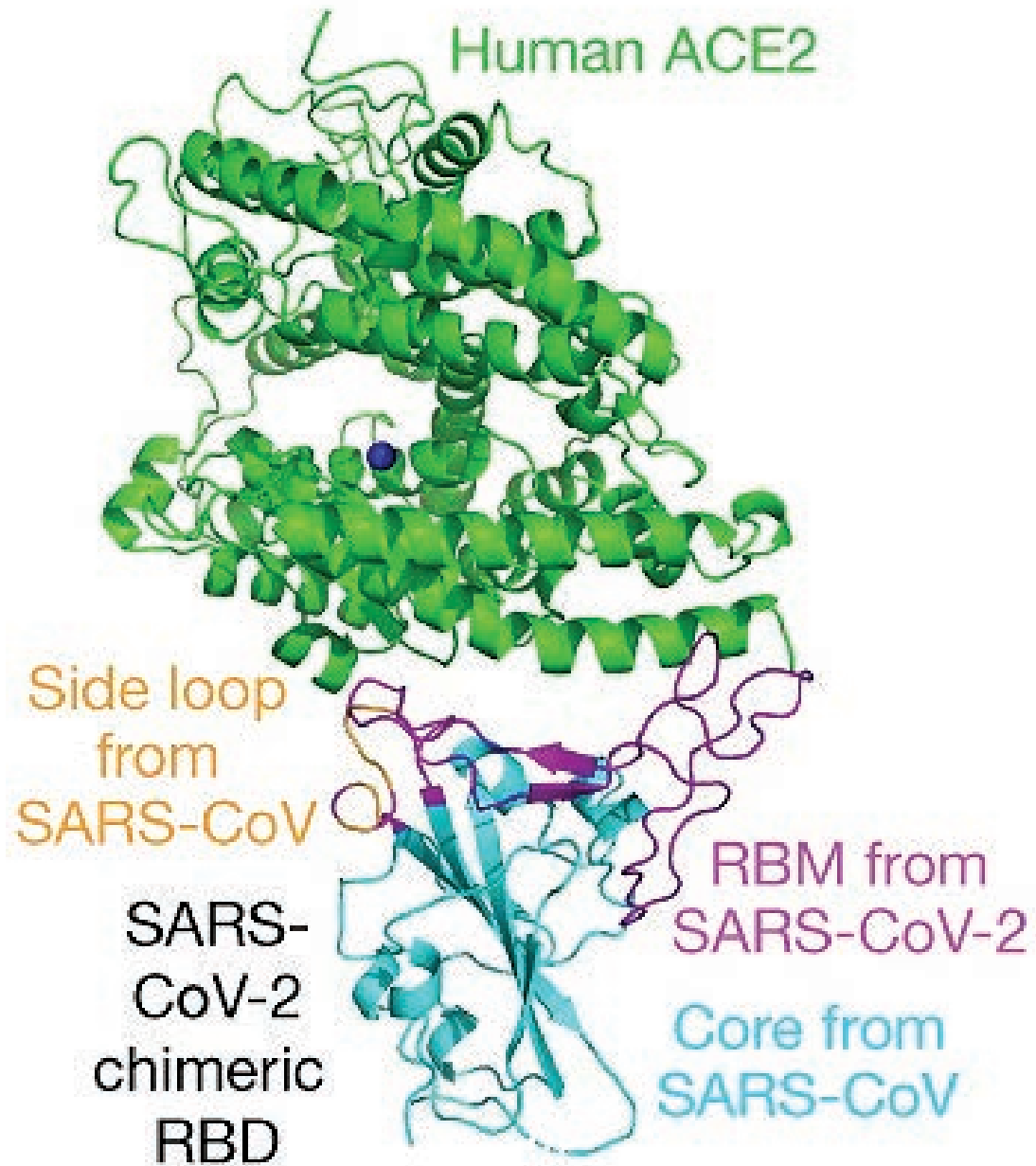


Fig. 1. Crystal structure of the engineered SARS-CoV-2 RBD in complex with hACE-2. hACE-2 is shown in green. The RBD core is shown in cyan. The receptor binding motif (RBM), which mediates contacts with hACE-2 is shown in magenta. A zinc ion in hACE-2 is shown in blue. From J. Shang et al., "Structural basis of receptor recognition by SARS-CoV-2," *Nature* **581**, 221 (14 May 2020). © 2020 Springer Nature Limited

A key to tackling the severe acute respiratory syndrome 2 (SARS-CoV-2)-driven pandemic is learning how the virus attaches to receptors on human cells. This mechanism would likely explain the levels of SARS-CoV-2 infectivity, how it jumped to humans from an animal host, and host range. SARS-CoV-2 and its close coronavirus relative, SARS-CoV, recognize the same receptor in humans called angiotensin-converting enzyme 2 (hACE-2). Researchers using the APS determined the crystal structure of the receptor-binding domain (RBD) of the spike protein of SARS-CoV-2—engineered to facilitate crystallization—in complex with ACE2. In comparison with the SARS-CoV RBD, an ACE2-binding site in SARS-CoV-2, RBD has a more compact, stable conformation. These structural features of SARS-CoV-2 RBD increase the likelihood of the coronavirus binding to hACE-2. Additionally, the researchers show that RaTG13, a bat coronavirus that is closely related to SARS-CoV-2, also uses hACE-2 as its receptor. The differences among SARS-CoV-2, SARS-CoV and RaTG13 in hACE-2 recognition shed light on the potential animal-to-human transmission of SARS-CoV-2. These studies provide guidance for intervention strategies that target receptor recognition by SARS-CoV-2.

The emergence of SARS-CoV-2 in China caused hundreds of thousands of deaths and overwhelmed health care systems around the globe. Following other notable recent coronavirus outbreaks, including SARS-CoV in 2002 and MERS-CoV in 2012, SARS-CoV-2 is the seventh coronavirus known to cause human disease.

Coronaviruses are a group of large, enveloped viruses with single-stranded RNA genomes. All coronaviruses share a similar means of infection: When the virus encounters a human cell, spike-shaped proteins on its surface attach to cell receptors called hACE-2, if the cell possesses them, allowing the virus to gain entry to the cell and begin replicating.

In some important ways, SARS-CoV-2 behaves very differently from other coronaviruses, including its close relative SARS-CoV, which was responsible for approximately 8000 infections and 775 deaths. While both SARS-CoV and SARS-CoV-2 replicate in the lungs, SARS-CoV-2 also efficiently infects the throat and the nose. However, because levels of hACE-2 are thought to be lower in the throat and nose, there has been a question about whether SARS-CoV-2 does a better job of clinging onto hACE-2.

To answer this question, researchers from the University of Minnesota used x-ray crystallography data obtained at the NE-CAT beamline 24-ID-E at the APS to create the first atomic-scale three-dimensional (3-D) map of the receptor binding domain (RBD) on the spike protein of a SARS-CoV-2 in complex with hACE-2 [1]. To facilitate crys-

tallization, the researchers designed a chimeric RBD that uses the core from the SARS-CoV RBD as the crystallization scaffold and the RBM from SARS-CoV-2 as the functionally relevant unit. They then compared the crystal structure with those of other coronaviruses, primarily SARS-CoV. (No live viruses are studied at the APS.)

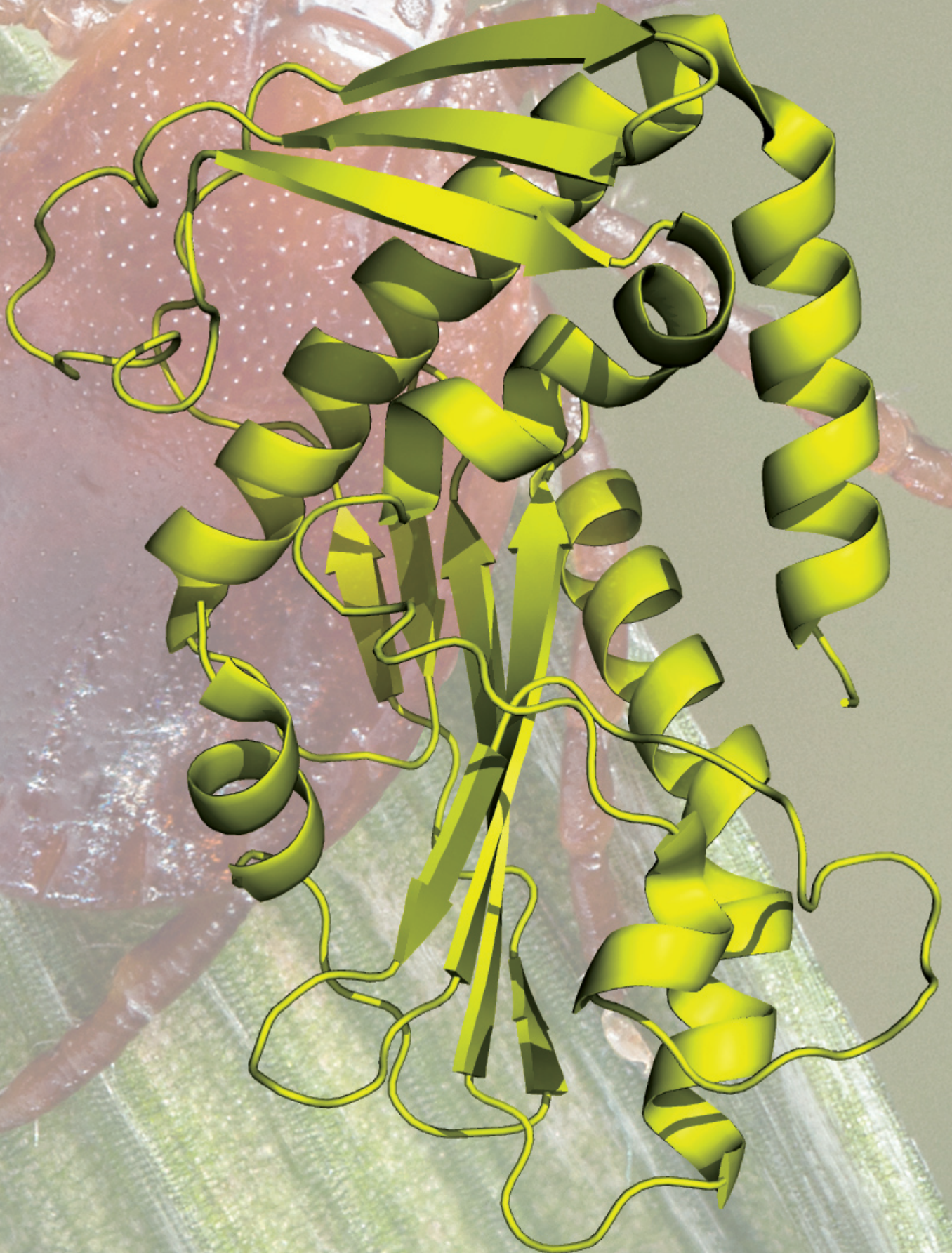
The 3-D structure of SARS-CoV-2 (Fig. 1) shows that the club-like spike proteins it uses to establish infections are more compact and have the potential to latch onto the hACE-2 receptor about four times more strongly than the spike proteins on SARS-CoV. In addition, several residue changes in the SARS-CoV-2 RBD stabilize two virus-binding hotspots at the RBD–hACE-2 interface. This results in the SARS-CoV-2 RBD having a tighter and more stable binding affinity for the human cells.

In theory, this finding would suggest that SARS-CoV-2 should infect humans more easily than SARS-CoV, which it does. Yet, a more recent publication from the researchers used a biochemical technique called a protein pull-down assay to show that although SARS-CoV-2 RBD has a higher hACE2-binding affinity than SARS-CoV RBD, the hACE2 binding affinity of the entire SARS-CoV-2 spike is comparable to or lower than that of SARS-CoV spike. The researchers hypothesize that the reason for this is likely due to the SARS-CoV-2 RBD being less accessible than that of SARS-CoV.

Binding affinity, however, is not the sole determinant

“3-D” cont’d. on page 98

Repurposing Existing Treatments to Fight Emerging Viral Pathogens



Bunyaviruses, as defined by Merriam-Webster, are spherical or pleomorphic single-stranded RNA viruses that are usually transmitted by the bite of an arthropod (think: mosquito) or in the bodily secretions of rodents. They include the hantaviruses and are the causative agents of Rift Valley fever, sandfly fever, and some forms of encephalitis and hemorrhagic fever. Experts have been tracking a couple of new bunyaviruses that have circulated in China and in the United States since about 2009. These viruses, the severe fever with thrombocytopenia syndrome virus (SFTSV) found in East Asia, and the heartland virus (HRTV) identified in the U.S., belong to a family of RNA viruses that are likely to be spread by ticks. SFTSV, in particular, can cause serious disease with an estimated 12%-30% mortality rate. Unfortunately, there are no currently approved drugs to treat infections caused by these viruses and no vaccines available. However, one approach to treatment may be found in the identification of similarities between these viruses and other, more well-known viruses to identify potential drug targets. Building on this concept with a structural biology approach enabled by the extreme-brightness x-rays from the APS, a research team has identified a potential treatment for SFTSV and HRTV and other related viruses.

RNA viruses replicate inside host cells by expressing a polymerase that transcribes RNA and replicates the viral genome to build new virions (a complete virus particle that consists of an RNA or DNA core with a protein coat sometimes with external envelopes and that is the extracellular infectious form of a virus). One interesting feature of bunyaviruses is that their RNA polymerases do not have the usual capping domain needed to provide an RNA primer cap for starting transcription. Instead, they have a “cap-snatching” domain at the N-terminus of the polymerase that uses endonuclease enzyme activity to clip off a host RNA primer cap to use for transcription and translation of viral proteins. The most well-known cap-snatching polymerase is from influenza A virus (IAV), and baloxavir marboxil (BXM), an endonuclease inhibitor, was recently approved for treatment of IAV infection. Based on the hypothesis that the cap-snatching domain from SFTSV might present a target for a similar inhibitory approach, the researchers from the Washington University School of Medicine and the University of Southern California set out to structurally and functionally characterize this domain.

< Fig. 1. SFTSV is transmitted by the *Haemaphysalis longicornis* tick (CDC/James D. Gathany; Public Health Image Library ID#: 22873). Shown is the x-ray crystal structure of the SFTSV endonuclease domain determined at SBC-XSD.

The work started with expression of just the cap-snatching domain of the SFTSV RNA polymerase. After confirming that the domain was a monomer in solution by size exclusion multi-angle light scattering (SEC-MALS), the researchers were able to solve the crystal structure of the protein to 2.4 Å using data collected at the SBC-XSD 19-ID beamline at the APS. The structure revealed some features that confirmed the cap-snatching activity of the domain, including the conserved amino acids needed for the catalytic endonuclease activity of the protein, and a general fold similar to IAV and other cap-snatching viral polymerases in the family.

However, the SFTSV structure also revealed some unique features. The domain has a unique beta cap structure on the N-terminal exposed surface that has only been observed in one other family member and a completely unique alpha helix at its C-terminal end.

Functional assays showed that the N-terminal cap domain could not be removed without completely destabilizing the structure. However, assessment of the unique helix was more interesting. Removal of the helix resulted in increased endonuclease activity of the domain and other physical tests showed that this region is highly flexible, suggesting it controls access to the active site of the en-

“Existing” cont’d. on page 98

New Zika Virus Vaccine May Also Protect Against Dengue Virus

Zika virus infection has caused widespread cases of neurological pathology and congenital neurologic defects. Rapid vaccine development has led to a number of candidates capable of eliciting potent Zika virus-neutralizing antibodies. Despite advances in vaccine development, it remains unclear how Zika virus vaccination affects immune responses in humans with prior immunity to the flavivirus family of viruses, to which the Zika and dengue viruses belong. A team of researchers have now shown that a single-dose immunization of a Zika virus vaccine in a person previously infected with dengue virus elicited potent cross-neutralizing antibodies to both Zika virus and dengue virus. The research team isolated one antibody in particular, called MZ4, and used two U.S. Department of Energy x-ray light sources including the APS to determine that the antibody targets a novel site of vulnerability centered on the domain I/III linker region of the Zika virus envelope. The researchers also discovered that MZ4 rapidly eliminates Zika virus in Zika-infected mice. Finally, the team showed that vaccination in Puerto Rican individuals with prior flavivirus experience yielded similar cross-neutralizing potency after a single vaccination, suggesting a potential benefit of Zika virus vaccination in locations with a high incidence of flavivirus infection. These results demonstrate the potential for MZ4 to be part of the prevention toolbox for these diseases. A vaccine based on this antibody may be able to elicit both Zika- and dengue-virus-protective immune responses with unique potential as a prevention tool in regions where both dengue and Zika are prevalent.

Since 2015, an outbreak of the Zika virus has had devastating effects on children and families across the western hemisphere. Although no longer declared an international public health emergency, cases of Zika virus infection are still occurring, and the threat of another epidemic remains. While Zika virus infections are generally not severe, this infection among pregnant women can lead to severe birth defects in the newborn baby including microcephaly and severe mental retardation. As with most other flavivirus infections, there is no known cure for Zika virus infection and researchers continue to search for an effective vaccine.

A few years ago, scientists developed a vaccine against the Zika virus and performed a series of Phase 1 clinical trials in humans. They found the vaccine to be both safe and effective in generating robust immune responses against the Zika virus.

Now, a multi-institution team of many of those same researchers has analyzed the antibody responses of trial participants following vaccination with the Zika vaccine who had previously been naturally infected with dengue virus in two separate phase I trials (located both in the

contiguous U.S., and Puerto Rico), and compared these responses to participants with no prior exposure to dengue. While study participants with prior dengue exposure experienced a sharp increase in antibodies following just one dose of the novel Zika vaccine, the dengue-naïve participants required two vaccinations to reach a similar increase in antibody production to Zika. However, this level of antibody response in the dengue-naïve participants was specific for Zika virus only and insufficient to thwart dengue infection.

In a separate series of experiments, the researchers, using a unique B-cell sorting strategy, isolated and characterized multiple antibodies from a clinical trial participant previously exposed to dengue. One of these antibodies, MZ4, demonstrated high neutralization potency against both Zika virus and dengue virus serotype 2. Potent activity against dengue virus serotype 3 was also observed, as well as modest neutralization against serotypes 1 and 4. Although no neutralization activity was detected to flaviviruses WNV, YFV or JEV, the antibody MZ4 had broad neutralization against Zika virus strains from American, Asian, and African lineage. *“Zika” cont’d. on facing page*

“Zika” cont’d. from previous page

The researchers then administered antibodies MZ4 and MZ1 prior to either Zika or dengue infection in mice and found that it fully prevented the accumulation of virus particles in the blood of mice. MZ4 also protected against the dissemination of virus into mouse brain, spleen, and lymph nodes.

To better understand how MZ4 recognizes the Zika virus, diffraction data for the MZ1 Fab antibody and the MZ4 Fab antibody to a final resolution of 2.05 Å and 2.95 Å, respectively (Fig. 1), and diffraction data for MZ4-ZIKV E complex to a final resolution of 4.3 Å were collected at the SBC-XSD 19-ID x-ray beamline of the APS. Diffraction data for MZ1-ZIKV E crystals were collected at the NE-CAT 24-ID-E beamline at the APS to a final resolution of 4.2 Å. MZ24 Fab diffraction data were collected at the National Synchrotron Light Source-II (NSLS-II) AMX 17-1 beamline to a final resolution of 2.11 Å.

The researchers used this data to identify the binding site of the MZ4 antibody as the DI/DIII linker region of the Zika virus envelope. The atomic level understanding of the epitope explains the level of cross-neutralization seen by this family of antibodies and provides insight for future vaccine design and clinical studies of broadly protective vaccines and therapeutics. – Chris Palmer

See: Vincent Dussupt^{1,2}, Rajeshwer S. Sankhala^{1,2}, Gregory D. Gromowski¹, Gina Donofrio^{1,2}, Rafael A. De La Barrera¹, Rafael A. Larocca^{3,4}, Weam Zaky^{1,2}, Letzibeth Mendez-Rivera^{1,2}, Misook Choe^{1,2}, Edgar Davidson⁸, Michael K. McCracken¹, James D. Brien⁶, Peter Abbink^{3,4}, Hongjun Bai^{1,2}, Aubrey L. Bryan⁵, Candace Hope Bias¹, Irina Maljkovic Berry¹, Nubia Botero¹, Tanya Cook¹, Nicole A. Doria-Rose⁷, Ariadna Grinyo i Escuer⁵, Justice Akuoku Frimpong⁸, Aviva Geretz^{1,2}, Mayda Hernandez⁵, Bradley S. Hollidge⁸, Ningbo Jian^{1,2}, Kareem Kabra⁵, David J. Leggat⁷, Jinyan Liu^{3,4}, Amelia K. Pint⁶, Wiriya Rutvisuttinunt¹, Ian Setliff⁹, Ursula Tran^{1,2}, Samantha Townsley^{1,2}, Benjamin J. Doranz⁵, Mor-

gane Rolland^{1,2}, Adrian B. McDermott⁷, Ivelin S. Georgiev⁹, Rasmi Thomas^{1,3}, Merlin L. Robb³, Kenneth H. Eckels¹, Elizabeth Barranco¹⁰, Michael Koren¹, Darci R. Smith^{8†}, Richard G. Jarman¹, Sarah L. George¹¹, Kathryn E. Stephenson^{3,4}, Dan H. Barouch^{3,4}, Kayvon Modjarrad¹, Nelson L. Michael¹, M. Gordon Joyce^{1,2*} and Shelly J. Krebs^{1,2**}, “Potent Zika and dengue cross-neutralizing antibodies induced by Zika vaccination in a dengue-experienced donor,” *Nat. Med.* **26**,

228 (February 2020). DOI: 10.1038/s41591-019-0746-2

Author affiliations: ¹Walter Reed Army Institute of Research, ²Henry M. Jackson Foundation for the Advancement of Military Medicine, ³Harvard Medical School, ⁴Ragon Institute of MGH, ⁵Integral Molecular, ⁶Saint Louis University School of Medicine, ⁷National Institutes of Health, ⁸U.S. Army Medical Research Institute of Infectious Diseases, ⁹Vanderbilt University Medical Center, ¹⁰Ponce Health Sciences University, ¹¹Saint Louis University School of Medicine and St. Louis VA Medical Center †Present address: [†]Naval Medical Research Center

Correspondence:

* gjoyce@eidresearch.org,

** skrebs@hivresearch.org

This work was primarily funded by the U.S. Department of the Army and the Defense Health Agency (O130602D16) to K.M. This work was supported by a cooperative agreement

(W81XWH-07-2-0067) between the Henry M. Jackson Foundation for the Advancement of Military Medicine and the U.S. Department of Defense under the leadership of N.L.M. and M.R. In addition, this work was supported by NIH contract no. HHSN272201400058C to B.J.D. SBC-XSD is operated by UChicago Argonne for the U.S. Department of Energy (DOE) Office of Biological and Environmental Research under contract no. DE-AC02-06CH11357. The Northeastern Collaborative Access Team beamlines, which are funded by the National Institute of General Medical Sciences from the National Institutes of Health (NIH) P30 GM124165. The Eiger 16M detector on the 24-ID-E beamline is funded by a NIH-ORIP HEI grant (S10OD021527). The National Synchrotron Light Source-II, a U.S. DOE Office of Science User Facility is operated for the DOE Office of Science by Brookhaven National Laboratory under contract no. DE-SC0012704. This research used resources of the Advanced Photon Source, a U.S. Department of Energy (DOE) Office of Science User Facility operated for the DOE Office of Science by Argonne National Laboratory under Contract No. DE-AC02-06CH11357.

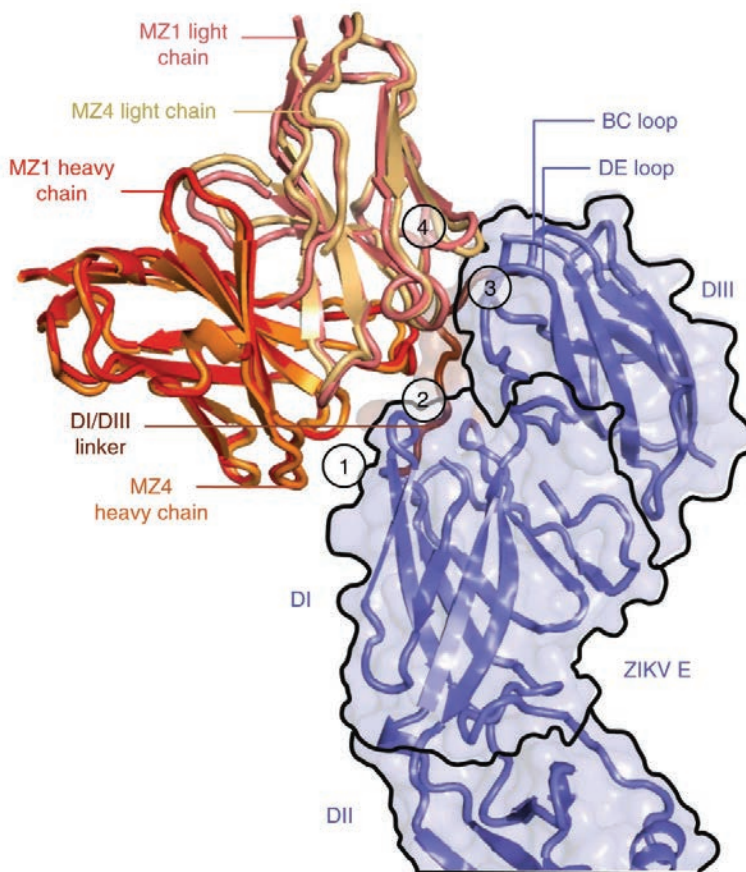


Fig. 1. Crystal structure of human antibody MZ1 and MZ4 in complex with ZIKV E glycoprotein.

“3-D” cont’d. from page 93

of infectivity success. The researchers’ new paper also demonstrates that SARS-CoV-2 does a better job of evading the human immune system. It’s likely this aspect of the virus that ultimately determines its ability to infect more humans than SARS-CoV.

The researchers went on to compare the structure of SARS-CoV-2 with related strains found in bats and pangolins. They found that both animal strains could bind to the same hACE-2 receptor. This evidence supports previous work suggesting the human coronavirus came from bats either directly, or via pangolins acting as an intermediate host. To infect humans, however, the bat or pangolin coronavirus would have needed to undergo mutations to better attach to the human receptor.

The knowledge gained through the biochemical assays and the creation of 3-D crystal structures of SARS-CoV-2 not only provides a better understanding of the mechanisms involved in the infectivity of the virus, but also sheds light on its animal origin and offers guidance on vaccine and antiviral drug designs. – [Chris Palmer](#)

See: [1] Jian Shang, Gang Ye, Ke Shi, Yushun Wan, Chuming Luo, Hideki Aihara, Qibin Geng, Ashley Auerbach, and Fang Li*, “Structural basis of receptor recognition by SARS-CoV-2,” *Nature* **581**, 221 (14 May 2020). DOI: 10.1038/s41586-020-2179-y

Author affiliation: University of Minnesota

Correspondence: * lifang@umn.edu

This work was supported by National Institutes of Health (NIH) grants R01AI089728 and R01AI110700 (to F.L.) and R35GM118047 (to H.A.). We thank staff at the Northeastern Collaborative Access Team for assistance in data collection. The Northeastern Collaborative Access Team beamlines are funded by the National Institute of General Medical Sciences from the National Institutes of Health (P30 GM124165). The Eiger 16M detector on the 24-ID-E beamline is funded by a NIH-ORIP HEI grant (S10OD021527). This research used resources of the Advanced Photon Source, a U.S. Department of Energy (DOE) Office of Science User Facility operated for the DOE Office of Science by Argonne National Laboratory under Contract No. DE-AC02-06CH11357.

[2] Jian Shang, Yushun Wan, Chuming Luo, Gang Ye, Qibin Geng, Ashley Auerbach, and Fang Li*, “Cell entry mechanisms of SARS-CoV-2,” *Proc. Natl. Acad. Sci. U.S.A.* **117**(21), 11727 (May 26, 2020). DOI: 10.1073/pnas.2003138117

Author affiliation: University of Minnesota

Correspondence: * lifang@umn.edu

This work was supported by National Institutes of Health Grants R01AI089728 and R01AI110700 (to F.L.). This research used resources of the Advanced Photon Source, a U.S. DOE Office of Science User Facility operated for the DOE Office of Science by Argonne National Laboratory under Contract No. DE-AC02-06CH11357.

“Existing” cont’d. from page 95

zyme. Further functional assessments of the SFTSV cap-snatching domain showed that it is stabilized by manganese ions and that these are also a cofactor for catalysis. Mutation of the conserved catalytic amino acids confirmed their importance in the endonuclease activity of the protein.

The final step was to test known inhibitors of related viral polymerases to see if they might identify a drug that could be repurposed for treatment of SFTSV and HRTV. The team tested several influenza endonuclease inhibitors and showed that one of them, the IAV inhibitor BXM, inhibited the SFTSV and HRTV endonucleases with similar efficacy to the IAV endonuclease in their in vitro assay and also inhibited SFTSV and HRTV viral plaque formation in a viral replication assay.

Further structural model analysis supports the conclusion that BXM binds to and stabilizes the SFTSV and HRTV polymerases in a similar manner to IAV and this stabilization inhibits their enzymatic activity.

Taken together, these results promise to have a global impact by identifying effective new treatments for SFTSV, HRTV, and related emerging viral pathogens.

– [Sandy Field](#)

See: Wenjie Wang¹, Woo-Jin Shin², Bojie Zhang¹, Younho Choi², Ji-Seung Yoo², Maxwell I. Zimmerman¹, Thomas E. Frederick¹, Gregory R. Bowman¹, Michael L. Gross¹, Daisy W. Leung¹, Jae U. Jung^{2*}, and Gaya K. Amarasinghe^{1**}, “The Cap-Snatching SFTSV Endonuclease Domain Is an Antiviral Target,” *Cell Rep.* **30**, 153 (January 7, 2020). DOI: 10.1016/j.celrep.2019.12.020

Author affiliations: ¹Washington University School of Medicine,

²University of Southern California

Correspondence: * jaeujung@med.usc.edu,

** gamarasinghe@wustl.edu

Research was supported by National Institutes of Health (NIH) grants R01AI107056 and R01AI140758 (D.W.L.); R01AI123926 (G.K.A.); U19AI109945 and U19AI109664 (G.K.A.); R01GM12400701 (G.R.B.); and CA200422, AI116585, AI129496, AI140705, and AI140718 (J.U.J.); as well as by the Fletcher Jones Foundation (J.U.J.), National Science Foundation (NSF) CAREER Award MCB-1552471 (G.R.B.), and U.S. Department of Energy (DOE) Integrated Diffraction Analysis (IDAT) grant contract DE-AC02-05CH11231. The mass spectrometry was supported by the National Institute of General Medical Sciences (NIGMS) of the NIH (grant P41GM103422). SBC-XSD is operated by the University of Chicago, Argonne, for the U.S. DOE Office of Biological and Environmental Research under contract DE-AC02-06CH11357. This research used resources of the Advanced Photon Source, a U.S. DOE Office of Science User Facility operated for the DOE Office of Science by Argonne National Laboratory under Contract No. DE-AC02-06CH11357.

A Novel, Potent Pharmaceutical for the Treatment of Prostate Cancer

Prostate cancer is a debilitating, age-related disease that is a leading cause of cancer death in men. Although research efforts have developed treatment options to improve patient outcomes, the overall mortality rate remains high compared to other cancer types. As such, there is a dire need for improved therapeutics that can increase patient survival. With this clinically paramount goal in mind, the research team in this study developed a novel, high-potential pharmaceutical for the treatment of prostate cancer. This compound, named “ABBV-744,” is a potent and specific inhibitor of the BET protein family. In a mouse prostate cancer model, treatment with ABBV-744 reduced tumor volume and caused fewer side effects compared to a previously identified BET inhibitor. X-ray diffraction data were collected at the APS to better understand the interaction between ABBV-744 and its protein target. While this novel compound ultimately needs to undergo rigorous clinical testing to assess its safety and efficacy, it harbors exciting potential for the treatment of prostate cancer.

In biology, epigenetic modifications refer to gene regulatory mechanisms that are independent of DNA sequence. A classic example of this is histone acetylation. DNA is the blueprint used for the construction of genes; a process referred to as transcription. Since our cells contain an inordinate amount of DNA, it must be very strategically packaged and organized by proteins called histones. When the chemical group acetyl is transferred to a histone, it changes its chemical structure and promotes the utilization of DNA to produce genes. This promotion of gene expression is reversed by the removal of an acetyl group from histones. Thus, histone acetylation and deacetylation play very important regulatory roles in biology.

Genes are ultimately translated into proteins, which are the primary cellular workers. Proteins that are part of the bromodomain and extraterminal (BET) family are epigenetic readers that recognize acetyl groups on histones. They additionally bind to acetylated histones, thereby regulating the expression of genes. Key protein members of this family include BRD2, BRD3, BRD4, and BRDt, each of which contains the two different bromodomains BD1 and BD2. Previously, inhibitors of both bromodomains have shown modest activity in cancer clinical trials. Unfortunately, these inhibitors have been associated with undesirable side effects such as a low blood platelet count and gastrointestinal toxicity. The genetic suppression of the

BET gene *Brd4* in mice causes similar adverse symptoms. Since a desirable oncology drug is one that can combat cancer with minimal or tolerable side effects, ideally a new generation of BET inhibitors would be designed that can more safely mediate anti-cancer effects.

These researchers, from AbbVie, theorized that the inhibition of just one bromodomain (i.e., BD1 vs. BD2) may mediate anti-cancer effects more safely. To test this, they performed a medical chemistry screen to identify ABBV-744, a potent and selective BD2 domain inhibitor. To better understand the interaction between this pharmaceutical and the BD2 domain, x-ray diffraction data were collected at the IMCA-CAT 17-ID beamline at the APS.

This drug was anti-proliferative in acute myeloid leukemia and prostate cancer cell lines. More impressively, in a mouse model of prostate cancer, ABBV-744 was able to reduce tumor volume while minimizing gastrointestinal and platelet side effects. These side effects were notably milder compared to an inhibitor of both bromodomains. A detailed molecular analysis also revealed that ABBV-744 preferentially inhibits the expression of Androgen Receptor (AR)-dependent genes.

– Stephen Taylor

See: Emily J. Faivre, Keith F. McDaniel, Daniel H. Albert, Srinivasa R. Mantena, Joshua P. Plotnik, Denise Wilcox, Lu Zhang, Mai H. Bui, George S. Sheppard, Le Wang, Vasudha Sehgal, “Cancer” cont’d. on page 101

Mamba Snake Toxin Unlocks Potential for Future Drug Discoveries

Venomous animals are prevalent in wildlife, from small ants, marine snails, and snakes to giant lizards. As these creatures evolve to increase their ability to capture prey and defend themselves from predators, their venom is a natural arsenal of protein-modifying agents. One of the toxin groups produced by mamba snakes in their venom is the muscarinic toxin (MT) family, which has binding affinity for a family of proteins referred to as muscarinic acetylcholine receptors (mAChRs). These receptors play important roles in the nervous system and help regulate many key central and peripheral functions. In fact, muscarinic antagonists are known to cause memory disturbances in animals and humans. An international team of researchers determined the crystal structure of MT7 in a complex with M1AChR. The researchers collected structural x-ray data at the APS that revealed important mechanistic insights. In addition to uncovering why MT7 has such a high specificity for M1AChR, the team demonstrated that MT7 could be modified to be selective for a different muscarinic acetylcholine receptor subtype. This latter finding is especially exciting as it suggests that muscarinic toxins can be customized to create potent drugs capable of targeting other kinds of receptors. Thus, the authors have created the possibility of exploiting snake venom to improve patient health.

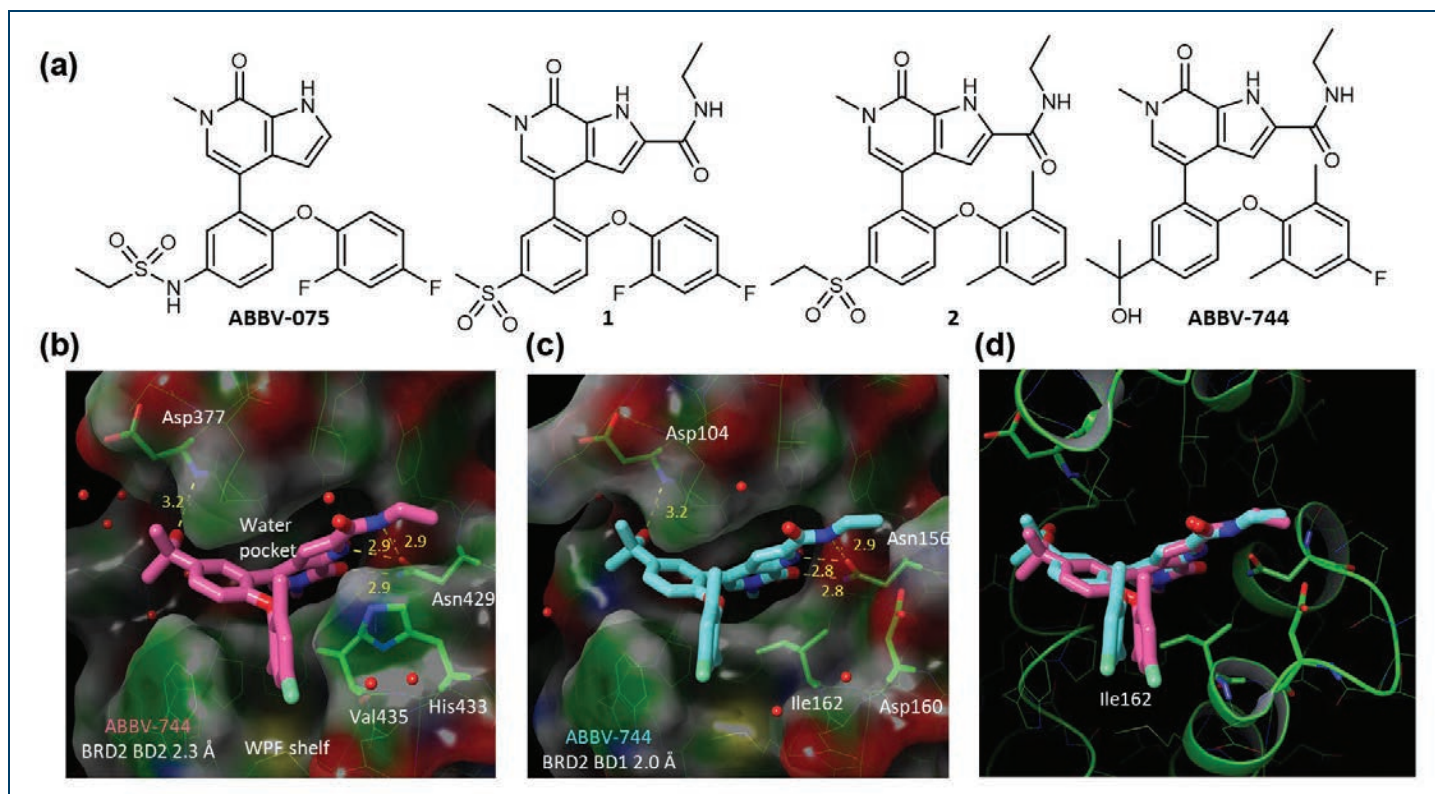
Mamba snakes (of the genus *Dendroaspis*, which literally means “tree asp”) are highly venomous animals native to a variety of regions in sub-Saharan Africa. The black mamba, in particular, is especially dangerous and has claimed many human lives. Mambas are either arboreal (tree-dwelling) or terrestrial (land-dwelling) and hunt a plethora of different animals, including birds and small mammals. The small MT toxins isolated from the venom of these snakes are so named because they bind to the mAChR family of protein receptors. Located in cellular membranes, these receptors mediate important cellular actions such as neuronal firing and smooth muscle contraction in response to binding of the neurotransmitter acetylcholine. There are five different subtypes of mAChRs. Out of these five subtypes, the toxin MT7 has an extremely high specificity towards the M₁AChR subtype. The binding of MT7 to M₁AChR alters the functionality of this receptor as well as its ability to bind to downstream signaling molecules. In addition to its connection to the snake toxin MT7, M₁AChR has been reported to have an association with the devastating age-related neurodegenerative disorder Alzheimer’s disease. Thus, both MT7 and

M₁AChR have tangible connections to human health.

The high-resolution crystal structure of MT7 complexed with M₁AChR was obtained at the GM/CA-XSD x-ray beamline 23-ID-D of at the APS. Figure 1 displays the crystal structure of MT7 from the green mamba snake in complex with muscarinic acetylcholine receptor 1. As seen in this illustration, MT7 engages into the extracellular pocket of M₁AChR. An analysis of the structure revealed how MT7 influences the function of M₁AChR and also identified why, on a molecular level, M₁AChR has such a high affinity for MT7. The team also demonstrated that MT7 could be modified to exhibit selectivity towards the M₂AChR subtype.

Not only do these data help us better understand the molecular mechanisms by which mamba snake venom induces deleterious effects, but the authors have found a way to customize the snake toxin MT7 to selectively target another important receptor. This has massive implications for drug discovery, and it suggests that further customizations could allow for the creation of potent drugs targeting other receptor proteins. – Alicia Surrao

“Mamba” cont’d. on facing page



Xiaoyu Lin, Xiaoli Huang, Xin Lu, Tamar Uziel, Paul Hessler, Lloyd T. Lam, Richard J. Bellin, Gaurav Mehta, Steve Fidanze, John K. Pratt, Dachun Liu, Lisa A. Hasvold, Chaohong Sun, Sanjay C. Panchal, John J. Nicolette, Stacey L. Fossey, Chang H. Park, Kenton Longenecker, Lance Bigelow, Maricel Torrent, Saul H. Rosenberg, Warren M. Kati, and Yu Shen*, "Selective inhibition of the BD2 bromodomain of BET proteins in prostate cancer," *Nature* **578**, 306 (13 February 2020).

DOI: 10.1038/s41586-020-1930-8

Author affiliation: AbbVie, Inc.

Correspondence: * yu.shen@abbvie.com

IMCA-CAT is supported by the companies of the Industrial Macromolecular Crystallography Association through a contract with Hauptman-Woodward Medical Research Institute. This research used resources of the Advanced Photon Source, a U.S. Department of Energy (DOE) Office of Science User Facility operated for the DOE Office of Science by Argonne National Laboratory under contract no. DE-AC02-06CH11357.

"Mamba" cont'd. from previous page

See: Shoji Maeda^{1*}, Jun Xu², Francois Marie N. Kadji³, Mary J. Clark⁴, Jiawei Zhao², Naotaka Tsutsumi¹, Junken Aoki³, Roger K. Sunahara⁴, Asuka Inoue³, K. Christopher Garcia¹, Brian K. Kobilka^{1,2**}, "Structure and selectivity engineering of the M1 muscarinic receptor toxin complex," *Science* **369**, 161 (2020).

DOI: 10.1126/science.aax2517

Author affiliations: ¹Stanford University School of Medicine, ²Tsinghua University, ³Tohoku University, ⁴UC San Diego School of Medicine

Correspondence: * shojim@stanford.edu,

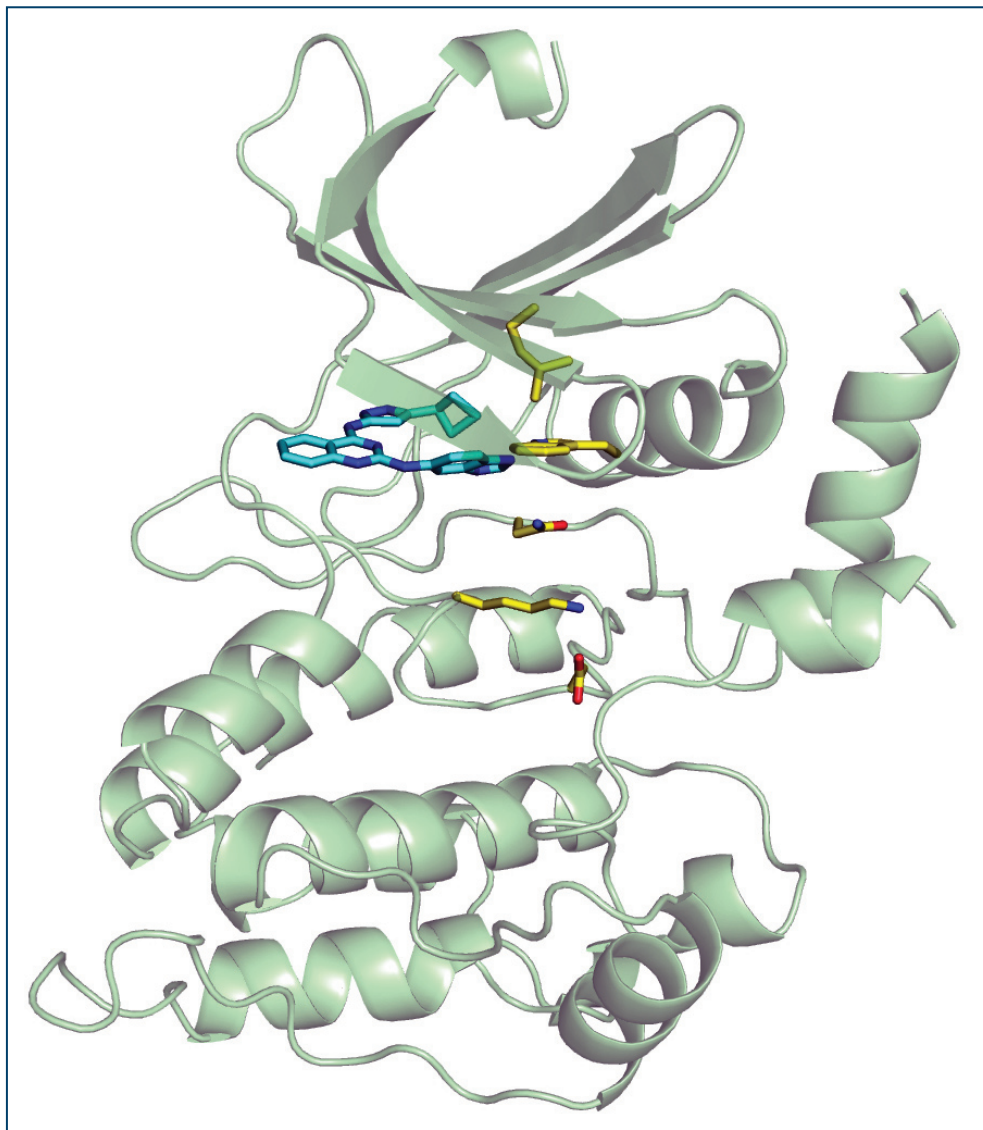
** kobilka@stanford.edu

Fig. 1. ABBV-744 is a potent and highly selective inhibitor of the BD2 domain of BET family proteins. (a) Chemical structure of indicated compounds. (b) Co-crystal structure of ABBV-744 (pink) in complex with BD2 of BRD2. (c) Co-crystal structure of ABBV-744 (blue) in complex with BD1 of BRD2. (d) Overlay of the co-crystal structure of ABBV-744 in complex with BD2 of BRD2 (pink) and with BD1 of BRD2 (blue), displayed on the BRD2BD1 protein (green). From E. J. Faivre et al., "Selective inhibition of the BD2 bromodomain of BET proteins in prostate cancer," *Nature* **578**, 306 (13 February 2020).

We thank staff at the GM/CA-XSD beamlines for technical assistance and support for data collection. The work was supported by National Institutes of Health (NIH) grant R01GM083118 for R.K.S. B.K.K. was funded by R01NS028471. K.C.G. was funded by NIH R01AI125320, the Mathers Foundation, and the Howard Hughes Medical Institute. A.I. was funded by the PRIME 18gm5910013 and the LEAP 18gm0010004 from the Japan Agency for Medical Research and Development (AMED) and the Japan Society for the Promotion of Science (JSPS) KAKENHI 17K08264. J.A. was funded by the LEAP 18gm0010004 from AMED. B.K.K. is Chan Zuckerberg Biohub investigator. GM/CA-XSD is funded in whole or in part with Federal funds from the National Cancer Institute (ACB-12002) and the National Institute of General Medical Sciences (AGM-12006). This research used resources of the Advanced Photon Source, a U.S. Department of Energy (DOE) Office of Science User Facility operated for the DOE Office of Science by Argonne National Laboratory under Contract No. DE-AC02-06CH11357.

Solving the Structure of a Clinically Interesting Protein Associated with Schizophrenia

The psychiatric disorder schizophrenia, which causes hallucinations and delusions, has been shown to be associated with mutations in the gene ULK4. Further supporting a functional role for ULK4 in the brain, inhibition of this protein in mice disrupts the development of the cerebral cortex. Although the data strongly suggest an important neurological role for ULK4, very little is known about this protein, but impactful work by researchers who carried out studies at the APS has helped make this protein considerably less enigmatic. Their work provides a high-resolution structure of ULK4 and demonstrates that it can bind to the energy molecule ATP. In addition to these findings, the authors identified small molecules capable of directly binding ULK4. These small molecules will make for invaluable research tools that will help facilitate future research into the biological role of ULK4. Given that schizophrenia is one of the most severe psychiatric disorders, these data are highly significant and create the possibility of developing novel anti-psychotic therapeutics.



In mammals, there are five proteins that make up the ULK family: ULK1, ULK2, ULK3, ULK4, and STK36. Deletion mutations in the gene ULK4 were previously found in patients diagnosed with schizophrenia as well as in patients doubly diagnosed with schizophrenia and bipolar disorder. Schizophrenia, which is one of the most severe psychiatric disorders that requires lifelong treatment, can present with symptoms such as hallucinations and delusions. Bipolar disorder is also a lifelong condition that can present with delusional or hallucinatory symptoms. Given the serious, chronic nature of these neuropsychiatric disorders, the abovementioned finding regarding ULK4 is clinically significant. Further corroborating a functional role for ULK4 in the brain, inhibiting ULK4 in mice perturbs the development of the cerebral cortex. The cerebral cortex is an important outer layer of the brain that fulfills many critical functions, such as receiving sensory information. Mice lacking the related genes ULK1 and ULK2 display both neurological and nerve fiber defects. These collective data suggest that ULK4 plays a paramount role in mammalian brain function.

Outside of these findings, very little is known about ULK4. The protein is specific to neurons and is classified as a pseudokinase. Kinase enzymes have the ability to transfer a phosphate group to a target, a process referred to as “phosphorylation,” that plays an important regulatory function biologically. For example, the phosphorylation of a protein can make it either active or inactive. Unlike kinase enzymes, pseudokinase enzymes have a modified kinase domain that is presumably inactive: ULK1 and ULK2 are capable of transferring phosphates to targets while ULK4 is unable to do this. This raises the intriguing question of what ULK4 is doing on a molecular level.

Exciting answers to this question were provided in a recent study by researchers from the Icahn School of Medicine at Mount Sinai and Yale University. This work unveiled the first-ever structure of ULK4. Figure 1 displays the structure of the ULK4 pseudokinase domain bound to an inhibitor, as determined at the LS-CAT beamline 21-ID-D at the APS. This high-resolution structure discovered by the authors confirmed the absence of phosphotransfer ac-

tivity (i.e., the lack of an ability to transfer a phosphate group to a target) and revealed that ULK4 strongly binds to the molecule ATP. This is a highly intriguing finding as ATP is what cells use for energy. (ATP contains three phosphoryl groups and the cleavage of one of these phosphates produces useable energy.) The authors additionally identified a magnesium-independent mechanism by which ULK4 binds to ATP. This mechanism involves the rare utilization of a hydrophobic bridge in the active site (i.e., binding region) of ULK4. Lastly, the work identifies various small molecules that are capable of physically interacting with ULK4 and have the potential to accelerate our understanding of ULK4’s biological role.

Taken together, these data have significantly illuminated the biological role of ULK4. While many interesting questions remain to be solved, it is now known that ULK4 directly binds ATP. In addition, knowing the structure of ULK4 will accelerate future research into how ULK4 affects brain health. Knowledge of the structure also allows for the development of potent, sensitive drugs targeting ULK4. Given ULK4’s connection to psychiatric disorders, this may ultimately lead to the development of novel drugs that improve patient health. – Alicia Surrao

See: Susmita Khamrui¹, Peter M. U. Ung^{1,2}, Cody Secor¹, Avner Schlessinger¹, and Michael B. Lazarus^{1*}, “High-Resolution Structure and Inhibition of the Schizophrenia-Linked Pseudokinase ULK4,” *J. Am. Chem. Soc.* **142**, 33 (2020).

DOI: 10.1021/jacs.9b10458

Author affiliations: ¹Icahn School of Medicine at Mount Sinai, ²Yale University

Correspondence: * michael.lazarus@mssm.edu

This work was supported by U.S. National Institutes of Health grants K22CA201103 and GM124838 (M.B.L.) and GM108911 (A.S.). Use of the Life Scireces Collaborative Access Team facility at APS Sector 21 was supported by the Michigan Economic Development Corporation and the Michigan Technology Tri-Corridor (Grant 085P1000817). This work was supported in part through the computational resources and staff expertise provided by the Department of Scientific Computing at the Icahn School of Medicine at Mount Sinai. This research used resources of the Advanced Photon Source, a U.S. Department of Energy (DOE) Office of Science User Facility operated for the DOE Office of Science by Argonne National Laboratory under Contract No. DE-AC02-06CH11357.

< Fig. 1. Structure of the ULK4 pseudokinase domain bound to an inhibitor. The inhibitor is shown in cyan and interesting residues in the active site are highlighted in yellow. PDB code 6U5L.

Probing the Kinetics of Cooperation in Hemoglobin

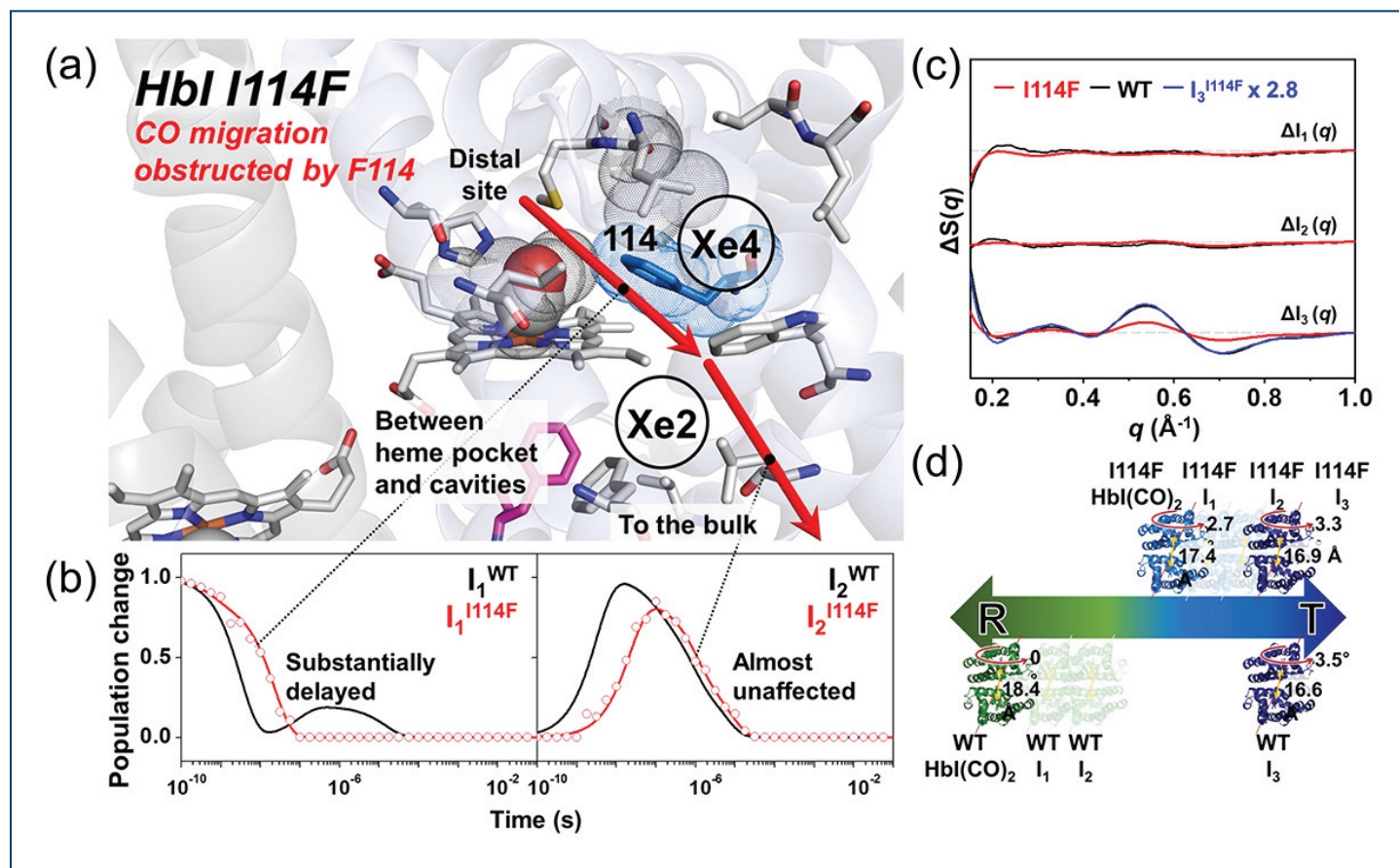
Hemoglobin (Hb) is one of the most essential proteins of life. It is a red blood cell protein that carries oxygen from our lungs to our cells and has been extensively studied as a classic example in biology of cooperative binding and release of a ligand through allosteric regulation. The structure of Hb has been known since 1959 and consists of four subunits that each contain an oxygen-binding heme group. The binding of each oxygen increases the affinity of the other subunits for oxygen through conformational changes. Then, when the loaded hemoglobin reaches its destination, the unloading of one oxygen causes another shape change in the other subunits and they all unload. However, although the model for hemoglobin oxygen binding cooperativity between a low-affinity “T” state and a high-affinity “R” state is well established, the molecular and kinetic details are quite complex and are still emerging. One of these details is the dynamic relationship between ligand migration pathways through the molecule to the bulk solvent and the resultant structural changes that occur within the protein molecule as the ligand is released. Recent work from a group carrying out research at the APS made important new findings about this critical biological function. The detailed structural changes that this work reveals may contribute to future technological applications with direct relevance to structure-based drug design projects in which cooperative binding is a desired feature.

The work made use of the availability of a model system for studying Hb using a version of the molecule (Hbl) that only has two subunits. Thus, Hbl provides a model for studying cooperative binding in a system with fewer moving parts. Also, mutated forms of Hbl have been made that change the kinetics of ligand migration within the molecule, allowing for comparisons to the known wild-type structures. In this case, the team from the Institute for Basic Science (Korea) was interested in a mutant Hbl (Hbl I114F) in which a small amino acid, isoleucine, has been changed to a bulky phenylalanine to slow the migration of the ligand from the interior of the protein out to the bulk solvent. This set the stage for answering questions about how the migration of the ligand was related to cooperative structural changes in the protein.

In order to discover differences between the mutant and the wild-type Hb, the team from the Institute for Basic Science (Republic of Korea) used time-resolved x-ray solution scattering (TRXSS) at the BioCARS beamline 14-ID-B of the APS to analyze the dissociation of carbon monoxide (CO), a well-known ligand that binds to Hb at the oxygen binding site and can be dissociated with a laser pulse.

The first step was to compare the kinetic framework of CO dissociation to that of the wild-type protein (Fig. 1a). TRXSS data showed that, similar to the wild-type protein, the migration of CO from Hbl I114F goes through three distinct structural intermediate states, I_1 , I_2 , and I_3 . However, in the Hbl I114F mutant, the ligand appears to take a different path, and proceeds through the intermediate steps between I_1 and I_2 at a slower rate than in the wild-type protein (Fig. 1b). The next transition from I_2 to I_3 occurs at a similar rate to the wild-type protein (Fig. 1b), but the final transition is totally different and suggests that the CO migrates out of the protein into the bulk solvent during the I_2 to I_3 structural transition (Fig. 1c).

Taken together, these data suggest that the ligand-bound state of the Hbl I114F mutant is closer to the T state of the wild-type protein than the ligand-bound R state of the wild-type protein, a significant difference (Fig. 1d). This provides a direct link between the movement of the ligand out of the protein and the overall structural changes that occur between the R and T states in response, furthering our understanding of how hemoglobin performs its remarkable function. — Sandy Field



See: Hanui Kim, Jong Goo Kim, Srinivasan Muniyappan, Tae Wu Kim, Sang Jin Lee, and Hyotcherl Ihee*, "Effect of Occluded Ligand Migration on the Kinetics and Structural Dynamics of Homodimeric Hemoglobin," *J. Phys. Chem. B* **124**, 1550 (2020). DOI: 10.1021/acs.jpcc.9b11749
 Author affiliation: Institute for Basic Science
 Correspondence: *hyotcherl.ihee@kaist.ac.kr

This work was supported by the Institute for Basic Science (IBS-R004). We acknowledge BioCARS staff for support and helpful discussions. The use of BioCARS was supported by the National Institutes of Health (NIH) National Institute of General Medical Sciences Grant P41GM103543. The time-resolved setup at Sector 14 was funded in part through collaboration with P. Anfinrud (NIH/National Institute of Diabetes and Digestive and Kidney Diseases, NIDDK) through the Intramural Research Program of the NIDDK. This research used resources of the Advanced Photon Source, a U.S. Department of Energy (DOE) Office of Science User Facility operated for the DOE Office of Science by Argonne National Laboratory under Contract No. DE-AC02-06CH11357.

Fig. 1. (a) Close-up views of the heme environment of crystal structures of Hbl(CO)₂ for the I114F mutant (I114F). Heme and some residues forming secondary docking sites (Xe4 and Xe2 sites) are represented by the gray sticks, and heme-bounded CO molecules are shown as spheres. (b) A comparative study with WT shows occluded ligand migration by I114F decelerates the I₁-to-I₂ transition but that the transitions from I₂ to I₃ are not delayed and have rates similar to those of WT. (c) SADS curves of three intermediates for I114F (red) and WT (black). (d) Schematic summary of the structural transition for WT and I114F. In WT, the structures of I₁ and I₂ are close to that of the R state of WT and the structure of I₃ is close to that of the T state of WT. In I114F, because the starting structure of R-T transition is already shifted toward the T state of WT, all of I₁, I₂, and I₃ have structures close to the T state of WT.

Two Keys, One Protein, Diverse Pathways

In biology class, students learn about the lock-and-key analogy to protein-ligand interactions. The lesson goes, one ligand binds to a protein prompting a structural change that in turn elicits a change in function, much like a key unlocks a door. But, as with most things, the reality is much more complicated. Using structural data collected at the APS, researchers uncovered the way a single G protein-coupled receptor (GPCR) adopts two distinct conformations, with distinct functions, depending on which of two ligands binds to it. It's as though a single lock can open a door into two different locations depending on which of two different keys are used. The implications go far beyond biology class; this research may have clinical ramifications, as GPCRs are a major drug-target class.

GPCRs are a large group of proteins that span the cell membrane and capture ligand agonists outside the cell, relay the signal across the membrane, and trigger a chain reaction within the cell, culminating in a physiological response such as a change in blood pressure. As the name suggests, GPCRs activate heterotrimeric G proteins (a 3-protein complex), but the receptors can also turn on another type of protein called β -arrestin. An activated G protein and a β -arrestin can each start their own signaling cascades and activate downstream pathways inside the cell. Scientists had previously observed that particular ligands (biased agonists) seemed to direct GPCR activity toward either G protein or β -arrestin activation pathways, but the mechanism for how different ligands cause the GPCR to prefer to turn on different intracellular proteins was unknown.

To solve the mystery, the multi-institutional team focused on a particular GPCR: the angiotensin II type 1 receptor (AT1R). This well-characterized GPCR helps regulate blood pressure and is a target of medications for hypertension and diabetic nephropathy. It is a good model system for studying how biased agonists work because scientists have found that making small changes to angiotensin II – the small peptide hormone produced by the body to activate AT1R – can trigger the receptor to preferentially activate G proteins or β -arrestin. Without these small changes, angiotensin II naturally activates both G protein and β -arrestin pathways. The β -arrestin-biased ligands that promote only β -arrestin pathways are of particular clinical interest, though, as they may have dual benefits in the treatments of both hypertension and heart failure.

The researchers generated three types of crystals for structural characterization: AT1R bound to natural angiotensin II and two different β -arrestin-biased angiotensin

II analogs. They took their crystals to the GM/CA-XSD x-ray beamline 23-ID-B at the APS. There, they collected diffraction data with a micron-sized x-ray beam, and solved high-resolution structures for each crystal at between 2.7 Å to 2.9 Å resolution (Fig. 1).

An analysis of the differences between each structure and previous structures of the AT1R in an inactive state provided some clues on the origins of biased agonism. The key finding was that the AT1R can assume more than one activated state, depending on whether natural angiotensin II or a β -arrestin-biased angiotensin II analog is bound. In addition, differences among the structures were seen not only right around the binding site of the ligands, which faces outside the cell, but also deeper within the AT1R protein. This helps to explain how information about the bound ligand is propagated all the way across the cell membrane, causing different responses inside the cell. Angiotensin II promoted more dramatic structural rearrangements in AT1R than the other analogs. Most notably, the researchers identified particular structural features that seemed to determine the bias. Both β -arrestin-biased ligands and angiotensin II caused a rearrangement of an asparagine in a network of amino acid residues deep within the protein, suggesting that movement of this amino acid allows AT1R to adopt a specific conformation on the inner side of the cell membrane, triggering β -arrestin signaling. Only the natural angiotensin II promoted the flipping of a second asparagine in this same region, altering the connectivity of a network of amino acids that extends towards the inside of the cell and may trigger the receptor to activate G proteins.

The observation that certain residues play an outsized role in biased agonism prompted the researchers to look beyond AT1R to other members of the GPCR family. While

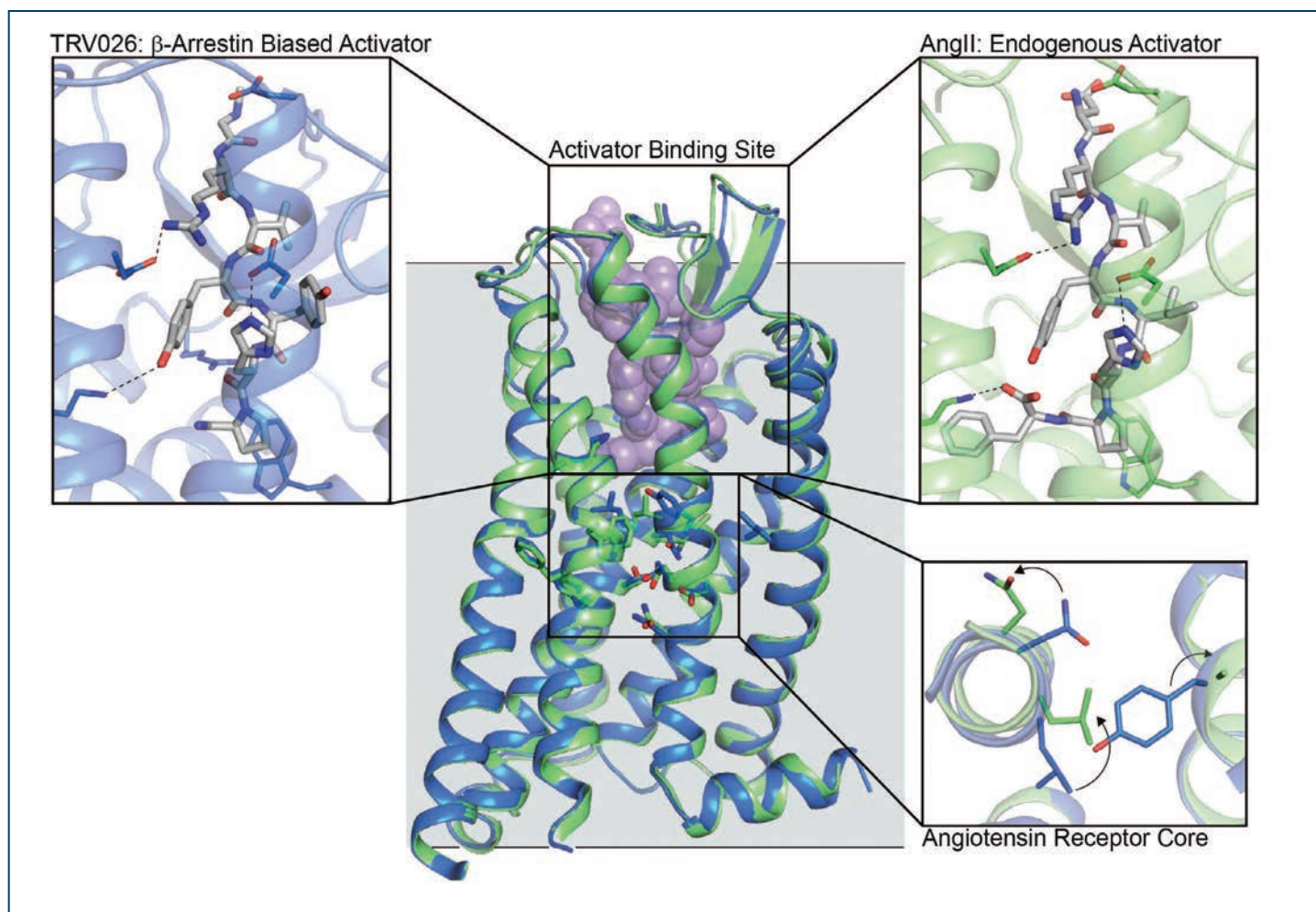


Fig. 1. Crystal structures of Angiotensin II type 1 receptor in complex with angiotensin II (green) and a β -arrestin biased activator (blue) determined at the GM/CA-XSD structural biology facility at the APS.

this polar core tends to be well conserved among GPCRs, the researchers proposed that receptors that are most similar to AT1R in this region may be particularly inclined to show biased signaling.

In 2018, about a third of all FDA-approved medications targeted GPCRs, with 108 GPCRs serving as drug targets for heart disease, diabetes, asthma, acid reflux, and cancer among other conditions. Biased agonists are of particular interest for the development of next-generation pharmaceuticals as the ability to control the extent to which G-proteins or β -arrestin are activated could help reduce or eliminate undesirable side effects. With a greater understanding of the molecular underpinnings of biased agonism, new approaches to drug development may now be possible. – Erika Gebel Berg

See: Laura M. Wingler^{1*}, Meredith A. Skiba², Conor McMahon², Dean P. Staus¹, Alissa L. W. Kleinhenz^{1,3}, Carl-Mikael Suomivuori^{4,5}, Naomi R. Latorraca^{4,5†}, Ron O. Dror^{4,5}, Robert J.

Lefkowitz^{1*}, and Andrew C. Kruse^{2**}, “Angiotensin and biased analogs induce structurally distinct active conformations within a GPCR,” *Science* **367**, 888 (21 February 2020). DOI: 10.1126/science.aay9813

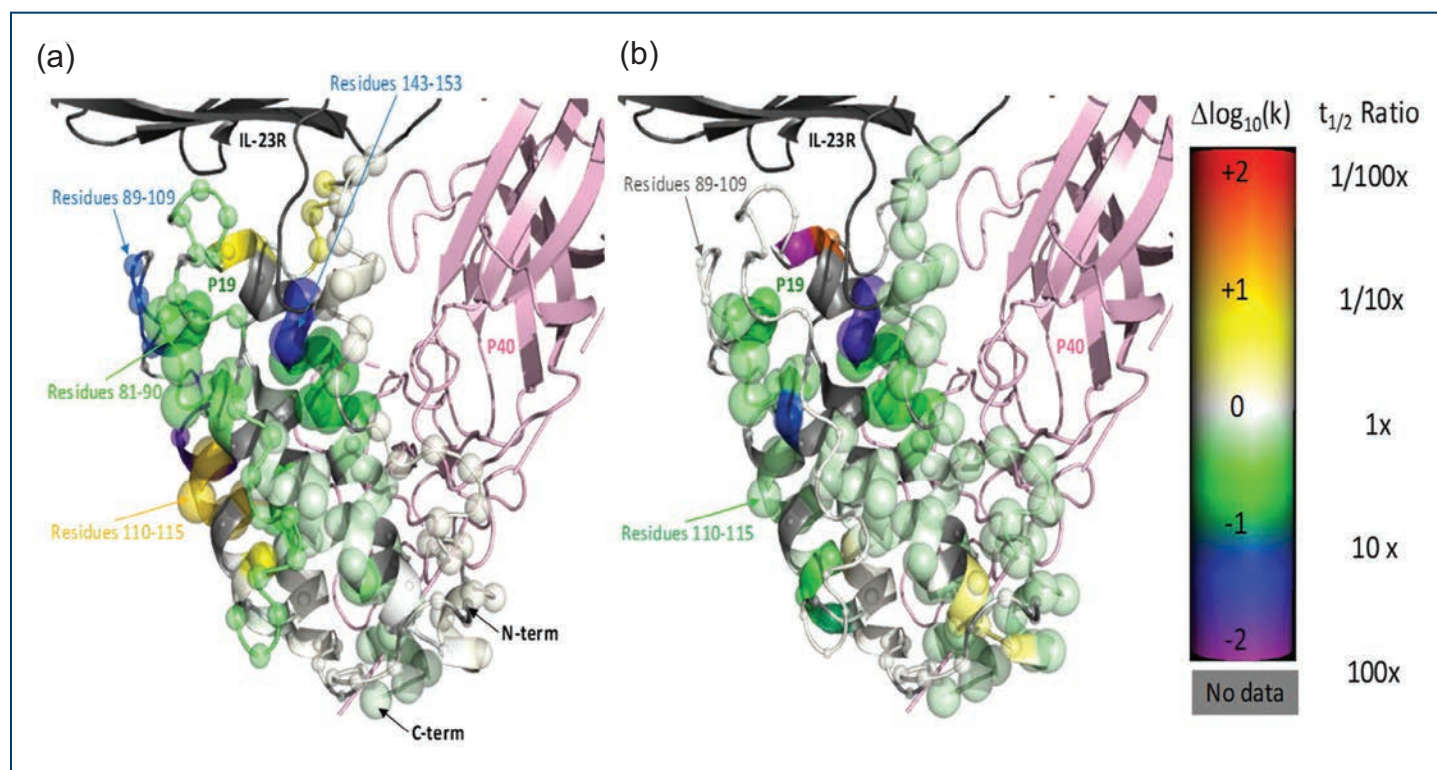
Author affiliations: ¹Duke University Medical Center and Howard Hughes Medical Institute, ²Harvard Medical School, ³University of Michigan, ⁴Stanford University, ⁵Stanford University School of Medicine [†]Present address: University of California, Berkeley

Correspondence: * lefko001@receptor-biol.duke.edu,
** andrew_kruse@hms.harvard.edu

Funding was provided by the Sigrid Jusélius Foundation (C.-M.S.); the International Human Frontier Science Program Organization (LT000916/2018-L) (C.-M.S.); the Mandel Center for Hypertension and Atherosclerosis at Duke University (R.J.L.); the Vallee Foundation (A.C.K.); the Smith Family Foundation (A.C.K.); and National Institutes of Health (NIH) grants R01GM127359 (R.O.D.), R01HL16037 (R.J.L.), and DP5OD021345 (A.C.K.). A.L.W.K. is a Howard Hughes Medical Institute Medical Research Fellow. R.J.L. is an investigator with the Howard Hughes Medical Institute. We thank the staff at the GM/CA-XSD beamlines for technical assistance and support of data collection. GM/CA@APS is supported by the NIH National Institute of General Medical Sciences (AGM-12006) and the National Cancer Institute (ACB-12002), and the Eiger 16M detector was funded by NIH grant S10 OD012289. This research used resources of the Advanced Photon Source, a U.S. Department of Energy (DOE) Office of Science User Facility operated for the DOE Office of Science by Argonne National Laboratory under Contract No. DE-AC02-06CH11357.

Bringing Phages and Yeast Together for Peptide Discovery

Finding peptides that bind to proteins of interest—such as those that play key roles in human diseases and disorders—can be expensive and time-consuming. In the past few decades, this process has been greatly facilitated through phage display. This technique involves engineering the gene for various peptides in frame with the phage coat protein, prompting the phage, a virus that can infect and kill bacteria, to display the peptide on its surface. Although this method has led to the discovery of hundreds of potential target-specific hits, these hits must still be synthesized to confirm binding as a free peptide, which adds considerable effort and cost, and has low yield. Furthermore, to identify peptides that bind to specific regions of interest on the target protein, researchers have traditionally used a method called alanine mutation, which substitutes alanine for other individual amino acids at a particular site to change binding propensity. However, the process of cloning, expressing, purifying, and characterizing each alanine mutation is also laborious and time consuming. To get around these challenges and smooth the process of discovering functional peptides, users of the APS tried a new tactic: They combined phage display with a related platform called yeast display, incorporating target proteins and their alanine-mutated variants into the cell walls of yeast. The authors of this study suggest that this approach could be applied to any target protein that can be displayed on yeast, narrows the number of proteins that ultimately require synthesis, and enriches the population of promising target-specific peptides providing a reliable and cost-effective way to improve peptide discovery.



As a model target protein, the researchers selected interleukin 23 (IL-23), a chemical messenger that plays a key role in several autoimmune diseases. Although IL-23 is composed of multiple subunits, they were particularly interested in one known as p19, which provides a unique binding area that's not shared by other interleukin 12.

The team created peptide libraries of different lengths against IL-23—including cyclic 12, 15, and 18 libraries of random amino acids, as well as one linear library 15 amino acids long—displayed on phages. They also created yeast that displayed wild-type IL-23 or alanine-mutated variants of the p19 subunit in complex with p40 on their surfaces.

To validate whether a phage-displayed peptide could bind to a yeast-displayed target, the researchers tested this concept with phage that displayed a key binding region of an antibody (Fab) that had already been discovered to bind to the p19 region of IL-23. Although a naked phage didn't bind to the yeast displaying wild-type IL-23 or any of its alanine mutants, the one displaying part of the previously discovered antibody bound to nearly all of these, with the exception of yeast carrying a mutation in a residue that's known to be a major site for receptor binding.

With evidence that this approach is feasible, the researchers tested the binding of the peptides as displayed on phage to wild-type and select alanine mutants of p19 displayed on yeast. Consequently, they identified several different phage-peptides in their library that bound strongly to yeast displaying wild-type IL-23 and not to the p19 alanine mutants that correspond to the peptide binding site. Using a technique called hydrogen deuterium exchange mass spectrometry, they confirmed p19-specific binding: While the p40 subunit of wild-type IL-23 had significant deuterium uptake when it was exposed to this hydrogen isotope, suggesting that it remained open and ex-

posed, the p19 subunit didn't take up much deuterium, suggesting that its binding to these peptides blocked deuterium exchange.

To further investigate binding, the researchers used the LRL-CAT 31-ID-D beamline at the APS to perform x-ray crystallography, which allowed them to see crystal structures of these phage peptides bound and unbound to IL-23 (Fig. 1), providing additional confirmation that these peptides bound to the p19 subunit.

To provide even more confirmation that these phage-displayed peptides targeted IL-23, and specifically p19, the researchers synthesized free peptides of four of the most promising phage-displayed peptides and showed that these could successfully compete with IL-23 receptors to bind to IL-23 proteins. Additional protein-protein interaction assays, known as AlphaLISA and TR-FRET, further showed that these four peptides blocked IL-23 from binding to its receptor.

Finally, the researchers showed that this whole process of identifying promising phage-displayed peptides using yeast-displayed proteins could be accelerated using a cell sorting technique. – [Christen Brownlee](#)

See: Priyanka Pandya¹, Robert O. Sayers¹, Joey P. Ting¹, Shaghayegh Morshedian¹, Carina Torres¹, Justine S. Cudal¹, Kai Zhang¹, Jonathan R. Fitchett¹, Qing Zhang¹, Feiyu F. Zhang², Jing Wang², Jim D. Durbin³, Juan J. Carrillo³, Alfonso Espada⁴, Howard Broughton⁴, Yuewei Qian², and Sepideh Afshar^{1*}, "Integration of phage and yeast display platforms: A reliable and cost effective approach for binning of peptides as displayed on-phage," *PLoS ONE* **15**(6), e0233961 (June 1 2020). DOI: 10.1371/journal.pone.0233961

Author affiliations: ¹Eli Lilly Biotechnology Center, ²Lilly Research Laboratories, ³Eli Lilly and Company, ⁴Centro de Investigación Lilly

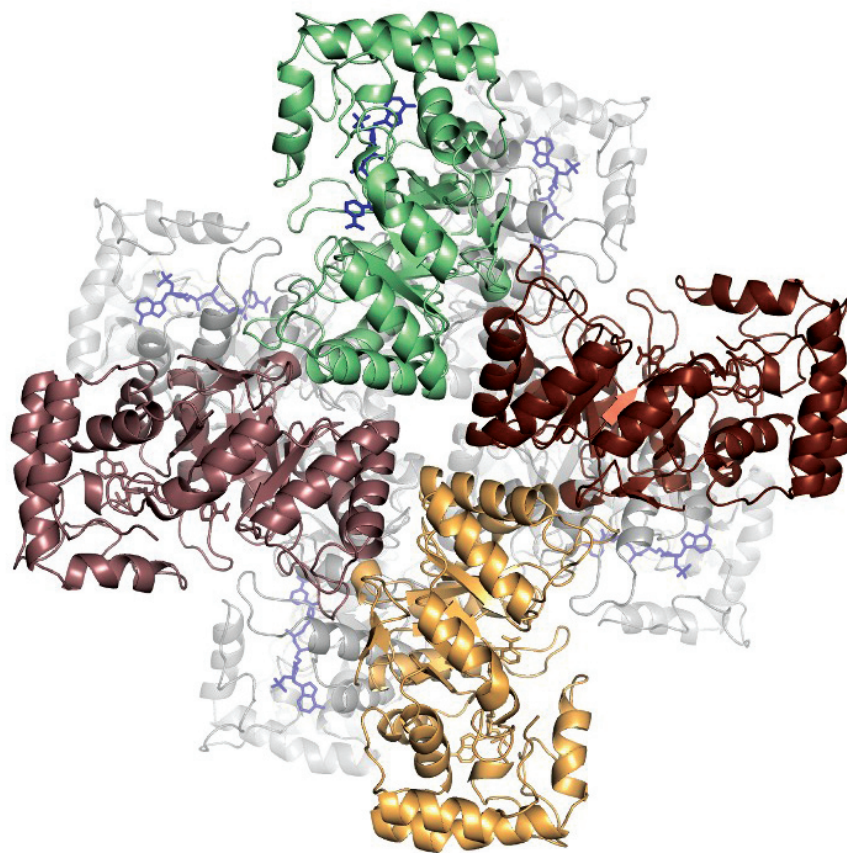
Correspondence: * s.afshar@lilly.com

Use of the Lilly Research Laboratories Collaborative Access Team (LRL-CAT) beamline at Sector 31 of the Advanced Photon Source was provided by Eli Lilly Company, which operates the facility. Use of the Advanced Photon Source, an Office of Science User Facility operated for the U.S. Department of Energy (DOE) Office of Science by Argonne National Laboratory, was supported by the U.S. DOE under Contract No. DE-AC02-06CH11357-

< Fig. 1. Structure of IL-23 unbound (a) and bound (b) determined at LRL-CAT. From P. Pandya et al., "Integration of phage and yeast display platforms: A reliable and cost effective approach for binning of peptides as displayed on-phage," *PLoS ONE* **15**(6), e0233961 (June 1 2020).

Preventing a Bacterium from Getting a Taste of Its Own Medicine

Mithramycin (MTM) is an anticancer antibiotic produced by the gram-positive bacterium *Streptomyces argillaceus*. The enzymes MtmOIV and MtmW were found to catalyze the final two reactions in mithramycin's biosynthetic pathway, the Baeyer-Villiger opening of the fourth ring of premithramycin B (PMB), creating a C3 pentyl side chain, followed closely by reduction of the distal keto group on the new side chain. Unexpectedly, the completion of this biosynthetic pathway yields only a small amount of active MTM and a large amount of an inert form of MTM, dubbed iso-MTM. Iso-MTM was then observed to non-enzymatically convert to the toxic MTM species in the presence of magnesium ions. The reason for this roundabout series of production steps is presumably a previously unobserved form of self-resistance to MTM, which is toxic to gram-positive bacteria. X-ray crystallography carried out at the APS to examine the high-resolution structures of MtmW in complex with the co-substrate NADP⁺ and polyethylene glycol suggests a catalytic mechanism for MtmW. The results and structures also show that the assembly of MtmW closely resembles the ring-shaped β subunit of a vertebrate ion channel, suggesting the enzyme may play a role in exporting iso-MTM out of the cell prior to its activation to a toxic agent. This unusual transporter-mediated mechanism may shed light on the production of other potentially clinically useful natural products.



Small-molecule natural products, which have evolved structurally to exert specific biological functions over millions of years, provide the producer organisms with evolutionary advantages. As chemical warfare agents, these molecules usually bind house-keeping elements of the competing organisms and inhibit their normal life cycles. Such natural products, however, may create similar threats to the producing organisms themselves. To avoid self-destruction, many natural-product biosynthetic gene clusters encode not only enzymes for their production, but also additional regulatory factors to control the expression of the genes, transporters to ensure the toxic molecule is efficiently expelled from the producer organism, or dedicated resistance mechanisms, such as enzymes that inactivate the product molecules that linger in the cytoplasm.

The producer of the anticancer antibiotic mithramycin, the bacterium *Streptomyces argillaceus*, appears to have evolved a rather intriguing form of protection against such self-destruction. Besides being an antibacterial agent, MTM is a potent transcriptional inhibitor targeting G/C-rich promoters that has been found to inhibit growth of cancer cells dependent on oncogenic transcription. Specifically, MTM is a highly potent antagonist of the bone and soft tissue cancer Ewing sarcoma and prostate cancers that depend on similar oncogenic transcription mechanisms.

To gain a better understanding of the final biosynthetic steps of mithramycin for the development of potential drugs to treat Ewing sarcoma and prostate cancers, researchers from the University of Kentucky and the University of Texas Health Science Center focused on the enzymes responsible for the generation of mithramycin's C3-side chain. They discovered that the enzymatic cooperation of the enzymes MtmOIV (a Baeyer–Villiger monooxygenase) and MtmW (a ketoreductase) is essential for MTM formation, through the creation of a transient complex.

< Fig. 1. An inter-subunit channel view into the crystal structure of the octamer of the MtmW-NADP⁺ complex. NADP⁺ (stick representation) is shown in blue.

Surprisingly, the researchers discovered that this biosynthetic pathway actually produces scant amounts of MTM and large amounts of a stereoisomer of MTM that is biologically inert. This inert form, called iso-MTM, is converted to MTM in the presence of environmental magnesium ions, presumably after the compound has been expelled from the organism that produced it.

The research team then used x-ray diffraction data collected on the SER-CAT synchrotron beamline 22-ID at the APS to determine the crystal structures of MtmW in two forms, with the apo-MtmW crystallized in one form (diffracting to 1.8 Å resolution) and its complex with NADP⁺ in the other form (2.1 Å resolution, Fig. 1). Additionally, the similarity of the crystal structures of MtmW to a ring-shaped β subunit of a vertebrate ion channel Kvb indicated that the activity of MtmW may be coupled to channeling mithramycin out of the organism through the transmembrane channel MtrAB.

The formation and export of an inert precursor (iso-MTM) would explain the self-resistance of the producing organism to the toxic MTM. This somewhat unusual self-resistance mechanism may be used by *Streptomyces argillaceus* and other bacteria. Knowledge of this mechanism may help in the discovery and utilization of other natural products with important uses. – Chris Palmer

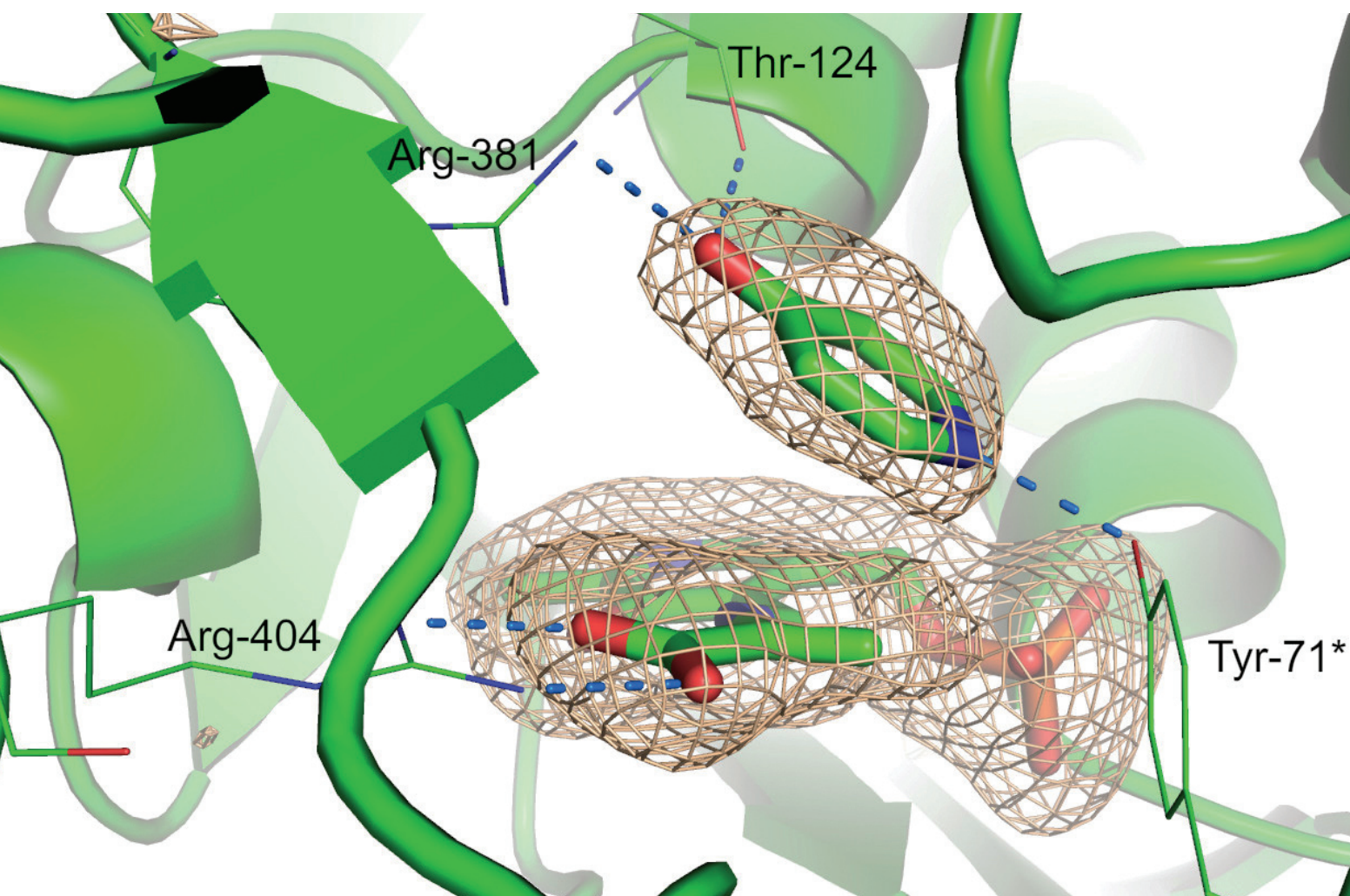
See: Ryan Wheeler¹, Xia Yu^{1,2}, Caixia Hou¹, Prithiba Mitra¹, Jhong-Min Chen¹, Frank Herkules³, Dmitri N. Ivanov³, Oleg V. Tsodikov^{1*}, and Jrgen Rohr^{1,**}, “Discovery of a Cryptic Intermediate in Late Steps of Mithramycin Biosynthesis,” *Angew. Chem. Int. Ed.* **59**, 826 (2020). DOI: 10.1002/anie.201910241

Author affiliations: ¹University of Kentucky, ²Central South University Changsha, ³University of Texas Health Science Center
Correspondence: * oleg.tsodikov@uky.edu, ** jrohr2@uky.edu

The work was supported by National Institutes of Health (NIH) grants CA 091901 and GM 1051977 to J.R. The Southeast Regional Collaborative Access Team is supported by its member institutions (see www.ser-cat.org/members.html), and equipment grants (S10_RR25528, S10_RR028976 and S10_OD027000) from the NIH. This research used resources of the Advanced Photon Source, a U.S. Department of Energy (DOE) Office of Science User Facility operated for the DOE Office of Science by Argonne National Laboratory under Contract No. DE-AC02-06CH11357.

Enzyme-Assisted Molecular Strain Contributes to Successful Reaction

Tyrosine (or L-tyrosine) is a non-essential amino acid used by the human body for communication within cells and to build proteins. Additionally, it can be converted by the body into important molecules such as dopamine and melanin. One form of industrial synthesis of L-tyrosine involves a reaction catalyzed by the enzyme tyrosine phenol-lyase in the presence of vitamin B6, which has been widely studied for its role in disease prevention. Although tyrosine phenol-lyase also catalyzes reactions with other amino acids, the reaction involving L-tyrosine differs from the others. To understand these differences, scientists have investigated the chemical structure of a set of intermediate molecules created during these reactions, varying both the amino acid used and the form of the enzyme. Recent results from studies carried out at the APS show that the strain under which the L-tyrosine amino acid exists during the reaction can explain the special characteristics of the reaction. By understanding the specific conformational changes of reactions catalyzed by tyrosine phenol-lyase, the work by the research team in this study improves our understanding of vitamin B6-related reactions within the human body.



A key characteristic of this reaction is that it is reversible, meaning that the products can recombine to create more reactants. Thus, the reactant, L-tyrosine can be synthesized from inexpensive materials such as phenol, ammonia, and pyruvic acid. No spontaneous chemical reaction can transform these materials into this valuable reactant. Another special characteristic of this reaction is that the phenol molecule –unusually–takes a pair of electrons with it when the L-tyrosine molecule is cleaved and contributes to a fast reaction. When tyrosine phenol-lyase catalyzes reactions with other, similar amino acids, they are not reversible and the product does not exhibit the same behavior. To explain these characteristics, the team of researchers from the University of Georgia, Oak Ridge National Laboratory, Tennessee Wesleyan University, and The University of Manchester (UK) investigated the shape, or conformation, of the amino acid. By pursuing this avenue of investigation, they built on their previously published results showing that, in similar, related reactions, the substrate—the molecule on which the enzyme acts—is deformed due to strain.

The team looked at a large set of reactions, involving four amino acids as substrates and three different versions of the enzyme. (Not each combination of enzyme and amino acid were paired in this study.) The team investigated the conformation and thermodynamic properties of the intermediate molecules created by the L-tyrosine to phenol and ammonium pyruvate reaction, rather than the final chemical products. These intermediate molecules, called aminoacrylates, occur in many reactions involving vitamin B6. Determining their structure allowed the team to assess how the different conformations of the amino acid affected the reversibility and phenol characteristics of the reactions catalyzed by tyrosine phenol-lyase.

After synthesizing the enzymes and amino acids, the team used the SER-CAT 22-ID and 22-BM x-ray beam-lines at APS to take diffraction data of both the enzymes and the amino acids. They modeled the intermediate molecules' conformations from that data. They also took kinetic data of the reactions using high-pressure stopped-flow spectrophotometry at a range of pressures and temperatures.

< Fig. 1. Depiction of an aminoacrylate (lower center) formed as an intermediate molecule in the production of the amino acid L-tyrosine catalyzed by tyrosine phenol-lyase.

The team found that the structures of all the intermediate aminoacrylates, depicted in Fig. 1, were identical, independent of the amino acid used in the reaction. However, there were thermodynamic differences between the L-tyrosine reactions and those of the other amino acids, including values for enthalpy, entropy, compressibility, and apparent activation volume. The rate of formation was higher for the L-tyrosine reaction than the one that used S-ethyl-L-cysteine. Additionally, the reaction of S-ethyl-L-cysteine did not exhibit an interaction similar to that of L-tyrosine with the enzyme during catalysis. The team's use of a perdeuterated version of tyrosine phenol-lyase (in which all significant hydrogen atoms within the molecule were replaced with deuterium) gave them insight into the dynamic motions of the enzyme that occurred during the reactions.

Based on the differences measured for the L-tyrosine reaction as compared with the other amino acids, the team concluded that interacting with the tyrosine phenol-lyase enzyme changed the conformation of the L-tyrosine during the formation of the intermediate molecule. They further concluded that the conformational change in the amino acid due to the enzyme allowed the reaction to be reversible and the phenol leaving group to be good.

– Mary Alexandra Agner

See: Robert S. Phillips^{1*}, Steven Craig¹, Andrey Kovalevsky², Oksana Gerlits³, Kevin Weiss², Andreea I. Iorgu⁴, Derren J. Heyes⁴, and Sam Hay⁴, “Pressure and Temperature Effects on the Formation of Aminoacrylate Intermediates of Tyrosine Phenol-lyase Demonstrate Reaction Dynamics,” ACS Catal. **10**, 1692 (2020). DOI: 10.1021/acscatal.9b03967

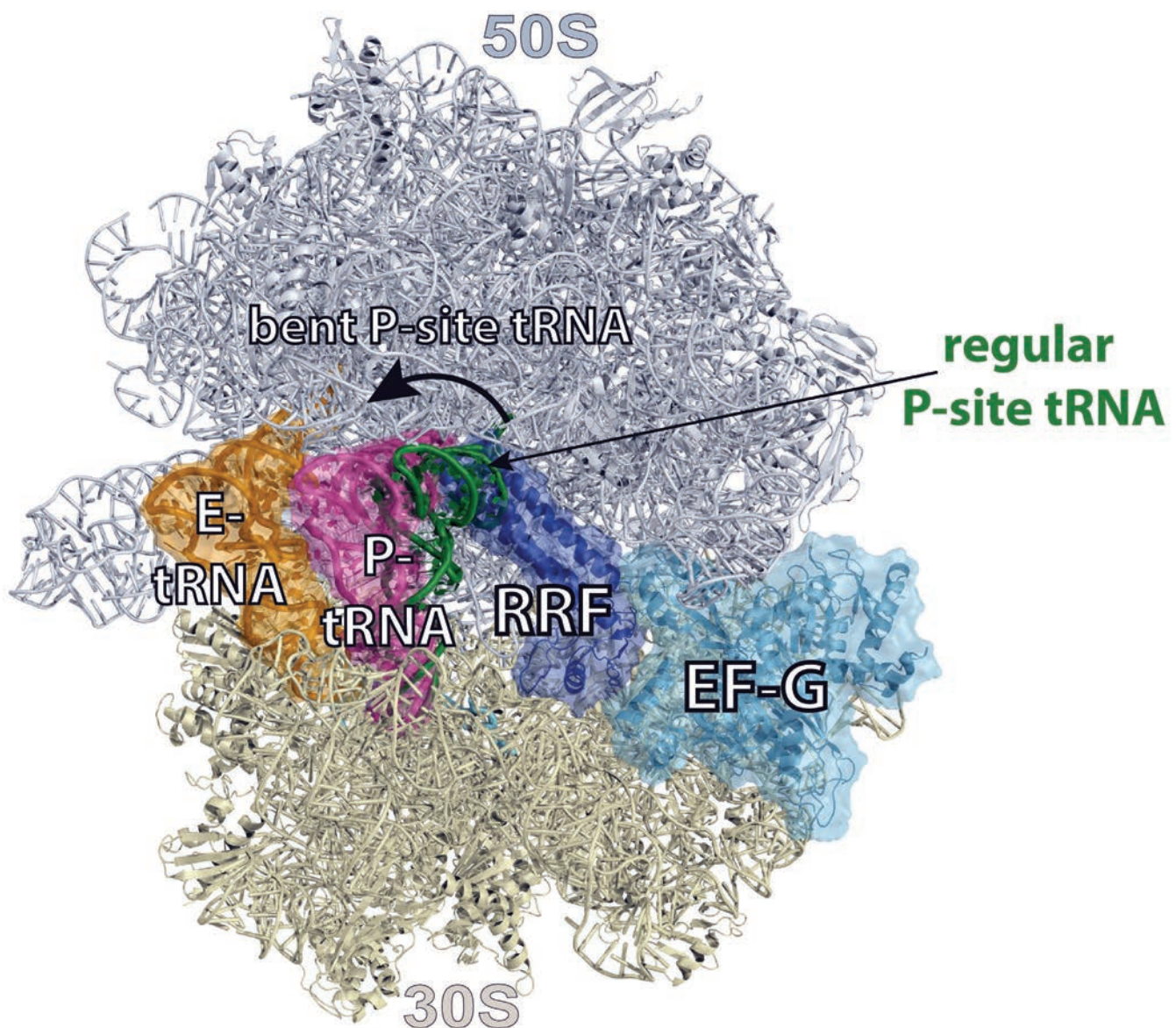
Correspondence: * plp@uga.edu

Author affiliations: ¹University of Georgia, ²Oak Ridge National Laboratory, ³Tennessee Wesleyan University, ⁴The University of Manchester

The Southeast Regional Collaborative Access Team is supported by its member institutions (see <https://www.ser.aps.anl.gov/www.ser-cat.org/members.html>) and equipment grants (S10 RR25528 and S10 RR028976) from the National Institutes of Health. This research used resources of the Advanced Photon Source, a U.S. DOE Office of Science User Facility operated for the DOE Office of Science by Argonne National Laboratory under contract no. DE-AC02-06CH11357.

Transfer RNA Conformation Aids Efficient Ribosome Recycling

Suffering from a surplus of shipping boxes? No matter how large your recycling bins are, it's always frustrating to have to trim down the cardboard to fit inside. This dissociative aspect of recycling extends to even the microscopic level. Ribosomes, important cellular machines, also break apart as they're recycled. It's necessary for ribosomes to dissociate after completing their work so that the molecules bound to them will be released for other tasks. But understanding exactly how ribosomes dissociate can be as frustrating as being stuck with a dull box cutter and a pile of boxes. Recent research by a team of collaborators used the APS to determine the previously-unseen structure of the ribosome molecular complex near the beginning of the recycling process, yielding insight into the conditions that facilitate ribosome dissociation.



Ribosomes are formed from two subunits, one smaller, one larger; the two subunits are connected by bridges. The ribosome's function within the cell is to translate messenger RNA into large polypeptide chains, or proteins. Proteins act as antibodies, enzymes, and messengers, as well as playing other key roles within the cell. Not surprisingly, RNA translation involves many molecules, whose shape, or conformation, could affect the ribosome after it has finished its work. Some of these molecules help bring the raw materials to the ribosome, and some of them bind to the ribosome, moving between different sites on the ribosome as translation occurs. At the point when the ribosome reads the genetic command to end translation, the ribosome complex is comprised of the ribosome itself plus the following molecules: a bound messenger RNA molecule (which provides the instructions for the ribosome's work), two bound transfer RNA molecules (which help the ribosome build the protein), a ribosome recycling factor molecule (which helps split the ribosome into its subunits and release messenger RNA), an elongation factor G molecule (which moves transfer RNA molecules during translation), and guanosine 5'-triphosphate (which provides fuel for the ribosome's work). The relative position and conformation of these molecules at the point when the ribosome's work is finished all potentially impact how the ribosome dissociates.

To determine those relative positions and conformations, the team collected x-ray diffraction data of the ribosome complex of the bacteria *Thermus thermophilus* using the NE-CAT beamline 24-ID-C at the APS and beamline BL17U at the Shanghai Synchrotron Radiation Facility. The team determined the structure of the ribosome complex from the diffraction data and found marked differences between this structure and those described in previously-published research, indicating that their data had been collected during a different point in the translation process from that of the previous efforts. The first difference was that the transfer RNA molecule in the peptidyl site was bent nearly 30°, with its cytosine-cytosine-adenine tail in an unexpected location, as shown in Fig. 1. Secondly, the elongation factor was in its compact shape, able

< Fig. 1 The ribosome complex just prior to recycling, including all the major molecules and the two parts of the ribosome itself (labeled 50S and 30S), but focusing on the changes to the transfer RNA molecule.

to influence the positioning of the ribosome recycling factor and, thus indirectly, the ribosome subunits.

Since the structure shows the ribosome complex at a single moment in the translation process, the team drew the following conclusions about how the molecules were relating to each other based on their conformations. With the transfer RNA molecule in the peptidyl site bent and its tail located differently from its expected place, the phosphate portions of that molecule and the ribosome interact non-favorably, potentially creating enough molecular tension to push apart the ribosome subunits. The team also concluded that additional tension could be created by the way the compact shape of the elongation factor was influencing the ribosome recycling factor: causing the latter to rotate toward the bridges between the ribosome subunits. These conclusions were supported by other published results which show that the presence of transfer RNA molecules aid efficient ribosome recycling.

– Mary Alexandra Agner

See: Dejian Zhou¹, Takehito Tanzawa², Jinzhong Lin^{1*} and Matthieu G. Gagnon^{2**}, “Structural basis for ribosome recycling by RRF and tRNA,” *Nat. Struct. Mol. Biol.* **27**, 25 (January 2020). DOI: 10.1038/s41594-019-0350-7

Author affiliations: ¹Fudan University, ²University of Texas Medical Branch

Correspondence: * linjinzhong@fudan.edu.cn,
** magagnon@utmb.edu

This work was supported by grants from the National Key R&D Program of China (no. 2017YFA0504602) and the National Natural Science Foundation of China (no. 31770784) (to J.L.), and by startup funds from the University of Texas Medical Branch (to M.G.G.), by a McLaughlin Fellowship from the Institute for Human Infections and Immunity at the University of Texas Medical Branch (to M.G.G.), by a Rising Science and Technology Acquisition and Retention Program award (to M.G.G.), and by an endowment from Sealy and Smith Foundation to Sealy Center for Structural Biology at the University of Texas Medical Branch. The Northeastern Collaborative Access Team beamlines are funded by the National Institute of General Medical Sciences from the National Institutes of Health (grant no. P41-GM103403 to NE-CAT). The Pilatus 6M detector on 24-ID-C beamline is funded by the NIH-ORIP HEI Grant (no. S10-RR029205 to NE-CAT). This research used resources of the Advanced Photon Source, a U.S. Department of Energy (DOE) Office of Science User Facility operated for the DOE Office of Science by Argonne National Laboratory under contract no. DE-AC02-06CH11357.

Structural Analyses Reveal Key Insights into Clinically Relevant Nanomachines

N-terminal region of pseudo A₂ domains

AntC	RAPRYAAVSDLP	PRNADGTLDTAA	GELP	VLDIAE	AAGAWERGI	AAL	PGVRS	AAVEL	EDVPO	1691			
CesA	-----	MMEMKR	VEEHDH	IFVFN	-----	E	LENEC	RRYGR	SNLAIMLEKHGV	55			
CesB	PKSQI	ISMSSLPL	TRKEG	IDRQQL	PSLL	GLT	ADDEE	MLQSY	-----	GKEK	IAITYE	WFR	139
CrpD	LPCIY	VPVSAL	PLTS	FGGE	VEVGL	ASIS	LDSE	LINT	WEEQ	IGSQAE	LDK	VAVT	TEPNV
HctE	-----	NLPL	TGKGL	DES	ALQ	LE	V	DS	ELV	SRW	EQQL	RSI	PEIE
HctF	-----	PVSSL	PLTGKGL	DES	ALQ	LE	V	DS	ELV	SRW	EQQL	RSI	PEIE
KtzG	-----	-----	-----	-----	-----	MTT	AD	IG	PD	ALAE	IAAE	ART	APG
StsApre	-----	MKP	STIN	QTS	RHES	MDAIL	-----	Q	-----	DV	KT	IL	Q
StsB	VPAAL	VLVPSL	PRKES	GA	VDTE	ALL	AID	VL	DEE	ERR	KIE	ERT	AID
Vlm1	-----	-----	-----	-----	-----	-----	-----	-----	-----	-----	-----	-----	-----
Vlm2	PVDD	VTVS	CLPL	DDG	AVD	YVSL	RQ	AA	LD	AP	RL	AE	LE
StsAobs	-----	MKP	STIN	QTS	RHES	MDAIL	-----	Q	-----	DV	KT	IL	Q



N-terminal region of pseudo A₂ domains

AntC	RAPRYAAVSDLP	PRNADGTLDTAA	GELP	VLDIAE	AAGAWERGI	AAL	PGVRS	AAVEL	EDVPO	1691			
CesA	-----	MMEMKR	VEEHDH	IFVFN	-----	E	LENEC	RRYGR	SNLAIMLEKHGV	55			
CesB	PKSQI	ISMSSLPL	TRKEG	IDRQQL	PSLL	GLT	ADDEE	MLQSY	-----	GKEK	IAITYE	WFR	139
CrpD	LPCIY	VPVSAL	PLTS	FGGE	VEVGL	ASIS	LDSE	LINT	WEEQ	IGSQAE	LDK	VAVT	TEPNV
HctE	-----	NLPL	TGKGL	DES	ALQ	LE	V	DS	ELV	SRW	EQQL	RSI	PEIE
HctF	-----	PVSSL	PLTGKGL	DES	ALQ	LE	V	DS	ELV	SRW	EQQL	RSI	PEIE
KtzG	-----	-----	-----	-----	-----	MTT	AD	IG	PD	ALAE	IAAE	ART	APG
StsApre	-----	MKP	STIN	QTS	RHES	MDAIL	-----	Q	-----	DV	KT	IL	Q
StsB	VPAAL	VLVPSL	PRKES	GA	VDTE	ALL	AID	VL	DEE	ERR	KIE	ERT	AID
Vlm1	-----	-----	-----	-----	-----	-----	-----	-----	-----	-----	-----	-----	-----
Vlm2	PVDD	VTVS	CLPL	DDG	AVD	YVSL	RQ	AA	LD	AP	RL	AE	LE
StsAobs	-----	MKP	STIN	QTS	RHES	MDAIL	-----	Q	-----	DV	KT	IL	Q

Fig. 1. Structure of a depsipeptide module, in which the PCP domain is disordered. (Photo credit: Larissa Ulisko and Martin Schmeing)

Humans are currently living longer lives than ever before. Our improved longevity is, in part, thanks to the development of effective drugs that can treat infection and disease. The antibiotic daptomycin, for example, can treat complicated bacterial skin and blood infections. Another example is the immunosuppressant cyclosporin, which can help prevent someone from rejecting a vital organ transplant. Yet another example is the antifungal drug caspofungin, which can be given intravenously to treat patients with a serious fungal infection. What do these three very different drugs have in common? They are each produced by enzymes referred to as nonribosomal peptide synthetases, which are nanomachines that construct a variety of molecules that are utilized in the clinic. Research at the APS has significantly furthered our understanding of how these nanomachines synthesize molecules. The researchers in this study revealed the structural basis of this synthetic process and these novel findings create the exciting possibility of designing new, effective drugs to improve human health.

In biology, proteins can be thought of as the primary molecular workers. They are responsible for carrying out various cellular tasks, such as transporting resources or waste from one part of a cell to another. Enzymes are an especially important protein type as they have a unique ability to accelerate chemical reactions. A key example would be the multi-domain class of enzymes referred to as nonribosomal peptide synthetases (NRPSs). These enzymes, which are made up of different sections called modules, can be likened to assembly line machines in factories. NRPSs are nanomachines that add building blocks to a growing molecular chain. The molecular product built by NRPSs is referred to as a nonribosomal peptide or depsipeptide. The term “nonribosomal” means that these molecules are built outside of ribosomes, which are more classical molecular machines that synthesize proteins. Peptides are made up of amino acid building blocks and the term “depsipeptide” describes a peptide with a unique chemical structure (i.e., where one or more amide groups are replaced with an ester group). Depsipeptides contain both hydroxyl acid and amino acid residues, the former of which are often derived from α -keto acid substrates. Keto acids play important biological roles—e.g., keto acids are converted into energy in response to lengthy periods of food deprivation, sometimes known as intermittent fasting.

NRPS enzymes have significant clinical relevance; they produce a plethora of different drugs, such as daptomycin, cyclosporin, and caspofungin. Daptomycin is an antibiotic that can be injected to treat bacterial blood infections as well as complicated skin infections. For organ transplant recipients, the immunosuppressant cyclosporine can prevent transplant rejection. Caspofungin is an antifungal drug that can treat fungal infections of the blood and esophagus. Specific examples of depsipeptides that serve important societal roles include the piscicide antimycin, the anti-cancer agent cryptophycin, and the insecticide beauvericin. Many of these important compounds—such as antimycin and cryptophycin—derive their hydroxyl acid residues from α -keto acid substrates. NRPS enzymes and depsipeptides therefore have palpably useful roles for the promotion of human health.

In this study by researchers from McGill University (Canada) and Yale University, substantial structural insights have been gleaned into NRPSs. The researchers have unveiled the architecture of NRPS modules and identified the mechanism by which α -keto acids are incorporated into the assembly process. Figure 1 displays the surprising architecture for modules that use α -keto acids. Since many nonribosomal depsipeptides derive their hydroxyl acid residue from α -keto acids, this sheds light onto a paramount part of nonribosomal depsipeptide synthesis. Molecular x-ray crystallography studies were performed at the NE-CAT beamlines 24-ID-C and 24-ID-E, and at the Canadian Light Source beamline 08ID-1 to obtain important structural data.

This research opens important possibilities for future research. Since a key part of nonribosomal depsipeptides—the hydroxyl acid residue—are often derived from α -keto acids, these findings advance our collective understanding of how these medically useful molecules are produced. With this knowledge, it is theoretically possible to manipulate this machinery to produce new, potent drugs capable of further improving human health.

– Alicia Surrao

See: Diego A. Alonzo¹, Clarisse Chiche-Lapierre¹, Michael J. Tarry¹, Jimin Wang², and T. Martin Schmeing^{*}, “Structural basis of keto acid utilization in nonribosomal depsipeptide synthesis,” *Nat. Chem. Biol.* **16**, 493 (May 2020).

DOI: 10.1038/s41589-020-0481-5

Author affiliations: ¹McGill University, ²Yale University

Correspondence: * martin.schmeing@mcgill.ca

This work was supported by a Canada Research Chair and NSERC Discovery Grant no. 418420 to T.M.S. The Northeastern Collaborative Access Team beamlines are funded by the National Institute of General Medical Sciences from the National Institutes of Health (NIH) (P30 GM124165). The Eiger 16M detector on 24-ID-E is funded by a NIH-ORIP HEI grant (S10OD021527). This research used resources of the Advanced Photon Source, a U.S. Department of Energy (DOE) Office of Science User Facility operated for the DOE Office of Science by Argonne National Laboratory under Contract No. DE-AC02-06CH11357.

Double-Safe in the Time of the Pandemic: **Jeff McGhee**



Environmental, Geological, and Planetary Science

In Situ Imaging of Methane Hydrate Formation and Dissolution

Methane hydrates are abundant in nature under conditions of high pressure and low temperature. They are important as a resource of clean-burning hydrocarbon fuel, but have a negative environmental impact if the methane dissociates and enters the atmosphere. Dynamic *in situ* three-dimensional (3-D) x-ray imaging, with short scanning times and high-resolution, improves researchers' understanding of the chemical and physical processes of gas-hydrate formation and dissolution, which is crucial for developing safer and more efficient techniques for methane hydrate exploration and utilization. This work attempts to better understand the formation and dissociation of methane gas hydrates using synchrotron tomography at the APS. A technique new to the study of gas hydrates—four-dimensional x-ray imaging—revealed the time evolution of hydrate morphology, matrix composition, pore structure, and the hydrates' effects on the physical properties of rocks. Using short scanning times and high resolution, the high-brightness x-rays from the APS revealed fast processes, i.e., water movement and gas hydrate formation and dissociation.

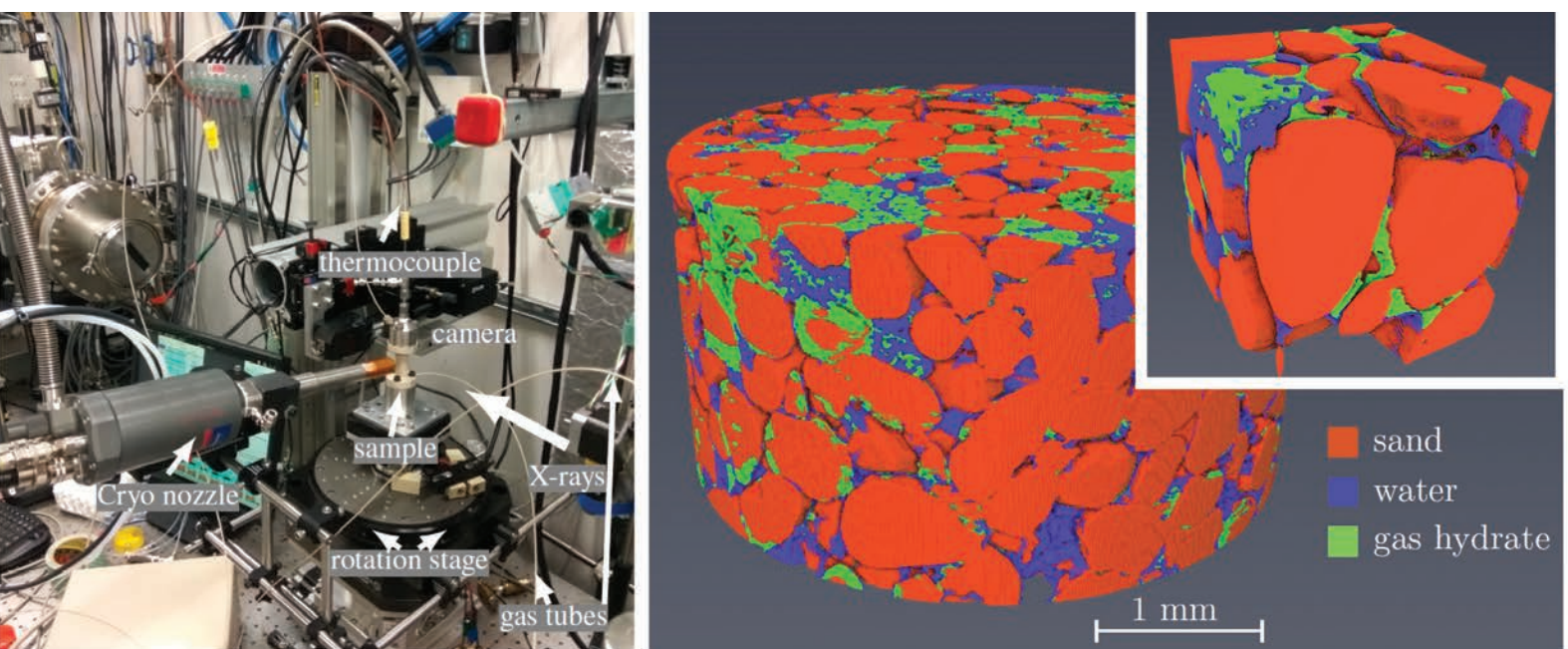


Fig. 1. Left: Set-up of the tomography experiments at the 2-BM-B beamline of the APS; and (right) x-ray computed tomographic image of gas hydrate growth in a sample, obtained at the beamline.

Methane hydrates—solid crystals of methane enclosed in a cage of water molecules—are most common in permafrost and deep-ocean sediments under conditions of high pressure (>35 bars) and low temperature (<10° C). In the oceans, microorganisms convert organic materials into methane deep in a sediment pile. Deep sediments are too warm for hydrate stability, so the methane bubbles up into cooler sediments, where it is incorporated into methane hydrates.

Methane hydrates are plentiful along continental margins where organic material is abundant and temperature and pressure conditions are favorable. If conditions change, for instance, the ocean temperature rises, the hydrate structure dissociates and releases the methane (a potent greenhouse gas) into the atmosphere. Interest in methane hydrates is high because they are a clean-burning hydrocarbon fuel and are more abundant than conventional and shale resources combined. Methane that escapes into the atmosphere is a greenhouse gas and may contribute to the rise in global temperatures. However, researchers must learn more about chemical and physical processes during gas-hydrate formation and dissolution in order to develop efficient and safe techniques for utilizing them.

First, the researchers in this study filled the environmental cell with wet sand and introduced methane gas via high-pressure tubes at the top and bottom of the cell, under controlled temperature and gas pressure. Next, they used dynamic *in situ* three-dimensional imaging to study the rock structure during the formation/dissociation cycle using x-ray computed tomography at the XSD Imaging Group's 2-BM-D x-ray beamline of the APS. To get the desired spatial and temporal resolution, the acquisition time for one data set ranged from one-half minute to several minutes.

High-resolution and variable scanning times of geologic sediments exposed complicated structures with small pores and mineral particles, gas, and multi-phase liq-

uids. *In situ* imaging also revealed dynamic processes during gas-hydrate formation and dissociation. In addition to the previously known shell formation, gas hydrates form in gas pockets or inside water volumes. The researchers observed short, fast movements of water punctuated by periods of water immobility that may have been caused by cryogenic water suction during hydrate formation.

Dissociation in self-preservation mode (pressure drop at negative temperature) is different for each type of gas hydrate. Hydrates formed in water volumes are more stable than those formed in gas pockets, so each dissociates at a different speed. Interestingly, the stability of gas-hydrate accumulations and their production rates depends on their history prior to formation.

In the future, faster imaging will improve the researchers' ability to understand the kinetics of gas hydrate formation and dissociation, which could optimize the methodology of methane hydrate production. Performing the experiments in a larger chamber will allow the researchers to measure the acoustic properties of the samples during methane hydrate formation. This will help them develop methods to interpret geophysical data for acoustic well logging and seismic exploration.

– Dana Desonie

See: Viktor V. Nikitin^{1*}, Geser A. Dugarov², Anton A. Duchkov^{2,3}, Mikhail I. Fokin², Arkady N. Drobchik², Pavel D. Shevchenko⁴, Francesco De Carlo⁴, and Rajmund Mokso¹, “Dynamic in-situ imaging of methane hydrate formation and self-preservation in porous media,” *Mar. Petrol. Geol.* **115**, 104234 (2020). DOI: 10.1016/j.marpetgeo.2020.104234

Author affiliations: ¹Lund University, ²Institute of Petroleum Geology and Geophysics SB RAS, ³Novosibirsk State University, ⁴National Laboratory

Correspondence: * viktorn.nikitin@maxiv.lu.se, vnikitin@anl.gov

The work is supported by the Swedish Research Council grant (2017-00583). This research used resources of the Advanced Photon Source, a U.S. Department of Energy (DOE) Office of Science User Facility operated for the DOE Office of Science by Argonne National Laboratory under Contract No. DE-AC02-06CH11357.

A Comparison of Large and Supersized Rhyolitic Eruptions in Taupo, New Zealand

Researchers used the APS to investigate one large and one supersized eruption of high-silica rhyolite magma in the Taupo Volcanic Center (TVC), New Zealand. The compositions and textures of the rock samples reveal differences in the magmatic processes that formed them. To understand volcanic hazards, and also the formation and evolution of the continental crust, it is necessary to know where and for how long these magmas reside in the crust, plus the timing and path over which they erupted.

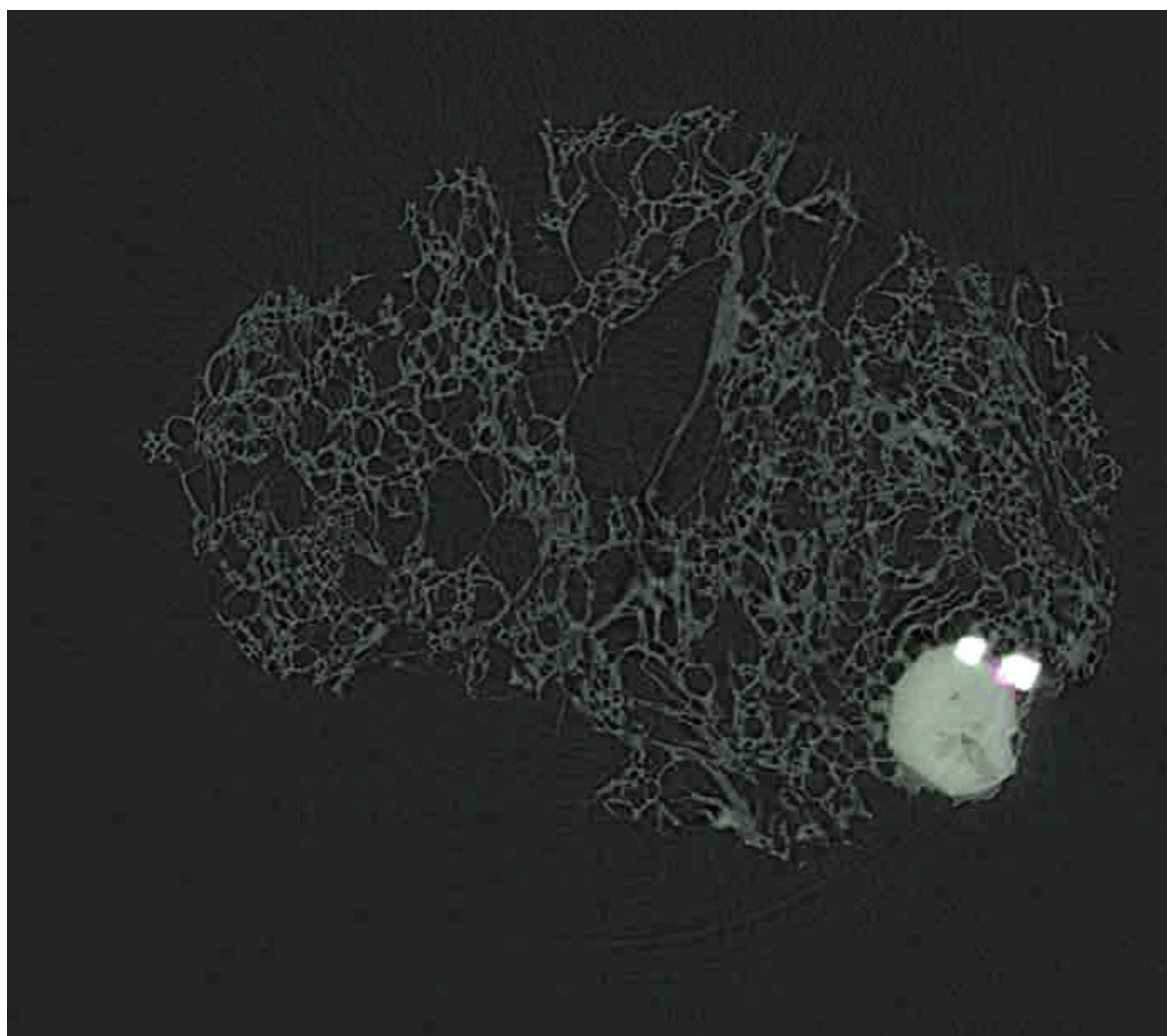


Fig. 1. X-ray tomogram of a piece of pumice with an overlay of a zirconium map, obtained at the GSECARS beamline at the APS. Several crystals are visible; the one that is artificially colored pink is zircon, a high-zirconium phase.

For the past 1.6 million years, the sideways and downward movement of the Pacific Plate beneath the North Island of New Zealand has fueled explosive volcanic activity. In the middle is the TVC, where large, explosive, caldera-forming silicic volcanism has occurred intermittently for about 61,000 years. The volcanism was “hyperactive” for about 24,000 years, from the Oruanui supereruption 25,400 years ago to the Taupo eruption 1,720 years ago.

Supereruptions are rare in Earth history, and the Oruanui was the most recent. This voluminous high-silica rhyolitic event ejected 530 km³ (approximately 127 cu mi) of material. The second largest eruption in the TVC, the Taupo eruption, produced an order of magnitude smaller volume (35 km³, or about 8 cu mi). Many smaller eruptions, primarily of dacite and lower silica rhyolite, occurred in between the two large eruptions.

Igneous rocks, and the minerals in them, lock away the secrets of their magmatic history in their compositions and textures (sizes, shapes). Volcanic rocks, like the pumice the researchers used in this study, contain different kinds of crystals and glass. Phenocrysts are larger crystals whose sizes and compositions help to record the history of crystallization in the magma prior to eruption. Microlites are tiny crystals that grow just before or during an eruption and reveal secrets about eruptive processes. For this study, the researchers analyzed crystal and glass compositions and textures to learn about the crustal storage conditions, longevity, and eruption of the TVC magmas.

Using rhyolite-MELTS geobarometry on glass compositions, the researchers in this study found that both magmas crystallized in the upper crust but at different pressures, consistent with differences in their compositions. The Oruanui magma was more evolved than the Taupo magma and crystallized at lower pressures (50-250 MPa versus 280-470 MPa). Previous studies showed that the Oruanui and Taupo magmas did not exist in the crust simultaneously, and that the TVC magmatic system was rebuilt after the Oruanui explosion. The researchers found a trend from shallow storage of an older, mature system (Oruanui) to deep storage of a younger, less mature system (Taupo) as the magmatic structure was being recon-

structed. This is similar to a trend seen during a 100,000-year ignimbrite flare-up, when several supereruptions occurred. This led the researchers to suggest that the modern TVC may currently be flaring-up for another sequence of large-to-giant eruptions.

Using crystal size distributions, which they determined from tomographic images (Fig. 1) collected at the GSECARS 13-BM-D x-ray beamline at the APS, and titanium-in-quartz diffusion chronometry, the researchers found that the two magmas crystallized over similarly short time periods (decades to centuries) even though the volume of the two eruptions was so different. This suggests that longer residence times are not necessarily correlated with larger eruptions, and that large-to-giant volumes of crystal-poor silicic magma are unstable in the upper crust.

The researchers also noticed important textural differences in the tomographic images from the two eruptions. Rock textures reveal important characteristics about the conditions and processes of eruption. Microlites are scarcer in Oruanui rocks than in Taupo rocks, and the researchers believe that the difference they see in microlite textures is related to the differences in the magma storage depths. The shallower storage depth of the Oruanui magma could have resulted in shorter ascent times, less chance of the magma stalling, and/or lower liquidus temperatures. – Dana Desonie

See: Ayla S. Pamukçu^{1*}, Kylie A. Wright², Guilherme A. R. Gualda², and Darren Gravley³, “Magma residence and eruption at the Taupo Volcanic Center (Taupo Volcanic Zone, New Zealand): insights from rhyolite-MELTS geobarometry, diffusion chronometry, and crystal textures,” *Contrib. Mineral. Petr.* **175**, 48 (2020). DOI: 10.1007/s00410-020-01684-2

Author affiliations: ¹Stanford University, ²Vanderbilt University, ³University of Canterbury

Correspondence: * apamukcu@stanford.edu

Funding was provided by a National Science Foundation (NSF) EAPSI Fellowship to A. Pamukcu, a Vanderbilt University VUSRP to K. Wright, and NSF grant EAR-1151337 to G. Gualda. GeoSoilEnviroCARS is supported by the NSF—Earth Sciences (EAR-1128799, EAPSI-1209584) and U.S. Department of Energy (DOE) GeoSciences (DE-FG02-94ER14466). This research used resources of the Advanced Photon Source, a U.S. DOE Office of Science User Facility operated for the DOE Office of Science by Argonne National Laboratory under Contract No. DE-AC02-06CH11357.

A Deeper Look into the Surface Chemistry and Mineralogy of Titan

In our Solar System, Saturn's largest moon, Titan, is currently the most promising candidate to harbor extraterrestrial life. Its thick atmosphere and the liquid hydrocarbon oceans beneath its icy surface are rich with organic compounds that offer tantalizing hints of past or present biological activity. In addition, there is a methane-based cycle similar to the hydrological cycle on Earth. NASA's upcoming Dragonfly mission is intended to closely explore this spectacular world by placing a rotorcraft lander capable of analyzing multiple surface sites. As a follow-up to the brief mission of the 2005 Huygens lander, Dragonfly will provide a far more extensive portrait of Titan's biotic environment. To accurately identify and interpret the fruits of Dragonfly's explorations in light of astrobiology will require a deeper understanding of the fundamental chemistry of the particular organic mixtures that might be found on Titan. Toward this end, a group of researchers using high-brightness APS x-rays investigated various mixtures of two of the most common organic compounds, benzene and acetonitrile.

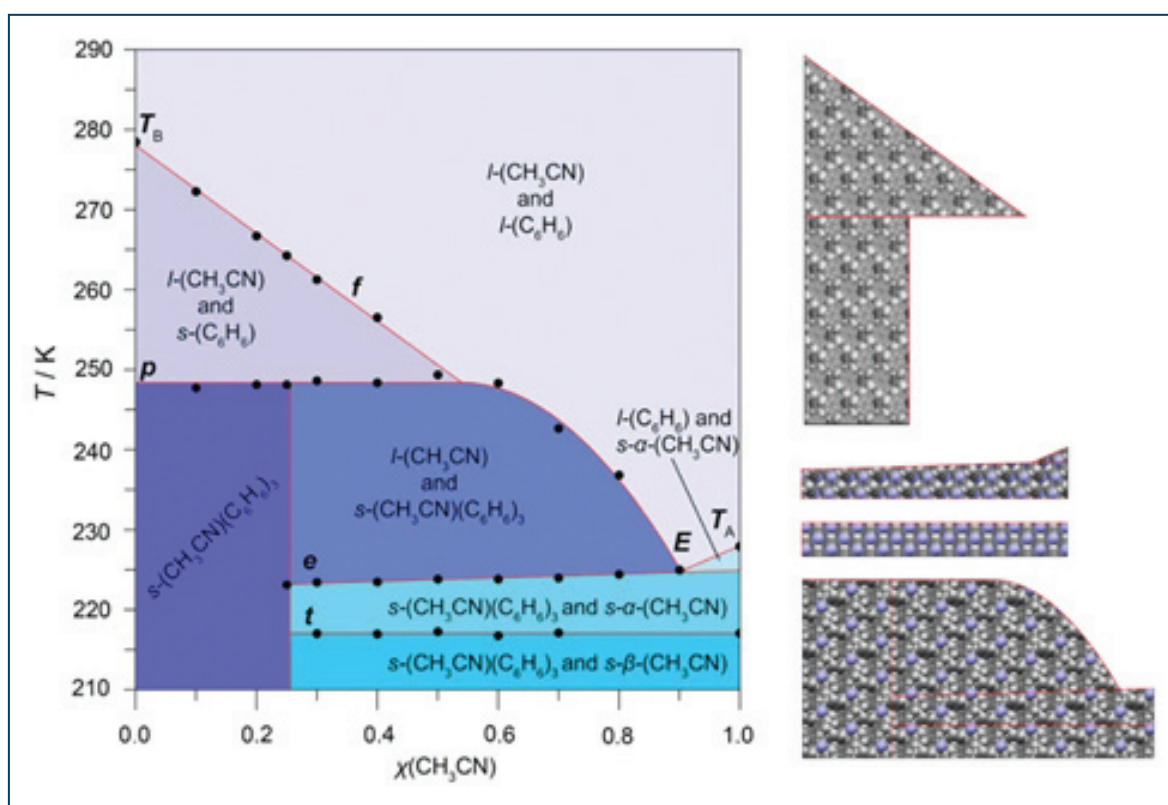


Fig. 1. Temperature-composition liquid-solid phase diagram of acetonitrile and ethane and crystal packing diagrams of characteristic crystalline phases.

Earlier studies of these two compounds suggested the possibility of co-crystallization, but at an unknown phase and temperature and without any structural information. The structure and interaction of such molecules at the cryogenic conditions of extraterrestrial environments have gained added relevance with space exploration, and such data has remained largely unaddressed in prior research. To fill in some of these gaps, the researchers studied the temperature-composition phase diagram of the benzene-acetonitrile system (Fig. 1) using calorimetric methods, finding a complex phase diagram indicating a possible peritectic phase transition at 248 K and occurrence of distinct crystalline states.

To obtain detailed structural information on the different phases below the fusion and peritectic boundary lines, the experimenters from Southern Methodist University, the National Institute for Standards and Technology, the University of Delaware, and Argonne employed *in situ* powder x-ray diffraction (PXRD) at various temperatures using the APS 17-BM x-ray beamline operated by the XSD Structural Science Group for rapid data acquisition. This showed that a solid benzene phase is present above the peritectic line from 245 K to 263 K. The crystalline benzene reacts with liquid acetonitrile, and a secondary phase develops below 245 K which displays a co-crystal with 1:3 acetonitrile:benzene stoichiometry, forming on cooling at a temperature of 227 K. When heated, the cocrystal remains stable until a melting temperature of 245 K.

The structural analysis of the diffraction pattern of related to the cocrystal was leading to two options. Energy optimization on isolated crystal structures confirmed the experimental model, described in an ordered *R3* packing. The cocrystal is polar, with benzene molecules forming hexagonal channels in a trigonal structure containing acetonitrile molecules. The polar structure raises interesting possibilities for pyroelectric, piezoelectric, ferroelectric, and other properties that could have potential astrobiological implications.

The experimenters investigated the stability of the acetonitrile:benzene cocrystal in a more representative Ti-

tanean environment through *in situ* contact with liquid ethane. Because ethane and acetonitrile share the same molecular diameter, they can both fit inside the benzene structure, forming a ternary system. The x-ray diffraction pattern of this structure is considerably different than that of either crystal in pure form, which suggests the existence of mixed or non-stoichiometric phases, and also raises the prospect that the detection of this cocrystal might serve as a marker for the past presence of ethane at Titanian sites.

With the more detailed chemical detection and analyses that Dragonfly will make possible on Titan, the present work is a significant step toward a more comprehensive picture of the to be expected mineralogy of Titan, particularly those aspects that might point to active biological processes. As we've already seen as far back as the Viking missions to Mars, the mere presence of organic molecules doesn't necessarily indicate the presence of life. However, a better understanding of the unique chemical environment of an extraterrestrial world will make it easier to distinguish false positives from a major scientific discovery. – Mark Wolverson

See: Christina A. McConville¹, Yunwen Tao¹, Hayden A. Evans², Benjamin A. Trump², Jonathan B. Lefton¹, Wenqian Xu³, Andrey A. Yakovenko³, Elfi Kraka¹, Craig M. Brown^{2,4}, and Tomče Runčevski^{1*}, “Peritectic phase transition of benzene and acetonitrile into a cocrystal relevant to Titan, Saturn’s moon,” *Chem. Commun.* **56**, 13520 (2020). DOI: 10.1039/d0cc04999a

Author affiliations: ¹Southern Methodist University, ²National Institute of Standards and Technology, ³Argonne National Laboratory, ⁴University of Delaware

Correspondence: * truncevski@smu.edu

T.R. and C.A.M. thank the Robert A. Welch Foundation (Grant No.: N-2012-20190330) for financial support. C.A.M. thanks the Texas Space Grant Consortium graduate fellowship. H.A.E. thanks the National Research Council (USA) for financial support through the Research Associate Program. We thank SMU for providing generous computational resources. This research used resources of the Advanced Photon Source, a U.S. Department of Energy (DOE) Office of Science User Facility operated for the DOE Office of Science by Argonne National Laboratory under Contract No. DE-AC02-06CH11357.

Keeping Heavy Metals Out of the Food Chain

Mining activities can release toxic heavy metals into waterways, where they poison marine life and can potentially spread into the food chain. Simplistic models of heavy metal dispersion sometimes suggest that much of the material would settle into sediments near its source. However, in Spain, testing of the waters of the Rio Tinto, one of the most heavily metal contaminated river systems in the world, has shown that significant amounts of certain metals, including up to 9% and 4% of the global river transport of zinc (Zn) and copper (Cu) respectively, make it out into the ocean. Significant amounts of arsenic (As), chromium (Cr), lead (Pb), and cadmium (Cd) are also washed into the ocean this way. A team of researchers suspected iron-metabolizing bacteria might play a role in the metals' mobility. They used the APS to analyze particulate matter and sediment samples from the Rio Tinto and its estuary. The data they collected help us understand the complex ways in which iron(II)-oxidizing microorganisms, mineral phases, and hydro(geo)chemical fluctuations caused by the mixing of fresh and saltwater interact to transport heavy metals (As, Cr, and Pb) from the mining sites to the ocean.

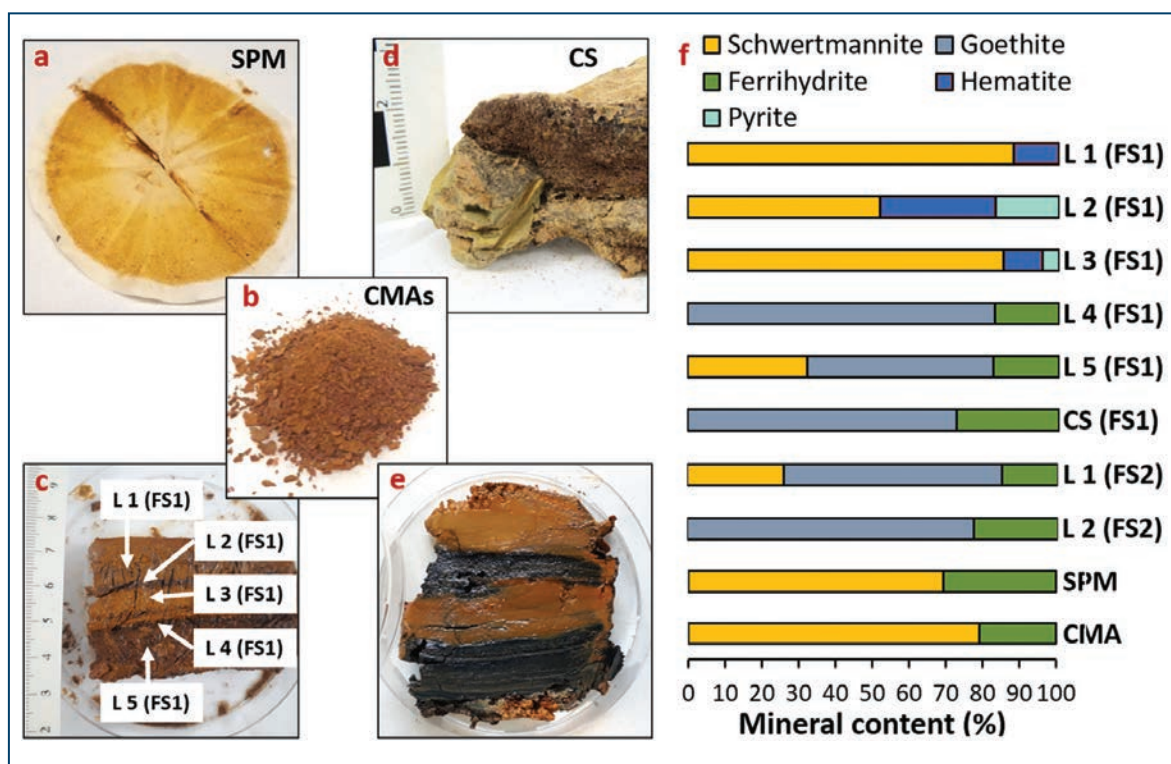


Fig. 1. The content of the various iron minerals in different types of sediments, particulate matter sampled in the Rio Tinto and microbially produced cell-mineral aggregates: a) coarse-grained suspended particulate matter sampled from the upper river, b) cell-Fe(III) mineral aggregates, c) layered sediment from the upper river, d) underlying consolidated sediment from the upper river, e) layered sediment with orange and black layers from the estuary, f) results of the iron K-edge EXAFS for samples, showing iron mineral content. FS1 = field site 1, FS2 = field site 2, CS = consolidated sediment, SPM = suspended particulate matter, and CMA = cell-Fe(III) mineral aggregates. From S.M. Abramov et al., "Role of biogenic Fe(III) minerals as a sink and carrier of heavy metals in the Rio Tinto, Spain," *Sci. Total Environ.* **718**, 137294 (20 May 2020). © 2020 Elsevier B.V. All rights reserved.

The Rio Tinto in the province Huelva of Spain, flows through an area with many mines, tailing and waste piles. The unique geochemistry of the river (i.e., pH = 2.3) and flow path can oxidize sulfide mineral naturally exposed along the riverbank. All of these hydro(geo)chemical processes contribute to the transport of heavy metals over a variety of distances. Some of these metals, such as Zn and Cu, are necessary for life in trace amounts. However, at the high concentrations found in the Rio Tinto, most of these heavy metals are determinantal to life and many (such as Pb, Cr, and A), are toxic even at low levels.

Despite the toxic heavy metals and high acidity of the water, a robust population of acidophilic iron metabolizing bacteria live in the water and sediments of the upper and middle reaches of the Rio Tinto. These bacteria oxidize iron-²⁺ ions (Fe(II)) to iron-³⁺ (Fe(III)) as they live and reproduce. Although able to survive in the heavy metal infused water, the toxicity seriously slowed bacterial growth and reproduction by an order of magnitude. Nevertheless, the oxidation and reduction of Fe(II) and Fe(III) by the bacteria can play a key role in immobilizing heavy metals within minerals. Lead, chromium and arsenic all form compounds with, or are easily adsorbed by, iron sulfate minerals such as schwertmannite. These metals tended to precipitate and fall into the sediment, but could also adsorb to suspended particulate matter, along with bacterial cells, and continue to float about the river. It was demonstrated that up to 100% of As and Cr can be transported to the ocean via associations with particulate matter. Conversely, aluminum, copper, cobalt and cadmium did not precipitate out, even when there was an abundance of adsorption sites, because of the high acidity of the water.

Heavy metals associated with particulate matter in the Rio Tinto can either be kicked back up into the water by turbulence and the flux of salty and fresh water, or be buried into sediment and eventually mineralized. Samples of sediment collected from the middle course of the Rio Tinto showed a gradual transformation of schwertmannite and ferrihydrite (two semistable Fe mineral phases that adsorb heavy metals) into more consolidated, crystalline goethite and hematite (Fig. 1).

At the estuary, due to the mixing of saltwater with acidic freshwater and subsequent flocculation of solutes, the composition of the sediment was more complex. The sediment was characterized by distinct layers of orange and black material (Fig. 1.) Though both layers were rich in Fe(III) minerals, the black layers were enriched with hydro-

gen sulfide released by sulfate-reducing bacteria. The abiotic or biotic reduction of sulfate produces sulfide, which reacts with dissolved heavy metals leading to the precipitation of metal sulfides. These sulfides can act as a sink for heavy metals, and thus, lead, arsenic, cadmium and zinc were all found in these sulfidic layers in higher concentrations.

The researchers used the MR-CAT 10-BM and 10-ID x-ray beamlines at the APS to perform extended x-ray absorption fine structure (EXAFS) analysis on suspended particulate matter, river sediments and microbially produced cell-mineral aggregates. The MR-CAT facility at APS has the only insertion-device beamline in the United States dedicated to this type of analysis, and is uniquely good at illuminating the structures of molecules at the interface of biology and geology, such as the microbially-influenced Fe-containing minerals of the Rio Tinto.

Overall, the analysis showed two divergent pathways of immobilized heavy metals in the Rio Tinto system. Longitudinal pathways provide continuous transport of immobilized heavy metals into the ocean, while sedimentation pathways provide continuous burial of heavy metals in the sediments. Multiple sources, multiple sinks, and the microorganisms in the river all contribute to the varied fates of heavy metals flowing through the water. – Kim Krieger

See: Sergey M. Abramov^{1*}, Julian Tejada², Lars Grimm¹, Franziska Schädler¹, Aleksandr Bulaev³, Elizabeth J. Tomaszewski^{1,4}, James M. Byrne¹, Daniel Straub¹, Harald Thorwarth², Ricardo Amils⁵, Sara Kleindienst¹, Andreas Kappler¹, “Role of biogenic Fe(III) minerals as a sink and carrier of heavy metals in the Rio Tinto, Spain,” *Sci. Total Environ.* **718**, 137294 (20 May 2020). DOI: /10.1016/j.scitotenv.2020.137294
Author affiliations: ¹University of Tuebingen, ²University of Applied Forest Sciences Rottenburg, ³Research Center of Biotechnology of the Russian Academy of Sciences, ⁴University of Delaware, ⁵Autonomous University of Madrid
Correspondence: * sergey.abramov@uni-tuebingen.de

This study was supported by a grant from the German Research Foundation (DFG) to Andreas Kappler (KA 1736/43-1). Daniel Straub is funded by the Institutional Strategy of the University of Tübingen (DFG, ZUK 63) and further supported by the Collaborative Research Center 1253 CAMPOS (DFG, Grant Agreement SFB 1253/1 2017). Sara Kleindienst is funded by an Emmy-Noether fellowship (DFG, grant No 326028733). MR-CAT operations are supported by the Department of Energy and the MR-CAT member institutions. We would like to thank Joshua Wright (APS), Sarah Balgooyen, Emma Trainer and Lily Schacht for help with data collection. This research used resources of the Advanced Photon Source, a U.S. Department of Energy (DOE) Office of Science User Facility operated for the DOE Office of Science by Argonne National Laboratory under Contract No. DE-AC02-06CH11357.

Double-Safe in the Time of the Pandemic: **Elroy Chang**



Nanoscience

Using Cutting-Edge Nanoscale Imaging to Gain Molecular Insights about Parkinson's Disease

Parkinson's disease is a devastating, age-related neurodegenerative disease that severely affects movement and progressively worsens. There are no therapies that are disease-modifying. As such, there is a need for therapeutics that can delay or reverse cell death pathways. Since Parkinson's disease is presently incurable, any research results revealing the mechanisms underlying this disease or any other related neurodegenerative disease are highly valuable. Recent work by a research team using high-brightness x-rays from the APS provided exciting, nanoscopic insights into this neurodegenerative disorder that could help identify pathways for the development of disease-modifying therapeutics to preserve or restore neuronal health in Parkinson's disease patients.

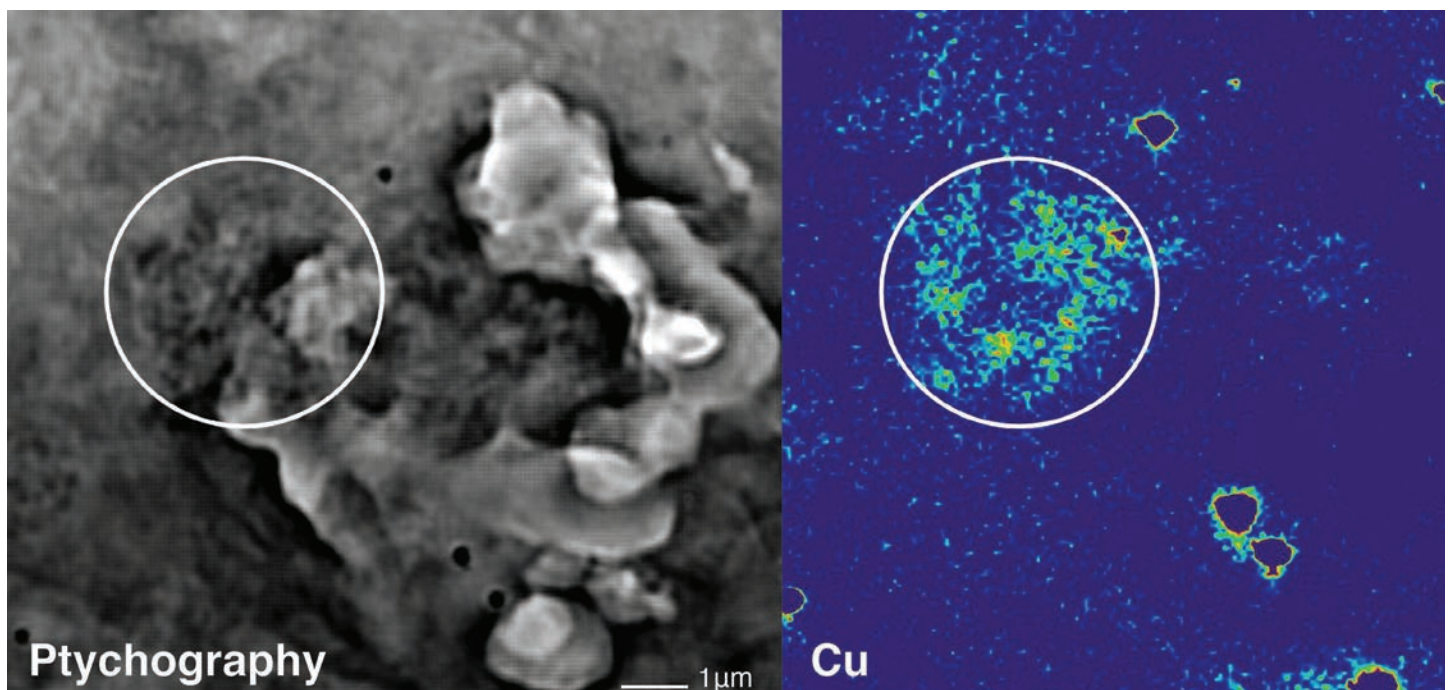
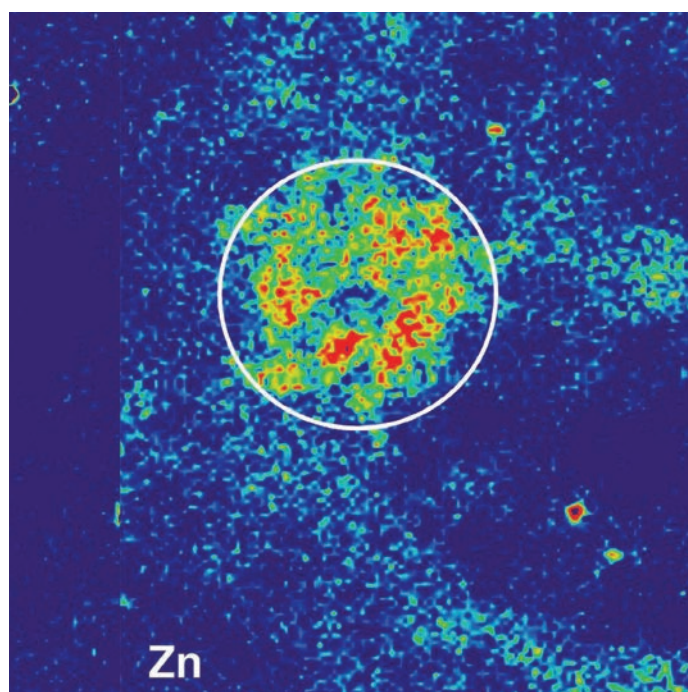


Fig. 1. X-ray ptychography (left) and quantitative x-ray fluorescence microscopy (middle and right) of SOD1 aggregates in the substantia nigra demonstrating distinct elemental fingerprints for copper (Cu) and zinc (Zn) binding.

Many neurodegenerative diseases exhibit an accumulation of molecular aggregates in the brain. For example, Alzheimer's disease is characterized by the accumulation of amyloid-beta peptide and fibrillary tangles comprised of hyperphosphorylated tau; amyotrophic lateral sclerosis (or Lou Gehrig's disease) presents with aggregations of superoxide dismutase 1 (SOD1) in the spinal cord; and alpha-synuclein protein deposits (termed Lewy bodies) are present in the brains of Parkinson's disease patients. Although it is still unknown what causes these neurodegenerative disorders, prevalent theories suggest that these molecular aggregates directly lead to neuronal death and onset of the disease.

Parkinson's disease is the second most common age-related neurodegenerative disorder and the most prevalent neurodegenerative movement disorder. Symptoms include a reduced ability to perform unconscious movements (e.g., blinking), muscle stiffness, slowed movement, shaking, balance problems, stooped posture, speech alterations, and writing difficulty. In Parkinson's disease, the presence of Lewy bodies serves as a definitive disease diagnosis. Additionally, the accumulation of other essential proteins has been found in the brains of Parkinson's disease patients, including the aggregation of SOD1 antioxidant protein as well as the normal aging deposits of neuromelanin.

The researchers in this study from The University of Sydney, Queensland University of Technology, The University of Melbourne, and the University of Technology



Sydney (all Australia) gained significant structural and molecular insights into Parkinson's disease. This work, carried out in collaboration with colleagues from Argonne, paired x-ray ptychography and x-ray fluorescence microscopy (XFM) using the hard x-ray nanoprobe located at the XSD Microscopy Group's beamline 9-ID-B at the APS to study the Lewy Body, SOD1, and neuromelanin molecular aggregates in the post-mortem brains of Parkinson's disease patients. By combining XFM and x-ray ptychography using the same x-ray source, the researchers were able to obtain nanometer structural and elemental resolution without disturbing the natural state of the sample. They found that neuromelanin exhibits a distinctly disor-

dered structure with a unique elemental composition. Although they observed that SOD1 protein aggregates and Lewy bodies exhibit a similar structure, these protein aggregates exhibited a unique elemental fingerprint in comparison to that of neuromelanin aggregates.

Another finding was that copper binding was impaired in SOD1 protein aggregates (Fig. 1). Since copper binding is required for SOD1 to function normally, this dysfunction may contribute to the pathogenesis of Parkinson's disease. This is especially interesting given that mutations in SOD1 are also associated with the neurodegenerative disease amyotrophic lateral sclerosis.

These findings in human brain tissue are highly significant and advance our understanding of Parkinson's disease. In addition to providing key insights into potential pathogenic mechanisms, these data contribute to our understanding of how this disease presents on a molecular level. Moreover, this analytical technique could be theoretically utilized to better understand molecular aggregates associated with other major diseases. Future studies should build upon these findings to develop novel interventions that can help patients suffering from neurodegenerative diseases like Parkinson's disease. – Stephen Taylor

See: Sian Genoud¹, Michael W. M. Jones², Benjamin Guy Trist¹, Junjing Deng³, Si Chen³, Dominic James Hare^{1,4,5*}, and Kay L. Double^{1**}, "Simultaneous structural and elemental nano-imaging of human brain tissue," *Chem. Sci.* **11**, 8919 (2020).

DOI: 10.1039/D0SC02844D

Author affiliations: ¹The University of Sydney, ²Queensland University of Technology, ³Argonne National Laboratory, ⁴The University of Melbourne, ⁵University of Technology Sydney

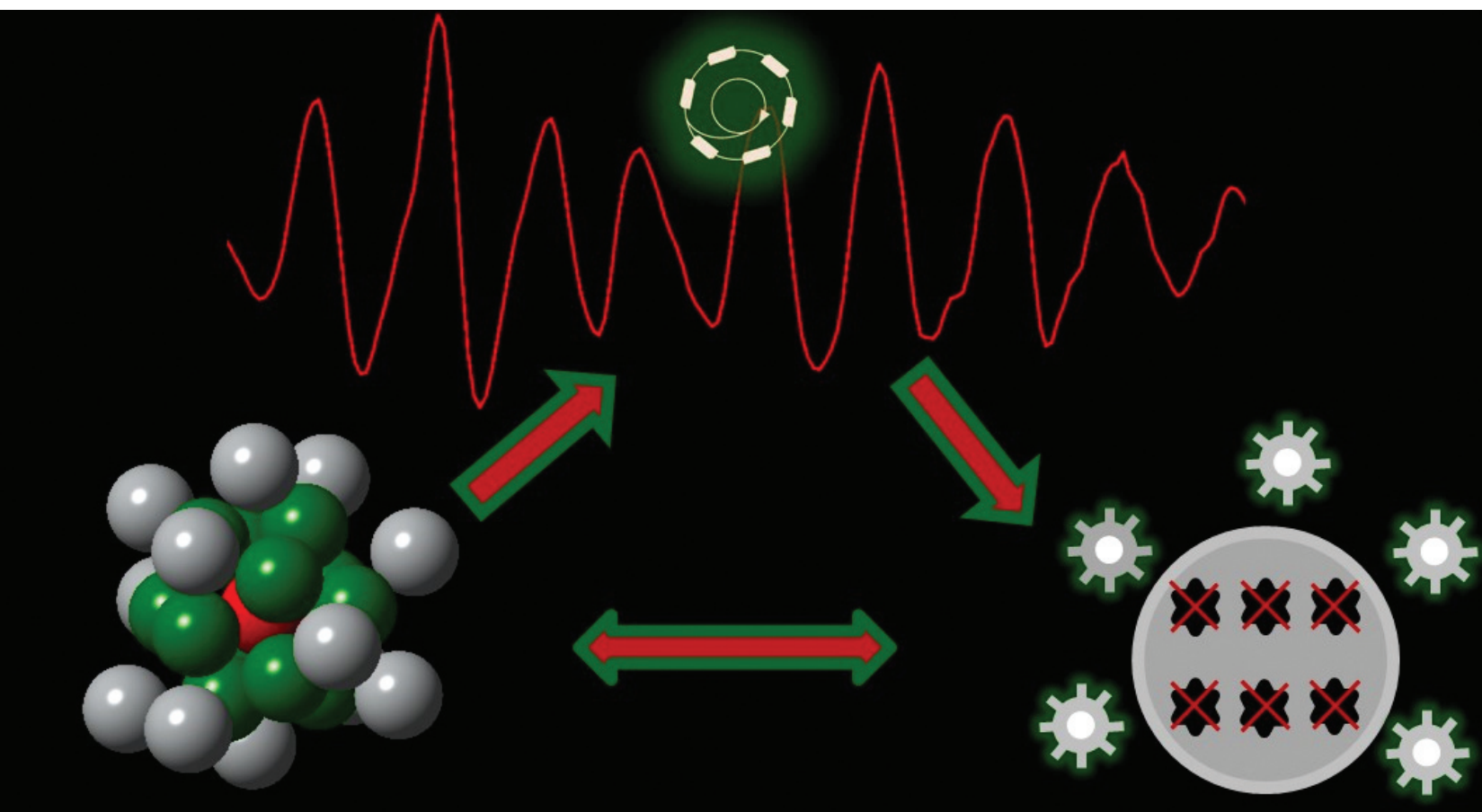
Correspondence: ** kay.double@sydney.edu.au

* dominic.hare@unimelb.edu.au

The Australian Research Council (ARC) Centre of Excellence for Advanced Molecular Imaging (CE140100011), and National Health and Medical Research Council (NHMRC) grants (GNT1122981; GNT1181864) schemes funded this work. This study was supported by ForeFront, a large collaborative research group dedicated to the study of neurodegenerative diseases and funded by the National Health and Medical Research Council of Australia Program Grant (1132524), Dementia Research Team Grant (1095127), Neuro-Sleep Centre of Research Excellence (1060992), and the ARC Centre of Excellence in Cognition and its Disorders Memory Program (CE10001021). D.J.H. wishes to acknowledge research and material support from Agilent Technologies through the NHMRC Career Development Industry Fellowship program (GNT1122981). Implementation of the Bionanoprobe was supported by NIH ARRA grant SP0007167. The authors would like to thank Evan Maxeey for the technical support at the Bionanoprobe beamline. This research used resources of the Advanced Photon Source, a U.S. Department of Energy (DOE) Office of Science User Facility operated for the DOE Office of Science by Argonne National Laboratory under Contract No. DE-AC02-06CH11357.

Silver Nanostructures Show Promise for Improved Medical Probes

Thermometers are a hot topic this year. Not just the devices themselves, but the disposable plastic covers that allow you to reuse the thermometer by keeping its parts separate from the microbes living in your body. But disposable plastic isn't the only way to make a medical device more hygienic: the material of the device itself could have intrinsic properties that make it less amenable to hosting microbes. The field of materials science has identified, and continues to investigate, these antibacterial materials, which include some nanostructures composed primarily of silver. The multi-year efforts of a research team shows that the atomic arrangements of the silver nanostructures—as revealed by x-ray absorption spectroscopy at the APS—can be used to characterize their antibacterial properties, allowing for improvements to medical probes. These results show that better characterization of the geometrical and electronic properties of silver nanostructures would allow for the use of the nanostructures' antibacterial properties in future medical applications, including but not limited to an improved thermometer.



Scientists quantify the intrinsic ability of a material to inhibit the growth of bacteria by calculating its antibacterial activity value. This value is determined by applying microbes to materials and counting the number of viable cells remaining after a specified period of time has elapsed. Many types of bacteria can be used for these calculations; for example, the JIS Z 2801 international standard specifies strains of *Staphylococcus aureus* and *Escherichia coli*. Because materials exhibit a range of antibacterial activity values—the silver nanostructures examined by the team all have different values—scientists are still working to improve their understanding of how the properties of a material contribute to its antibacterial activity value.

The team of researchers from Dalhousie University (Canada) investigated three types of silver nanostructures: silver nanoclusters (particles with diameters of less than 2 nm), silver nanocrystals (crystals having one dimension smaller than 100 nm and organized in a face-centered cubic lattice), and silver nanoalloys (a combination of particles of silver and other metals smaller than 100 nm). The two types of nanoclusters characterized by the team both had high antibacterial activity values, indicating they are effective at inhibiting bacterial growth. Two of the nanocrystals studied (those with cysteine and polyvinylpyrrolidone ligands) spanned a range of antibacterial activity values and did not inhibit growth with the same efficacy. A silver-plated gold nanoalloy had the highest antibacterial activity value of all the nanoalloys the team examined.

The breadth of antibacterial activity values found in the silver nanostructures implies that the ability of the nanostructure to inhibit bacterial growth is a function of its molecular geometry, those physical and electronic characteristics which determine the position of the atoms. These include bond lengths and coordination numbers (the number of atoms bonded to a given atom in a molecule). To discover the geometry of the silver nanostructures, the team used x-ray absorption spectroscopy—both x-ray absorption near-edge structure measurements and extended x-ray absorption fine structure measurements—at the XSD Spectroscopy Group's 20-BM-B x-ray beamline at

the APS. Figure 1 shows a simplified version of the synchrotron x-ray absorption spectroscopy process used. The team took both multi-edge and multi-element measurements, allowing them to also infer information about the structural information from a non-central metal atom and about the d-electron behavior of transitional metals, respectively. Together with advanced modeling, including density functional theory, this allowed the researchers to establish the geometrical characteristics of the nanostructures.

The team used the geometrical results to characterize the antibacterial activity values for the nanostructures. The silver nanoclusters had higher antibacterial activity values than predicted, based on the bonds between silver atoms. The team found that the differences in structure between the nanocrystals with cysteine ligands and those with polyvinylpyrrolidone ligands allowed for the release of differing amounts of silver ions; the polyvinylpyrrolidone ligands hold silver ions less tightly than the cysteine ligands, allowing the silver ions to disperse and inhibit bacterial growth. For the silver nanoalloys, the team found that the location rather than the concentration of silver plays the most important part in increasing the antibacterial activity value: nanoalloys with a silver coating, rather than a high silver composition, had the highest antibacterial activity values for the nanoalloys studied.

– Mary Alexandra Agner

See: Andrew G. Walsh, Ziyi Chen, and Peng Zhang*, “X-ray Spectroscopy of Silver Nanostructures toward Antibacterial Applications,” *J. Phys. Chem. C* **124**, 4339 (2020).

DOI: 10.1021/acs.jpcc.9b09548

Author affiliation: Dalhousie University

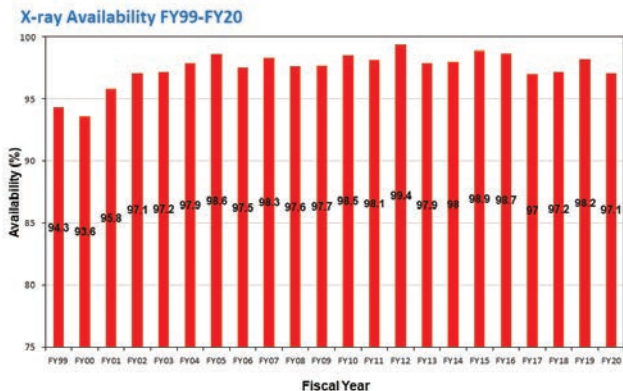
Correspondence: * peng.zhang@dal.ca

The financial support from NSERC Canada is gratefully acknowledged. This research used resources of the Advanced Photon Source, an Office of Science User Facility operated for the U.S. Department of Energy (DOE) Office of Science by Argonne National Laboratory, and was supported by the U.S. DOE under Contract No. DE-AC02-06CH11357 and the Canadian Light Source (CLS) and its funding partners. The CLS is supported by the CFI, NSERC, NRC, CIHR, the University of Saskatchewan, the Government of Saskatchewan, and Western Economic Diversification Canada.

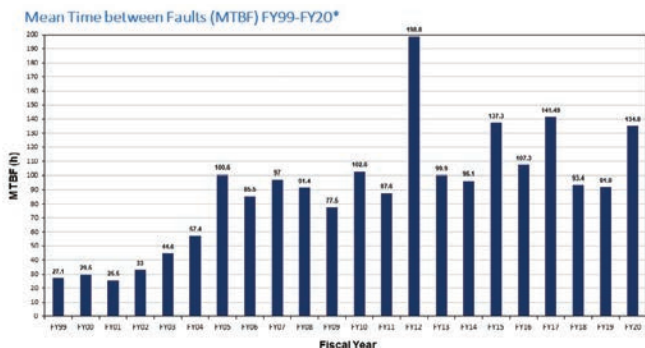
< Fig. 1. Synchrotron x-ray absorption spectroscopy can be used to determine structural and electronic information about silver (Ag) nanostructures from different atom positions, which can be used to understand the antibacterial activities of these materials.

APS X-RAY AVAILABILITY AND RELIABILITY

In fiscal year 2020*, the APS x-ray source continued to function as a highly reliable delivery system for synchrotron x-ray beams for research. Several factors support the overall growth in both the APS user community and the number of experiments carried out by that community. But there is a direct correlation between the number of x-ray hours available to users; the success of the APS experiment program; and the physicists, engineers, and technicians responsible for achieving and maintaining optimum x-ray source performance. Below are definitions of important measures for the delivery of x-ray beam to users (latest data shown graphically).



X-ray Availability: The number of hours that beam is available to users divided by the number of hours of scheduled beam delivery prior to the beginning of a run. The specific definition of available beam is that the APS main control room has granted permission to users to open shutters, and there is more than 50-mA stored beam in the storage ring.



Storage Ring Reliability: A measure of the mean time between beam losses (faults), or MTBF, calculated by taking the delivered beam and dividing by the total number of faults. The APS targets, and routinely exceeds, 70 h MTBF. A fault is defined as complete unavailability of beam either via beam loss or removal of shutter permit not related to weather. A fault also occurs when beam has decayed to the point where stability and orbit can no longer be considered reliable (50 mA).

* While the highlights in, and title of, this report cover calendar year 2020, data on accelerator performance and user statistics are measured on the basis of fiscal years.

TYPICAL APS MACHINE PARAMETERS

LINAC

Output energy	425 MeV
Output beam charge	0.3–3 nC
Normalized emittance	5–20 mm-mrad
Frequency	2.856 GHz
Modulator pulse rep rate	30 Hz
Gun rep rate	2–26 Hz
(1-13 pulses, 33.3 ms apart every 0.5 s)	
Beam pulse length	8–15 ns
Bunch length	1–10 ps FWHM

PARTICLE ACCUMULATOR RING

Nominal energy	425 MeV
Circumference	30.66 m
Cycle time	0.5 s or 1 s
Fundamental radio frequency (RF1)	9.77 MHz
12th harmonic RF frequency (RF12)	117.3 MHz
RMS bunch length	0.34 ns
(after compression)	

INJECTOR SYNCHROTRON (BOOSTER)

Nominal extraction energy	7.0 GeV
Injection energy	425 MeV
Circumference	368.0 m
Ramping rep rate	2 Hz or 1 Hz
Natural emittance	132 nm-rad (nominal)
	87 nm-rad (actual)
Booster RMS bunch length	100 ps
Radio frequency	351.935 MHz

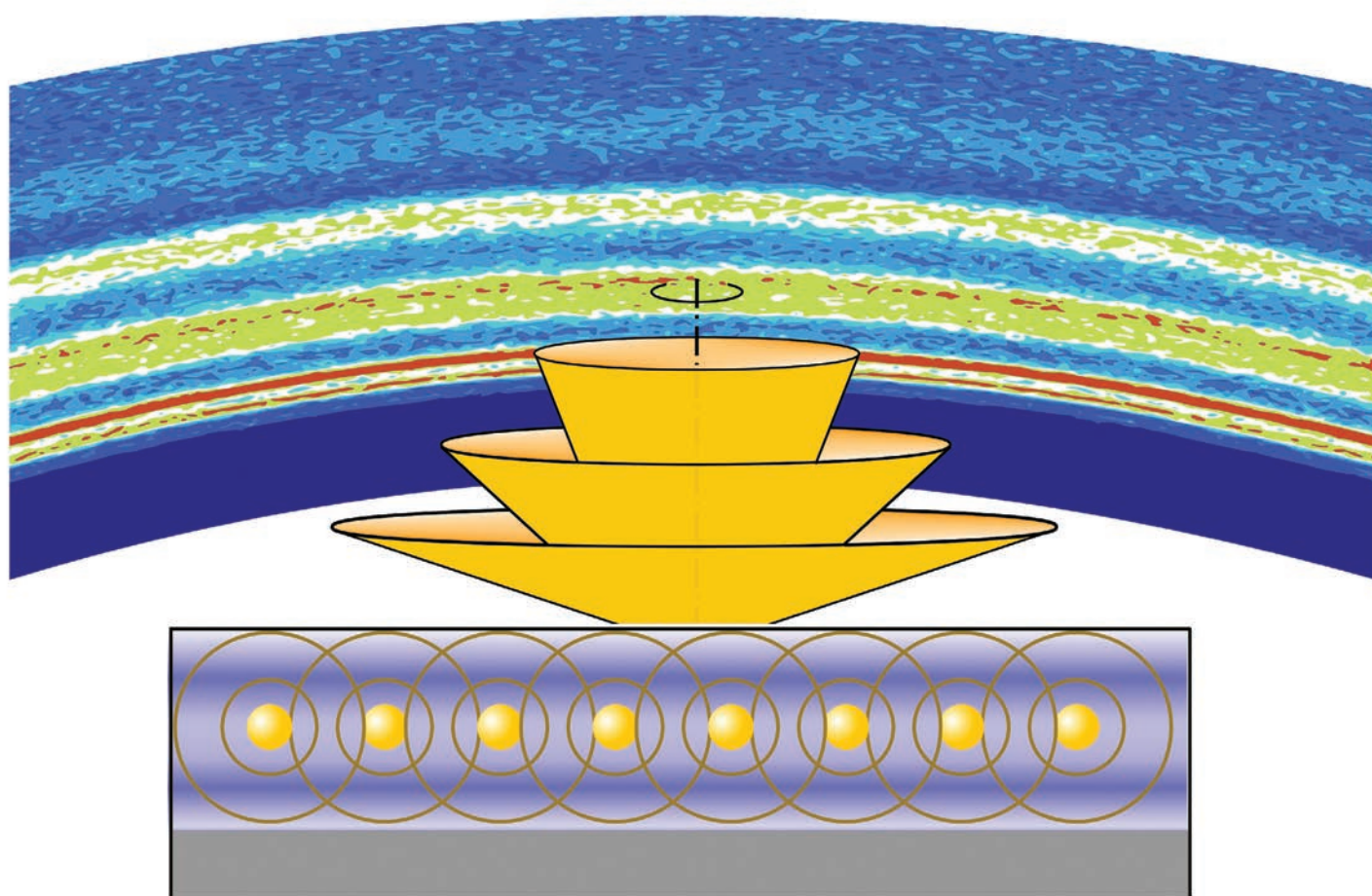
STORAGE RING SYSTEM

Nominal energy	7.0 GeV
Circumference	1104 m
Number of sectors	40
Length available for insertion device	5.0 m
Nominal circulating current, multibunch	100 mA
Natural emittance	2.5 nm-rad
RMS momentum spread	0.096%
Effective emittance	3.1 nm-rad
Vertical emittance	0.040 nm-rad
Coupling (operating)	1.5%
Revolution frequency	271.555 kHz
Radio frequency	351.935 MHz
Operating number of bunches	24 to 324
RMS bunch lengths	33 ps to 25 ps
RMS bunch length of 16 mA in hybrid mode	50 ps

Novel Accelerator and X-ray Techniques and Instrumentation

An X-ray Waveguide Probe into Ultra-thin Nanostructure Films

With ultra-thin nanostructure films now an indispensable component of many electronic and photonic technologies, the ability to accurately observe and characterize their morphology and dynamics is crucial for achieving their optimal design and synthesis techniques. But currently available structural probes are rather limited in their sensitivity, resolution, and *in operando* ability to probe nanometer-size films. Researchers from the APS have demonstrated a new technique using x-ray fluorescence holography (XFH) that exploits the characteristics of these ultra-thin films to serve as a waveguide that creates a detailed fluorescence hologram that can provide a sub-nanometer spatial resolution of film structure. Because of its flexibility and ability to be used for *in situ* and time-resolved studies, it can be used in conjunction with other techniques such as grazing-incidence small-angle x-ray scattering (GISAXS) or reflectivity studies, providing the power to address a broad range of questions concerning ultra-thin film nanostructures.



The technique, which the team calls “x-ray waveguide fluorescence holography” (XWFH, Fig. 1), is similar to XFH techniques used in crystallography in that it forms holograms through the interference of reference and object waves. Unlike the three-dimensional normal and inverse XFH modes processes, XWFH combines them in a mixed mode to produce a two-dimensional distribution, with the layered thin film nanostructure creating an x-ray standing wave that modulates the normally isotropic fluorescence wave.

The research team used the XWFH technique to study the structure and kinetics of gold nanoparticle monolayers sandwiched between two polymer layers. A model-independent reconstruction algorithm based on dynamical scattering theories was used to reconstruct the results of the XWFH scans along with simultaneous reflectivity and GISAXS data. The experiments were conducted at the XSD Time Resolved Research Group’s 7-ID-C x-ray beamline at the APS.

To avoid loss of x-ray signal and decreased signal-to-noise ratio due to penetration of the film’s palladium substrate, the incident angle in this work was kept at 0.125° for both the XWFH and GISAXS measurements. This also allowed the optimal enhancement of the electric field within the gold monolayer, which lead to the formation of the x-ray standing wave that acted as a waveguide. The resulting fluorescence of the gold atoms then exited the waveguide at discrete exit angles, forming a concentric cone-shaped hologram collected at the detector.

Three types of samples were used, with polymer layers of different molecular weights (low [LL], high [HH], and both [LH]) to allow *in situ* studies of the diffusion kinetics of the gold nanoparticles under annealing. The annealing process altered the monolayer’s electron density profile as well as atomic number density, thus providing valuable information on its rheological properties. Both the XWFH and GISAXS techniques showed that the density of the layer smoothed out and decreased as annealing proceeded. Meanwhile, the reflectivity measurements were

< Fig. 1. The principle of XWFH. Fluorescence from emitting atoms is dynamically modulated by a thin-film waveguide to give a concentric cone-like hologram when leaving the film. The distribution of the fluorescent atoms can be obtained with a high spatial resolution by reconstructing the hologram with a dynamical XWFH algorithm.

relatively insensitive to these changes, which the investigators note is largely due to the greater sensitivity of XWFH and GISAXS to the electric field changes in the waveguide. The LL and HH samples showed the fastest and slowest diffusion kinetics, respectively, with the mixed samples in between.

The mixed-mode XWFH technique can also be simplified by performing it either in grazing-incidence (GIXRF, grazing-incidence x-ray fluorescence) or grazing-exit (GEXRF, grazing-incidence x-ray fluorescence) configurations, each with particular advantages and disadvantages. In the GIXRF configuration, a dominant standing x-ray wave above the film substrate provides an extremely sensitive means to probe the nanostructure, but this requires a highly collimated and precisely aligned incident x-ray beam. The GEXRF technique does not require quite the same precision and is well-suited for *in situ* and time-resolved studies, but also creates a large elastic scattering background that makes data interpretation and reconstruction more difficult. The current work avoids these problems by combining both approaches, so that the characteristics of grazing-incidence and grazing-exit angles complement each other.

The dynamical reconstruction algorithm of the XWFH hologram used by the experimenters includes all of the elastic and fluorescence energies engaged by the x-ray standing wave, allowing element-specific nanostructures to be characterized with high resolution.

The XWFH concept and reconstruction strategies can combine with the novel coherent surface scattering imaging (CSSI) technique to provide high-resolution chemical and structural information for thin films. A one-of-kind CSSI beamline is under design and development for the APS Upgrade. – [Mark Wolverton](#)

See: Zhang Jiang*, Joseph W. Strzalka, Donald A. Walko, and Jin Wang, “Reconstruction of evolving nanostructures in ultrathin films with X-ray waveguide fluorescence holography,” *Nat. Commun.* **11**, 3197 (2020). DOI: 10.1038/s41467-020-16980-5

Author affiliation: Argonne National Laboratory

Correspondence: * zjiang@anl.gov

Z.J. was supported by the U.S. Department of Energy (DOE) Early Career Research Program. The project is partially supported by an Argonne Laboratory Directed Research and Development fund. This research used resources of the Advanced Photon Source, a U.S. DOE Office of Science User Facility operated for the DOE Office of Science by Argonne National Laboratory under Contract No. DE-AC02-06CH11357.

Using X-Rays and Rare Earth Elements to Generate Ultra-High Resolution Images

For centuries, microscopy has been an invaluable tool for understanding nature. Fluorescence microscopy in particular can image a diverse array of molecules. For example, a molecule can be conjugated to a special protein that emits green light. Such conjugation allows researchers to identify a molecule in a cell or tissue by finding regions that fluoresce green. While this technique is incredibly powerful, it is challenging to obtain an optical resolution better than 200 nm. In recent work carried out at two DOE x-ray light sources, including the APS, a novel tool was developed to obtain impressive spatial resolutions (e.g., 36 nm) in intact cells. This was accomplished by adapting lanthanide-binding tags in conjunction with x-ray fluorescence microscopy. Since lanthanide-binding tags offer many unique advantages, this novel work may allow for previously inaccessible structures and molecules to be imaged at a high resolution.

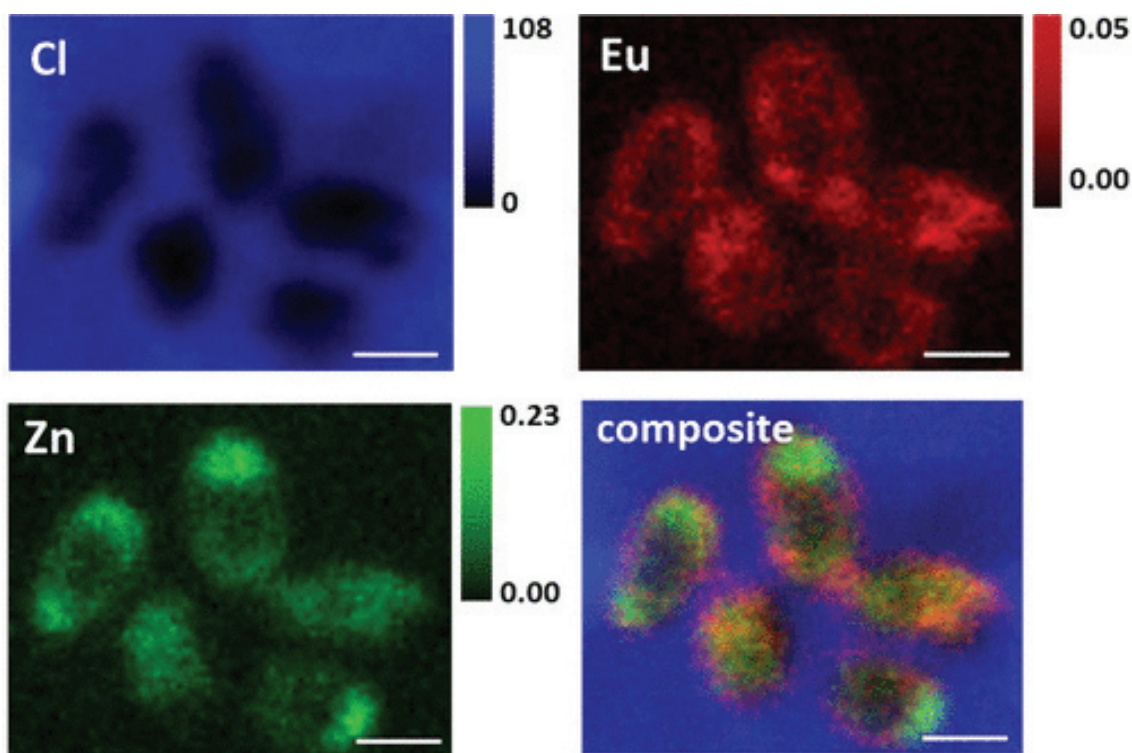


Fig. 1. X-ray fluorescence microscopy images from the APS Bionanoprobe showing the distribution of chlorine (Cl), europium (Eu), zinc (Zn), and the overlay of Eu (red), Zn (green), and Cl (blue) in *E. coli* cells expressing OmpA-LBT and incubated with 5- μm Eu. Images were collected with zone plate optics and an 85-nm beam size. Scale bar is 2 μm , and concentration units are $\mu\text{g}/\text{cm}^2$.

Many key discoveries have been made by knowing the location and activity of a given molecule or a group of molecules. Highlighting how important fluorescence microscopy is in science, the 2014 Nobel Prize in Chemistry was awarded to three individuals for advancements in fluorescence microscopy that allow for super-resolution imaging. Prior to the advent of super-resolution microscopy, light microscopy could not reliably obtain a resolution greater than 200 nm or distinguish objects less than 200 nm apart. This is problematic because many objects, such as many viruses, are smaller than 200 nm.

One unique form of fluorescence microscopy is x-ray fluorescence microscopy, which utilizes x-ray beams to perform imaging. Recent technological advances have made x-ray fluorescence microscopy quite powerful and this technique has been used to study important biological processes, such as fertilization, Alzheimer's disease, Parkinson's disease, chemotherapy, and malaria. However, this technique has historically not been capable of super-resolution and has been limited to ~300 nm laterally (two dimensions) and ~1,000 nm axially (three dimensions). Unlike traditional fluorescence microscopy, there is also a dearth of x-ray sensitive tags that can be paired with molecules to image them.

Recent work by researchers from Brookhaven National Laboratory, Boston University, Argonne, Oregon Health Science University, and MIT directly addressed these challenges. The resolution obstacle discussed above was solved by using advanced optics including high-resolution zone plates and the multilayer Laue x-ray lenses, which allows for spatial resolutions approaching 10 nm, a ~20-fold improvement over the conventional diffraction resolution limit. The latter tagging problem was addressed by customizing short peptides (15-20 amino acids long) referred to as lanthanide-binding tags.

The metallic chemical (rare-earth) elements with atomic numbers (proton numbers) 57-71 make up the lanthanide series. Other techniques have used lanthanide binding tags for important research techniques such as nuclear magnetic resonance spectroscopy, magnetic resonance imaging, photoluminescence, and x-ray crystallography. Creatively, these researchers have adapted lanthanide-binding tags for x-ray fluorescence microscopy. The tags are well-suited to biological imaging because lanthanide elements are extremely rare within living organisms. The authors present a variety of beautiful, colored images in bacteria to demonstrate that the tags can be used for two- and three-dimensional imaging. Figure 1 shows a tri-colored, high-resolution image of bacteria.

The Bionanoprobe, which was at LS-CAT beamline 21-ID-D and now is at the XSD Microscopy Group's beamline 9-ID-B, both at the APS, was used to perform two-dimensional x-ray fluorescence microscopy. The Hard X-ray Nanoprobe beamline 3-ID at the DOE's National Synchrotron Light Source II (NSLS-II) at Brookhaven National Laboratory was used for the three-dimensional x-ray nanotomography work.

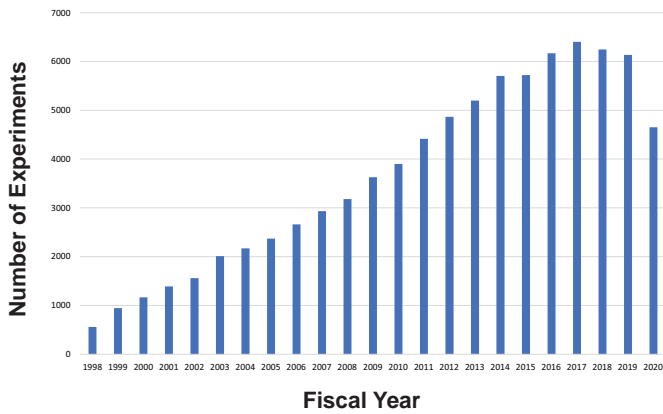
This research demonstrates that x-ray imaging can be performed in the X, Y, and Z dimensions using lanthanide-binding tags. Since these tags have an incredibly high affinity for lanthanides, they can be used at low, non-toxic concentrations. Protein sequences are amenable to their incorporation and their small size means that they don't hinder a protein's ability to carry out its physiological functions. These data demonstrate that this approach can be used to generate high-quality images with a nanoscale resolution. Since x-rays have a long penetration depth, this method could be feasibly applied to imaging in tissues. Future research should build upon these findings and aim to explore what novel insights can be gleaned from the unique combination of lanthanide-binding tags and x-ray imaging. – Alicia Surrao

See: Tiffany W. Victor¹, Katherine H. O'Toole², Lindsey M. Easton², Mingyuan Ge¹, Randy J. Smith¹, Xiaojing Huang¹, Hanfei Yan¹, Yong S. Chu¹, Si Chen³, Doga Gursoy³, Martina Ralle⁴, Barbara Imperiati⁵, Karen N. Allen², and Lisa M. Miller^{*}, "Lanthanide-Binding Tags for 3D X-ray Imaging of Proteins in Cells at Nanoscale Resolution," *J. Am. Chem. Soc.* **142**, 2145 (2020). DOI: 10.1021/jacs.9b11571

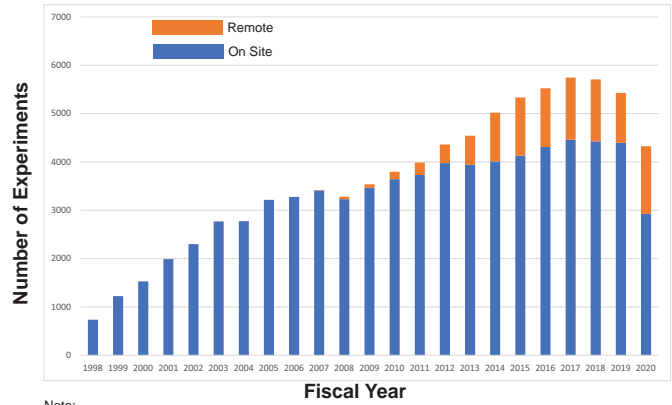
Author affiliations: ¹Brookhaven National Laboratory, ²University, ³Argonne National Laboratory, ⁴Oregon Health Science University, ⁵Massachusetts Institute of Technology
Correspondence: * lmill@bnl.gov

This work was supported by the U.S. Department of Energy (DOE) Office of Biological and Environmental Research as part of the "Environment Sensing and Response" Scientific Focus Area of the BER Genomic Science Program. T.W.V. was partially supported by the National Institutes of Health T32 Grant 5T32GM092714 and a Director's Postdoctoral Fellowship at NSLS-II. B.I. and K.N.A. were supported by National Science Foundation MCB-1615252 and MCB-1614608, respectively. The Life Sciences Collaborative Access Team is supported by the Michigan Economic Development Corporation and the Michigan Technology Tri-Corridor (Grant 085P1000817). This research used beamline 3-ID (HXN) at the National Synchrotron Light Source II, a U.S. DOE Office of Science User Facility operated for the DOE Office of Science by Brookhaven National Laboratory under Contract No. DE-SC0012704. This research used resources of the Advanced Photon Source, a U.S. DOE Office of Science User Facility operated for the DOE Office of Science by Argonne National Laboratory under Contract No. DE-AC02-06CH11357.

Number of APS Experiments by Fiscal Year

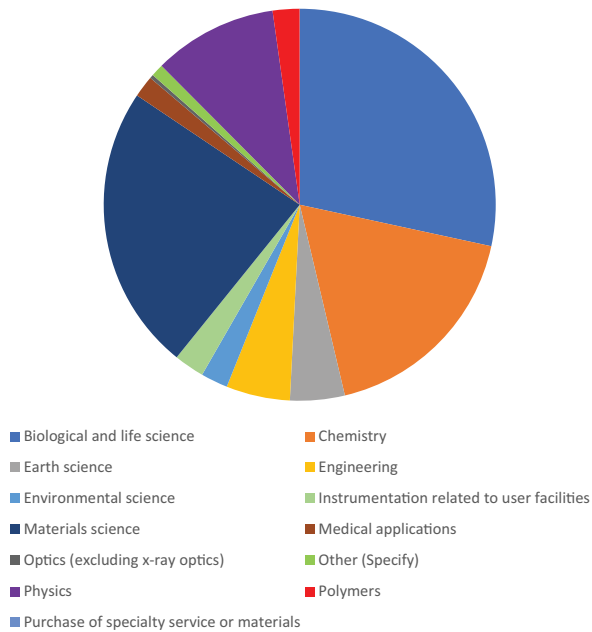


APS On-Site and Remote Users by Fiscal Year

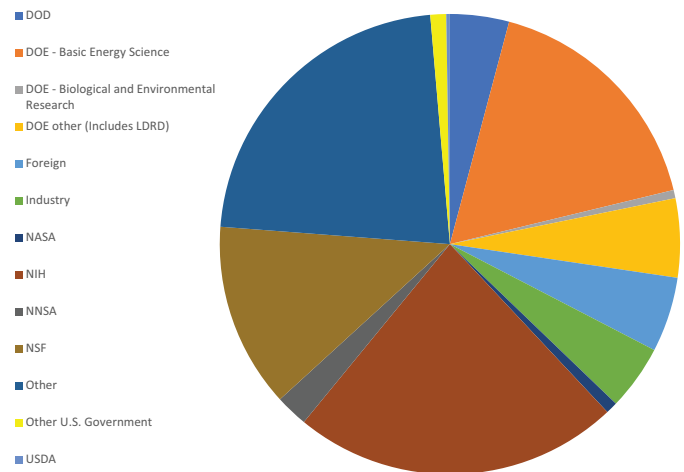


Note:
 1) Prior to FY14, mail-in users were not included in the Remote category.
 2) In FY20, a new BES user counting policy has been applied so that only one unique user is associated with mail-in experiments and the user is only counted once in the whole population.

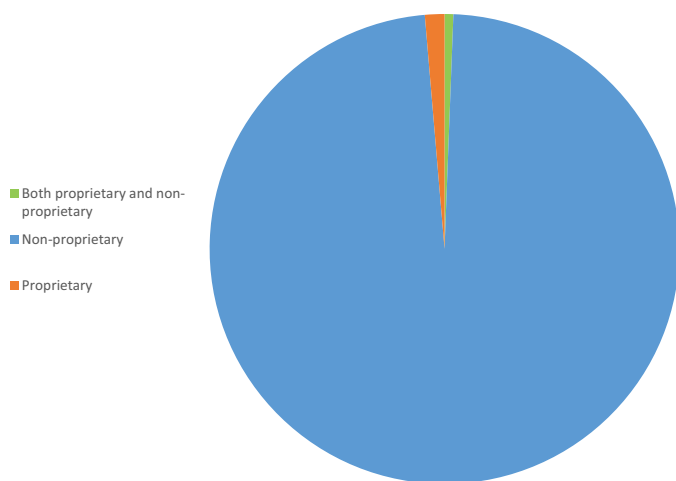
APS Users by Experiment Subject - FY20



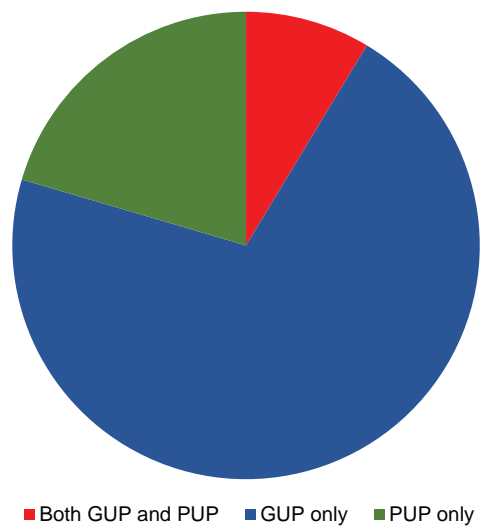
APS Users by Source of Support - FY20



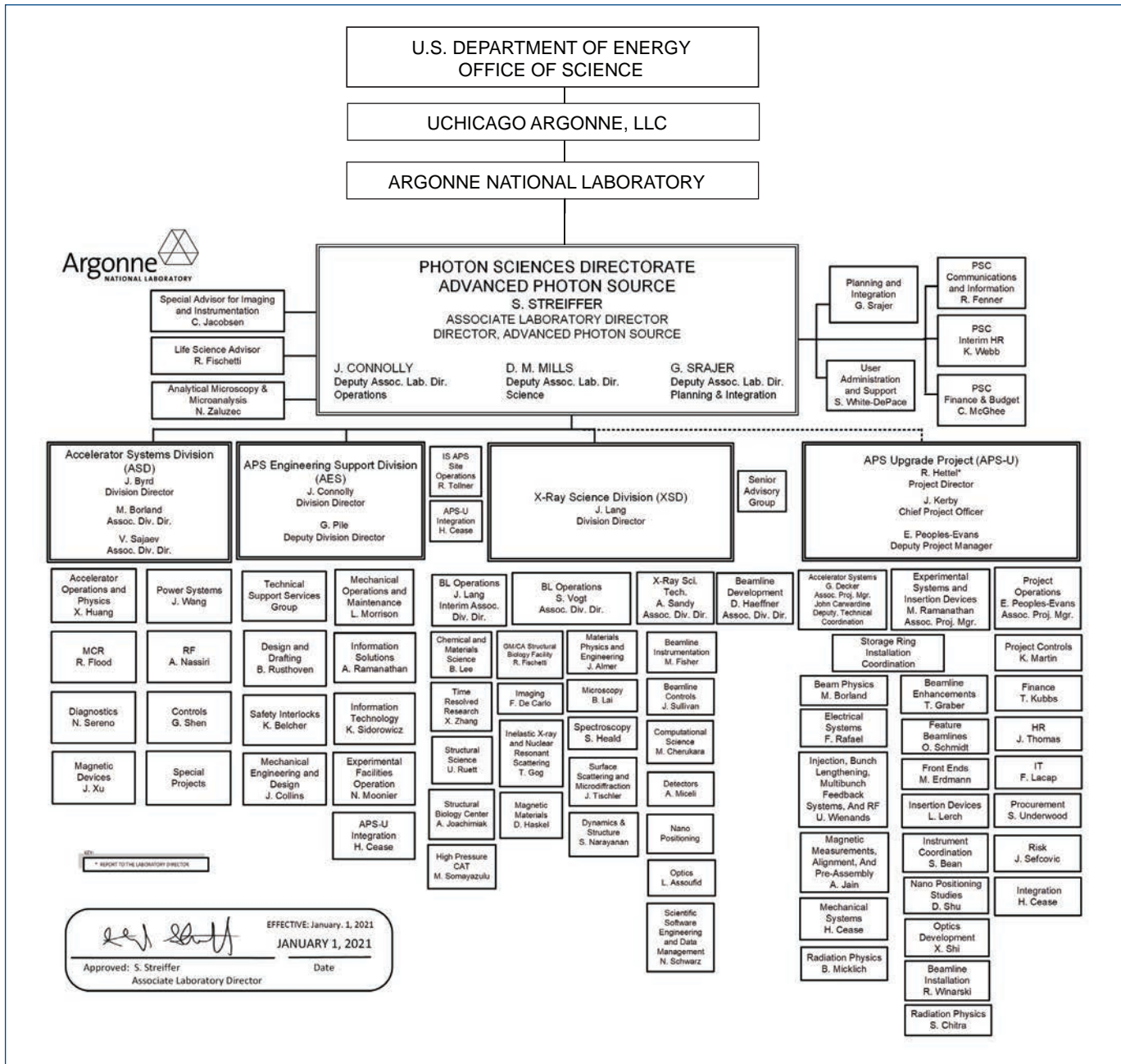
APS Users by Proprietary Type - FY20



APS Users by User Type - FY20



Photon Sciences Directorate Organization Chart



APS SOURCE PARAMETERS

UNDULATOR A (31 INSERTION DEVICES [IDs] IN 25 SECTORS)

Period: 3.30 cm

Length: 2.1 m in sectors 16, 21, 23, 24, 28, 34; 2.3 m in Sector 6;
2.4 m in sectors 1, 2, 5, 7, 8, 9, 10, 11, 15, 17, 18, 19, 20, 22, 26, 28,
31, 32, 33

Minimum gap: 10.5 mm

B_{\max}/K_{\max} : 0.892 T/2.75 (effective; at minimum gap)

Tuning range: 3.0–13.0 keV (1st harmonic)

3.0–45.0 keV (1st–5th harmonic)

On-axis brilliance at 7 keV (ph/s/mrad²/mm²/0.1%bw):

4.1×10^{19} (2.4 m), 4.0×10^{19} (2.3 m), 3.3×10^{19} (2.1 m)

Source size and divergence at 8 keV:

Σ_x : 276 μm Σ_y : 11 μm

Σ_x : 12.7 μrad (2.4 m), 12.8 μrad (2.3 m), 12.9 μrad (2.1 m)

Σ_y : 6.7 μrad (2.4 m), 6.8 μrad (2.3 m), 7.1 μrad (2.1 m)

2.30-CM UNDULATOR (2 IDs IN SECTORS 11, 14)

Period: 2.30 cm Length: 2.4 m

Minimum gap: 10.5 mm

B_{\max}/K_{\max} : 0.558 T/1.20 (effective; at minimum gap)

Tuning range: 11.8–20.0 keV (1st harmonic)

11.8–70.0 keV (1st–5th harmonic, non-contiguous)

On-axis brilliance at 12 keV (ph/s/mrad²/mm²/0.1%bw): 6.9×10^{19}

Source size and divergence at 12 keV:

Σ_x : 276 μm Σ_y : 11 μm

Σ_x : 12.3 μrad Σ_y : 5.9 μrad

2.70-CM UNDULATOR (5 IDs IN SECTORS 3, 12, 14, 35)

Period: 2.70 cm

Length: 2.1 m in Sector 12; 2.4 m in sectors 3, 14, and 35

Minimum gap: 10.5 mm

B_{\max}/K_{\max} : 0.698 T/1.76 (effective; at minimum gap)

Tuning range: 6.7–16.0 keV (1st harmonic)

6.7–60.0 keV (1st–5th harmonic, non-contiguous)

On-axis brilliance at 8.5 keV (ph/s/mrad²/mm²/0.1%bw):

5.7×10^{19} (2.4 m), 4.7×10^{19} (2.1 m)

Source size and divergence at 8 keV:

Σ_x : 276 μm Σ_y : 11 μm

Σ_x : 12.7 μrad (2.4 m), 12.9 μrad (2.1 m)

Σ_y : 6.7 μrad (2.4 m), 7.1 μrad (2.1 m)

3.00-CM UNDULATOR (8 IDs IN SECTORS 12, 13, 16, 21, 23, 27, 34)

Period: 3.00 cm

Length: 2.1 m in sectors 12, 13, 16, 21, 23, 34; 2.4 m in Sector 27

Minimum gap: 10.5 mm

B_{\max}/K_{\max} : 0.787 T/2.20 (effective; at minimum gap)

Tuning range: 4.6–14.5 keV (1st harmonic)

4.6–50.0 keV (1st–5th harmonic)

On-axis brilliance at 8 keV (ph/s/mrad²/mm²/0.1%bw):

4.8×10^{19} (2.4 m), 3.9×10^{19} (2.1 m)

Source size and divergence at 8 keV:

Σ_x : 276 μm Σ_y : 11 μm

Σ_x : 12.7 μrad (2.4 m), 12.9 μrad (2.1 m)

Σ_y : 6.7 μrad (2.4 m), 7.1 μrad (2.1 m)

3.50-CM SMCO UNDULATOR (SECTOR 4)

Period: 3.50 cm Length: 2.4 m

Minimum gap: 9.75 mm

B_{\max}/K_{\max} : 0.918 T/3.00 (effective; at minimum gap)

Tuning range: 2.4–12.5 keV (1st harmonic)

2.4–42.0 keV (1st–5th harmonic)

On-axis brilliance at 7 keV (ph/s/mrad²/mm²/0.1%bw): 3.7×10^{19}

Source size and divergence at 8 keV:

Σ_x : 276 μm Σ_y : 11 μm

Σ_x : 12.7 μrad Σ_y : 6.7 μrad

3.60-CM UNDULATOR (SECTOR 13)

Period: 3.60 cm

Length: 2.1 m

Minimum gap: 11.0 mm

B_{\max}/K_{\max} : 0.936 T/3.15 (effective; at minimum gap)

Tuning range: 2.2–11.8 keV (1st harmonic)

2.2–40.0 keV (1st–5th harmonic)

On-axis brilliance at 6.5 keV (ph/s/mrad²/mm²/0.1%bw): 2.8×10^{19}

Source size and divergence at 8 keV:

Σ_x : 276 μm Σ_y : 11 μm

Σ_x : 12.9 μrad Σ_y : 7.1 μrad

1.72-CM UNDULATOR (3 IDs IN SECTORS 30, 35)

Period: 1.72 cm

Length: 4.8 m (2 x 2.4 m) in Sector 30; 2.4 m in Sector 35

Minimum gap: 10.6 mm

B_{\max}/K_{\max} : 0.330 T/0.53 (effective; at minimum gap)

Tuning range: 23.7–26.3 keV (1st harmonic)

On-axis brilliance at 23.7 keV (ph/s/mrad²/mm²/0.1%bw):

1.0×10^{20} (4.8 m), 4.4×10^{19} (2.4 m)

Source size and divergence at 23.7 keV:

Σ_x : 276 μm Σ_y : 11 μm

Σ_x : 11.6 μrad (4.8 m) 11.9 μrad (2.4 m)

Σ_y : 4.3 μrad (4.8 m), 4.9 μrad (2.4 m)

1.80-CM UNDULATOR (SECTOR 32)

Period: 1.80 cm

Length: 2.4 m

Minimum gap: 11.0 mm

B_{\max}/K_{\max} : 0.244 T/0.41 (effective; at minimum gap)

Tuning range: 23.8 - 25.3 keV (1st harmonic)

71.4 - 75.9 keV (3rd harmonic)

On-axis brilliance at 23.8 keV (ph/s/mrad²/mm²/0.1%bw): 2.8×10^{19}

Source size and divergence at 23.8 keV:

Σ_x : 276 μm Σ_y : 11 μm

Σ_x : 11.9 μrad Σ_y : 4.9 μrad

IEX 12.5-CM QUASI-PERIODIC POLARIZING UNDULATOR (SECTOR 29)

Period: 12.5 cm

Length: 4.8 m

Circular polarization mode:

Max. currents: horizontal coils 34.4 A, vertical coils 20.7 A

K_{\max} : 2.73 (effective; at max. currents)

B_{\max} : 0.27 T (peak; at max. currents)

Tuning range: 0.44–3.5 keV (1st harmonic)

On-axis brilliance at 1.8 keV (ph/s/mrad²/mm²/0.1%bw): 1.4×10^{19}

Linear horizontal polarization mode:

Max. current: vertical coils 47.6 A

K_{\max} : 5.39 (effective; at max. current)

B_{\max} : 0.54 T (peak; at max. current)

Tuning range: 0.24–3.5 keV (1st harmonic)

0.24–11.0 keV (1st–5th harmonic)

On-axis brilliance at 2.1 keV (ph/s/mrad²/mm²/0.1%bw): 1.1×10^{19}

Linear vertical polarization mode:

Max. current: horizontal coils 50.3 A

K_{\max} : 3.86 (effective; at max. current)

B_{\max} : 0.37 T (peak; at max. current)

Tuning range: 0.44–3.5 keV (1st harmonic)

0.44–11.0 keV (1st–5th harmonic)

On-axis brilliance at 2.1 keV (ph/s/mrad²/mm²/0.1%bw): 1.1×10^{19}

Fast polarization switching not required

Source size and divergence at 2 keV:

Σ_x : 276 μm Σ_y : 13 μm

Σ_x : 13.9 μrad Σ_y : 8.8 μrad

12.8-CM CIRCULARLY POLARIZING UNDULATOR (SECTOR 4)

Period: 12.8 cm

Length: 2.1 m

Circular polarization mode:

Max. currents: horizontal coils 1.34 kA, vertical coils 0.40 kA

K_{\max} : 2.85 (effective; at max. currents)

B_{\max} : 0.30 T (peak; at max. currents)

Tuning range: 0.4–3.0 keV (1st harmonic)

On-axis brilliance at 1.8 keV (ph/s/mrad²/mm²/0.1%bw): 3.1×10^{18}

Linear horizontal polarization mode:

Max. current: vertical coils 0.40 kA

K_{\max} : 2.85 (effective; at max. current)

B_{\max} : 0.30 T (peak; at max. current)

Tuning range: 0.72–3.0 keV (1st harmonic)

0.72–10.0 keV (1st–5th harmonic)

On-axis brilliance at 2.1 keV (ph/s/mrad²/mm²/0.1%bw): 2.3×10^{18}

Linear vertical polarization mode:

Max. current: horizontal coils 1.60 kA

K_{\max} : 3.23 (effective; at max. current)

B_{\max} : 0.34 T (peak; at max. current)

Tuning range: 0.58–3.0 keV (1st harmonic)

0.58–10.0 keV (1st–5th harmonic)

On-axis brilliance at 2.1 keV (ph/s/mrad²/mm²/0.1%bw): 2.3×10^{18}

Switching frequency (limited by storage ring operation): 0–0.5 Hz

Switching rise time: 50 ms

Source size and divergence at 2 keV:

Σ_x : 276 μm Σ_y : 12 μm

Σ_x : 16.7 μrad Σ_y : 12.7 μrad

1.80-CM SUPERCONDUCTING UNDULATOR

(2 IDs IN SECTORS 1, 6)

Period: 1.80 cm

Length: 1.1 m

Gap: 9.5 mm (fixed)

Max. current: 450 A

B_{\max}/K_{\max} : 0.962 T/1.61 (effective; at maximum current)

Tuning range: 11.2–24.7 keV (1st harmonic)

11.2–150.0 keV (1st–13th harmonic, non-contiguous)

On-axis brilliance at 13 keV (ph/s/mrad²/mm²/0.1%bw): 3.2×10^{19}

Source size and divergence at 13 keV:

Σ_x : 276 μm Σ_y : 11 μm

Σ_x : 13.2 μrad Σ_y : 7.5 μrad

3.15-CM HELICAL SUPERCONDUCTING UNDULATOR

(SECTOR 7)

Period: 3.15 cm

Length: 1.2 m

Coil winding diameter: 31.0 mm

Max. current: 450 A

B_{\max}/K_{\max} : 0.413 T/1.213 ($B_x=B_y$ effective; at maximum current)

Tuning range: 6.0–13.0 keV (1st harmonic)

On-axis brilliance at 6.0 keV (ph/s/mrad²/mm²/0.1%bw): 2.2×10^{19}

Source size and divergence at 6 keV:

Σ_x : 276 μm Σ_y : 11 μm

Σ_x : 14.7 μrad Σ_y : 10.0 μrad

APS BENDING MAGNET

Critical energy: 19.51 keV

Energy range: 1–100 keV

On-axis brilliance at 16 keV (ph/s/mrad²/mm²/0.1%bw): 5.4×10^{15}

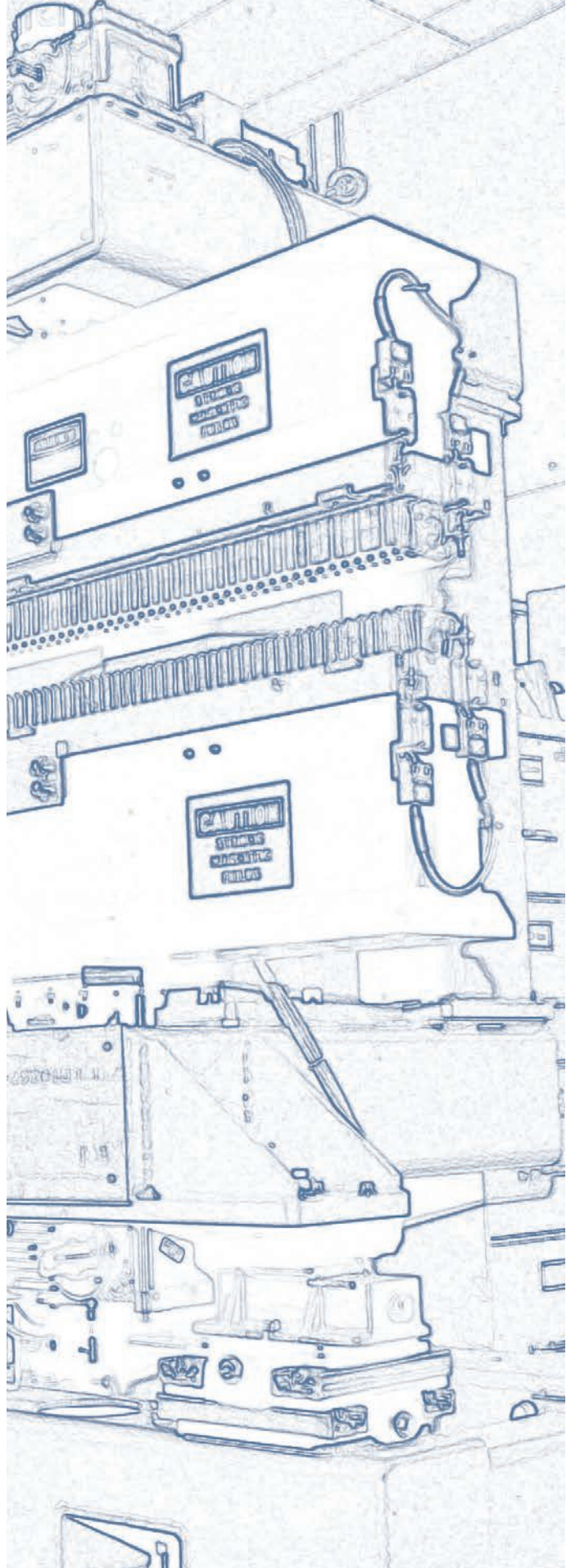
On-axis angular flux density at 16 keV (ph/s/mrad²/0.1%bw): 9.6×10^{13}

Horizontal angular flux density at 6 keV (ph/s/mradh/0.1%bw): 1.6×10^{13}

Source size and divergence at the critical energy:

Σ_x : 92 μm Σ_y : 31 μm

Σ_x : 6 mrad Σ_y : 47 μrad



Acknowledgments

APS Science 2019 Editorial Board:

John Byrd (ANL-ASD), John Connolly (ANL-AES), Robert Fischetti (ANL-PSC), Robert Hettel (ANL-PSC), Jim Kerby (ANL-PSC), Jonathan Lang (ANL-XSD), Dennis Mills, (ANL-PSC), George Srajer (ANL-PSC), Stephen Streiffer (ANL-PSC), Stefan Vogt (ANL-XSD)

Reviewers:

Vukica Srajer (BioCARS); Thomas Irving (Bio-CAT); Binhau Lin (ChemMatCARS); Yogendra Gupta, Sheila Heyns, and Paulo Rigg (DCS), Denis Keane (DND-CAT); Michael Becker, Robert Fischetti, and Janet Smith (GMCA-XSD); Mark Rivers, and Steve Sutton (GSECARS); Maddury (Zulu) Somayazulu (HPCAT-XSD); Lisa Keefe (IMCA-CAT); Jordi Benach (LRL-CAT); Keith Brister (LS-CAT); Carlo Segre (MR-CAT); Kay Perry (NE-CAT); Andrzej Joachimiak (SBC-XSD); John Patrick Rose and Bi-Cheng Wang (SER-CAT); Ahmet Alatas, Jonathan Almer, Francesco De Carlo, Paul Fenter, Thomas Gog, Daniel Haskel, Steve Heald, Barry Lai, Byeongdu Lee, Suresh Narayanan, Uta Ruett, Jon Tischler, Alec Sandy, Shastri and Xiaoyi Zhang (XSD)

Unless otherwise noted, the research highlights in this report were written by:

Mary Alexandra Agner (marymary@alum.mit.edu)
Christen Brownlee (christenbrownlee@gmail.com)
Erika Gebel Berg (erikagebel@gmail.com)
Vic Comello (ANL-CPA - retired) (vcomello@anl.gov)
Dana Desonie (desonie@cox.net)
Sandy Field (sfield@fieldscientific.com)
Philip Koth (philkoth@comcast.net)
Kim Krieger (mskrieger@gmail.com)
Tien Nguyen (tmnguyen5@gmail.com)
Chris Palmer (crpalmer2009@gmail.com)
Neil Savage (neil@stefan.com)
Alicia Surrao (alicia@untoldcontent.com)
Stephen Taylor (stephen@untoldcontent.com)
Mark Wolverton (exetermw@earthlink.net)

Photography: Wes P. Agresta, Mark L. Lopez (both ANL-CPA)

Aerial photograph of the APS: John Hill (Tigerhill Studio, <http://www.tigerhillstudio.com>)

Publications, contracts, rights and permissions, circulation: Jessie L. Skwarek (ANL-PSC)

Printing oversight: John Schneider (ANL-CPA)

Editorial, project coordination, design, photography: Richard B. Fenner (ANL-PSC)

Our thanks to the corresponding authors and others who assisted in the preparation of the research highlights, to the users and APS personnel who wrote articles for the report, and our apologies to anyone inadvertently left off this list. To all: your contributions are appreciated.



Advanced Photon Source
Argonne National Laboratory
9700 S. Cass Ave.
Lemont, IL 60439 USA
www.anl.gov • www.aps.anl.gov